HEINRICH HEINE
UNIVERSITÄT DÜSSELDORF

The incorporation of an unnatural amino acid to study the nucleotide binding domain of the ABC transporter HlyB from *Escherichia coli*

Inaugural-Dissertation

zur Erlangung des Doktorgrades

der Mathematisch-Naturwissenschaftlichen Fakultät

der Heinrich-Heine-Universität Düsseldorf

vorgelegt von

Miroslav Kirov

aus Pazardzhik

Düsseldorf, März 2014

Aus dem Institut für Biochemie
der Heinrich-Heine-Universität Düsseldorf

Gedruckt mit der Genehmigung
der Mathematisch-Naturwissenschaftlichen Fakultät
der Heinrich-Heine-Universität Düsseldorf

Referent: Prof. Dr. Lutz Schmitt
Korreferent: PD. Dr. Ulrich Schulte

Tag der mündlichen Prüfung

Table of Contents

1 Summary

ABC transporters perform fundamental cellular processes like the import of nutrients or the export of drugs and toxins. They use the same energy source, ATP hydrolysis, to fuel these different processes. The investigation of their ATPase domains can contribute to better understand the principles of substrate translocation of ABC transpoprters. This knowledge might be applied for example in the research and in drug development against cancer cells, which utilize the ABC transporter ABCB1 to export drugs as one mechanism to obtain resistance. Therefore, a detailed understanding of how these proteins perform ATP hydrolysis is of major interest.
In this work the nucleotide binding domain (NBD) of the ABC transporter HlyB from *E. coli* was used as a model system to investigate the mechanism of ATP hydrolysis via protein caging. By means of this strategy the protein was reversibly inactivated ("caged") by the conjugation to a photolabile protecting group. The aim was to trap the protein in different states of its ATP hydrolysis cycle by incorporation of the photo-caged amino acid DMNB-L-serine and to relieve the trapping by photolysis of DMNB-L-serine to study the ATP hydrolysis cycle in more detail. For this purpose, serines located in the Walker A motif or the D-loop, which are essential for the ATPase activity of HlyB NBD, were replaced with the unnatural amino acid DMNB-L-serine, which can be converted to L-serine by photolysis.
Before the incorporation of the unnatural amino acid, the expression of HlyB NBD in *S. cerevisiae* was established by the screening of different parameters (expression plasmid, temperature or growth medium). Furthermore, different serines mutants were characterized to determine whether the according serine is essential for ATP hydrolysis. Subsequently, the incorporation of DMNB-L-serine into HlyB NBD was established in *S. cerevisiae* and the resulting mutants were purified successfully. It was not possible to reactivate the Walker A mutant (S504DMNB-L-serine) by photolysis. In contrast, the D-loop mutant (S634DMNB-L-serine) showed ATPase activity as a function of the incubation time, which reached 70 % of the activity of the wild type protein after photolysis. The characterisation of the photolysed protein indicated that the NBD still hydrolysed ATP in a cooperative fashion, however its catalytic properties deviated from the properties of the wild type protein. Based on the involvement of the D-loop in the ATP-ADP transition of the nucleotide bound HlyB NBD, the regained activity of the D-loop mutant indicated that this region is dynamic and flexible. Based on its role in the inter-monomer communication, the manipulation of the D-loop probably disrupts the allosteric communication between the monomers in the HlyB NBD dimer.

Zusammenfassung

ABC Transporter sind für essentielle zelluläre Prozesse wie z. B. den Import von Nährstoffen, die Resistenz gegen unterschiedliche Xenobiotika oder die Sekretion von Toxinen verantwortlich. Die Energie für den aktiven Transport ihrer Substrate gewinnen sie durch die Hydrolyse von ATP. Durch die Untersuchung der ATPase Domäne kann ein besseres Verständnis der Prinzipien des aktiven Transports dieser Membranproteine erlangt werden. Dieses könnte z. B. in der Forschung oder in der Entwicklung von Wirkstoffen gegen Krebszellen eingesetzt werden, die den ABC-Transporter ABCB1 zum Export von Xenobiotika verwenden. Aus diesem Grund würde eine detaillierte Aufklärung des Mechanismus der ATP-Hydrolyse weitere wichtige Erkenntnisse dafür liefern.
In dieser Arbeit wurde die Nukleotid-bindende Domäne (NBD) des ABC Transporters Haemolysin B (HlyB) aus *E. coli* als Modellsystem verwendet, um den Mechanismus der ATP-Hydrolyse mittels Protein-„Caging“ zu untersuchen. Mit dieser Strategie wurde das Protein inaktiviert, indem eine photolabile Schutzgruppe eingebaut wurde. Für die ATP-Hydrolyse essentielle Serine des Walker A Motivs oder des D-Loops wurden gegen die nicht natürliche, photolabile Aminosäure DMNB-L-Serin mutiert. Diese kann mittels Lichtbestrahlung zu L-Serin photolysiert werden. Diese Strategie sollte es ermöglichen, die HlyB NBD in bestimmten Zuständen ihres katalytischen Zyklus zu arretieren und anschließend nach Photolyse zu reaktivieren.
Vor dem Einbau von DMNB-L-Serin wurde die HlyB NBD Expression in *S. cerevisiae* etabliert, indem unterschiedliche Parameter (Expressionsplasmid, Temperatur oder Nährmedium) analysiert wurden. Darüber hinaus wurden unterschiedliche Serin-Mutanten charakterisiert, um zu überprüfen, ob die entsprechenden Serine essentiell für die ATPase Aktivität des Proteins sind. Im Anschluss wurde der DMNB-L-Serin-Einbau in *S. cerevisiae* etabliert und die entsprechenden HlyB NBD Mutanten aufgereinigt. Eine Walker A Mutante (S504DMNB-L-Serin) zeigte keine Aktivität, jedoch führte Lichtbestrahlung zu keiner Reaktivierung. Im Gegensatz dazu zeigte eine D-Loop Mutante (S634DMNB-L-Serin) nach erfolgreicher Photolyse eine zeitabhängige ATPase Aktivität, die 70 % der Aktivität des Wildtypproteins erreichte. Obwohl diese photolysierte Mutante Kooperativität bei der ATP Hydrolyse zeigte, wichen ihre katalytische Eigenschaften von denen der Wildtyp HlyB NBD ab. Aufgrund der beobachteten Mitwirkung des D-Loops als „Scharnier“ bei dem Übergang von ATP- zur ADP-gebundenen HlyB NBD, deuteten die Ergebnisse darauf hin, dass der D-Loop dynamisch und flexibel ist. Die Beteiligung des D-Loops an der Monomer-Monomer Wechselwirkungen innerhalb des HlyB NBD Dimers ließ vermuten, dass die Mutation von Serin 634 aus dem D-loop die allosterische Kommunikation zwischen den Monomeren unterbrach.

2 Introduction

2.1 ABC transport proteins

Selective transport across biological membranes is one of the key features of the cell. Membrane proteins play a crucial role in this task and can be grouped into different classes – channels, primary active transporters, secondary active transporters and group translocators (*11*). The proteins from the class of the primary transporters, among them the ABC transporters, usually use direct chemical energy (e.g. hydrolysis of nucleotides) to fuel the transport process (*12*). ABC transporters usually utilize the energy stored in ATP for active transport of their substrates (*13*).These proteins constitute a large family of proteins and are widespread in all three kingdoms of life (*14*).

The classification of ABC proteins is based on the primary sequence. The presence of the conserved motifs Walker A (G-x-x-G-x-G-K-S-T)[1], Walker B ($\phi\phi\phi\phi$DE)[2] and the ABC signature motive, also called linker peptide or C-loop (LSGGQ), is characteristic of this protein superfamily (*15, 16*). The comparison of the sequences of ABC proteins results in three main classes: *(i)* class 1 contains all known exporters; *(ii)* class 2 consists of proteins that participate in different cellular processes other than transport; *(iii)* class 3 contains binding-protein-dependent ABC importers, disease-related proteins and not-characterised ABC proteins, some of which might be exporters (*17*).

2.2 Structural organisation of ABC transporters

Despite the huge substrate diversity of ABC transporters, these proteins share a common structural organisation. By combining X-ray crystallography and biochemical data, it was demonstrated that the functional unit of an ABC transporter (ABC proteins from class 1 and 3) consists of four domains – two transmembrane domains (TMDs) and two cytosolic ATP binding cassettes, also named nucleotide binding domains (NBDs) or ABC ATPases (*18*), (Figure 1).

[1] x means any amino acid

[2] ϕ means hydrophobic residue

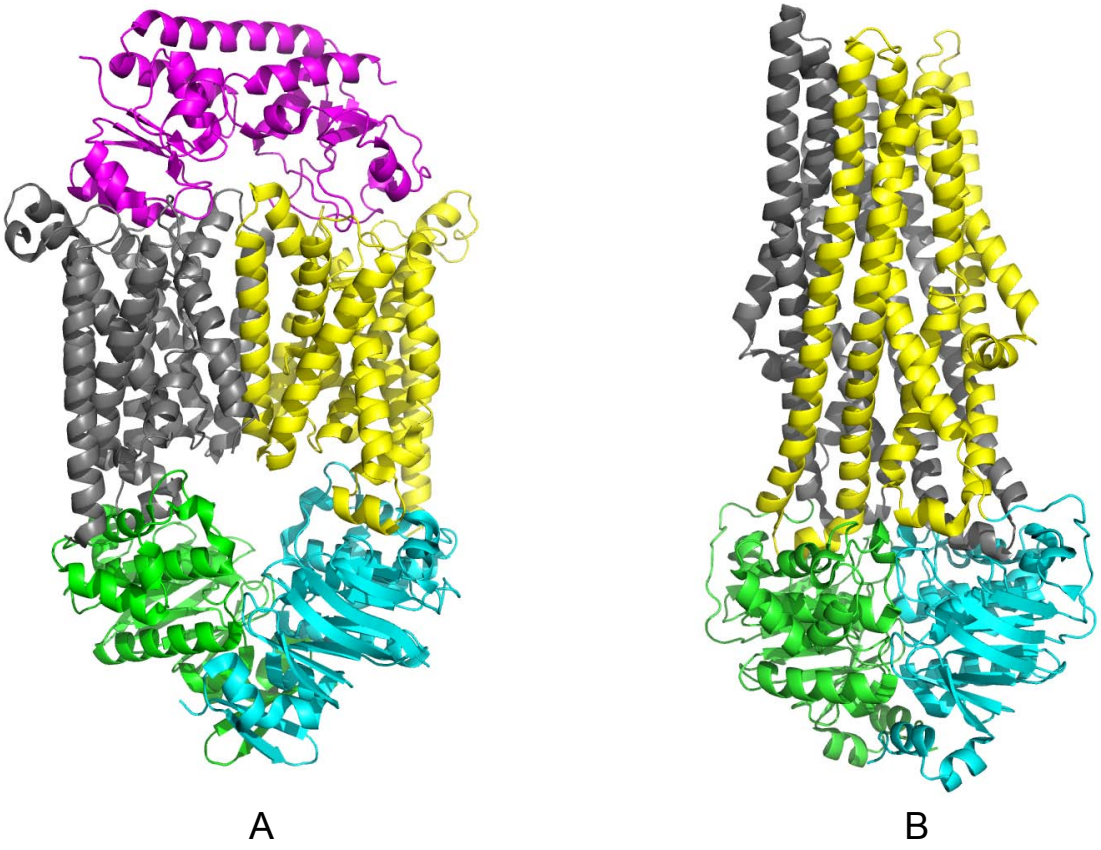

Figure 1: Structural organization of ABC transporters. The nucleotide binding domains are shown in green and cyan, the transmembrane domains are shown in yellow and grey. In magenta a substrate binding protein, found only in importers and also essential for function, is shown. **A:** Crystal structure of the vitamin B_{12} importer BtuCD from *E. coli* in complex with its substrate binding protein BtuF (*4*), PDB code 2QI9. **B:** Crystal structure of the exporter Sav1866 from *S. aureus* (*9*), PDB code 2HYD.

A comparison of the different NBDs reveals a high degree of conservation in these domains, reflected in the conserved motifs Walker A and Walker B, the C-, D-, H-, Q-, and Pro-loop (*19*). Each loop-name corresponds to the highly conserved amino acid found in the according loop. In contrast TMDs of ABC transporters do not show a high sequence conservation, which might explain the high diversity of transported substrates, which are also called allocrites (*20*). These four domains can be encoded on one (e.g. ABCB1), two (e.g. HlyB), three (e.g. YejFBE) or four (e.g. DppBCDF) polypeptide chains (*21*). The domains can associate to hetero- or homooligomers to form a functional ABC transporter. Both ABC importers and exporters are found in prokaryotes whereas in eukaryotes exporters are present (*12*). There are also indications for the presence of ABC importers in eukaryotes (*22-24*), however further evidence is needed to postulate the presence of these transporter proteins in

eukaryotes. Importers are crucial for the uptake of nutrients whereas exporters transport for example toxins, drugs, polysaccharides and lipids to the exterior (*18*). The domains of importers, which include also the essential substrate binding proteins (SBPs), are often encoded on different polypeptide chains (*25*). The domains of exporters are usually encoded on one or two (i.e. one TMD and one NBD fused together) polypeptide chains.

Some of the ABC transporters contain additional domains. One example is the regulatory domain (RD) of the nucleotide binding domain (MalK) of the maltose importer (*26*). It interacts with the transcriptional regulator MalT (*27*) or the enzyme IIA and it is able to regulate the transport activity of the ABC transporter (*27-30*).

Furthermore, next to NBDs and TMDs bacterial importers like the maltose import system from *E. coli* (*31*) or the vitamin B_{12} importer from *E. coli* (*32*) contain specific substrate binding proteins, which are essential for transport. These SBPs entrap the substrate with high affinity and load the transporter complex with it.

2.3 The nucleotide binding domain (NBD)

In this work one of the best-characterised ABC ATPases, the NBD of the ABC transporter HlyB from *E.coli*, was used as a model system to study the properties of ABC ATPases.

The nucleotide binding domains of ABC transporters are key players in the transport of allocrites across the cell membrane – they deliver the energy for this process by binding and hydrolysing ATP (*14, 33*). Mg^{2+} is essential for this reaction, in which ADP and phosphate are formed. The high-resolution X-ray structures of isolated ABC ATPases contributed greatly to improve the understanding of the structure-function relationships of these proteins. NBDs contain a Rec-A-like fold that is characterised by a central β-sheet, flanked by α-helices (*34*). Typically, NBDs show an L-shaped form (*3*), (Figure 2).

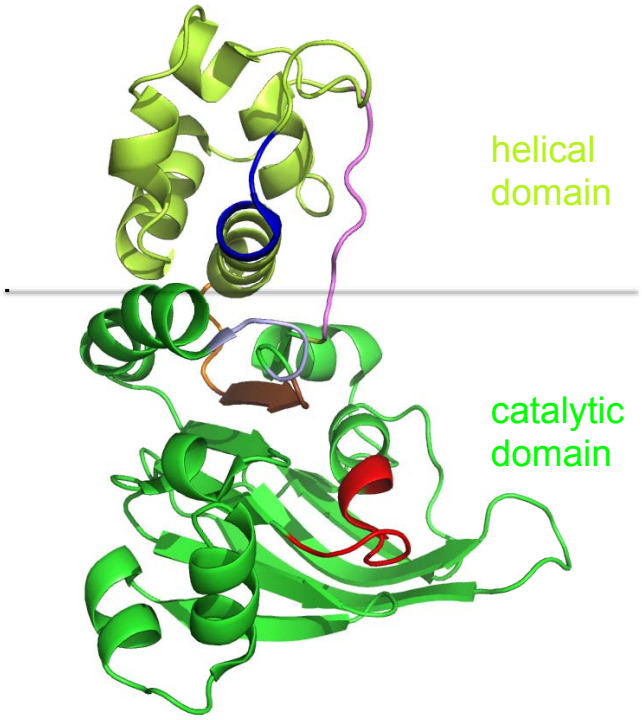

Figure 2: Cartoon representation of the three-dimensional structure of HlyB-NBD. The catalytic domain (lower section) is colored in green; the helical domain (upper section) is colored in limón green. Conserved motives are shown as follows: red – Walker A; brown – Walker B; blue – C-loop; light blue – D-loop; violet – Q-loop; orange – Pro-loop. This figure was generated using Pymol from the HlyB NBD X-Ray structure, PDB entry 1MT0 (*3*).

Based on their structure, the NBD can be divided in two domains – the helical domain (upper part, colored in limón green, Figure 2) and the catalytic domain (lower part, coloured in green, Figure 2). The helical part consists of α-helices while the catalytic domain consists of β-sheets and α-helices. The helical domain contains the diagnostic motif of the ABC transporters – the C-loop (shown in blue), which has the amino acid sequence LSGGQ (*35*). The catalytic domain contains the conserved Walker A motif, which has the consensus sequence G-X-X-G-X-G-K-S-T (Figure 2, red), where X means any amino acid (*36*). Another conserved sequence in the catalytic domain is the Walker B motif, which is characterized by the amino acids sequence ϕϕϕϕDE, where ϕ indicates a hydrophobic amino acid. Both domains of the NBD are connected via the Q-loop and the Pro-loop (Figure 2, marked in

violet and orange respectively). The names of the two latter mentioned loops are derived from highly conserved glutamine and proline residues in the corresponding loops. The D-loop (consensus sequence SALD), containing the highly conserved aspartate, is shown in light blue (*35*).

By now, several X-ray-structures of isolated NBDs have been published and they revealed basically the same monomeric architecture (Figure 3). For a review see (*37*).

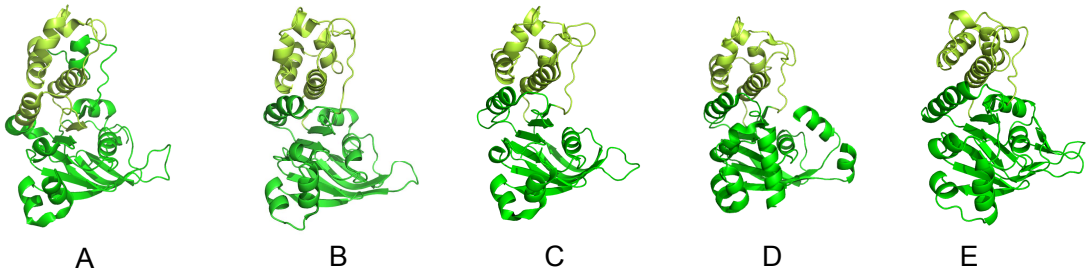

Figure 3: Comparison of the overall fold of different ABC-ATPases. The catalytical domain is shown in green (lower part) and the helical domain is in lemon green (upper part). **A:** TAP1-NBD (PDB-code: 2IXG); **B**: HlyB-NBD (PDB-code: 1MT0); **C**: MRP1-NBD1 (PDB-code: 2CBZ); **D**: CFTR-NBD1 (PDB-code: 1R0W); **E**: HisP (PDB-code: 1BOU).

ATP binding induces the formation of a dimer of the NBDs (*38*). The dimer represents the functional form of ABC ATPases, which was supported by structural and biochemical data (*5, 38*). All these data demonstrated that the binding of ATP drives a dimer formation in a so-called “head to tail” – arrangement. In Figure 4 dimer structures of isolated NBDs of different ABC transporters, solved via X-ray crystallography, are presented.

The nucleotide is bound between the Walker A motive of one monomer (*cis*-monomer) and the C-loop of the other monomer (*trans*-monomer). Consequently two molecules of ATP are required for the formation of one dimer with two binding sites (*1*). A detailed view of one binding pocket of the composite dimer of the HlyB NBD (*5*) is presented in Figure 5.

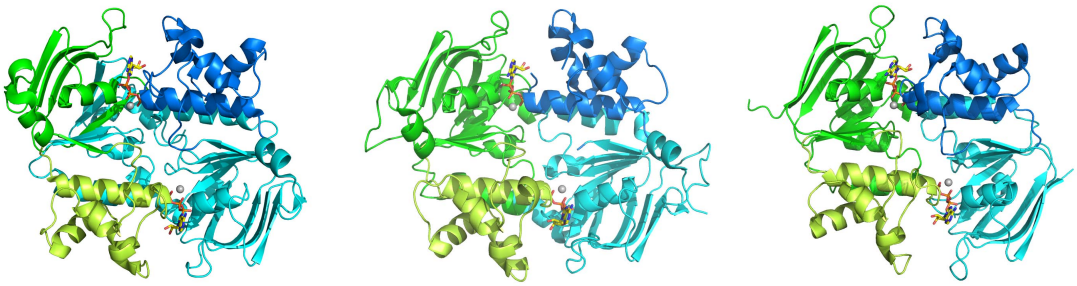

Figure 4: Comparison of three-dimensional structures of dimeric NBDs. The color code of the *cis*-monomer is the same as in **Figure 3**. In the *trans*-monomer the catalytic domain is colored in cyan, the helical domain is colored in marine blue. Both ATP molecules are shown in stick representation. The magnesium ions are shown as grey spheres. **A**: HlyB-NBD (PDB-code: 1XEF); **B**: TAP1-NBD (PDB-code: 2IXE); **C**: CFTR-NBD1 (PDB-code: 2PZE).

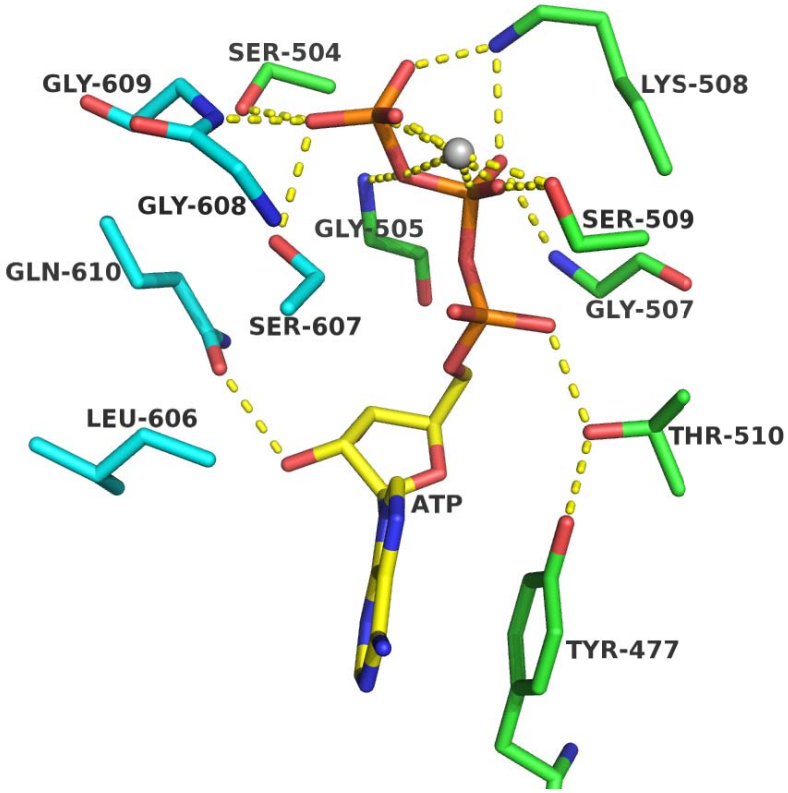

Figure 5: Coordination of ATP and a magnesium ion within the binding pocket of the HlyB NBD. The residues of the Walker A motif and the C-loop are shown. Furthermore Y477, which coordinates the adenine ring of ATP via π-π interactions, is shown. The hydrogen bonds and the salt bridges are depicted as dashed yellow lines. For a better overview only the side chains of the amino acids are shown, except for glycines. The carbon atoms of the Walker A motif are colored in green, the carbon atoms of the C-loop are colored in cyan. Oxygen atoms are colored in red, nitrogen atoms in blue. The carbon atoms of ATP are shown in yellow, the phosphorus atoms of ATP are shown in orange. The magnesium ion is shown as a silver sphere. The figure was prepared from the coordinates of the structure of HlyB NBD H662A, PDB code 1XEF, using Pymol.

A complex network of bonds stabilizes the dimer (hydrogen bonds, salt bridges, van der Waals- and hydrophobic interactions). This network enables the orientation of the whole system in the above-mentioned “head-to-tail” –

architecture. The adenine-ring of ATP is coordinated via π-π-interactions by an aromatic residue (*38*). This is Y477 in HlyB NBD (Figure 5) (*5*). The Walker A motif fixes ATP in a defined position via interactions with the triphosphate moiety (Figure 5). Most interactions are established between the Walker A motif and ATP via the β-phosphate. The residues of the Walker A motif participate in these interactions mainly by the nitrogen atoms of the peptide backbone (Figure 6). The network of interactions between HlyB NBD and ATP is shown schematically in Figure 6.

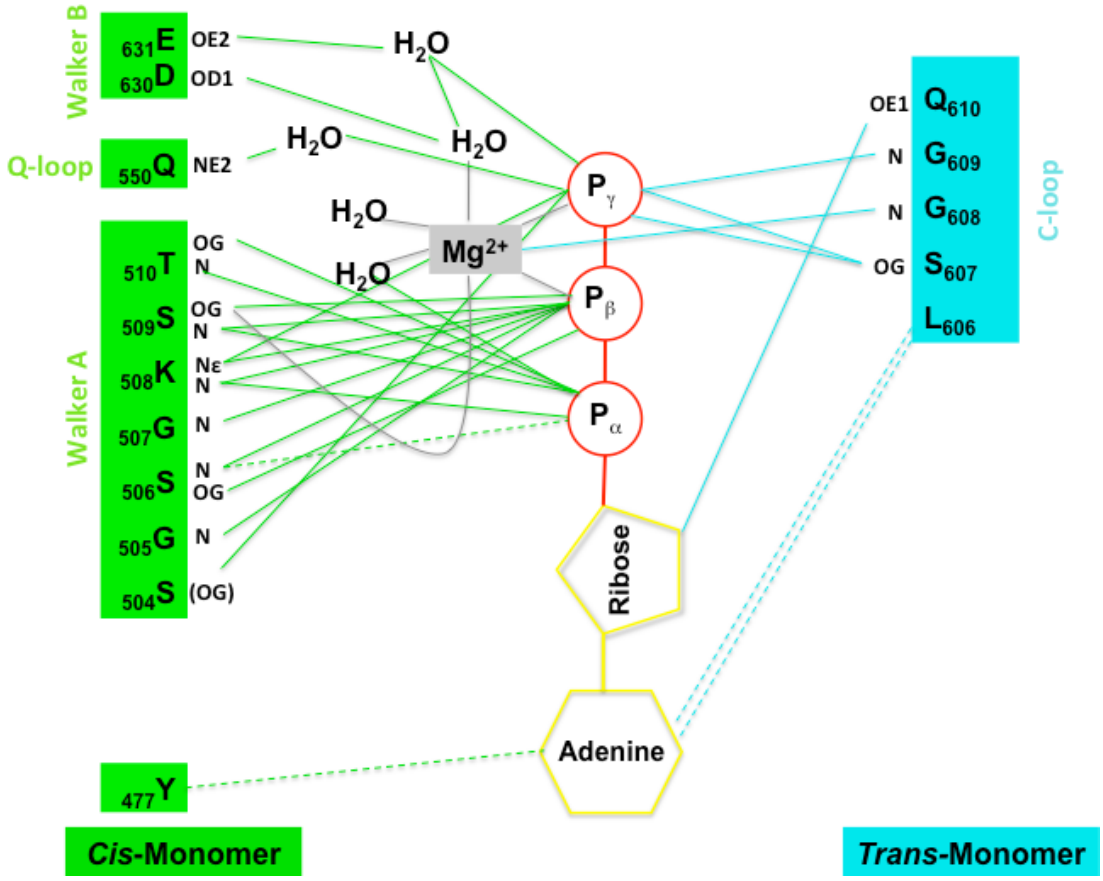

Figure 6: Schematic representation of the protein-nucleotide interactions within the composite dimer of HlyB NBD. The monomers are colored as in **Figure 5**. ATP is shown in the center. Solid lines represent hydrogen bonds or salt bridges, dashed lines mark hydrophobic- and van der Waals interactions. N – nitrogen atom of the peptide backbone, NE2 – nitrogen atom of a glutamine side chain, Nε – nitrogen atom of a lysine side chain, OG – oxygen atom of a serine side chain, OD1 – oxygen atom of an aspartate side chain, OE1 - oxygen atom of a glutamine side chain. This scheme was adapted from (*2*).

Apart from the Walker A motif and the C-loop water molecules play an important role for the protein—ATP interactions. Furthermore, water molecules participate in the coordination of the magnesium ion. Via water

molecules the highly conserved D630, E631 (both Walker B) and Q550 (Q-loop) contact the magnesium ion and / or the γ–phosphate (Figure 6).

The γ–phosphate is crucial for NBD dimerization (*12*). For example in the HlyB NBD the C-loop from the *trans*-monomer (via S607, G608 and G609) stabilizes the dimer by direct interactions with the γ–phosphate (Figure 6). Furthermore, upon nucleotide binding, the glutamine of the Q-loop contacts the γ–phosphate via a water molecule (Figure 6). After ATP binding this interaction mediates the movement of the Q-loop as a mechanical hinge, which pulls the whole helical domain towards the catalytic domain (*1*). Consequently, the signature motif shifts inward and is able to coordinate the γ–phosphate of ATP, which is also coordinated by the Walker A motif of the opposing monomer (*37*). In this way the nucleotide binding induces a rigid-body inward rotation of the helical relative to the catalytic domain in the range of 5 – 25° ("induced fit motion") depending on the ABC ATPase (*39*). ADP is not able to induce the formation of a dimer, which indicates that the γ–phosphate is essential for the dimerization (*5*).

The complex network of interactions within the nucleotide bound dimer is completed by symmetrical and asymmetrical protein-protein contacts between the *cis*- and *trans*-monomer, as revealed from the dimeric structures of HlyB NBD (*1, 2*). These structures showed the decisive role of the cofactor Mg^{2+}, which induces asymmetry in the dimer. The D-loop is also involved in monomer-monomer interactions within the ATP/Mg^{2+} - bound dimer as a possible sensor of structural changes in the opposite monomer (*1*).

2.4 Transport of allocrites across the membrane and coupling to the ATP-hydrolysis cycle

As mentioned above, the functional unit of an ABC transporter comprises two NBDs and two TMDs, which can be organised in different ways. For an efficient allocrite transport each of these units is required. This implies that the transport process is highly synchronized, and therefore communication and a coupling mechanism between the domains are required. Such coupling was shown for example via comparative analysis of the X-ray structures of BtuCD, HI1470/71, ModBC and Sav1866 (*40*) and via mutational studies of

Tap1/Tap2 (*41, 42*), $MalFGK_2$ (*43*) and CFTR (*44*). Basically, intra-cytosolic loops (ICLs) from the TMDs contact the NBDs in a cleft between the catalytic and the helical domain. This cleft is formed in an area around the Q-loop (*32, 39*). The coupling mechanism among different ABC transporters shows some variations (*45, 46*). In ABC exporters one TMD interacts with both NBDs via two ICLs while in ABC importers one TMD contacts one NBD via a single ICL (*19*). The TMD-NBD communication is transmitted via extensive interactions between the ICLs and the Q-loop, which could be shown via genetical studies (*43*), crosslinking experiments (*47*) and structural studies (*31, 32, 48-50*). Furthermore, an adjacent structural diverse region (SDR) in the helical domain, unique to each NBD, interacts with the TMDs (*3*). This helps to explain the specificity of a given NBD to its cognate TMD in ABC transporter with TMDs and NBDs encoded on different polypeptide chains (*3*). ICLs do not share high sequence similarity. However, they share the same secondary structure - α-helix (coupling helix) at the apex of an ICL (*9, 31, 48, 51*). According to the number of ICLs per TMD (see above) there are two coupling helices per TMD in ABC exporters while in importers there is one coupling helix per TMD (*19*). The interactions between coupling helices and Q-loops are essential for the function of ABC transporters. Due to the architecture of the interaction interface between the coupling helices and the Q-loop the latter one could control the allosteric interaction between the NBDs and the allocrite-binding sites of the TMDs (*19*). Furthermore, the Q-loop can control the NBD-NBD communication (*1, 19*). This cross talk enables the transmission of conformational changes between domains. Furthermore, it reflects a mechanism, which in general assures efficient transport initiation and ATPase stimulation after substrate binding (*52*). In this way it is possible to avoid a waste of ATP in the absence of transport substrate. Cross talk between TMDs and NBDs was experimentally shown by mutational studies of the histidine permease ($HisQMP_2$) and the maltose importer ($MalFGK_2$), where mutations in the coupling regions (both TMDs and NBDs) led to uncoupled hydrolysis of ATP in futile cycles without transport substrate (*53, 54*). However, there are also ABC transporters with high basal ATPase activity without bound allocrite (*55*).

Based on structural and biochemical data two general models for allocrite transport have been established – the “Alternating Access Switch Model” (or “Processive Clamp” model (*26, 56*)), based on the transport model from (*57*) and the “Alternating Catalytic Site Model” (*58*) (or “Constant Contact Model” (*59-61*)).

The key difference between these models is the formation of a symmetrical closed “sandwich” dimer with two bound ATPs in the NBDs, which dissociates after sequential nucleotide hydrolysis and the NBDs are completely separated after the hydrolysis (*62*). This is the scenario in the “Alternating Access Switch Model”, which was developed from a detailed structural analysis of full length ABC transporters and isolated NBDs (*63, 64*). Three main stages appear in this model (*65*): I) in the apo form (resting state) the allocrite binds with high affinity to the substrate binding protein (ABC importers) or to the TMDs (exporters), which initiates the transport cycle (and the ATP hydrolysis cycle, however, this is not observed in all ABC transporters). The subsequent conformational changes are transferred to the NBDs via the coupling helix (importers) or the coupling helices (exporters); II) ATP can bind now with higher affinity to the NBDs, which leads to the formation of the composite dimer, which is held together by the nucleotides. This conformational change, also considered as a power stroke, is transmitted to the TMDs. As a consequence, the TMDs reorient (“switch”) towards the opposite membrane site (from an inward-facing orientation to an outward-facing orientation). In this conformation the ABC transporter has a lower affinity for its allocrite. This leads to an allocrite release. III) ATP hydrolysis in the NBDs follows this release by generating excess of negative charges resulting in an electrostatic repulsion, which induces the opening of the dimer thereby enabling the dissociation of P_i and ADP (*38*). In the case of HlyB NBD, not charge excess, but rather conformational changes upon ATP hydrolysis drives the dimer disassembly with the Walker B/D-loop region acting as a hinge in the ATP-ADP transition (*1*). The dimer opening induces the return of the TMDs in their high-affinity conformation.

The “Alternating Catalytic Site Model” is supported by biochemical and biophysical data. It has been derived from data for ABCB1 and is based on asymmetry in the NBD dimer during the transport cycle (*58*). This model is

described by a couple of key points: I) The allocrite binding initiates the transport cycle. This cycle is driven by the ATP hydrolysis within the dimeric NBD and its monomers remain in constant contact during the transport cycle (*59*). The ATPase activity is coupled to the transport and shifts within the NBD dimer sequentially between two states, where one site is occupied with ATP and the other one is empty (*63*). II) Every hydrolysed ATP molecule results in dimer destabilisation (usually due to electrostatic repulsion). This conformational change in the NBD dimer is transmitted to the TMDs, which results in their conformational change and consequently in the transport of an allocrite across the membrane. III) Furthermore, the coupling between NBDs and TMDs ensures the transmission of conformational changes from TMDs to NBDs and vice versa. Experimental data from vanadate-induced trapping (*66*) and from experiments with ATP-γ-S (*67*) supported this model. They showed one bound molecule ATP, but never two simultaneously bound in the NBDs of ABCB1 during the transport process. Furthermore, data obtained vie electron microscopy (*60*) and via experiments with ATP-γ-S (*68*) supported the notion that at each step of the transport cycle the transporter dimer is asymmetric. From these results it was inferred, that during the transport cycle the NBDs of ABCB1 are differently (asymmetrically) occupied, for eyample with one ATP and one ADP, but never with two ATPs simultaneously.

As mentioned, the “Alternating Access Switch Model” is based on structural data and the “Alternating Catalytic Site Model” is based on biochemical and biophysical data. The main differences between both models are the symmetrical composite NBD-dimer of the transporter with two bound ATPs, which was observed in the “Switch model” either with non-hydrolysable ATP analogues (*69*), in the absence of the essential Mg^{2+} ions (*38, 70*), with inactive mutants (*1, 2*), disulfide cross-linking (*71*) or via vanadate-trapping experiments (*49*). Furthermore, the complete dissociation of this dimer (and not only opening) is observed during the transport process. Which model describes the catalytic cycle of HlyB NBD? Structural and biochemical analysis showed two ATP molecules in the binding pockets of the composite dimer (*1, 2*). Furthermore, the data suggested a sequential ATP hydrolysis, which leads to the dissociation of the dimer (*1*). These observations indicated

that rather the “Alternating Access Switch Model” describes the catalytic cycle of the HlyB NBD. Despite the detailed characterization of the catalytic cycle there are still open questions about the mechanism of ATP hydrolysis. How does HlyB NBD hydrolyze the two ATP in the composite dimer – simultaneously or in a sequential order? What is the exact mechanism of the ATP hydrolysis during the catalytic cycle of HlyB NBD between the stage of the composite dimer and the stage of the monomeric HlyB NBD? Furthermore, do ABC transporters hydrolyse ATP via a common mechanism? Which method could deliver the answers of these questions? These still open questions revealed that further investigation of the catalytic cycle is needed.
One of the often-mentioned issues in the investigation of the transporters catalytic cycle is the application of inactive mutants or the omitting of essential cofactors when generating intermediates. A possible approach to circumvent this problem is the trapping of intermediates, which can be reactivated with an external switch at a desirable point. For instance light could be used as such a switch (see below).

2.5 Caged compounds

Light is suitable for this purpose because it usually interacts with proteins without a negative influence on their structure and function at the appropriate wavelength. One of the approaches to utilize light as an external switch is the application of “caged compounds”, which has been applied for decades (*72, 73*). The concept of this approach is based on the idea that “caged compounds” are inhibited in their function by a labile, reactive group, which can be modified (e.g. removed) by irradiation with light. In this way the compound is reactivated (*73*). With such compounds dynamic studies of biological processes can be conducted, because they allow temporally defined manipulation by irradiation with light (*74*). For example, muscular contraction and regulation (*75-77*), mode of action of the Ion-pumping ATPases (*73, 78*), ion channels (*79, 80*), second messengers (*81*), receptors (*82*) or bacterial flagella and proton –motive force (*83, 84*) were studied by the application of caged compounds.

Two caging strategies are to be considered – either a small molecule (a compound of interest) or its interaction partner (the protein of interest) can be "caged" by a conjugation to a photolabile protecting group. There are many examples for the successful application of "caged" compounds like ATP-derivatives (*85, 86*), cAMP (*87*), "caged" Ca^{2+} (*88*), "caged" amino acids (*89, 90*) and others. Nevertheless, the strategy of the "caged" compounds bears some disadvantages. For instance, a modified ligand interacts with the protein of interest and hence interferes with its kinetic and binding properties (*8*) or even with the reaction mechanism (*91*).

2.6 Caged proteins

To avoid such problems, the second strategy, "caged" proteins, can be applied. The advantage of this approach is the (theoretical) possibility to label the protein of interest at any position with a photolabile protective ("caged") group of interest. This should allow an inactivation of the protein in its function and its controlled reactivation after irradiation with light. Another advantage of this strategy is the possibility of labelling different positions within the protein. This would facilitate control of the protein reaction mechanism at different stages. Furthermore, the application of this strategy requires detailed knowledge of the reaction mechanism of the protein of interest. Such labelling can be achieved by different methods – conjugation to natural amino acids, translational incorporation of unnatural amino acids, semisynthetic incorporation of unnatural amino acids or bio-orthogonal conjugation to unnatural amino acids (*92*). In this work caging of proteins by the approach of *in vivo* translational incorporation of an unnatural amino acid was performed (*93*). The basic concept of this approach is the integration of a novel amino acid into proteins by using the biosynthesis machinery of the cell. Firstly, the codon of a desired amino acid in the gene encoding the protein of interest is mutated against the "amber" stop codon. Then a special designed tRNA/aminoacyl-tRNA syntethase (tRNA/aaRS) pair is applied. This pair enables the suppression of an "amber" stop codon in the mRNA of the protein of interest during the protein biosynthesis at the ribosome and also the incorporation of a novel (unnatural) amino acid (*10*).

Each amino acid within the repertoire of the natural amino acids is encoded by one or more codons, which are recognized by specific tRNAs. The addition of a novel proteinogenic amino acid to the cell machinery requires the overcoming of some cellular limitations (*10*). A unique codon has to be assigned to the unnatural amino acid, which encodes only this new amino acid. This codon should not be present in a high frequency throughout the genes of the endogenous proteins because of possible negative impact on their and the cells function. The designed aaRS has to recognize only the novel compound and only the special designed tRNA. This tRNA has to recognize only its codon. Furthermore, the special tRNA needs to be accepted by the ribosome and the delivered unnatural amino acid has to be incorporated into the growing polypeptide chain (Figure 7). No endogeneous aaRS should recognize the special tRNA and load it with a natural amino acid. Furthermore, no endogenous aaRS should recognize the unnatural amino acid. Beyond that, such amino acid should be transported passively or actively into the cell. It also should be non-toxic and not metabolised by cellular enzymes.

One of the strategies for the assignment of a unique codon to an unnatural amino acid of interest is the suppression of the “amber” stop codon (*94*). This codon is the least-used stop codon in *E. coli* and *S. cerevisiae* (*93*). Moreover, it was reported that in some *E. coli* strains natural “amber” stop suppression does not lead to a ponderable impact on the cell growth (*95, 96*). The successful suppression of this stop codon and the incorporation of the unnatural amino acid with high fidelity requires a genetically engineered tRNA/aaRS pair (*97*). A successful approach for the development of these two components was described (*98-100*). This strategy includes the separate development of tRNA and aaRS and comprises a combination of positive and negative selection. Usually, in the first step via combination of negative and positive selection the orthogonal tRNA is selected from a tRNA library (*93*). In the second step via directed evolution an aaRS is developed, which aminoacylates its cognate tRNA with an unnatural amino acid of interest and no endogenous amino acid (*93, 98, 100*). This is usually achieved by modification of amino acids in the binding pocket of the aaRS, which are involved in the binding of amino acids. Via mutagenesis a library of mutants is

generated. These are subject to repetitive rounds of positive and negative selection. The resulting aaRS recognizes only the unnatural amino acid of interest and the according tRNA. Furthermore, the tRNA is also accepted by the ribosome for protein biosynthesis (Figure 7). Usually tRNA/aaRS pairs from archaea are used in bacteria and tRNA/aaRS pairs from bacteria are used in eukaryotes (*93, 98*). This is dictated by the evolutionary relationship between the kingdoms of life and in order to achieve high fidelity of incorporation or to avoid cross-reactions with endogenous amino acids and tRNA/aaRS pairs.

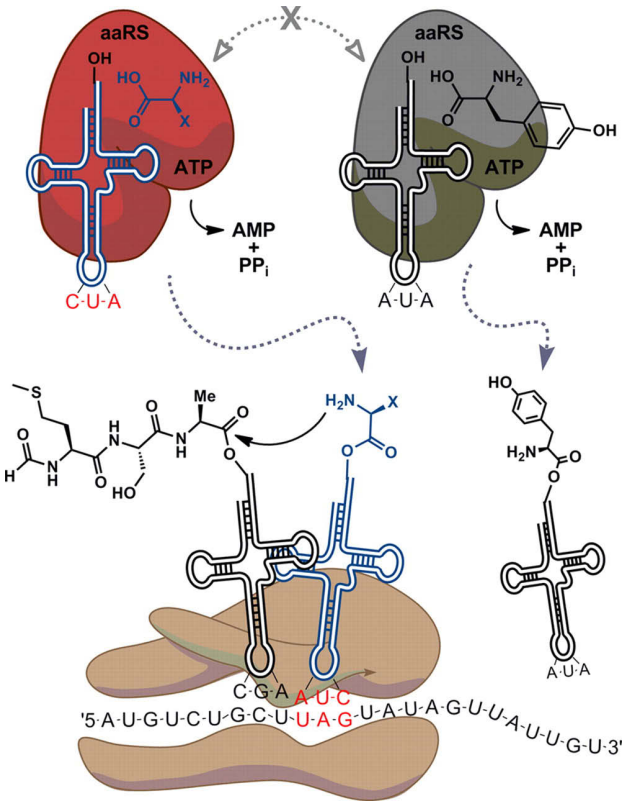

Figure 7: Incorporation of an unnatural amino acid into a nascent polypeptide chain by using the cell machinery via the “amber” stop codon strategy. The tRNA, which is developed for the unnatural amino acid of interest (side chain X), is colored in blue. Both the mentioned tRNA and the unnatural amino acid are recognized by the aminoacyl-tRNA synthetase (aaRS, colored in red), which has been developed via directed evolution. This aaRS reacts only with the tRNA of interest and loads it with the unnatural amino acid. The loaded tRNA is recognized by the ribosome (colored in brown), the “amber” stop codon (UAG, colored in red) is repressed and the unnatural amino acid is incorporated in the nascent polypeptide chain. An “amber” stop codon could be positioned at any position in the gene of interest via site directed mutagenesis. This allows (theoretically) the incorporation of the desired unnatural amino acid at any position in the polypeptide chain. This figure was adopted from (*10*).

Several unnatural amino acids were successfully incorporated into proteins (*10, 101*). The new reactive functional groups allowed the application of new

methods for the study of proteins. For instance, the “photo-caged” amino acid DMNB-L-Ser was successfully applied to study the influence of posttranslational phosphorylation on the transcription factor Pho4 (*102*). This allowed the inactivation of the protein by inhibition of its phosphorylation, which was reversed after irradiation with light. In this manner conclusions about the functional influence of the phosphorylation of different serines could be drawn.

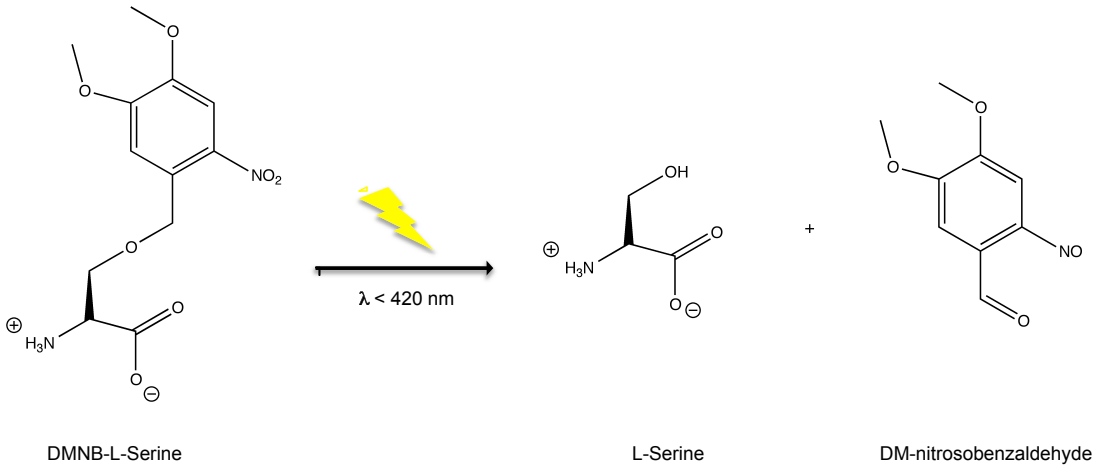

Figure 8: Photoreaction of DMNB-L-Serine upon irradiation with light. The flash, colored in yellow, symbolizes light. The nitro group of DMNB-L-Serine is reduced to a nitroso group, whereas the α-position of the aromatic moiety is oxidized. The photolysis reaction was modified from (*7*).

2.7 Aims and objectives

ABC transporters play a crucial role in the cells of all kingdoms of live by transport of wide range of substrates across biological membranes. The role of these proteins includes elimination of toxic compounds, continuous maintenance of biological membranes or import of vital substances (*25*). All these examples demonstrate the importance of further investigation and understanding of the basic mechanisms of these proteins.

Despite the major progress in the research of ABC transporters we are still far from a detailed understanding of the transport mechanism of these proteins. However, structural and biochemical analysis have resulted in the formulation of the “Alternating Access Switch Models”, based on structural data and of the “Alternating Catalytic Site Models”, based on biochemical data. The key difference is the oligomeric form of the NBDs before and after completion of an allocrite transport cycle. It is not understood until today whether the dimer completely dissociates or not during a “steady state” hydrolysis.

The aim of this work was to reveal more information about the hydrolysis cycle of the NBDs by the generation of temporary inactive intermediates, which can be reactivated by irradiation with light. For this purpose the “photo-caged”, unnatural amino acid DMNB-L-Ser was incorporated *in vivo* via the “amber” stop codon strategy in the isolated HlyB NBD. First, the incorporation of the unnatural amino acids has to be established. Then, DMNB-L-Ser has to be incorporated in the polypeptide chain of HlyB NBD at positions of serines, which are not essential for binding but for hydrolysis of ATP. This should enable the separation of the processes nucleotide binding and NBD dimerization by the generation of ATP-bound monomeric and dimeric intermediates. Their reactivation could reveal further information at molecular level about nucleotide binding at monomeric NBD, dimerization of ATP-bound monomer, mechanism of ATP hydrolysis and the way of ATP hydrolysis (sequential or simultaneous). The advantage of this method is that each “photo-caged” intermediate is trapped in and reactivated from the same starting position. This should increase the signal-to-noise ratio of the conducted experiments. Due to the fact that the utilized tRNA/aaRS pair

incorporates DMNB-L-Ser with high fidelity only in *S. cerevisiae* (*102*) the DMNB-L-Ser incorporation was performed in this yeast.

3 Materials and methods

3.1 Materials

3.1.1 Chemicals

(4-(2-hydroxyethyl)-1-piperazin-ethanesulfone acid)	Fluka
imidazole	
1,4-Dithiotreitol (DTT)	Roth
2(β)-mercaptoethanole	Roth
Acetic acid (CH_3COOH)	Normapur
Acrylamide/Bisacrylamide 37.5:1 30% (Rotiphorese)	Roth
Adenine	Fluka
Adenosine-5´-triphosphate (ATP)	Sigma-Aldrich
Agar-Agar	Serva
Agarose GTQ	Roth
Aluminum sulfate-hydrate ($Al_2(SO_4)_3*H_2O$)	Roth
Ammonium molybdate tetrahydrate	Fluka
($(NH_4)_6Mo7O_{24}*4H_2O$)	
Ammonium peroxidsulfate (APS)	Roth
Ammonium sulfate ($(NH_4)_2SO_4$)	Sigma
Ampicillin, sodium salt	Roth
Bromphenol blue	Sigma-Aldrich
CAPS (N-cyclohexyl-3-aminopropanesulfonic acid)	Roth
Coomassie brilliant blue G-250	Roth
Coomassie plus protein assay reagent	Bio-Rad
Dimethyl sulfoxide (DMSO)	Roth
Dipotassium hydrogen phosphate (K_2HPO_4)	VWR
DMNB-L-Serine	APAC international
Double distilled water	Millipore
EDTA-disodium salt	AppliChem
Ethanol abs. for molecular biology	Normapur
Ethanol techn.	Fluka
Ethidium bromide (EtBr)	Fluka

Glucose	Caesar & Loretz
Glycerol 99%	Grüssing
Glycerol, > 99.5%. p.a.	Roth
Glycine	Roth
HelmaEx	Hellma
Hepes	AppliChem
Hydrochloric acid (HCl) 37 %	Riedel-de-Haen
Isopropyl alcohol	Fluka
L-Arginine	Appli Chem
L-Glutamic acid	Roth
L-Histidine	Sigma
L-Isoleucine	Roth
L-Leucine	Merck
L-Methioinine	AppliChem/Roth
L-Phenylalanine	Merck
L-Threonine	Merck
L-Tryptophan	Roth
L-Tyrosine	Sigma-Aldrich
L-Valine	Roth
Lithium acetate (LiOAc)	Fluka
Magnesium chloride ($MgCl_2$)	Riedel-de-Haen
Malachite green	Sigma-Aldrich
Methanol	Roth
Monopotassium phosphate (KH_2PO_4)	Merck
Non-fat dry milk	Merck
Phosphoric acid (H_3PO_4)	Bernd Kraft Salze und Lösungen
Polyethylene glycol 4000 (PEG-4000)	Fluka
Potassium chloride (KCl)	Normapur
Potassium dihydrogen phosphate (KH_2PO_4)	Roth
Sodium acetate (NaOAc)	Fluka
Sodium azide (NaN_3)	Fluka
Sodium chloride (NaCl)	J.T. Baker

Sodium dodecyl sulfate	Serva
Sulfuric acid (H_2SO_4), 96 %	Fluka
TEMED (N,N,N´,N´-Tetra methylene diamine)	Merck
Trichloroacetic acid (TCA)	Fluka
Tris (Tris(hydroxyl methyl)-aminomethane)	Sigma
Tryptone/Peptone from casein	Difco
Tween 20	Fluka
Uracil	AppliChem/Serva
Water	Roth
Yeast extract	Difco
Yeast nitrogen base w/o ammonium sulfate and ammonium sulfate	Becton, Dickinson and company
Zink sulfate ($ZnSO_4$)	Sigma-Aldrich

3.1.2 Materials for molecular biology

3.1.2.1 Strains and plasmids

Table 1: Used strains and plasmids

Strain	*Genotype*	*Source*
E. coli XL1 blue	endA1 gyrA96(nalR) thi-1 recA1 relA1 lac glnV44 F'[::Tn10 proAB+ lacIq Δ(lacZ)M15] hsdR17(rK- mK+)	Agilent Genomics
S. cerevisiae YPH 500; haploid	ura3–52 lys2–801amber ade2–101ochre trp1–Δ63 his3–Δ200 leu2–Δ1, matα	Agilent Genomics

Table 2: Used plasmids

Plasmid	*Features*	*Source*
p426GPD-HlyB-NBD	*S. cerevisiae*; expression plasmid; GPD-Promoter; 2 µ-replicon; CYC1-terminator;URA3-marker; Amp^R	ATCC; #87361
p426TEF2-HlyB-NBD	*S. cerevisiae*; expression plasmid; TEF-Promoter; 2 µ-replicon; CYC1-terminator;URA3-marker; Amp^R	ATCC; #87369
p426CYC1-HlyB-NBD	*S. cerevisiae*; expression plasmid; CYC1-	ATCC;

	Promoter; 2 µ-replicon; CYC1-terminator;URA3-marker; Amp^R	#87385
p426ADH-HlyB-NBD	*S. cerevisiae*; expression plasmid; ADH-Promoter; 2 µ-replicon; CYC1-terminator;URA3-marker; Amp^R	ATCC; #87377
p426GAL1-HlyB-NBD	*S. cerevisiae*; expression plasmid; GAL1-Promoter; 2 µ-replicon; CYC1-terminator;URA3-marker; Amp^R	ATCC; #87333
426MET25-HlyB-NBD	*S. cerevisiae*; expression plasmid; MET25-Promoter; 2 µ-replicon; CYC1-terminator;URA3-marker; Amp^R	ATCC; #87325
pESCTrpLeuBHT252A	*S. cerevisiae* plasmid; TRP1-marker; Amp^R	(*102*)

3.1.2.2 Oligonucleotides

All oligonucleotides were synthesized by Eurofins MWG Operon. Primers were delivered in a lyophilized form and dissolved in nuclease-free, sterile water (Roth) to a concentration of 100 pmol/µL for long-term storage at -20 °C. Usually primers were used in reactions at a concentration of 10 pmol/µL. In Table 3 the primers are shown, which were used in this work.

Table 3: Used oligonucleotides

Primer name	*Primer sequence in 5´– 3´direction*
5for_B-NBD_N-His	CCAGAACTTAGTTTCGACGGATTCTAGAACTAGTGG ATCCATGCATCACCATCACCATCACGATATCAC
3rev_B-NBD_N-His	CGTGACATAACTAATTACATGACTCGAGGTCGACGG TATCGATTTAGTCTGACTGTAACTGATATAAGTAAC
5for_B-NBD_C-His	CCAGAACTTAGTTTCGACGGATTCTAGAACTAGTGG ATCCATGGATATCACTTTTCGTAATATCCGGTTTC
3rev_B-NBD_C-His	AACTAATTACATGACTCGAGGTCGACGGTATCGATT TAGTGATGGTGATGGTGATGGTCTGACTGTAACTGA TATAAGTA
H662A_5for_B-NBD	GTAAGGGCAGAACGGTTATAATCATTGCTGCGCGTC TGTCTACAGTAA

H662A_3rev_B-NBD	TTACTGTAGACAGACGCGCAGCAATGATTATAACCG TTCTGCCCTTAC
B-NBD-S504A_5for (*8*)	TATTGGTATTGTCGGACGTGCTGGTTCAGG
B-NBD-S504A_3rev (*8*)	TGTGCTTTTTCCTGAACCAGCACGTCCGAC
5_for_S504Amber	TGGTATTGTCGGACGTTAGGGTTCAGGAA
3_rev_S504Amber	TTCCTGAACCCTAACGTCCGACAATACCA
B-NBD S634Y 5for	TTTGATGAAGCAACCTATGCTCTGGATTATGAG
B-NBD_S634Y 3rev	CTCATAATCCAGAGCATAGGTTGCTTCATCAAA
NBD_S634Amb 5for	TTTGATGAAGCAACCTAGGCTCTGGATTATGAG
NBD_S634Amb 3rev	CTCATAATCCAGAGCCTAGGTTGCTTCATCAAA

3.1.2.3 Enzymes, additives and DNA ladders

dNTPs mix	Thermo Scientific / NEB
High-Fidelity Phusion DNA Polymerase	Thermo Scientific
High-Fidelity buffer 5x	Thermo Scientific
Restriction enzymes (ClaI; DpnI, SpeI)	NEB / Thermo Scientific
BSA (Bovine serum albumin)	Thermo Scientific / NEB
T4 DNA Ligase	NEB
T4 buffer	NEB
Fast AP (alkaline phosphatase)	Thermo Scientific
GeneRuler 1 kb DNA Ladder	Thermo Scientific

3.1.2.4 Antibodies

anti HlyB-NBD from rabbit	Prepared according to (*103*)
Anti-rabbit IgG(whole molecule)-Peroxidase antibody produced in goat	Sigma-Aldrich

3.1.2.5 DNA purification kits

Qiaquick Gel Extraction Kit	Qiagen
Qiaprep Miniprep Kit	Qiagen
NucleoBond Xtra Midi Kit	Macherey Nagel
QuickChange II XL Site-Directed Mutagenesis Kit	Agilent Technologies

3.1.2.6 Media and buffers

Cultivation media were prepared with distilled water. After media ingredients were weighed out and dissolved in water, they were autoclaved or sterilized by passing them through a filter with 0.22 µm pores. Media additives like antibiotics or glucose were separately sterilized and added to sterile solutions. Buffers were dissolved in water and if required also sterilized.

	LB-medium	LB-agar
10 g/L	Tryptone/Peptone from casein	LB-medium with 1.5% (w/v) Agar
5 g/L	Yeast extract	
10 g/L	Sodium chloride	

	YPD-medium	YPD-agar
20 g/L	Tryptone/Peptone from casein	YPD-medium with 2% (w/v) Agar
10 g/L	Yeast extract	
20 g/L	Glucose	

Glucose for YPD was produced separately as 20% solution and added to YP-medium separately to final concentration of 2%.

Antibiotics

	Concentration in stock solution	Final concentration
Ampicillin	100 mg/mL (in water)	100 µg/mL

(Amino acid) Mix for selective Drop Out (DO) medium

	mg/L final concentration	g/14.5 g mix
Adenine	40	0.4
L-arginine	20	0.2
L-tyrosine	30	0.3
L-isoleucine	30	0.3
L-phenylalanine	50	0.5
L-glutamic acid	100	1.0
L-aspartic acid	100	1.0
L-threonine	200	2.0
L-serine	400	4.0
L-valine	150	1.5
L-methionine	150	1.5
L-lysine	180	1.8

Additives for selective Drop Out medium

	Quantity	*Final concentration*	*Sterilization*
100xURA	0.2 g uracil in 50 mL H_2O	40 mg/L	autoclavable
100xHIS	0.3 g L-histidine in 50 mL H_2O	60 mg/L	autoclavable
50xLEU	1.3 g L-leucin in 100 mL H_2O	260 mg/L	autoclavable
100xTRP	0.4 g L-tryptophan in 50 mL H_2O	80 mg/L	Filtration

Stock solution for selective 2x Drop Out medium

3.4 g	Yeast nitrogen base without amino acids and $(NH_4)_2SO_4$
2.86 g	Amino acid mix for selective Drop Out medium
10 g	$(NH_4)_2SO_4$
In 740 mL	Total volume

pH is adjusted to 5.6 with 10 M NaOH, then 185 mL aliquots are prepared and autoclaved.

Yeast Drop Out media and plates

250 mL	4% Agar (for agar plates) or sterile water (for liquid medium)
185 mL	2x Drop Out medium Proper combination of 5 mL each 100xHIS, 100xTRP, 100xURA and 10 mL 50xLEU
50 mL	20% glucose
500 mL	Total volume

Buffers for yeast transformation

LATE		PLATE	
100 mM	Lithium acetate	100 mM	Lithium acetate
10 mM	Tris-HCl pH 7.5	10 mM	Tris-HCl pH 7.5
1 mM	EDTA	1 mM	EDTA
		40% (v/v)	PEG4000

Buffers for Agarose gel-electrophoresis

TAE buffer	10x Sample buffer
400 mM Tris-Acetate pH 8	40% (v/v) Glycerol
1 mM EDTA	0.25% Xylene cyanol
	0.25% Bromophenol blue
	Dissolve in 10x TAE buffer

Buffer for preparation of yeast whole cell lysates (YEX)

1.85 M NaOH

7.5% 2(β)-mercaptoethanole

3.1.3 Materials for protein chemistry

Buffer for SDS-Polyacrylamide gel electrophoresis and western blot

Stacking gel buffer		Separation gel buffer	
Tris/HCl pH 6.8	0.5 M	Tris/HCl pH 8.8	1.5 M

SDS running buffer		Western blot transfer buffer	
Tris	50 mM	Tris	50 mM
Glycine	190 mM	Glycine	190 mM
SDS	0.1% (w/v)	SDS	0.1% (w/v)
		Methanol	20% (v/v)

pH 8.3 is automatically set after buffer contents are dissolved in water.

SDS-PAGE 5x sample buffer	
Tris/HCl pH 6.8	0.1 M
SDS	4% (w/v)
Bromphenol blue	0.02% (w/v)
Glycerol	40% (v/v)

Usually DTT was added to SDS-PAGE 5x sample buffer to a final concentration of 20 mM DTT.

SDS-gels mixture

Separation gel			Stacking gel		
Percentage	10%	12.5%	Percentage	3%	4.5%
30 % Acrylamide/ Bisacrilamide (37.5/1)	3.3 mL	4.2 mL	30 % Acrylamide/ Bisacrylamide (37.5/1)	0.55 mL	0.75 mL
1.5 M Tris; pH 8.8	2.5 mL	2.5 mL	0.5 M Tris; pH 6.8	1.25 mL	1.25 mL
10% SDS	100 µL	100 µL	10% SDS	50 µL	50 µL
MQ Water	4 mL	3.2 mL	MQ Water	3.1 mL	2.9 mL
TEMED	10 µL	10 µL	TEMED	7.5 µL	7.5 µL
10% APS	50 µL	50 µL	10% APS	25 µL	25 µL

TBS buffer		TBS-T buffer	
Tris pH 8.0	20 mM	Tris pH 8.0	20 mM
NaCl	250 mM	NaCL	250 mM
		Tween20	0.1% (v/v)

Blocking solution for Western blot

TBS-T buffer

5% dry milk

0.05% NaN_3

Colloidal coomassie staining solution according to (*104*)	Final concentration
Coomassie brilliant blue G-250	0.02% (w/v)
Aluminum sulfate	5% (w/v)
Ethanol (96%)	10% (v/v)
Phosphoric acid (85%)	2% (v/v)

Destaining solution according to (*104*)	Final concentration
Ethanol (96%)	10% (v/v)
Phosphoric acid (85%)	2% (v/v)

IMAC buffers

LI buffer		HI buffer	
50 mM	KP_i pH 8.0	50 mM	KP_i pH 8.0
150 mM	KCl	150 mM	KCl
20% (v/v)	Glycerol	20% (v/v)	Glycerol
2 mM	Imidazole	300 mM	Imidazole

SEC buffer		Analytical SEC buffer	
50 mM	CAPS-NaOH pH 10.4	50 mM	Malonic acid pH 5.8
20% (v/v)	Glycerol	100 mM	Sodium acetate
		5% (v/v)	Glycerol

Buffers for ATPase measurements

ATPase assay buffer	ATPase STOP-buffer
100 mM HEPES pH 7.0	20 mM H_2SO_4
20% (v/v) glycerol	

Malachite green solution	Tween20	Ammonium molybdate
0.122 % (w/v) malachite green 20 % (v/v) H_2SO_4	11% (w/v) Tween20	7.5% (w/v)

Coloring solution for ATPase assays was always freshly prepared by mixing Malachite green solution, Ammonium molybdate solution and Tween20 solution in a ratio 50:12.5:1. It was stored in the dark for max. 2 hours before use.

Buffer for TNP-ATP binding measurements
100 mM HEPES, pH 7.0
20% (v/v) glycerol

3.1.4 Markers for electrophoresis

GeneRuler 1kb DNA Ladder	Thermo Scientific
PageRuler Prestained Protein Ladder	Thermo Scientific
PageRuler Unstained Protein Ladder	Thermo Scientific
Precision Plus Protein Unstained Standards	Bio-Rad

3.1.5 Columns for chromatography

IDA 1 mL HiTrap Chelating	GE Healthcare
IDA 5 mL HiTrap Chelating	GE Healthcare
Superdex 75 10/300 GL	GE Healthcare
Superdex 200 PC 3.2/30	GE Healthcare
Superose 12 PC 3.2/30	GE Healthcare

3.1.6 Other materials

Amicon Ultra 15 (MWCO 10 kDa) Centrifugal filter	Merck Millipore
Amicon Ultra 4 (MWCO 10 kDa) Centrifugal filter	Merck Millipore
BioTrace PVDF Transfer Membrane (Western Blot)	Pall Corporation
BioTrace NT Transfer Membrane (Western Blot)	Pall Corporation
Blotting Paper	Whatman

Western Lightning Ultra (Western Blot detection)	Perkin Elmer
96 Well PS-Microplates, Flat bottom	Greiner Bio One
Reaction tubes 1.5 mL	Eppendorf
Reaction tubes 2 mL	Eppendorf
PCR reaction tubes	Greiner Bio One
Pipettes Pipetman P10, P20, P100, P200, P1000	Gilson
Pipette tips	Sarsted

3.1.7 Devices and instruments

ÄKTA Basic purification system	GE Healthcare
ÄKTA Explorer purification system	GE Healthcare
ÄKTA Purifier purification system	GE Healthcare
ÄKTA Prime Plus purification system	GE Healthcare
ÄKTA Micro purification system	GE Healthcare
Microplates reader FLUOstar OPTIMA	BMG Labtech
ChemiGenius^2 Bio imaging system	Syngene
Cary 50 Scan UV/VIS-spectrophotometer	Varian
Ultrospec 10 Cell density meter	GE Healthcare
FluoroLog-3	Horiba Scientific
Nanodrop ND-1000	Peqlab
Fluorescence half-micro cuvette OS 104F, 1400 µL	Hellma
Fluorescence ultra-micro cuvette QS 105.250, 100 µL	Helma
Sorvall Ecolution RC centrifuge	Thermo Scientific
Avanti J-26 XP centrifuge	Beckman Coulter
Sorvall Discovery 90SE Ultra centrifuge	Thermo Scientific
Sorvall Discovery M120SE Ultra centrifuge	Thermo Scientific
Optima L-90K Ultra centrifuge	Beckman Coulter
Megafuge 1.0 R centrifuge	Thermo Scientific
Eppendorf 5417R centrifuge	Eppendorf
Eppendorf 5415D centrifuge	Eppendorf
LaminAir Heraues LB-48-C clean bench	Thermo Scientific
Constant Systems TS Series Benchtop Cell Disruptor	Constant Systems
NesLab RTE 740 temperature controller	Thermo Scientific

Incubator Heraeus	Thermo Scientific
Horizontal cooling shaker Multitron	Infors HT
15 L autoclavable single wall bioreactor	Applikon
Balances	Kern
Milli-Q^{50} Plus system	Merck Millipore
Thermocycler T-personal	Whatman Biometra
Thermoblock, Thermomixer compact	Eppendorf
pH Meter	Schott
Magnetic stirrer NeoLab D-6011	NeoLab
Vortex-genie 2	Scientific Industries
Mini-PROTEAN 3 Precast Gels system	Bio-Rad
Mini-PROTEAN 3 4-gel vertical electrophoresis system	Bio-Rad
DNA horizontal electrophoresis unit	Chem. Werkstatt Uni Duesseldorf
PowerPac HC power supply	Bio-Rad
Power Source 250 V	VWR

3.2 Methods

3.2.1 Molecular biology methods

3.2.1.1 Standard PCR

This technique was applied for the amplification of genes for cloning. Following contents are required for the performance of PCR: template DNA, thermostable DNA polymerase, oligonucleotide DNA primer pair, reaction buffer, magnesium ions and deoxynucleotides (dNTPs). DNA amplification was achieved via the following reaction sequence: DNA denaturation (generation of single stranded DNA, 98 °C), primer annealing (primer hybridization on the single stranded DNA template, 50 °C), elongation step (DNA elongation by a DNA polymerase, 72 °C). These steps are repeated in a cyclic manner in the same sequence as described above to produce large amounts of the desired gene product. Usually an initial denaturation step preludes the cyclic reaction mode. The primers are present in large excess

compared to the gene template. Phusion High-Fidelity DNA polymerase (Thermo Scientific) was used in this work. A typical PCR program, accomplished in a Biometra T-personal thermo cycler, is presented in Table 4. After the initial denaturation (step 1) the reaction cycle (steps 2 – 4) was repeated 35 times. After this mode, a step of final elongation was accomplished. The aim of that step was the elongation of each single stranded DNA template in the solution. Depending on the primer properties hybridization temperature was varied.

A typical reaction mixture for a standard PCR is shown in Table 5. Reaction buffer was High Fidelity buffer from Thermo Scientific. Total reaction volume amounted to 50 µL. Typically the reaction was initiated via “Hot-start”. In this case PCR was started after the initial denaturation step by addition of 0.5 µL Phusion polymerase.

Table 4: Typical program for standard PCR.

Step Nr.	Duration (*105*)	T [°C]	
1	120	98	
2	50	98	
3	40	50	x 35
4	30	72	
5	420	72	

Table 5: Reaction mix for standard PCR.

High-Fidelity buffer 5x (Thermo Scientific)	10 µL
Primer 5’ – 3’ forward (10 pmol/µL)	3 µL
Primer 3’ – 5’ reverse (10 pmol/µL)	3 µL
dNTPs mix (10 mM)	1 µL
Template DNA (100 ng/µL)	1 µL
H_2O dest.	31.5 µL
Total volume	49.5 µL
Start PCR program -> add 0.5 µL DNA polymerase after initial denaturation	

3.2.1.2 Site directed mutagenesis

This method is a modification of the standard PCR. It results in a mutation of the desired bases in the gene of interest. Mutations are introduced via oligonucleotide DNA primers only in circular plasmids. Usually, the mutation is positioned in the middle of the primer. The flanking regions on both sites of the mutation are chosen to be normally about 20 bases long, resulting in primer lengths of ca. 40 – 50 base pairs. PCR with such primers leads to a production of DNA plasmids containing the desired mutation. Each amplified (new) DNA molecule is not methylated, in contrast to the template DNA. This difference is used in the step after the PCR where the restriction endonuclease DpnI is added. This enzyme recognizes and digests methylated or hemi-methylated DNA. This results in an elimination of the template DNA, which does not contain the desired mutation.

In this work the gene of interest was within a plasmid. After introducing point mutations via the site directed mutagenesis PCR, the DNA was processed with DpnI. Subsequently, competent *E. coli* XL1 cells were transformed with the linear, mutated plasmid DNA. The bacterial cells ligate the linear DNA, which results in a circular plasmid construct.

Reaction buffer and dNTPs mix were the same like described for the standard PCR. The reaction volume was 30 µL, Phusion DNA polymerase (Thermo Scientific) was used in a “Hot-start” reaction. Typical reaction mixture for site directed mutagenesis PCR is shown in Table 6.

Table 6: Reaction mix for a site directed mutagenesis PCR.

High fidelity buffer 5x (Thermo Scientific)	6 µL
Primer 5’ – 3’ forward (10 pmol/µL)	1 µL
Primer 3’ – 5’ reverse (10 pmol/µL)	1 µL
dNTPs mix (10 mM)	0.6 µL
Template DNA (100 ng/µL)	0.6 µL
DMSO	0.9 µL
H_2O dest.	20.9 µL
Total volume	30 µL
Start PCR program -> add 0.3 µL DNA polymerase after initial denaturation	

Table 7 presents the PCR program usually used for this method. In some cases the hybridization temperature was adjusted depending on the primer properties.

Table 7: Typical programm for site directed mutagenesis PCR.

Step Nr.	Duration (*105*)	T [°C]	
1	60	95	
2	60	95	
3	60	55	x 35
4	240	72	
5	600	72	

3.2.1.3 Restriction digest of DNA

Digestion of DNA was performed with restriction endonucleases. These enzymes recognize specific nucleotide sequences and cut the DNA molecule. Typical protocol for restriction digestion in this work is shown in Table 8. In this work the restriction endonucleases *ClaI* and *SpeI* (NEB) were used. The reaction was performed in NEB buffer 4 for 1 hour at 37 °C.

Table 8: Standard protocol for DNA restriction digestion in this work.

DNA (15 µg)	x µL
5 µL NEB buffer	1 µL
ClaI (15 U)	3 µL
SpeI (15 U)	1.5 µL
BSA 100x	0.5 µL
H_2O dest.	Add to 50 µL
Total volume	50 µL
-> 1 h incubation at 37 °C	

3.2.1.4 Dephosphorylation of DNA

This method was applied to facilitate insertion of linear DNA-fragments into digested plasmids. During DNA ligation cutted plasmids could religate without insertion of the desired gene. To prevent this, the free phosphate group of the linearized vector at the 5'-end is removed by addition of the enzyme Alkaline Phosphatase. In a cloning procedure, the DNA fragment containing the gene of interest provides the required 5'-phosphate group. In this work the Fast Alkaline Phosphatase (Thermo Scientific) was used for dephosphorylation. The usually used protocol for this reaction is shown in Table 9.

Table 9: Protocol for DNA dephosphorylation.

50 µg digested plasmid DNA in appropriate NEB buffer	50 µL
Fast AP (Thermo Scientific)	2 µL
Total volume	52 µL
-> 1 h incubation at 37 °C -> inactivation for 10 min. at 65 °C	

After completion of the reaction, the enzyme was inactivated by heating to 65 °C for 10 min.

3.2.1.5 DNA ligation

Digested DNA fragments with compatible ends can be fused to one (circular) piece in a reaction called ligation. This process is catalyzed by a ligase. This enzyme concatenates two DNA chains by the formation of a phosphodiester bond between the 5'-end of one DNA fragment (insert) and the 3'-end of another DNA molecule (plasmid) in an ATP dependent fashion.

In this work the T4 DNA Ligase (Thermo Scientific) was used. The reaction mixture was prepared according to the protocol of the manufacturer. Plasmid and gene inserts were mixed in different ratios in order to find the optimal reaction conditions. After reaction completion, different amounts of the ligation reaction were used for transformation of *E. coli*. Table 10 shows the general protocol applied for this reaction.

Table 10: Standard protocol for DNA ligation.

Gene insert (45 ng)	x µL
Digested plasmid (300 ng)	x µL
T4-buffer (Thermo scientific)	2 µL
T4-Ligase (Thermo scientific)	1 µL
H_2O dest.	Add to 20 µL
Total volume	20 µL
-> 2 h incubation at 22 °C -> apply to transformation	

3.2.1.6 Transformation of E. coli

Competent *E. coli* cells are capable of taking up DNA. In general, there are two methods for transformation – heat shock at 42 °C and electroporation. In this work the heat shock method in combination with competent cells, prepared via the $RbCl_2$ – method, was used (*106*).

For the preparation a single colony of *E. coli* XL1 blue cells (Agilent Technologies) from an agar plate was inoculated into a 250 mL flask with 20 mL SOC medium and 12.5 µg/mL tetracycline. This pre-culture was grown over night in a horizontal shaker at 200 rpm and 37 °C. On the next day, 2.5 mL of the pre culture was diluted in 250 mL 2xYT medium in 2 L flask. The cells were further cultivated in a shaker at 200 rpm and 37 °C until an OD_{600} of approx. 0.5 was reached. The cells were separated from the medium by centrifugation in ice-cooled centrifugation bottles for 10 minutes at 4 °C and 4400x g (Avanti® J-26XP centrifuge, JA-10 rotor). Working on ice, the supernatant was then removed. The cells were resuspended in 83 mL buffer RF1 and afterwards incubated for 1 hour on ice. Bacteria were pelleted by centrifugation at 4400x g (Avanti® J-26XP centrifuge, JA-10 rotor) and 4 °C for 10 minutes. Working on ice, the supernatant was removed. The cell pellet was gently resuspended in 20 mL buffer RF2. After this step, the cells were incubated on ice for 15 minutes. Then, the cell suspension was dispensed in 100 µL aliquots in pre-cooled micro-centrifuge tubes (-80 °C), flash frozen in liquid nitrogen and stored at -80 °C.

During transformation the desired DNA (plasmids usually 1-10 ng, ligation mixtures 100 ng) was added to freshly thawed competent cells (100 µL). The reaction mixture was incubated for 30 min on ice and subjected to heat shock at 42 °C for 1 min. The cells were then incubated for 2 min on ice. Afterwards, 1 mL of 37 °C LB medium was added and the cells were incubated for 1 hour at 37 °C and 600 r.p.m. in a heat block. Afterwards, the supernatant was separated by centrifugation at room temperature and 6000x g (Eppendorf microcentrifuge 5415D). The cells were then resuspended in 100 µL LB medium and spread on a selective LB-Agar plates.

3.2.1.7 Transformation of S. cereviae

Competent yeast cells were transformed with DNA by the lithium acetate (LiAc) method in combination with heat shock at 42 °C (*107*). An environment, enriched with lithium, enhances the ability of *S. cerevisiae* to uptake DNA efficiently (*108*). The transformation efficiency is even more enhanced by a heat shock at 42 °C, when PEG is added and with yeast cells in their mid-log growth phase.

In this work, *S. cerevisiae* transformation was performed as described above. For the preparation of competent cells a single colony from a YPD agar plate was inoculated in 5 ml YPD pre-culture and grown at 30 °C in horizontal shaker at 200 r.p.m. over night. On the next morning the main culture of 50 mL YPD medium was inoculated from the pre culture to an OD_{600} of 0.2. The cells were incubated at 30 °C and 200 r.p.m. until an OD_{600} of 0.8 – 1 was reached. Cells were harvested by centrifugation at 4 °C and 2800x g (Eppendorf microcentrifuge 5417R) and subsequently resuspended in 20 mL distilled water. Afterwards, they were pelleted again and the supernatant was removed. *S. cerevisiae* was then resuspended in 1 mL LiAc containing LATE buffer, transferred to Eppendorf tube and centrifuged for 5 min at 2800x g (Eppendorf microcentrifuge 5417R) and 4°C. After removal of the supernatant, the cells were resuspended in LATE buffer at a ratio of 5 µL/1 OD-unit. These cells were usually directly used for DNA transformation. Storage of the cells was performed at 4 °C.

Typically, 1-5 µg DNA was used for the transformation of 50 µL yeast cells with a concentration of 0.2 OD-units/µL. Subsequently, 300 µL PEG containing PLATE-buffer was added. The reaction mixture was incubated for 20 min at 30 °C, followed by heat shock at 42 °C for 20 min. The reaction solution was mixed during the heat shock by inverting the reaction vessel every 5 min. Cells were harvested by a centrifugation step for 10 min at 2800x g (Eppendorf microcentrifuge 5415D) and room temperature. Subsequently, the supernatant was removed and the transformed cells were resuspended in the according drop out medium. The yeast cells were spread on a selective agar plate, which were incubated for 2 – 6 days at 30 °C.

3.2.1.8 Agarose gel electrophoresis

When loaded onto an agarose gel in an electric field, DNA migrates toward the positive pole. Due to the sieve properties of agarose gels, larger DNA fragments migrate slower compared to smaller fragments during electrophoresis. The percentage of agarose in the gel depends on the size of the DNA fragment – the larger the fragment the lower the agarose concentration and vice versa. Analysis of the gel results requires visualization of the DNA. Different agents could be applied for this purpose – ethidium bromide, SYBR Green (I and II, Molecular Probes), OilGreen or PicoGreen (Molecular Probes) or methylene blue. The most common method is staining with ethidium bromide. This chemical agent intercalates between the bases and can be visualized with UV light. For the estimation of the fragment size, a DNA ladder with fragments of known molecular weight is applied on the same gel next to the samples. Comparison between the mobility of the samples and the ladder enables to determine the size of the DNA fragments of the samples.

The agarose percentage of the gels in this work was chosen according to the analyzed DNA. Visualization was performed via ethidium bromide. For size determination 1 kb DNA ladder (Thermo Fisher Scientific) was used.

3.2.1.9 Extraction of DNA

DNA extraction was performed in two different ways – via silica membrane columns or via anion exchange columns.

3.2.1.9.1 Isolation via silica membrane columns

This method is based on fact that in acidic milieu DNA adsorbs on silica in the presence of high concentrated chaotropic salt (*109*). Bound nucleic acids can be washed with buffer containing salt and ethanol and then eluted with water or TE-buffer.

This method was applied for the purification of DNA (plasmids or DNA fragments) out of agarose gels or out of cultivated cells (plasmids out of *E. coli* or *S. cerevisiae*) in this work. In both cases, commercially available kits for DNA purification were used (Qiaquick Gel Extraction Kit and Qiaprep Miniprep from Qiagen). The only difference between both procedures was the step before loading onto the column. When isolating plasmids out of cells, the cells were subjected to alkaline lysis and the resulting solution was applied onto the column. The first step when extracting DNA out of agarose gels was the excision of the ethidium bromide stained fragment out of the gel, followed by its dissolution. In both cases, the reagents supplied by the manufacturer were used. The DNA extraction was performed according to the protocol of the manufacturer (Qiagen).

3.2.1.9.2 Isolation via anion exchange columns

This method makes use of the nucleic acid property that at a pH above 2 the phosphate groups of DNA and RNA are negatively charged. When applied to a (column with) positive charged matrix it binds to it. DNA, RNA and proteins show different binding properties, which also depend on the pH and ionic strength. The use of buffers with different pH and ionic strength results in the elution of DNA separately from RNA and proteins.

In this work NucleoBond Xtra Midi kit (Macherey Nagel) was used for this purpose. Cells, containing the desired plasmid DNA, were ruptured by alkaline lysis (*110*). The resulting suspension was mixed with the according buffer and

loaded onto the anion exchange column. Only buffers supplied with the kit were used. The manufacturers protocol was followed.

3.2.1.10 Measurement of the DNA concentration

The concentration of the purified DNA was determined via absorption spectroscopy. Nucleic acids absorb UV light and show an absorption maximum at 260 nm. With a multiplication factor of 50, specific for double stranded DNA, and with the dilution factor, the DNA concentration can be calculated. Pure DNA shows a ratio of the UV absorption at 260 nm and 280 nm (A_{260} / A_{280}) of 1.8 – 2.0. In this work concentration of DNA was measured with a Nanodrop UV/Vis spectrophotometer (Peqlab).

3.2.1.11 Cultivation of microorganisms

3.2.1.11.1 Cultivation of *E. coli* for molecular biology

E. coli cells were cultivated at 37 °C in LB medium or on LB-Agar plates, both supplemented with the appropriate antibiotic to keep selection pressure. In this work only ampicillin was used as an antibiotic due to the fact that each plasmid used had β-lactamase as a selection marker. When cultivated in medium, the cell culture was typically inoculated from a single colony on an agar plate. These *E. coli* cultures were incubated in baffled flasks in a horizontal shaker at 37 °C and 200 r.p.m. for a time period up to 12-16 hours (over night). The culture volume was adjusted to be maximal 40 % of the total flask volume to allow sufficient aeration. The cells were harvested by centrifugation or used further as liquid culture.

When bacteria were streaked out on an LB-Agar plate, the cultivation was performed for 12-16 hours at 37 °C.

For long term storage, liquid cultures were supplemented with 20 % glycerol (final concentration), flash frozen with liquid nitrogen and stored at -80 °C.

3.2.1.11.2 Cultivation of *S. cerevisiae* for molecular biology

S. cerevisiae cells were cultivated either on agar plates or in liquid cultures with the appropriate medium. The growth medium was YPD or selective

medium of defined composition, lacking the desired amino acids for selection pressure, according to the plasmid encoded selection markers.
The cultivation on agar plates was performed after streaking out cells out of cryostock cultures or after DNA transformation (see 3.2.1.7). This cultivation was performed for 2-6 days at 30 °C. The obtained cells could be stored up to two weeks at 4 °C.
Liquid cultures of *S. cerevisiae* were inoculated from single cell colonies on agar plates or from other liquid cultures. The liquid cultures were cultivated in shaking baffled flasks at 20, 25 or 30 °C (depending on the experiment) in horizontal shaker at 200 r.p.m. The volume of the liquid was kept at maximal 40 % of the total flask volume.
Long-term storage of yeast cells was performed, as described for *E. coli* (see section 3.2.1.11.1).

3.2.1.11.3 Determination of the generation time of yeast cells

The generation time **g** of *S. cerevisiae* was determined to compare exactly the growth behavior of yeast cells under different conditions when the starting optical density differed. The following equations (Equation 1 and Equation 2) (*111*) were used for this purpose:

$$g = \frac{t}{n} \qquad \textbf{Equation 1}$$

$$n = 3.3\ (\log N - \log N_0) \qquad \textbf{Equation 2}$$

g	Generation time [h]
t	Duration of exponential growth [h]
n	Number of generations occurred during t
N	Optical density reading at a time point within a defined time period

N_0 Optical density reading at the start of a defined time period

The generation time **g** of the yeast cells was calculated from the exponential phase of the growth curve. Therefore, N_0 corresponded to the OD at the beginning of the exponential growth phase, whereas N corresponded to an OD at a defined time point within the exponential growth phase.

3.2.1.12 Preparation of yeast whole cell lysates

This method was used to analyze gene expression and protein content within *S. cerevisiae*. Cells were disrupted by alkaline lysis and then their content was analyzed via SDS-PAGE and subsequent Western blot.

Yeast cells of a certain OD were harvested via centrifugation at 4 °C at 20000x g. After a washing step with cold water, cells were resuspended in 1 mL ice-cold water. 150 µL ice-cold YEX buffer was mixed to the cells and this suspension was incubated for 10 min on ice. Subsequently, 150 µL of 50 % TCA (v/v) solution was added and the suspension was mixed by shaking. After 10 min incubation on ice, the mixture was centrifuged and the supernatant was removed. The pellet was air-dried and subsequently resuspended in 10 µL buffer, containing Tris-HCl with pH 8. Afterwards 40µL 1x reducing SDS-sample buffer per 1 OD-unit was added. The samples were then heated for 10 min at 95 °C (65 °C for membrane proteins) and analyzed via SDS-PAGE and Western blot.

3.2.2 Protein chemistry

3.2.2.1 Heterologous expression of HlyB NBD in S. cerevisiae and incorporation of DMNB-L-Ser

The gene of the NBD of the *E. coli* ABC transporter HlyB was heterologously expressed in the yeast *S. cerevisiae* either in shaking flasks or in a bioreactor. The gene was cloned in the plasmid p426GPD (provided by ATCC), resulting in the plasmid p426GPD-HlyB-NBD. YPH 500 yeast cells (Agilent Technologies) were transformed with this plasmid, which contains the constitutive promoter of the glyceraldehyde-3-phosphate dehydrogenase. The

plasmid for each mutant in this work, expressed on a preparative scale in yeast, was based on a modification of the p426GPD-HlyB-NBD plasmid.
The incorporation of the unnatural amino acid DMNB-L-Ser in HlyB NBD was performed in *S. cerevisiae* by using an orthogonal tRNA/aaRS-pair via the "Amber" stop codon strategy (*102*). Section 2.6 provides a detailed overview about this strategy. The unnatural amino acid was incorporated at different position of the protein by using the TAG stop codon, which was introduced via site directed mutagenesis (see 3.2.1.2). The plasmid, which encodes the aaRS/tRNA pair, was kindly provided by Prof. Peter G. Schultz, Scripps Institute, La Jolla, California (*102*). The photo caged amino acid DMNB-L-Ser was synthesized by APAC International.

3.2.2.1.1 Expression in shaking flasks

HlyB NBD expression in shaking flasks was performed in selective drop out medium (DO medium). For the expression of wild type HlyB NBD, DO medium lacking uracil was used, because the p426GPD-HlyB-NBD plasmid encodes a gene, which complemented the uracil auxotrophy of the used YPH 500 strain. This was used as a selection marker. Protein labeling with DMNB-L-Ser was performed in DO medium lacking uracil and tryptophan. For the incorporation of DMNB-L-Ser the aaRS/tRNA-pair was essential. This pair was encoded on the additional pESCTrpLeuBHT252A plasmid. This additional plasmid also coded for a gene, which complemented the tryptophane auxotrophy of the used YPH 500 strain. This was also used as a selectin marker.
Pre-cultures were inoculated with single colonies of yeast cells in 100 mL of an appropriate DO medium, supplemented with 2 % glucose. They were incubated at 25 °C in a horizontal shaker at 200 r.p.m. for 14 – 16 hours. Main cultures were inoculated from the pre-cultures to an OD of 0.3 and grown for 12 h under the same conditions as the pre-cultures. In the case of expression of DMNB-L-Ser-labeled HlyB NBD, 0.5 g of unnatural amino acid per liter of DO-Ura/-Trp medium was added immediately after the inoculation of the main culture. After 12 hours, the cells were harvested by centrifugation in a Sorvall Evolution RC centrifuge (SLC-6000 rotor) at 5000x g and 4 °C. Subsequently,

the cells were washed with LI buffer and directly disrupted for protein isolation or flash frozen in liquid nitrogen and stored at -80 °C.

3.2.2.1.2 Expression in a bioreactor

Fed-batch fermentation in a bioreactor was performed in YPD medium, supplemented with 2 % glucose and under continuous titration of glucose. Yeast cells (YPH 500, transformed with p426GPD-HlyB-NBD plasmid and pESCTrpLeuRSBH5T252A) were inoculated from a single colony in shaking flasks with DO-Ura medium (or DO-Ura/-Trp when labeling with DMNB-L-Ser). These pre-cultures were incubated for 14-18 hours in horizontal shaker at 25 °C and 200 r.p.m. Afterwards, a second pre-culture was inoculated by diluting the first pre-culture (dilution rate 1/10) in the according DO medium. The second pre-culture was incubated under the same conditions as the first one for 16-20 hours. Afterwards, the bioreactor containing 4 L YPD was inoculated with the second pre-culture such that the inoculum volume did not exceed 20 % of the total medium volume for fermentation. When an expression of DMNB-L-Ser-labeled HlyB NBD was performed, 0.5 g unnatural amino acid per liter total fermentation medium was added directly after the inoculation of the fermenter. Fermentation of yeast cells was performed for 11 hours at 25 °C with constant stirring (750 rev*min^{-1}) and air supply. After 8 hours of fermentation, glucose feed (2.62 g*L^{-1} medium *h^{-1}) was started and the sugar solution was constantly titrated to the medium for 3 hours. This was performed to increase the cell mass and the protein production rate during fermentation (*112*). After 11 hours of incubation in the bioreactor, the cells were harvested by centrifugation in a Sorvall Evolution RC centrifuge (SLC-6000 rotor) at 5000x g and 4 °C. Subsequently, the cells were washed with LI buffer, flash frozen in liquid nitrogen and stored at -80 °C.

3.2.2.2 Protein purification

The isolation of HlyB NBD (DMNB-L-Ser-labeled) was performed in two chromatography steps using the N-terminal 6xHis-Tag for IMAC (*113*), followed by a size exclusion chromatography (SEC), which separates proteins

according to their hydrodynamic radii (*114*). Protein purification was performed as described (*115*) with some modifications.

S. cerevisiae cells (5 mL alliquots), freshly harvested or thawed after storage at -80 °C, were resuspended in 30 mL LI buffer. The cells were lysed by three passages through a TS Series benchtop cell disruptor (Constant Systems) at 4 °C at a pressure of 2.7 kbar. Cell debris and membranes were separated from the soluble fraction by ultracentrifugation at 4 °C and 260 000x g in a Beckman Coulter L90k-Ultracentrifuge with a rotor type Ti 70. Afterwards, the pH of the supernatant was adjusted to pH 8 with 1 M potassium phosphate buffer (pH 8), which was followed by loading the soluble fraction onto a Zn^{2+}-loaded IDA HiTrap Chelating column (5 mL, GE Healthcare). Subsequently, the column was washed with 20 column volumes LI buffer. Bound HlyB NBD was eluted in a two-step imidazole gradient. In the first step, other column-bound proteins were removed by increasing the imidazole concentration to 30 mM. In the second step, the imidazole concentration was increased to 150 mM and HlyB NBD was eluted. The elution fractions containing the protein of interest were concentrated to a volume of a 500 µL and applied on the same day onto a Superdex 200 10/300 column. This column was pre-equilibrated with two column volumes of SEC buffer. The peak fractions with soluble HlyB NBD were collected and their CAPS concentration was adjusted to 100 mM by the addition of a buffer, containing 500 mM CAPS, 20 % glycerol and pH of 10.4. The protein purity was analyzed via SDS-PAGE. If necessary, the protein was concentrated by ultrafiltration employing an Amicon Ultra 10 kDa MW cut of centrifugal filter (Merck Millipore).

3.2.2.3 Determination of protein concentration

Protein concentration was measured by two methods – UV-Absorption at 280 nm and a colorimetric Bradford-assay.

The concentration of a protein in solution can be determined via its UV-absorption at 280 nm. At this wavelength UV-absorption is proportional to the number of aromatic residues in the polypeptide chain, yet tryptophan provides higher extinction coefficient than tyrosine and phenylalanine. Each polypeptide chain possesses its own molar extinction coefficient ε, which

depends on the number of aromatic residues. The protein concentration of a solution can be determined by measuring the absorption at 280 nm via the Lambert-Beer law, see Equation 3.

$$A = \varepsilon \cdot c \cdot \mathrm{d} \qquad \textbf{Equation 3}$$

A	Absorption at 280 nm
ε	Molar extinction coefficient [$M^{-1}*cm^{-1}$]
c	Protein concentration [Mol/L]
d	Path length (1 cm)

At known path length (1 cm), known extinction coefficient and measured absorption the protein molar concentration in Mol/L can be calculated. The protein concentration in mg/mL can be calculated using the molar mass of the protein. In this work ProtParam (www.expasy.org) was applied to calculate the theoretical molar mass and the extinction coefficient of HlyB NBD. The extinction coefficient of the wild type protein and the alanine mutants was calculated to be 17 420 $M^{-1}*cm^{-1}$, for the tyrosine mutants of HlyB NBD a value of 18 910 $M^{-1}*cm^{-1}$ was calculated. For DMNB-L-Ser an extinction coefficient of 2454 $M^{-1}*cm^{-1}$ at 280 nm was calculated from its UV/VIS-absorption (0.27, Figure 10), its concentration (0.11 mM) and a path length of 1 cm via the Lambert-Beer law. Via the method of Gill and von Hippel a value of 19874 $M^{-1}*cm^{-1}$ for the extinction coefficient of DMNB-L-Ser labeled HlyB NBD at 280 nm was calculated (*116*). The protein concentration was determined by measurement of the UV-Absorption at 280 nm with the Nanodrop UV/Vis spectrophotometer (Peqlab).

The concentration of the protein was also determined via the colorimetric Bradford assay. The dye Coomassie brilliant blue G-250 binds to a protein in an acidic buffer, which results in a shift of the absorption maximum of the dye from 465 nm to 595 nm (*117*). This shift is proportional to the protein concentration and can be utilized to calculate the protein content of a solution. In this work the kit from Thermo Scientific for Bradford concentration

measurements was applied. The recommended protocol of the manufacturer was followed.

3.2.2.4 SDS-Polyacrylamid gel electrophoresis

This method is performed under denaturating conditions and it was used to estimate protein purity. Proteins migrate in an electric field depending on their mass and net charge density. The proteins are mixed with the detergent sodium dodecyl sulfate (and heated), which destroys the non-covalent interactions within the native proteins and leads to a denaturation. The SDS anion binds to the main chain of the proteins, mask their net charge and convert them to anions. Because the negative charge density of these proteins is proportional to their mass, the proteins can be separated via SDS-PAGE based on their different molecular masses. Usually, polyacrylamide gels are composed of two parts – separation gel and stacking gel above it. Protein samples are loaded in the slots of the stacking gel. This gel has lower concentration of polyacrylamide (3-5 %) and prevents smaller proteins to run faster then bigger proteins. This induces protein stacking to a uniform front no matter how big is the mass difference between the proteins in the sample. As a consequence, when the protein front enters the separation gel (7-20 % polyacrylamide) each protein has the same starting point. In this work the Laemmli Tris-glycine gel system in combination with a BIO-RAD electrophoresis system was used (*118*). Usually, the stacking gel polyacrylamide concentration was 4.5 %, the separation gel was normally 12.5 %.

Usually, SDS-PAGE was performed for 90 min at 110 V. The protein visualization was performed by colloidal Coomassie staining solution (*104*). Routinely, the gel staining was performed for 2 h, the destaining over night.

3.2.2.5 Western blot

With this method a protein, immobilized on a membrane, can be detected via an antibody against an epitope of the protein. After separation via SDS-PAGE, proteins can be transferred to a membrane, which consists for example of nitrocellulose or PVDF. For this purpose in an electric field the

membrane is positioned on the positive pol and the negatively charged proteins migrate to the membrane. Afterwards, non-occupied binding sites on the membrane are blocked by membrane incubation with BSA. The membrane is incubated with an antibody against the protein of interest. The binding of the antibody to the protein can be detected, for example, via a chemiluminescence.

In this work Trans-Blot Semi Dry SD Transfer Cell (BIO-RAD) and PVDF- or nitrocellulose membrane (Pall Corporation) were utilized. The detection of HlyB NBD was performed with two antibodies. The primary antibody (isolated from rabbit) was diluted 1:5000 in TBST buffer, containing 5 % milk powder and 0.005% sodium azide. It was incubated for 1 h with the membrane, on which HlyB NBD was transferred. Subsequently, non-bound antibody was removed by washing with TBST buffer (3x 15 min). The secondary antibody (coupled to horseradish peroxidase (Sigma Aldrich)) was diluted 1:20000 in TBST buffer and incubated for 1 h with the HlyB NBD containing membrane. Non-bound antibody was removed via washing (3x 15 min) with TBST. The detection was performed via chemiluminescence by using Western lightning Ultra kit (Perkin Elmer). Recommended manufacturers protocols were applied.

3.2.2.6 ATPase activity

With this method the enzymatic activity of HlyB NBD was investigated. This protein hydrolyses ATP to ADP and inorganic phosphate. Therefore, a detection of free inorganic phosphate was performed and its quantity revealed the degree of enzymatic activity. The released inorganic phosphate was determined with a colorimetric assay. It is based on the formation of colored complex between phosphomolybdate and malachite green in acidic environment, which results in a green color of the solution in the presence of inorganic phosphate (*119*).

ATPase activity was measured at 25 °C in a buffer containing 100 mM HEPES, 20 % glycerol, 10 mM $MgCl_2$ and different ATP concentrations at pH of 7.0. The concentration of HlyB NBD and the incubation time varied depending on the experiment. The reaction was started with $MgCl_2$ or ATP. It

was stopped by adding 25 µL of the reaction mix to 175 µL STOP-solution containing 18 mM sulphuric acid, which leads to protein denaturation. Subsequently, 50 µL freshly prepared malachite green coloring solution was added to the inactivated assay mixture, followed by 10-15 min incubation. The quantification of the phosphate was performed by measuring the Absorbance of the solution at 620 nm in a FLUOstar Optima spectrometer (BMG Labtech) using Na_2HPO_4 solutions with different concentrations (4 – 24 µM) as a standard. Background ATPase activity was determined and subtracted from the obtained values by measuring the samples without protein or in the presence of EDTA. EDTA complexes the Mg^{2+} ions, which are essential for the ATPase activity.

The obtained results were analyzed with Michaelis-Menten equation (see Equation 4).

$$V = V_{max} \frac{(S)}{(S) + K_M}$$ **Equation 4**

V	Reaction velocity
V_{max}	Maximal velocity when each enzyme molecule is occupied with substrate
(S)	Substrate concentration
K_M	Michaelis-Menten constant

This equation describes enzymatic reactions of enzymes with one or more ligand-binding sites, which act independently of each other. Such enzymes yield hyperbolic velocity curves (*120*). V_{max} represents the maximal velocity of substrate conversion when each binding site is occupied with a ligand. For this purpose the substrate concentration ([S], ATP) has to be present in much higher concentration than the enzyme. K_M denotes the substrate concentration, at which the observed velocity is half the V_{max}. K_M is an intrinsic property of an enzyme, it describes the interaction between the protein and a particular substrate and is independent of both.

Obtained ATPase data was also analyzed with the Hill equation to examine whether heterologously expressed HlyB NBD hydolyses ATP in a cooperative way (see Equation 5).

$$V = V_{max} \frac{(S)^h}{{K_{0.5}}^h + (S)^h}$$ **Equation 5**

V	Reaction velocity
V_{max}	Maximal velocity when each enzyme molecule is occupied with substrate
(S)	Substrate concentration
$K_{0.5}$	Substrate concentration, at which reached conversion velocity is half the V_{max}
h	Hill coefficient, reflects the degree of cooperativity

The Hill equation describes allosteric enzymes. These proteins have more than one ligand binding sites, which act dependently on each other. When such enzymes bind substrate, this leads to structural changes, which result in modified affinities for the vacant binding sites (*120*). Usually, these catalysts yield sigmoidal curves when their activity is analyzed as a function of the substrate concentration. The binding of the first substrate molecule influences the binding of the second substrate molecule. The binding of the second substrate molecule influences the binding of the third substrate molecule and so on. Such an alteration of the binding properties is called cooperative binding. The cooperativity of the binding could be positive or negative. Positive cooperativity means that the binding of each ligand increases the probability for binding of a further ligand. In the case of negative cooperativity the opposite effect is observed. h is the Hill coefficient and describes the degree of cooperativity. If h is greater than one there is positive cooperativity, if h is less than one there is negative cooperativity. Hill coefficient of one means no cooperativity and the enzyme properties are described by the Michaelis-Menten kinetic.

3.2.2.7 TNP-ATP binding

This method enables the investigation of the binding properties of proteins towards ATP by using fluorescence as a reporter (*121*). As fluorescence reporter TNP-ATP was used (Figure 9).

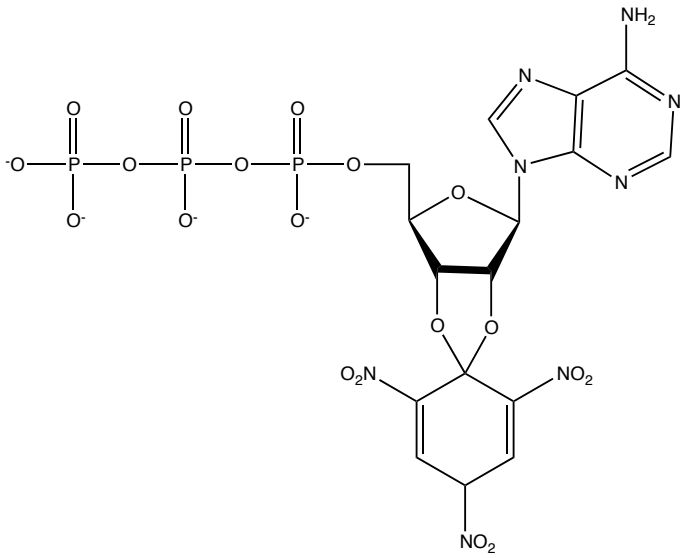

Figure 9: Chemical structure of TNP-ATP.

In fact, the trinitrophenyl-group shows higher fluorescence in hydrophobic environment than in hydrophilic environment (*122*). This means that binding of this nucleotide analog within a protein binding pocket can lead to an increase of the TNP-ATP fluorescence.

Binding experiments and data calculation were performed as described (*8*) in a Fluorolog-3 fluorescence-spectrometer (Horiba). In brief, TNP-ATP was titrated stepwise to 4 µM HlyB-NBD (wild type and mutants) in a 1 mL cuvette at 20 °C. During the titration, TNP-ATP up to 10 µM was added to the reaction mixture. The volume of the titrated TNP-ATP did not exceed 5 % of the total volume at the start of the reaction without nucleotide. The experiments were performed under continuous stirring in a buffer containing 100 mM HEPES, 20 % glycerol, pH 7.0. Fluorescence excitation of TNP-ATP was performed at 409 nm (excitation slit width usually 2 nm), fluorescence emission was recorded in the spectral range 450-600 nm (emission slit width usually 4 nm) with an increment of 1 nm and 1 sec integration time. Each data set was

measured for protein solution and for buffer solution. For a protein solution the titration should result in a curve with higher fluorescence compared to the buffer-only solution. This would indicate binding of TNP-ATP in the protein binding pocket.

Data were calculated according to (*123*). In these binding experiments the ligand TNP-ATP with a concentration L_0 was titrated to the protein HlyB NBD with a concentration P_0. Assuming equilibrium binding, HlyB NBD is present as free molecule (P_{free}) and as a protein/ligand complex (PL_N), see Equation 6. TNP-ATP is present as a free (L_{free}) and as a bound ligand ($N*PL_N$), see Equation 7. N denotes the number of ligand binding sites. The data calculation was performed assuming the existence of N independent ligand binding sites.

$$P_0 = \mathrm{P}_{free} + PL_N \qquad \textbf{Equation 6}$$

$$L_0 = \mathrm{L}_{free} + N \cdot PL_N \qquad \textbf{Equation 7}$$

The fluorescence of TNP-ATP was used as a reporter for nucleotide binding. Based on the equations above, the measured fluorescence can be described as the sum of the fluorescence of free ($F_{L,free}$) and bound ligand (F_{PLN}), as shown Equation 8.

$$F_{total} = \mathrm{F}_{L_{free}} + F_{PL_N} \qquad \textbf{Equation 8}$$

At low ligand concentrations the increase of the fluorescence is proportional to the TNP-ATP concentration, however at higher concentrations (above 6 µM) due to inner filter effects this is not the case (*123*). To correct these effects, the correction factors Q_1 and Q_2 were calculated from a polynomial function (see Equation 9). This correction was performed only for the control titration of TNP-ATP to a buffer solution.

$$\mathrm{F}_{L_{free}} = L_{free} \cdot Q_1 + L_{free}^2 \cdot Q_2 \qquad \textbf{Equation 9}$$

The TNP-ATP binding in the protein binding pocket can result in an increase of the TNP-ATP fluorescence, compared to its fluorescence as a free ligand in solution. This enhancement of the fluorescence (F_{PLN}) can be described by the enhancement factor γ, see Equation 10.

$$F_{PL_N} = N \cdot PL_N \cdot Q_1 \cdot \gamma \qquad \textbf{Equation 10}$$

The combination of Equation 8, Equation 9 and Equation 10 results in the description of the total fluorescence (F_{total}), see Equation 11.

$$F_{total} = L_0 \cdot Q_1 + L_0^2 \cdot Q_2 + N \cdot PL_N \cdot (Q_1 \cdot (\gamma - 1) - 2 \cdot L_0 \cdot Q_2) \qquad \textbf{Equation 11}$$

The unknown concentration of the protein-ligand complex (PL_N) in Equation 11 can be described using the law of mass action including the dissociation constant ($K_{D,PLN}$), see Equation 12. This is based on the assumption of independent HlyB NBD binding sites, which show the same affinity for TNP-ATP. The rearrangement of Equation 12 results in Equation 13, which describes the concentration of the protein-ligand complex as a function of $K_{D,PLN}$, L_0 and P_0.

$$K_{D_{PLN}} = \frac{L_{free} \cdot P_{free}}{PL_N} = \frac{(L_0 - N \cdot PL_N) \cdot (P_0 - PL_N)}{PL_N} \qquad \textbf{Equation 12}$$

$$N \cdot PL_N = \frac{1}{2}\left[\left(K_{D_{PLN}} + L_0 + N \cdot P_0\right) - \sqrt{(K_{D_{PLN}} + L_0 + N \cdot P_0)^2 - 4 \cdot N \cdot P_0 \cdot L_0}\right]$$

Equation 13

For reasons of simplicity, the term ($K_{D,PLN}$+L_0+NP_0) can be abbreviated as A. The combination of Equation 11 and Equation 13 results in Equation 14, which describes the measured fluorescence F_{total} for the titration of TNP-ATP to HlyB NBD.

$$F_{total} = L_0 \cdot Q_1 + L_0^2 \cdot Q_2 + \left[(0.5 \cdot Q_1 \cdot (\gamma - 1) - L_0 \cdot Q_2)\left[A - \sqrt{A^2 - 4 \cdot N \cdot P_0 \cdot L_0}\right]\right]$$

Equation 14

Since the term ($0.5*Q_1*(\gamma-1)-L_0*Q_2$) accounts for the maximal fluorescence and for reasons of simplicity, it can be written as F_{max}, which results in Equation 15.

$$F_{total} = L_0 \cdot Q_1 + L_0^2 \cdot Q_2 + \left[(F_{max}) \left[A - \sqrt{A^2 - 4 \cdot N \cdot P_0 \cdot L_0}\right]\right] \quad \textbf{Equation 15}$$

Equation 15 was applied to analyze the fluorescence data from the TNP-ATP titration to HlyB NBD. The constants Q_1 and Q_2 can be calculated from the fluorescence data from the control titration of TNP-ATP to the buffer-only solution. F_{max} can be determined via a titration of HlyB NBD to a fixed concentration of TNP-ATP. The ratio between the nucleotide fluorescence at its maximum (each nucleotide molecule in a complex with the protein, PL_N) and at its minimum (only free nucleotide, L_{free}) reveals the enhancement factor γ. With the measured F_{total}, $K_{D,PLN}$ can be fitted according to Equation 15.

3.2.2.8 Analytical size exclusion chromatography

This method allows the chromatographic separation of proteins, based on their different hydrodynamic radii. It was applied to investigate if purified HlyB NBD (wild type and mutants) are able to form a dimer upon addition of ATP. If nucleotide binding induces protein dimerization, the difference in the hydrodynamic radius between monomer and dimer can be detected via analytical size exclusion chromatography, which enables the separation of monomeric from dimeric protein.

In this work analytical SEC was performed at 4 °C in a buffer containing 50 mM malonate, 100 mM sodium acetate, 5% glycerol and pH 5.8, as described (*5*). HlyB NBD (wild type and the mutants) were diluted to a final concentration of 1.5 mg/mL (54 µM) in the buffer for analytical SEC and incubated for 1 h at 4 °C in the presence or absence of ATP. ATP was added to a final concentration of 1 mM. 50 µL samples were subjected to SEC analysis (*5*). When ATP was present in the sample solution the nucleotide was also added to the same final concentration to the buffer for SEC. No ATP was added to

the buffer for chromatography when the nucleotide was absent from the sample solution. The dimerization behavior was analyzed on a ÄKTA Micro FPLC system (GE) at a flowrate of 30 µL/min using Superdex 75 3.2/30, Superdex 200 3.2/30 or Superose 12 3.2/30 columns (each one from GE Healthcare). Prior to SEC the columns were equilibrated with 1.5 column volumes chromatography buffer. The protein detection was performed via UV absorption at 290 nm.

3.2.2.9 ESI-TOF mass spectrometry

This technique revealed if HlyB NBD was labeled with DMNB-L-Ser and if the DMNB-caging group was removed after irradiation with light (wavelength 355 nm). With this method it is possible to differentiate between ions based on their mass/charge ratio (*124*).

One of the possibilities to obtain ions is electrospray ionization (ESI) (*125*). The analyte solution is injected to a setup consisting of capillary and counter electrode. Between the capillary and the electrode is a potential difference. Due to the migration of the ions to the opposite pol, the liquid is “pulled”, which results in formation of the so-called “Taylor cone” (*126*). Because of the pulling ions containing drops dissociate from this cone to form a so-called “Nanospray” (*127*). During this process the droplets get smaller and smaller, which leads to a higher concentration of charges within a droplet and the electrostatic repulsion forces a “Coulomb explosion” (*128*). The result of this explosion are single ions, however formation of ions with more than one charges also occurs. Usually weak acids improve generation of positive ions (*125*).

Ion analysis was performed by double-quadrupole time of flight detector (QQTOF). Depending on the mass/charge ratio ions accelerate differently and have different flying speed. This leads to a typical distribution pattern of the detected signals. From this pattern the average mass of the analyte could be calculated back.

In this work a hybrid mass spectrometer QSTAR XL from Applied Biosystems was used. Before injection protein was first desalted using C_{18} tips (Proxeon, Thermo Fisher Scientific) and then the protein solvent was exchanged to 60 % methanol, containing 5 % formic acid. Obtained spectra were

deconvoluted via Analyst QS 1.1 software (Applied Biosystem). The measurement of the samples and the deconvolution of the obtained spectra were performed by Dr. Sabine Metzger from the BMFZ at the Heinrich Heine University Düsseldorf.

3.2.2.10 Properties of DMNB-L-Ser

In Figure 10 the absorption spectrum of DMNB-L-Ser is shown. It was measured at room temperature in a 100 µL ultra-micro cuvette (105.250-QS, Hellma analytics) with a path length of 1 cm. The measurement was performed on a Cary 50 Scan UV-Visible Spectrometer (Varian). The integration time was 0.1 s and the increment was 0.5 nm. The absorption maximum was observed at 350 nm.

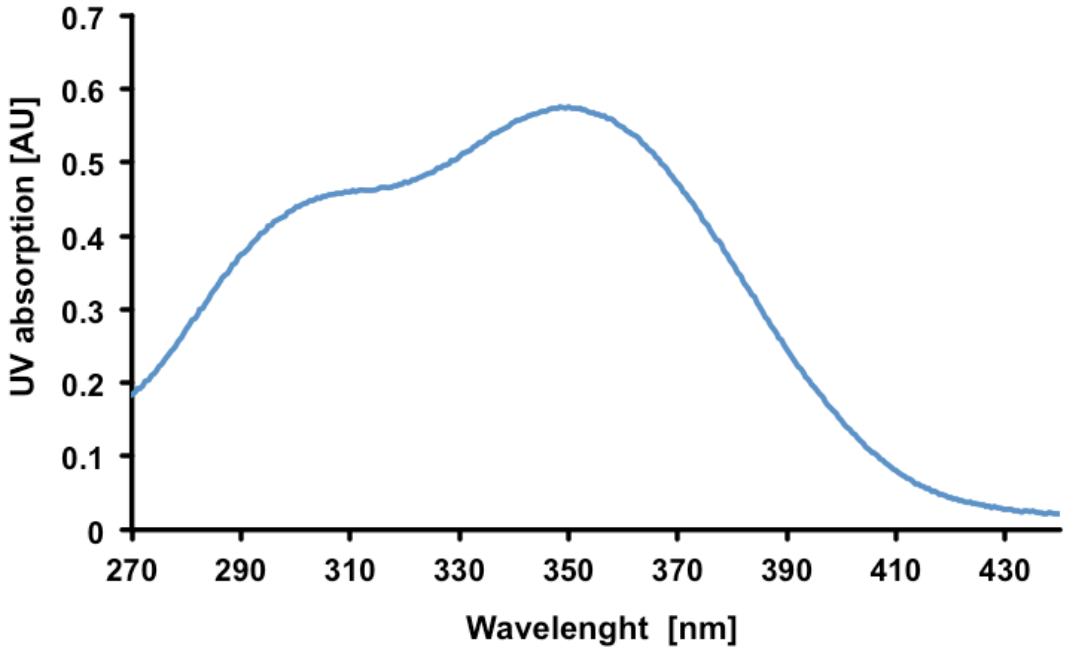

Figure 10: UV/VIS spectrum of 0.11 mM DMNB-L-Ser at room temperature in buffer containing 100 mM CAPS, 20 % glycerol, 10 mM DTT and pH 10.4.

3.2.2.11 Decaging of the DMNB-L-Ser labeled HlyB NBD

Based on the UV/VIS-absorption spectrum (Figure 10), the wavelength (355 nm) for the light irradiation of the DMNB-L-Ser labeled HlyB NBD was chosen. The decaging of the labeled protein was performed with a SplitLight 600 Flash lamp-pumped Nd:YAG Laser (InnoLas), which produced pulse-light

of a frequency of 10 Hz and a pulse-width of 7 ns. For this purpose, 355 nm light was applied. Usually, the pulse-energy amounted to 12 mJ. The irradiation was performed at room temperature for 1 sec up to 33 min, depending on the concentration of the samples. The samples were exposed to light in a 100 µL ultra-micro fluorescent cuvette (105.250-QS, Hellma analytics) with a path length 10 mm. During the experiment the samples were not mixed.

4 Results

4.1 Cloning of HlyB NBD into the p426-set of expression plasmids

The tRNA/aaRS pair for DMNB-L-Ser incorporation was derived from *E. coli*. In order to achieve the best possible DMNB-L-Ser incorporation fidelity, this pair was genetically engineered and showed the highest incorporation fidelity in *S. cerevisiae* (*102*). Therefore, the HlyB NBD gene was cloned in yeast plasmids and was subseguently expressed heterologously in *S. cerevisiae* (chapter 4.2.1.1).

The gene for HlyB NBD was inserted into a set of yeast vectors with different promoters (*129*). These promoters were derived from different genes encoding: GPD (glyceraldehyde-3-phosphate dehydrogenase, strong/constitutive active), TEF (translation elongation factor 1α, strong/constitutive active), CYC1 (cytochrome-c oxidase, weak/constitutive active), ADH (alcohol dehydrogenase, weak/constitutive active), MET25 (O-acetyl homoserine sulphydrylase, repressible) and GAL1 (galactokinase, inducible) (*129, 130*). The plasmids had the same multiple cloning sites (MCS), as shown in appendix (Figure 69), the same genetic markers (ampR, URA3), terminator (CYC1) and origin of replication (2µ). The vectors were purchased by ATCC and named as followed: p426GPD, p426ADH, p426TEF, p426CYC1, p426MET25 and p426GAL1 (*131*), see also Table 11.

The cloning was accomplished by restriction digestion and ligation. First, the HlyB NBD gene was amplified via PCR. Subsequent to the PCR the amplified gene and the plasmids were digested with the same restriction enzymes (*ClaI* and *SpeI*). Subsequently, the digested gene and the plasmids were fused via ligation, followed by the transformation of the ligated product in *E. coli*. The obtained plasmid constructs were verified by sequencing. For each plasmid construct the same procedure was used (Figure 11). Therefore only the production of the GPD-NBD-plasmid was shown as an example.

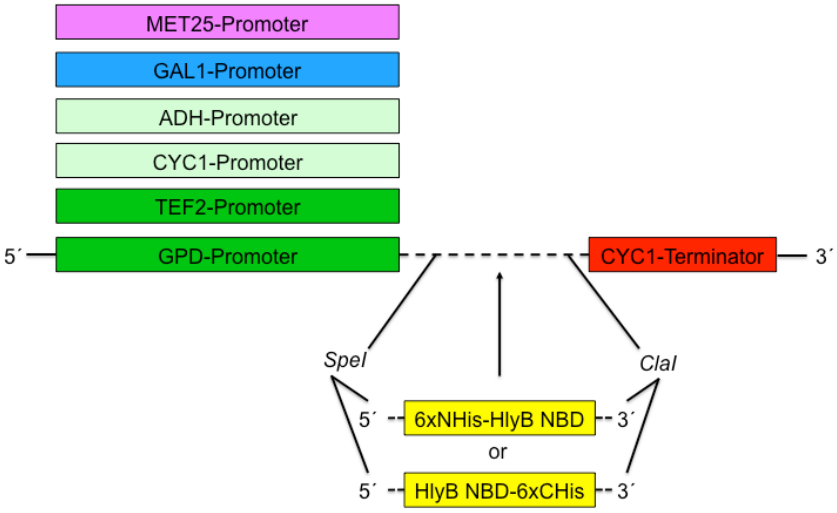

Figure 11: Cloning strategy. The HlyB NBD gene is presented in yellow. The relative digestion positions of the restriction enzymes, *SpeI* and *ClaI*, are depicted as solid lines. The relative DNA sites to be digested are shown as dashed lines. The used promoters are colored differently on the left site. The terminator region on the right site is colored red. The DNA, coding for the His-tag (6 histidines), was positioned relative to the NBD gene on the 5´-site (6xNHis) or on the 3´-site (6xCHis).

The gene for HlyB NBD was amplified out of the plasmid construct pESC-HIS-HlyB-NBD-$NHis_6$ (*132*). The primer pairs 5for_B-NBD_NHis and 3rev_B-NBD_NHis or 5for_B-NBD_CHis and 3rev_B-NBD_CHis were used for this purpose. Via the cloning strategy the His-tag was positioned at the N- or C-terminus. The restriction sites for the restriction enzymes *ClaI* and *SpeI* were also introduced via primers on the flanking regions of the PCR product. After a sodium acetate/ethanol precipitation of the amplified gene, it was digested simultaneously with *ClaI* and *SpeI*. The different plasmids were digested with these enzymes, dephosphorylated with alkaline phosphatase, applied onto an agarose gel and purified out of the gel. The PCR product and the according plasmid (both digested and purified) were mixed in ratios 1/1 or 3/1 and ligated via the T4-Ligase. With this cloning strategy different HlyB NBD containing plasmid constructs were generated, which differed in their promoters, as shown in Table 11. Afterwards, the ligation mixtures were transformed into *E. coli* XL1-blue® cells by heat shock (90 sec) and plated out on LB-Amp-selective medium. Grown bacterial colonies were inoculated in liquid LB-Amp medium for a subsequent plasmid isolation via mini prep. The cloning success was analyzed by restriction digestion of the isolated plasmids with *ClaI* and *SpeI*. Exemplarily the restriction digestion of the construct p426GPD-HlyB-NBD-$NHis_6$ is shown in Figure 12.

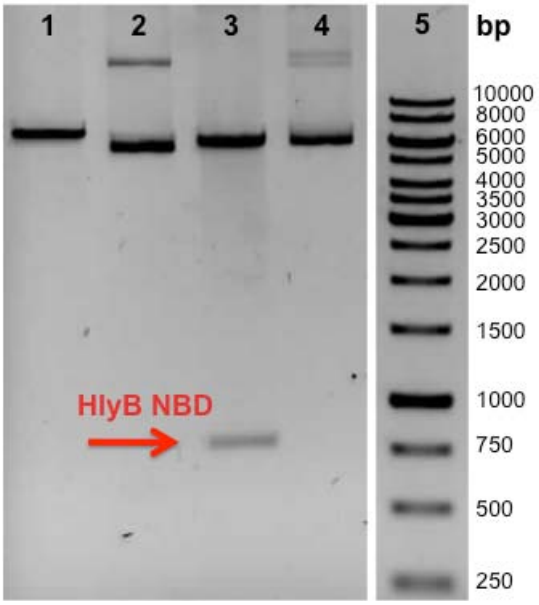

Figure 12: Restriction digestion of different preparations of the plasmid construct p426GPD-HlyB-NBD-NHis$_6$. Lane 1: clone 1, digested; lane 2: clone 1, not digested; lane 3: clone 2, digested; lane 4: clone 2, not digested; lane 5: GeneRuler^{TM} 1 kb DNA ladder. The red arrow indicates the NBD gene, which was digested out of the p426GPD-HlyB-NBD-NHis$_6$ plasmid.

The digestion of the plasmid from clone 2 (Figure 12, lane 3, indicated by a red arrow) revealed that a DNA fragment with the expected size of 760 base pairs has been inserted into the vector p426GPD. DNA sequencing confirmed the successful cloning of the HlyB NBD gene.

Table 11: Plasmid constructs with inserted HlyB NBD, achieved with the cloning procedure described above. The properties of the different promoter are summarized. Const. – constitutive active promoter.

Plasmid construct	*Promoter*
p426GPD-HlyB-NBD	GPD – strong/const.
p426TEF2-HlyB-NBD	TEF2 – strong/const.
p426CYC1-HlyB-NBD	CYC1 – weak/const.
p426ADH-HlyB-NBD	ADH – weak/const.
p426GAL1-HlyB-NBD	GAL1 – inducible
p426MET25-HlyB-NBD	MET25 – repressible

4.2 Expression of HlyB NBD in *S. cerevisiae*

4.2.1 Establishment of the HlyB NBD expression

4.2.1.1 Expression screening of different plasmids

To choose which construct to use in the further experiments, expression tests on analytical scale were performed. In these studies the expression levels of the HlyB NBD gene with an N-terminal His-tag from the different plasmid constructs were investigated. The aim was to establish the expression of HlyB NBD with an N-terminal 6x His-tag in *S. cerevisiae*.

Yeast cells, transformed with different plasmid constructs, were analyzed for their expression levels of HlyB NBD. The yeast cells containing plasmid constructs with constitutive active promoters (GPD-, TEF-, CYC1- and MET25-promoter, Figure 13) were cultivated at 25 °C in DO-URA liquid medium supplemented with 2 % glucose in a horizontal shaker at 200 rpm. At different time points samples were taken. The cells containing the plasmid construct with the inducible GAL1-promoter were treated the same way except that they were supplemented with 2 % galactose to induce the HlyB NBD expression. Subsequently, yeast whole cell lysates were prepared. The content of HlyB NBD was analyzed via Western blot (Figure 13).

The comparison between the expression levels of HlyB NBD from the different plasmids revealed distinct differences. Cells containing plasmids with the strong constitutive GPD- and TEF-promoter showed the highest levels of HlyB NBD expression, which was also observed in previous studies (*130*). Furthermore, these cells showed a stable HlyB NDB expression over time. Such stable expression of HlyB NBD was also observed in cells containing the plasmid with the constitutive weak promoter CYC1. However, the protein levels in this case were substantially lower in comparison to the p426GPD- and the p426TEF-construct, which was related to the properties of the promoters (GPD and TEF strong, CYC1 weak). The detected HlyB NBD quantities from the p426MET25-plasmid construct were similar to the quantities from the p426CYC1-plasmid. The NBD expression level of the cells with the MET25-plasmid construct decreased over time, which was surprising. Probably, this plasmid was less stable within yeast compared to the other plasmid constructs and the cells lost the majority of the plasmid copies after a

couple of generations, which resulted in the lower protein amount after 5 hours (Figure 13). HlyB NBD expression in yeast containing the plasmid with the GAL1-inducible promoter was detected as expected after induction (at time point 0 h) with galactose. 7 hours after the induction cells produced reasonable amounts of HlyB NBD, however it was below the protein level reached with the GPD- and the TEF-plasmid constructs.

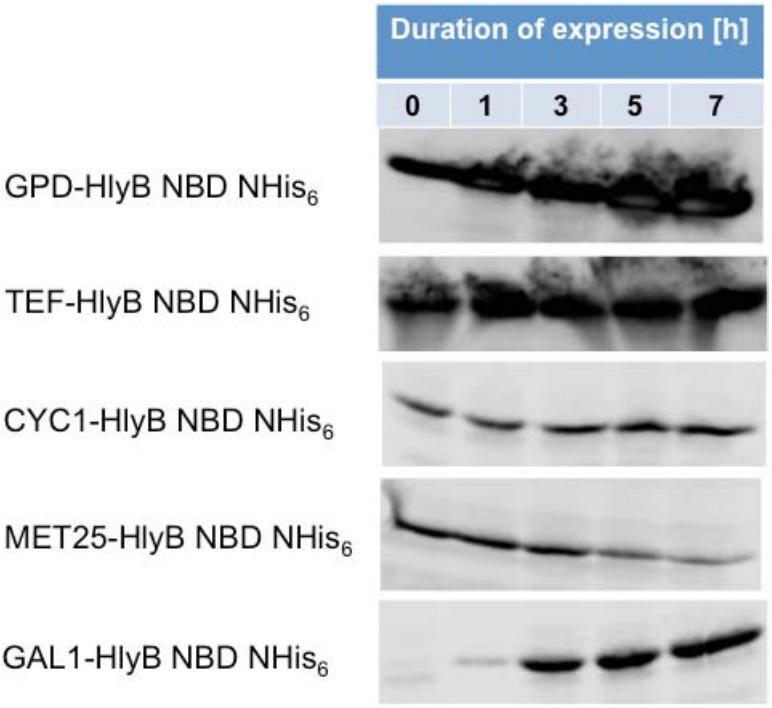

Figure 13: Western blot analysis of the expression of HlyB NBD in *S. cerevisiae*. Samples were taken at the indicated time points. Whole cell lysates were analyzed for their amount of NBD by using a monoclonal HlyB NBD antibody. The different labels describe plasmid constructs containing promoters with different properties – constitutive active (GPD-, TEF-, CYC1-), repressible (MET25-) or inducible (GAL1-). This was the reason why at the time point, 0 h, each construct, except the GAL1-construct, showed expression of HlyB NBD. The expression of HlyB NBD from the GAL1-plasmid construct was induced with 2 % galactose at the time point 0 h.

4.2.1.2 Expression of HlyB NBD in S. cerevisiae on preparative scale

Each plasmid construct was analyzed in expression studies on a preparative scale to establish the cultivation conditions for an optimal expression yield of HlyB NBD in *S. cerevisiae* YPH500^{TM}. To simplify matters, only the results of the best expressing construct (the GPD-construct) are presented.

The experiments were performed in horizontal shaker in shaking flasks in DO-URA medium supplemented with 2 % glucose as a carbon source. The cultivation temperature (20, 25 and 30 °C) and the addition of glycerol as

chemical chaperone (*133*) for possible enhancement of the expression levels were studied. For the analysis of the HlyB NBD amount yeast cells were lysed and the cell lysates were studied via Western blot. For that purpose OD-aliquots of the cultivated yeast cells were prepared and lysed, as described in "Materials and Methods". In Figure 14 the results of this expression study are summarized. As a positive control (+C) 100 ng pure HlyB NBD was analyzed.
The comparison between the expression levels in each condition (Figure 14 A, B, C) did not show significant differences. The amount of protein remained constant during time except for the HlyB NBD expression for 4 h and 6 h at 20 °C with glycerol (Figure 14 A, lanes 11 and 12). The analysis of these samples revealed lower protein amounts. However, after 8 h of incubation a level of HlyB NBD, as observed before the decline, was detected. This deviation did not correlate with the growth behavior of the yeast cells (Figure 15) and with the other analyzed samples. Therefore, the deviation was ascribed to the sample preparation. In general, the presence of glycerol resulted in lower cell densities. Furthermore, the higher the temperature, the higher the optical density of the cells (Figure 15).
An incubation temperature of 25 °C and a growth medium without glycerol were chosen for further experiments. This decision based on several facts and on the aim of obtaining the highest possible yield of the soluble protein. Due to reports of instability of the NBD during overexpression (*134, 135*), the application of expression conditions, which are as similar as possible to these of the homologous expression (*5, 115*), was planned. The optimal expression temperature for HlyB NBD in *E. coli* was established to be 20 °C (*115*). A HlyB NBD production in *S. cerevisiae* under these conditions was possible, however the yeast cells in DO-URA reached higher ODs at 25 °C than 20 °C (Figure 15). Furthermore, the expression of soluble HlyB NBD at 25 °C was demonstrated (*134*). The comparison of the NBD expression levels of the yeast cells at 20 and 25 °C showed no significant differences (Figure 14). This implied that when expressed at 25 °C due to the higher cell count the total amount of HlyB NBD would be higher than at 20 °C. Thus, a growth temperature of 25 °C and a duration of 10 hours in shaking flasks was chosen as expression conditions for the expression of HlyB NBD on preparative scale in *S. cerevisiae*.

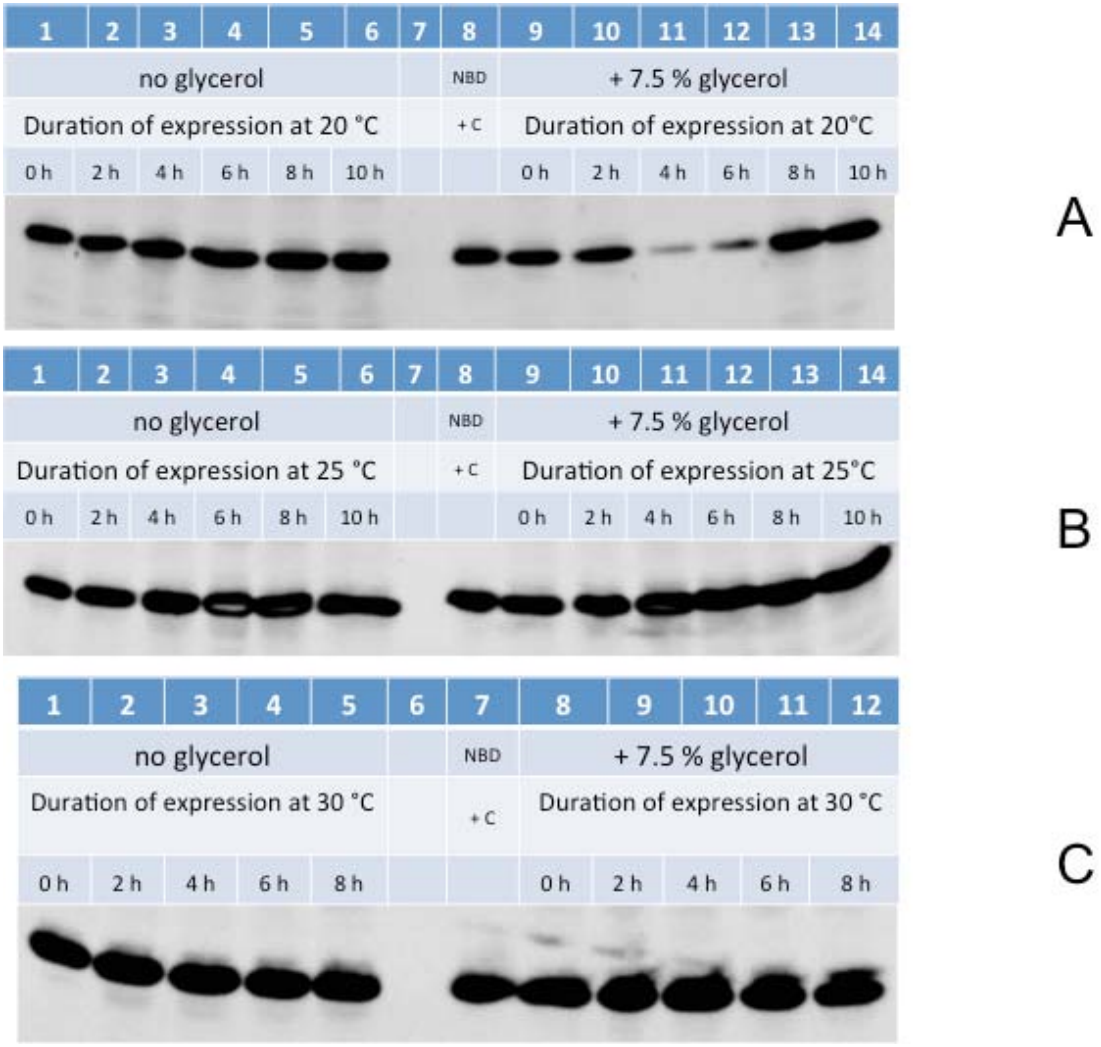

Figure 14: Expression of HlyB NBD in *S. cerevisiae* YPH500™ from the expression vector p426GPD in DO-URA liquid medium under different conditions. Western blot analysis of lysates of 0.5 OD-aliquots of whole yeast cells. The protein was detected by using monoclonal antibody against HlyB NBD. **A**: Incubation temperature of 20 °C with or without 7.5 % glycerol; **B**: Incubation temperature of 25 °C with or without 7.5 % glycerol; **C**: Incubation temperature of 30 °C with or without 7.5 % glycerol. +C: 100 ng HlyB NBD as positive control. h: hour.

The analysis of the NBD expression levels and of the growth of *S. cerevisiae* (Figure 14 and Figure 15) implied that the total yield of HlyB NBD would be even higher after expression at 30 °C. However, these conditions deviated significantly from the optimal conditions, established for the expression of HlyB NBD (*115*). Therefore, with regard of the stability of HlyB NBD during expression, 30 °C was not chosen as the temperature for the expression of HlyB NBD on preparative scale in *S. cerevisae*.

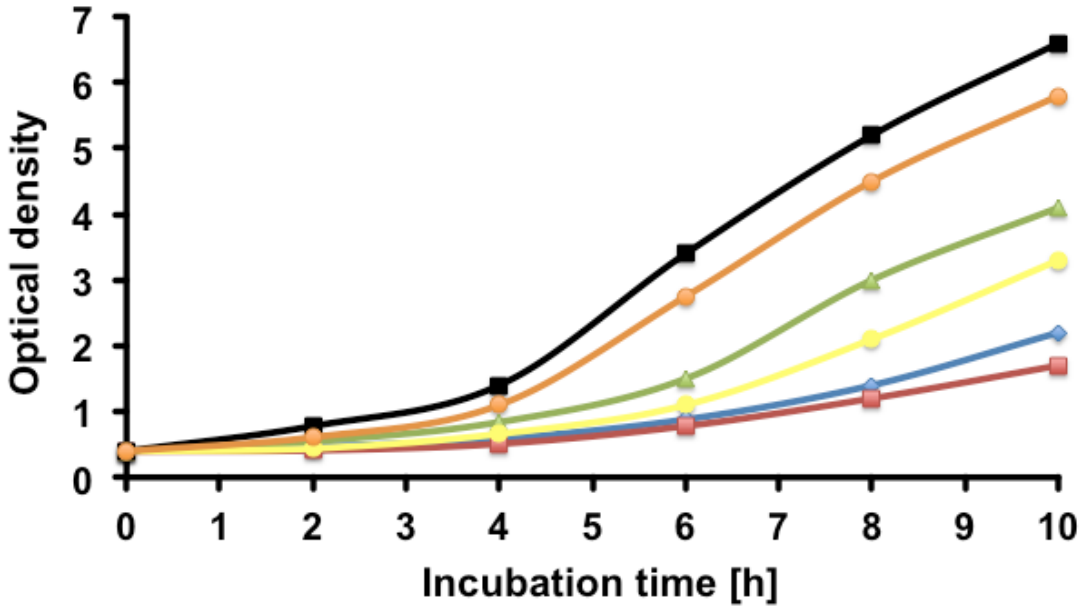

Figure 15: Growth curve of *S. cerevisiae* YPH500 with p426GPD-HlyB-NBD-NHis6 in DO-URA liquid medium at different temperatures and with or without glycerol. Different colors code different growth conditions. Red: 20°C +7.5% glycerol; dark blue: 20°C without glycerol; yellow: 25°C +7.5% glycerol; green: 25°C without glycerol; orange: 30°C +7.5% glycerol; black: 30°C without glycerol. h: hour.

Cells expressing the HlyB NBD mutants S504A and S634Y were cultivated as described above. The growth behavior of the cells expressing the mutant NBDs did not differ significantly from these of the wild type protein.

The expression of the NBD in yeast was also performed in a bioreactor. In previous studies it was already shown that a tight control of the aerobic growth conditions during fed-batch fermentation could result in increased amounts of the overexpressed protein (*112, 136*). Therefore, the protocol for fed-batch fermentation under aerobic conditions from (*112*) was used for the expression of HlyB NBD in this work, however with some modifications. The fermentation has been performed 11 hours in YPD liquid medium, which was stirred at 750 rev min^{-1}. The temperature was maintained at 25 °C, pH of the solution was kept at 5.6 during the entire procedure. The working volume was 5 L, the initial volume was 4 L. The saturation of the medium with dissolved oxygen was kept about 90 – 100 %. Two pre-cultures in a selective medium were prepared for the inoculum of the bioreactor. The first pre-culture was inoculated directly from the selective DO-URA agar plate and grown for approx. 17 hours in DO-URA liquid medium at 25 °C. The second pre-culture (the inoculum for bioreactor) was inoculated from the first pre-culture and

grown in DO-URA liquid medium at 25 °C for 20 h to obtain a high density of plasmid containing yeast cells. 1 L of the inoculum was added to the initial volume of the bioreactor (4 L). Together with the starting volume this resulted in a total working volume of 5 L. The starting OD of the fermentation culture was in the range of 0.9 – 1.1. After 8 hours of fermentation a feeding with glucose was started and performed for 3 hours. The feeding rate was 2.62 g glucose h^{-1} L^{-1} medium. Compared to the cultivation in shaking flasks (Figure 15, green curve), the yeast cells in the bioreactor clearly reached higher OD as shown in Figure 16.

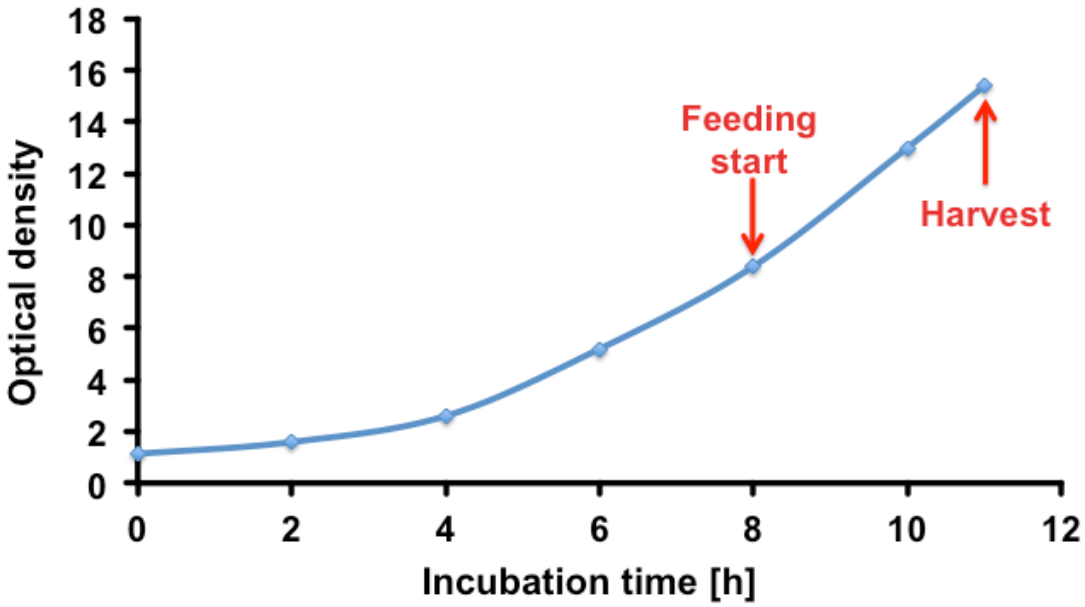

Figure 16: Growth curve of *S. cerevisiae* YPH500 containing p426GPD-HlyB-NBD-NHis6 in YPD medium at 25°C in a bioreactor. The blue curve depicts the OD of the yeast cells at different time points. The OD at the beginning (0 h) was adjusted to 1. OD: optical density, h: hours. Red arrows indicate the time points of feeding start and harvest.

A verification of the HlyB NBD expression during the fermentation was performed via Western blot (*6*). 0.5 OD-aliquots of the yeast cells were taken at the indicated time points during the growth analysis (Figure 16). Subsequently, cells were lysed, whole cell lysates were prepared and investigated via Western blot for the expression of HlyB NBD (Figure 17).

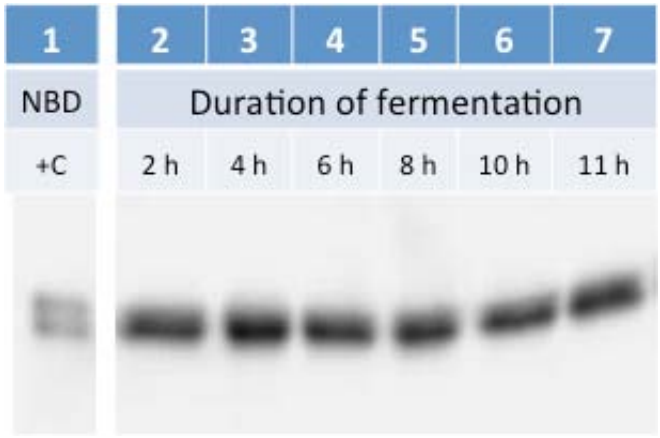

Figure 17: Expression analysis of HlyB NBD in yeast during fermentation. Analysis via Western blot of lysates of yeast cells (0.5 OD-aliquots) by using monoclonal HlyB NBD antibody. h: hour; **+C**: positive control, pure HlyB NBD.

A comparison between the expression levels of the protein at the different time-points during fermentation did not reveal significant differences. The pure HlyB NBD, used as a positive control (lane 1, Figure 17), was surprisingly detected as a double band. However, for HlyB NBD this was unusual (e.g. Figure 13, Figure 14) and did appear only in this case. Therefore, this double band was not considered as problematic. These results showed that fermentation in a bioreactor resulted in a stable HlyB NBD expression (Figure 17) and in a higher optical density of the yeast cells (Figure 16), compared to the expression in shaking flasks (Figure 15). The amount of HlyB NBD after the fermentation and the purification was 3 mg/L yeast cells (section 4.4.1.1).

4.2.2 Expression of DMNB-L-Ser-labeled HlyB NBD in *S. cerevisiae*

The labeling of HlyB NBD with DMNB-L-Ser was performed at three positions: S504 and S506 of the Walker A motif and S634 of the D-loop. In the case of S504 the labeling was performed both in shaking flasks and by fermentation. The incorporation of DMNB-L-Ser at positions S506 and S634 was performed only via fermentation.

The expression of HlyB NBD S504DMNB-L-Ser in shaking flasks resulted in an expression of a labeled protein. This conclusion was supported by the observation that in this expression system HlyB NBD was only produced in the presence of the unnatural amino acid (Figure 18 A). When DMNB-L-Ser

was absent, no HlyB NBD was detected. The expression of HlyB NBD S504DMNB-L-Ser was monitored via immunoblot analysis of OD-aliquots of yeast cells (Figure 18 A). These results also indicated that the expression yield of the labeled protein in shaking flaks decreased at some point between 12 and 24 hours, as this could be seen in lane 12 of Figure 18 A. As a consequence, the expression duration of the labeled HlyB NBD was limited to 12 hours. Nevertheless, this expression procedure did not result in sufficient HlyB NBD S504DMNB-L-Ser for biochemical studies. Therefore, the fermentation in a bioreactor was performed to increase the protein yield.

The fermentation procedure for the expression of a labeled protein at position 504 was conducted as described above (section 4.2.1.2, Figure 16) for wild type NBD. The only difference was the selective medium of the agar plates for the pre-cultures. In this case DO-URA/-TRP medium was used. DMNB-L-Ser was added to the fermentation culture after inoculation to a final concentration of 0.5 g/L. The growth behavior of the cells was similar to the growth behavior of yeast cells expressing wild type HlyB NBD. The expression of HlyB NBD S504DMNB-L-Ser was analyzed via Western blot of whole cell lysates, which is shown in Figure 18 B. This experiment demonstrated the presence of HlyB NBD in yeast cells. Before the addition of the unnatural amino acid (time point 0 h, lane 1, Figure 18 B) an extremely low amount of non-labeled protein was detected. This indicated the suppression of the “Amber” stop codon, which was independent from the unnatural amino acid. Furthermore, this suppression suggested an incorporation of natural amino acids in HlyB NBD by endogeneous aminoacyl-tRNA-synthetases. The addition of DMNB-L-Ser had as a consequence a significant increase of the intensity of the HlyB NBD band. This was strong evidence for the incorporation of the unnatural amino acid at position 504 and for the expression of HlyB NBD S504DMNB-L-Ser (Figure 18 B, lanes 4-10). The yield of the labeled protein after fermentation and purification was 0.06 mg/L yeast cells (see chapter 4.4.2.3).

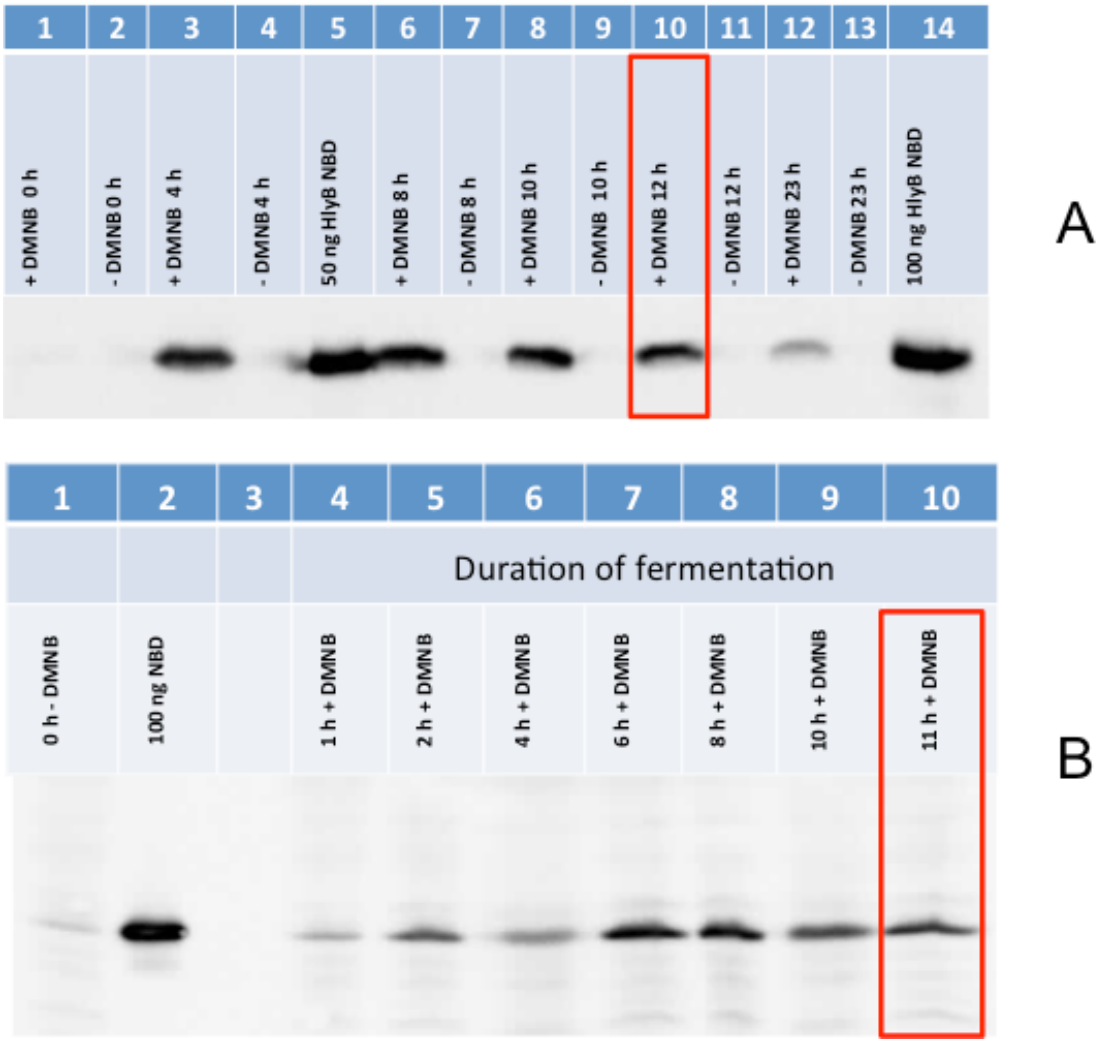

Figure 18: Western blot analysis of the expression of HlyB NBD S504DMNB-L-Ser in yeast in shaking flasks (A) or in a bioreactor (B). Lysates of OD-aliquots of yeast cells were analyzed by Western Blot. The detection was performed by using monoclonal HlyB NBD antibody. A red box marks the time point of cell harvest. **A**: Immunoblot analysis of the HlyB NBD S504DMNB-L-Ser expression in shaking flasks in the presence or absence of unnatural amino acid at different time points. In lanes 5 and 14 purified HlyB NBD is shown as positive control. h: hour. **B**: Western blot analysis of yeast whole cell lysates for HlyB NBD S504DMNB-L-Ser expression during fermentation in a bioreactor. Samples were taken at the indicated time points. The unnatural amino acid was added at the time point 0 h to the fermentation medium. The addition of DMNB-L-Ser resulted in the production of labeled protein. 50 and/or 100 ng pure HlyB NBD was applied as positive control; h: hour.

Furthermore, the amounts of labeled protein (in both cases – shaking flasks and fermenter) relative to the according positive control were compared. At the time point of cell harvest the detected NBD signal from the fermentation (lane 10, Figure 18 B) did not differ significantly from the protein signal of the shaking flasks experiment (Figure 18 A, lane 10). This comparison indicated that both expression strategies resulted in similar quantities of labeled protein per cell.

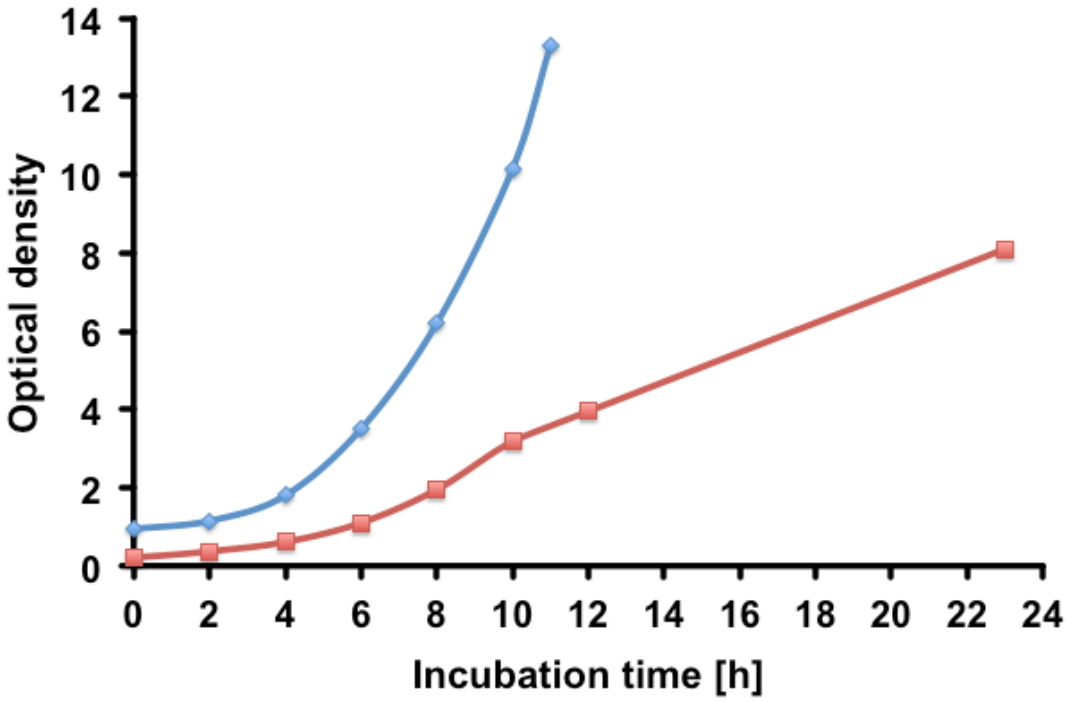

Figure 19: Comparison of the growth behavior between NBD S504DMNB-L-Ser producing yeast cells in shaking flasks (red line) and in bioreactor during fermentation (blue line). The feeding during the fermentation was performed as described for the yeast cells producing wild type HlyB NBD (**Figure 16**). The ODs at the beginning were different. The initial OD in the bioreactor was 0.9; the initial OD in the shaking flasks was 0.2. h: hours, OD – optical density.

However, the HlyB NBD S504DMNB-L-Ser producing yeast cells reached much higher optical densities during fermentation in a bioreactor than in shaking flasks (Figure 19). Due to the different starting optical densities of the yeast cell cultures in the bioreactor and in the shaking flasks (Figure 19), the generation times **g** of the cells under the different conditions (shaking flasks and bioreactor) were calculated as described in “Materials and Methods” (section 3.2.1.11.3).

The generation time of the yeast cells was calculated from the exponential phase of the growth curve, where the optical density increased in a linear manner. For the cells in the bioreactor **g** has been calculated for a time interval of 5 hours (between hour nr. 6 and 11). N_0 (OD after 6 h) was 3.5 and N (OD after 11 h) was 13.3, which resulted in a generation time of 2 h 37 min. The generation time of the cells in the shaking flasks was calculated for a time interval of 6 hours (between hour 6 and 12). N_0 was 1.1 and N was 3.95, which resulted in a longer generation time of 3 h 17 min. This result allowed the conclusion that the fermentation in a bioreactor would deliver more

labeled HlyB NBD S504DMNB-L-Ser because of a lower generation time. A lower generation time leads to higher cell densities and to higher protein yields per given time interval.

These results led to the decision to label HlyB NBD at position 634 only via fermentation. The experimental conditions were the same as in the case of the S504DMNB-L-Ser-labeling. The results of the expression of HlyB NBD S634DMNB-L-Ser are presented in Figure 20 A.

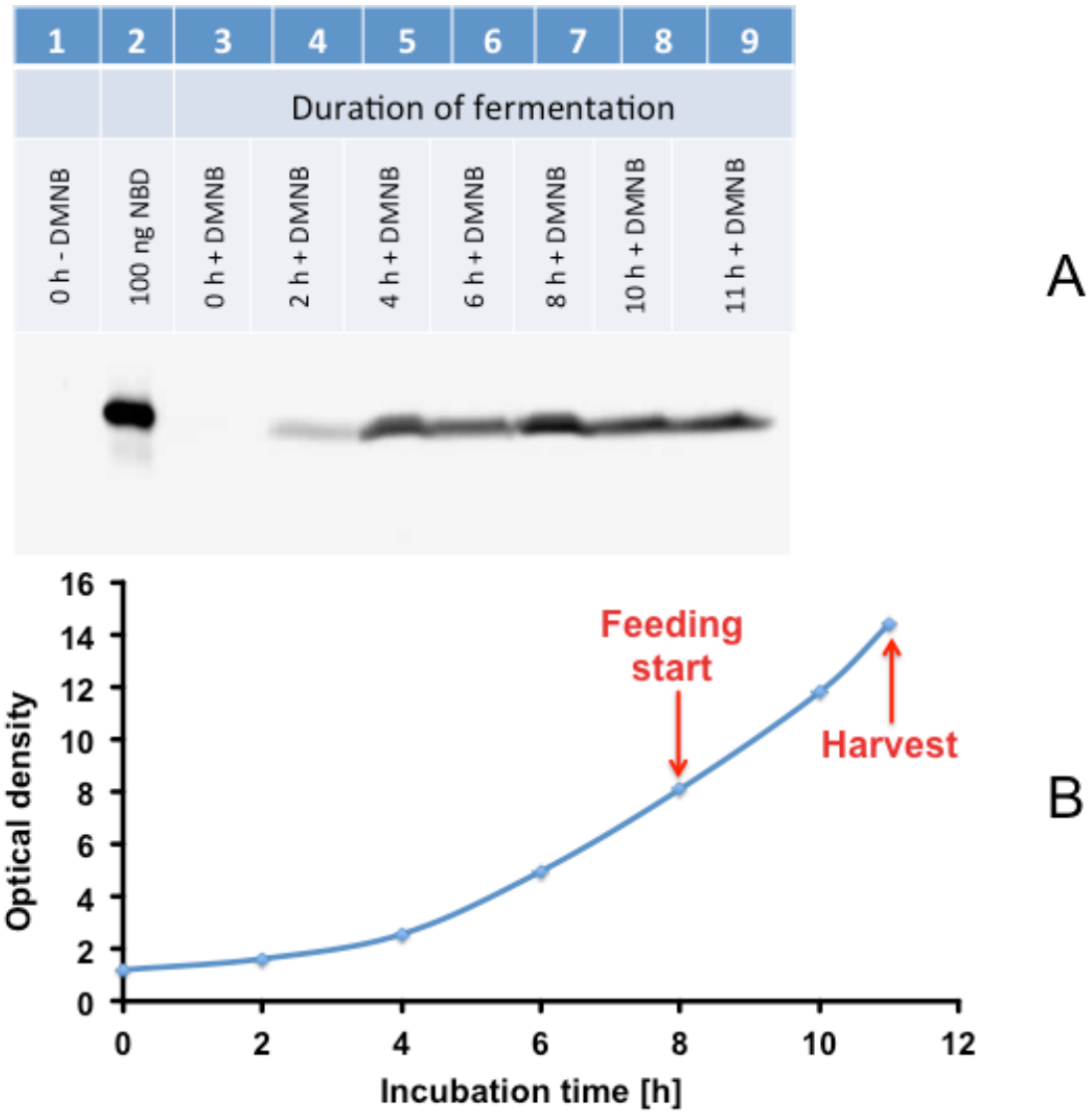

Figure 20: Immunoblot analysis of HlyB NBD S634DMNB-L-Ser production and the growth behavior of yeast cells during fermentation. A: Western blot analysis of yeast whole cell lysates for the expression of HlyB NBD S634DMNB-L-Ser during fermentation at different time points. The detection was performed with HlyB NBD antibody. h: hours. 100 ng pure HlyB NBD was applied as a positive control. **B**: Growth behavior of *S. cerevisiae* during fermentation in the presence of the unnatural amino acid DMNB-L-Ser. The feeding start and the cells harvest were performed as described for the yeast cells producing wild type HlyB NBD (**Figure 16**). The time points for feeding start and cells harvest are indicated by red arrows.

No labeled HlyB NBD could be detected without the unnatural amino acid (lane 1, Figure 20 A) or directly after its addition (lane 3). After 2 hours of expression HlyB NBD was detected (lane 4, Figure 20 A), which indicated that the expression of full length NBD was a result of the incorporation of DMNB-L-Ser at position 634. The amount of protein per cell after 2 hours of expression was lower compared to the protein amount after 4-11 hours of expression. Between the 4th and the 11th hour the expression level of the protein appeared to be stable. The growth behavior of the yeast cells (Figure 20 B) did not differ significantly from the *S. cerevisiae* cells producing wild type protein under the same conditions (Figure 16).

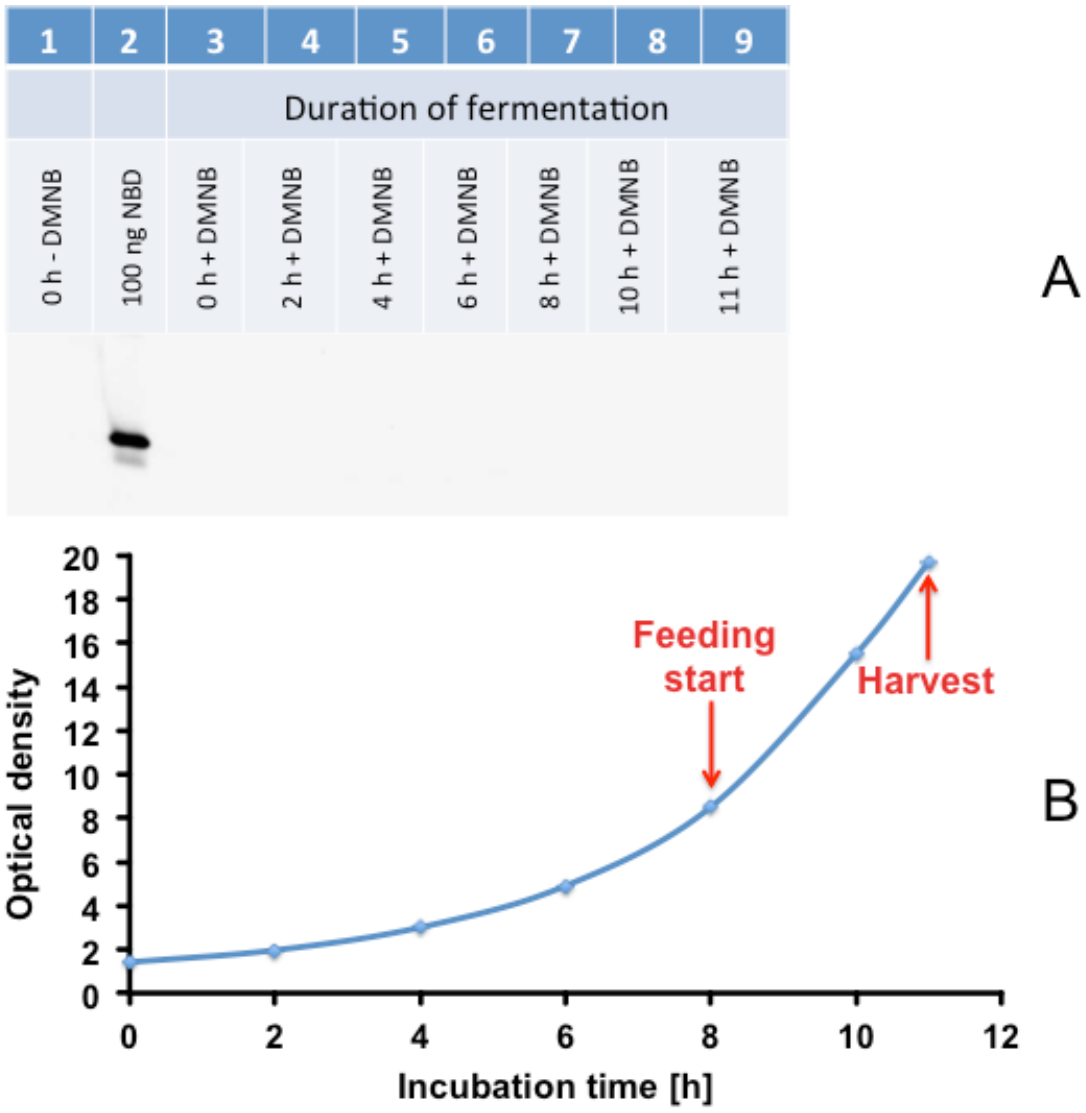

Figure 21: Western blot analysis of the HlyB NBD S506DMNB-L-Ser expression and the growth behavior of yeast cells during the fermentation. A: Western blot analysis of yeast whole cell lysates for expression of HlyB NBD S506DMNB-L-Ser during fermentation at different time points. The detection was performed by using HlyB NBD antibody. h: hours. 100 ng pure HlyB NBD was used as positive control. **B:** Growth behavior of *S. cerevisiae* during the fermentation in a bioreactor in the presence of the unnatural amino acids DMNB-L-Ser. The time points of the feeding start and the cells harvest are highlighted with red arrows.

The labeling of HlyB NBD with DMNB-L-Ser was also performed at position 506. The incorporation of the unnatural amino acid was performed via fermentation in a bioreactor under the same experimental conditions as for the mutants S504DMNB-L-Ser and S634DMNB-L-Ser. Figure 21 reveals the results of the expression of HlyB NBD S506DMNB-L-Ser. The yeast cells showed the same growth behavior (Figure 21 B) as the cells expressing HlyB NBD S504DMNB-L-Ser (Figure 19) or HlyB NBD S634DMNB-L-Ser (Figure 20 B). However, the immunoblot analysis (Figure 21 A) did not show the presence of HlyB NBD in the yeast cells. This revealed that the labeling with DMNB-L-Ser at position 506 was not successful.

4.3 Overview of the mutants of the HlyB NBD generated to study its catalytic cycle

In the following chapter an overview of the amino acids of HlyB NBD to be mutated is presented. The choice of these residues was based on the HlyB NBD H662A structure with bound ATP and Mg^{2+} (PDB code 1XEF). The chosen amino acids (Walker A motif and C-loop) were involved in interactions with ATP or in inter-monomer interactions (D-loop), see Table 12, Figure 5, Figure 6 and (*1, 2*).

Based on the HlyB NBD structure, mutation of these residues could impact the ability of HlyB NBD to dimerize upon nucleotide binding and/or its ability to hydrolyse ATP. Therefore, a mutagenesis of the mentioned amino acids could enable a trapping of the HlyB NBD at defined states, which correspond to the ATP-bound monomeric stage or the ATP-bound dimeric stage from its catalytic cycle (Figure 22). The unnatural photo-caged amino acid DMNB-L-Ser was employed for trapping of reactivatable inntermediates by incorporating it at different positions of the polypeptide chain of HlyB NBD (Table 12). It has already been used successfully for studying protein function (*102*). This unnatural amino acid can be converted photolytically to serine by irradiation with light (λ = 270 – 420 nm). For this reason, only serines and threonines were replaced with DMNB-L-Ser. The photolysis of DMNB-L-Ser should reactivate the “trapped” HlyB NBD intermediates and should lead to their simultaneous reactivation.

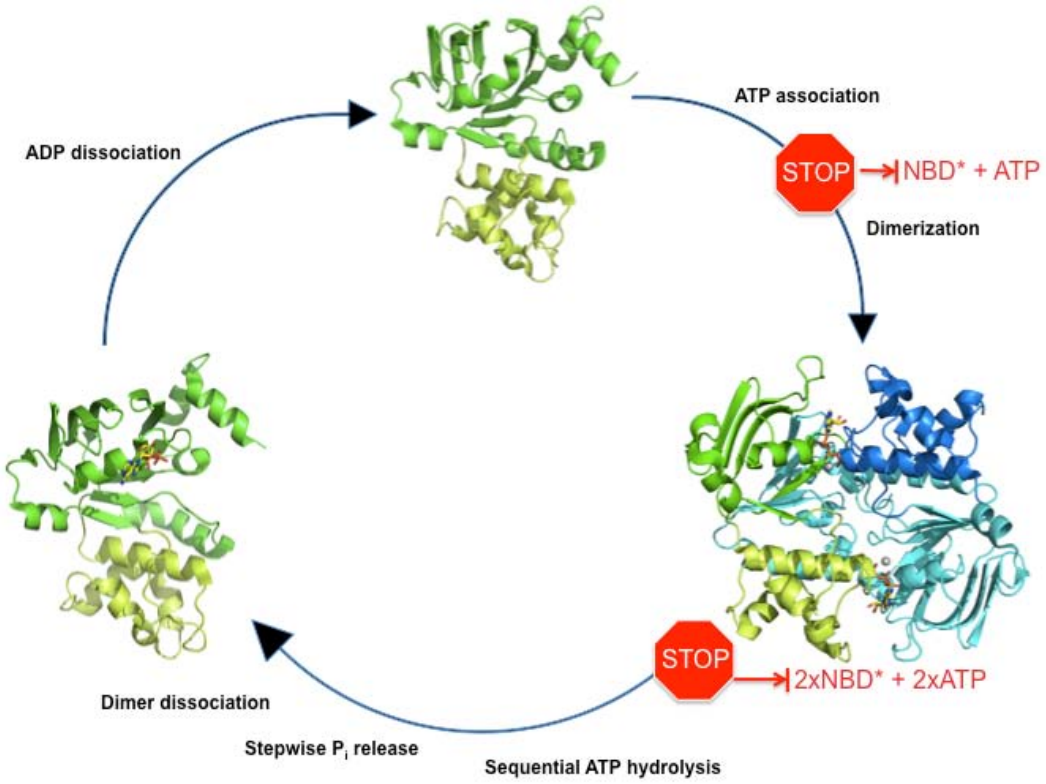

Figure 22: Catalytic cycle of HlyB NBD (*1*). The crystal structures of the substrate free monomeric HlyB NBD (PDB code 1MT0, (*3*)), ATP/Mg^{2+}-bound dimer (PDB entry 1XEF, (*2*)) and ADP-bound monomer (PDB entry 2FFA, (*1*)) are shown in a cartoon representation. The helical domain is colored in lemon green, the catalytical domain in green. In the dimeric form the second monomer is colored in blue (helical domain) and cyan (catalytical domain). ATP is showed in stick representation, the magnesium ions as a grey spheres. The biochemical properties of the HlyB NBD states, which are shown as crystal structures, are described (*1, 5*). Stop signs show which intermediates might be generated by the incorporation of DMNB-L-Ser and subsequently characterized. NBD* marks the monomeric state of the DMNB-L-Ser-labeled protein, 2xNBD* marks the dimeric state.

The reasons for the choice of a particular amino acid (of Walker A, C- or D-loop) for a substitution with DMNB-L-Ser are discussed in the following chapters (4.4.2 - 4.4.7). Each residue was first mutated to a natural amino acid (Ala or Tyr, see Table 12) to examine if the resulting mutant was ATPase deficient but still able to bind ATP. For these tests the according mutant (except S504A, (*8*)) was expressed in *E. coli* and purified, which compared to *S. cerevisiae* was more timesaving and resulted in higher protein yields. Mutants, which retained the ability to bind ATP (analyzed via the TNP-ATP binding assay), but were not able to hydrolyze it (analyzed via the ATPase activity assay), were also expressed in *S. cerevisiae*, purified from this host organism and characterized afterwards. This second step of characterization in yeast was necessary because the system for incorporation of DMNB-L-Ser was developed for *S. cerevisiae* (*102*). In case that the heterologous

expression in yeast did not impact the properties of a “suitable” mutant, DMNB-L-Ser was incorporated at the according position in the polypeptide chain of HlyB NBD. The resulting NBD-DMNB-L-Ser protein constructs were purified and characterized. The properties of each protein (Table 12) are described in section 4.4.

Table 12. Mutants of HlyB NBD, analyzed in this work. The different columns (from left to right) show the position of the mutated amino acids in the polypeptide chain, to which conserved motif they belong, the generated mutant and the according expression host. Usually, the Ala- and the Tyr-mutants (except S504A) were first expressed in *E. coli*, purified and characterized. The mutants, which retained the ability to bind ATP, but were ATPase inactive, were expressed afterwards heterologously in *S. cerevisiae* and then purified and characterized. In case the heterologous expression did not impact the properties of the mutant proteins, the unnatural amino acid DMNB-L-Ser was incorporated at the according position in the polypeptide chain of HlyB NBD.

Amino acid position	*Amino acid location*	*Mutant*	*Expression host*
S504	Walker A	S504A	*S. cerevisiae*
		S504DMNB-L-Ser	*S. cerevisiae*
S506	Walker A	S506Y	*E. coli*
		S506DMNB-L-Ser	*S. cerevisiae*
S509	Walker A	S509Y	*E. coli*
T510	Walker A	T510Y	*E. coli*
S607	C-loop	S607A	*E. coli, S. cerevisiae*
S634	D-loop	S634Y	*E. coli, S. cerevisiae*
		S634DMNB-L-Ser	*S. cerevisiae*

4.4 Characterization of HlyB NBD and selected mutants

4.4.1 Properties of HlyB NBD

The biochemical and the structural characterization of the isolated HlyB NBD from *E. coli* revealed that it binds ATP, which leads to the formation a dimer (*2, 5*). Within the dimer the two NBD monomers bind two ATP molecules (*1*). Each nucleotide is coordinated by the Walker A motif from one monomer and the C-loop from the other monomer in the so called “head-to-tail” dimer, as shown in Figure 23 A. For a better overview, the coordination of only one of the two ATP molecules bound is shown (Figure 23). The Walker A motif

wraps around the phosphate moiety of ATP coordinating each phosphate residue (*37*), whereas the C-loop contacts the γ-phosphate, the adenine ring and the ribose of the nucleotide (Figure 23 B). Other protein regions (Walker B motif and the Q-loop) are also involved in nucleotide coordination. These are shown in Figure 23 B.

The biochemical analysis of the ATPase activity of the purified HlyB NBD from *E. coli* revealed a positive cooperativity (*5*). However, it was planned to perform the labeling of the protein with DMNB-L-Ser in the heterologous host *S. cerevisiae*. Due to the heterologous expression, the wild type protein was first expressed and purified from *S. cerevisiae* and then characterized. The aim of this experiment was to examine whether the properties of the heterologous expressed protein differed from the properties of the homologous expressed protein.

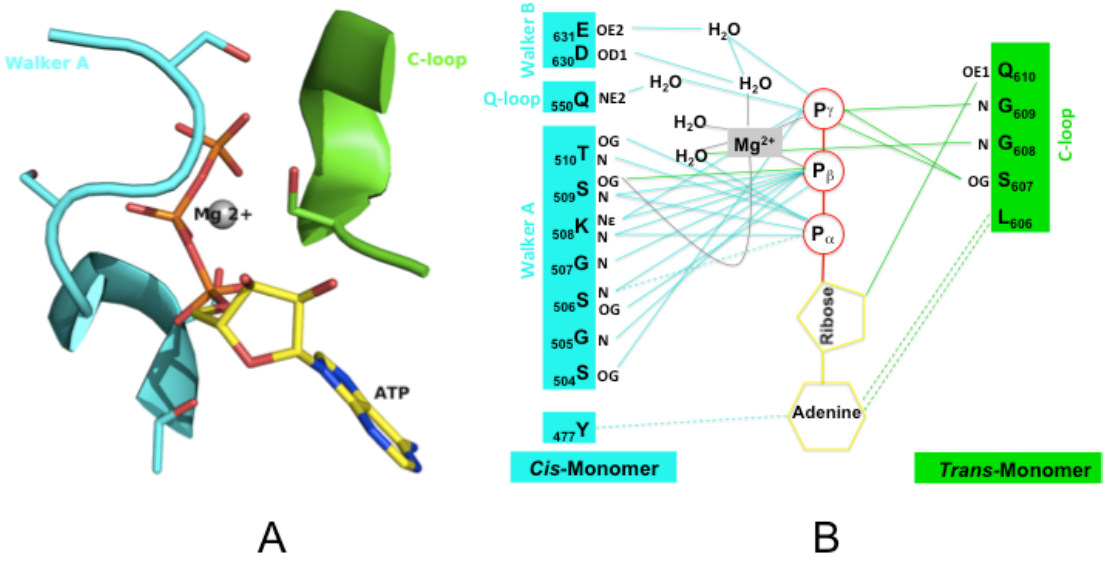

Figure 23: Structural organization within the binding pocket of the dimeric HlyB NBD with bound ATP and Mg^{2+}. A: Cartoon representation of the ATP binding pocket of HlyB NBD. For better overview only the Walker A motif from one monomer (colored in cyan) and the C-loop from the other monomer (colored in green) are shown. The side chains of the amino acids, which were mutated in this work, are shown in stick representation. The carbon atoms of HlyB NBD are colored according to the color code of their monomer. The nitrogen atoms are colored in blue, the oxygen atoms in red. The carbon atoms of ATP are colored yellow, the phosphorus atoms of the nucleotide are shown in orange. The magnesium ion is shown as a grey sphere. **B:** Schematic overview of the interactions within the composite dimer of HlyB NBD (*2*). The ATP molecule is shown between both monomers. The conserved motifs of the cis-monomer (Walker A, Walker B, Q-loop) are shown in cyan, the C-loop of the trans-monomer is shown in green. Solid lines represent hydrogen bonds or salt bridges, dashed lines mark hydrophobic- and van der Waals interactions. This figure was adapted from the structure of the Mg^{2+}/ATP-bound HlyB NBD H662A, PDB code 1XEF (*2*).

4.4.1.1 Purification of HlyB NBD from S. cerevisiae

Wild type HlyB NBD was expressed in *S. cereviasiae* YPH500^{TM} and purified via two steps, IMAC and SEC, as described in “Material and Methods”. After each step the purity was monitored by SDS-PAGE. For a better overview, only the chromatogram of SEC and the according SDS-gel are shown.

Figure 24 shows the result of the purification of wild type HlyB NBD. High protein purity could be achieved, as estimated from SDS-PAGE (Figure 24 A). SEC resulted in a major protein peak with a maximum at 10.8 mL. The yield of HlyB NBD was 1 mg/L in DO-URA medium when expressed in shaking flasks or 3 mg/L in YPD medium after fermentation. Routinely, after SEC the protein was concentrated by ultrafiltration up to 10 mg/mL in a buffer containing 100 mM CAPS, 20 % glycerol and 10 mM DTT at pH 10.4 and stored at 4 °C (*115*). In this buffer the protein remained stable for weeks without precipitation.

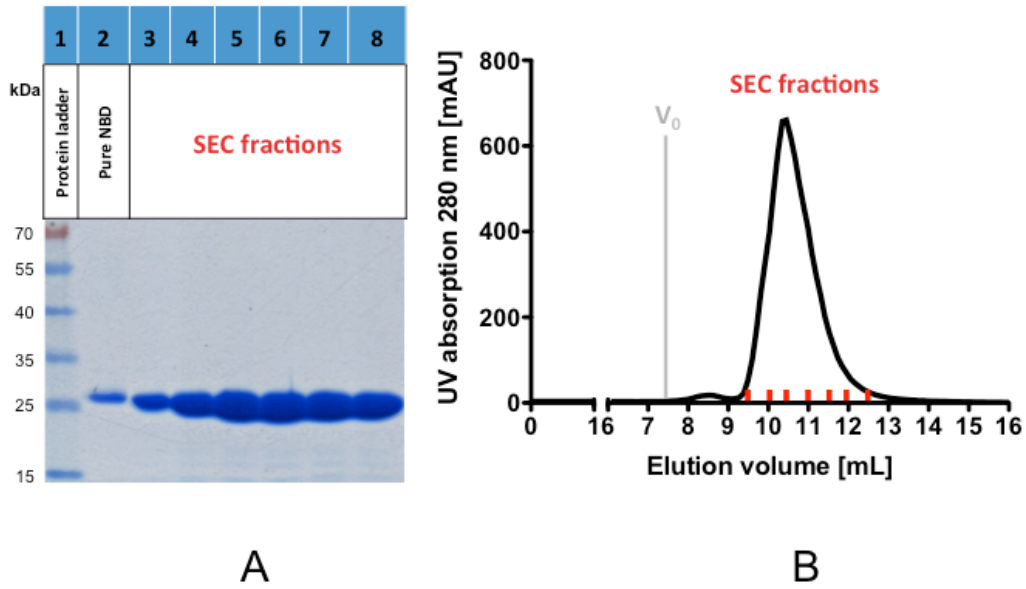

Figure 24: SEC of HlyB NBD from *S. cerevisiae* cells. A: SDS-PAGE analysis of the peak fractions of SEC (B). Pure HlyB NBD was employed as positive control. **B:** SEC of HlyB NBD using Superdex75 10/300 (GE Healthcare). V_0 denotes the void volume of the column. The protein detection was performed via UV absorption at 280 nm.

4.4.1.2 Characterization of the purified HlyB NBD

In CAPS-buffer the HlyB NBD was inactive as already described (*115*). The dilution of the NBD in a buffer containing 100 mM HEPES pH 7.0, 20 % glycerol, to a concentration of 1.1 µM led to recovery of the ATPase activity at

22 °C as shown in Figure 25. The reaction was started by adding $MgCl_2$ at a final concentration 10 mM.

The experimental data showed a non-linear dependency of the ATPase activity on the substrate concentration in the range between 0.1 and 1.2 mM ATP. The data were fitted according to the Michaelis-Menten (dashed line) or to the Hill equation (solid line). These fits were compared by two statistical approaches - the “Extra sum-of-squares F-test” and the “Akaike’s informative criterion approach” (AIC) using Graphpad Prism 5 version 5.0a (California, USA). Both approaches balance the goodness-of-fit with the change in the number of degrees of freedom. The goodness-of-fit is assessed by the sum-of-squares, which is the sum of the squares of the vertical distances of the data points from the best-fit-curve and indicates how well does a curve fit the data. A lower sum-of-squares means a lower deviation of the data points from the best-fit-curve and vice versa. The degrees of freedom reflect the number of adjustable parameters of a particular model. A simpler model (e.g. Michaelis-Menten) has fewer adjustable parameters than a more complicated model (Hill) and therefore more degrees of freedom. Both approaches for comparison (F-test and AIC) preferred clearly the data fit with the Hill equation. The AIC approach stated a probability of 99.7 % that the fit with the Hill equation is correct and a probabillity of 0.3 % that the Michaelis-Menten fit is correct. This analysis and earlier studies (*2, 5, 134*) supported a fit employing the Hill equation. This fit resulted in a sigmoidal form of the curve (Figure 25), which suggested positive cooperativity of the ATP hydrolysis of the yeast HlyB NBD.

The calculated value of 1.87 ± 0.24 of the Hill coefficient demonstrated that HlyB NBD from yeast hydrolysed ATP in a cooperative fashion, however it deviated fom the Hill coefficient of the *E. coli* NBD (1.31 ± 0.13). V_{max} was calculated to be 149 ± 7 nmol*min^{-1}*mg^{-1}, the kinetic constant $K_{0.5}$ = 0.24 ± 0.07 mM ATP. The turnover number of the heterologous expressed NBD was 4.1 ± 0.2 min^{-1}. The comparison of the kinetic parameters (Table 13) showed that the enzyme properties of HlyB NBD from yeast did not equal exactly the properties of HlyB NBD from *E. coli* (V_{max} 202 nmol*min^{-1}*mg^{-1}; k_{cat} 5.6 ± 0.7 min^{-1}; $K_{0.5}$ 0.36 mM), however they were similar.

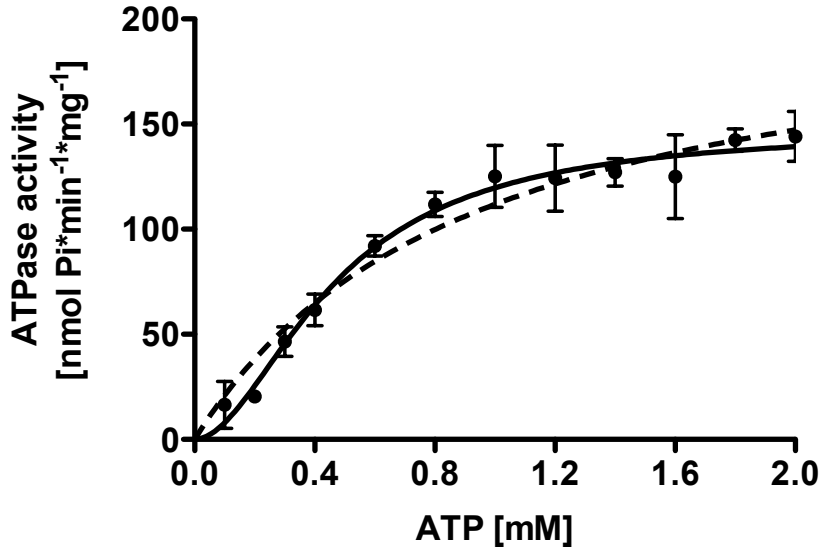

Figure 25: ATPase activity of HlyB NBD WT from *S. cerevisiae* as a function of the ATP concentration. The assay was performed in a buffer containing 100 mM HEPES; pH 7.0, 20 % glycerol, 10 mM $MgCl_2$ at 22 °C. The ATP concentration varied from 0.1 to 2 mM. The enzyme concentration was 1.1 µM. The solid line represents the analysis of the data according to the Hill equation, dashed line according to the Michaelis-Menten equation (formulas are shown in "Materials and Methods"). Each data point is an average of three independent experiments. Error bars represent standard deviation.

Table 13: Kinetic parameters of wild type HlyB NBD, purified from *E. coli* (homologous expression) or from *S. cerevisiae* (heterologous expression).

HlyB NBD	V_{max} [nmol*min^{-1}*mg^{-1}]	k_{cat} [min^{-1}]	$K_{0,5}$ [mM]	*h*
E. coli (*5*)	202 ± 16	5.6 ± 0.7	0.36 ± 0.05	1.31 ± 0.13
S. cerevisiae	149 ± 7	4.1 ± 0.2	0.24 ± 0.07	1.87 ± 0.24

These data and their comparison with the functional properties of HlyB NBD from *E. coli* indicated that the ATPase activity of HlyB NBD from *S. cerevisiae* also follows the rule of the Hill kinetics. This implied that ATP binding leads to the formation of a dimer, which is the active oligomeric form and that the yeast protein also hydrolyzes ATP in a cooperative fashion.

The nucleotide binding properties of the wild type HlyB NBD from yeast were investigated by analysing the ability of the protein to bind TNP-ATP (*8*). This molecule is an ATP analog, which contains the fluorophore TNP. TNP-ATP shows higher fluorescence in a hydrophobic environment than in a hydrophilic (*122*). Therefore, the binding in the hydrophobic protein binding pocket would

enhance the TNP-ATP fluorescence. A high number of ATPases show binding of TNP-ATP (*121, 137*). Hence, the alteration of the TNP-ATP fluorescence can be applied to determine the binding affinity of the NBD-nucleotude complex (*8*). The experiments were conducted at 20 °C in a buffer containing 100 mM HEPES, 20 % glycerol, pH 7.0. The sample volume was 1.2 mL. The protein concentration was 4 µM. TNP-ATP was titrated to the sample in a stepwise fashion. The nucleotide titration to HlyB NBD resulted in a binding curve, as shown in Figure 26. The control experiment with a solution containing only buffer showed an increase of the TNP-ATP fluorescence (blue color) with clearly lower fluorescence intensities. This led to the conclusion that the NBD from *S. cerevisiae* binds TNP-ATP. The calculated dissociation constant was 0.6 ± 0.2 µM, which is similar to the K_D of the *E. coli* NBD (0.8 µM, (*8*)). The correction factors Q_1 and Q_2 regarding the inner filter effects are shown in the appendix.

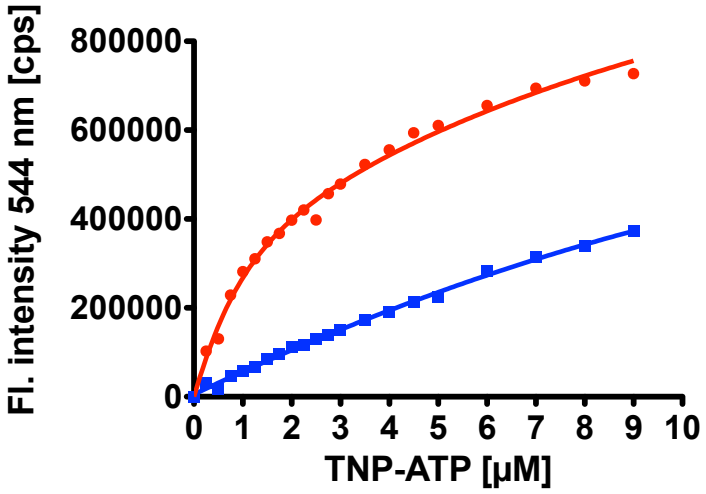

Figure 26: Analysis of the TNP-ATP binding by wild type HlyB NBD from *S. cerevisiae*. The experiment was performed at 20 °C in a buffer containing 100 mM HEPES, 20 % glycerol, pH 7.0. The protein concentration was 4 µM. The data of the TNP-ATP titration to the HlyB-NBD containing solution at 544 nm emission are displayed in red. The data of the TNP-ATP titration to the solution with only buffer are shown in blue. The data were calculated and fitted as described (*8*), see also chapter 3.2.2.7. Cps: counts per second.

The ATPase data shown above (Figure 25), suggested a positive cooperativity of HlyB NBD for ATP hydrolysis. This involves protein dimerization upon nucleotide binding. Therefore, the ATP induced dimerization of the heterologous expressed HlyB NBD was investigated by

analytical SEC. This allowed further comparison between the properties of the proteins, expressed in *E. coli* and in *S. cerevisiae*.

Analytical SEC was performed in a buffer containing 50 mM malonate, 100 mM sodium acetate, 5% glycerol and pH 5.8, as already established (*5*). The enzyme concentration was 50 µM. ATP was present in the solution at a final concentration of 1 mM (red line) or not present (blue line).

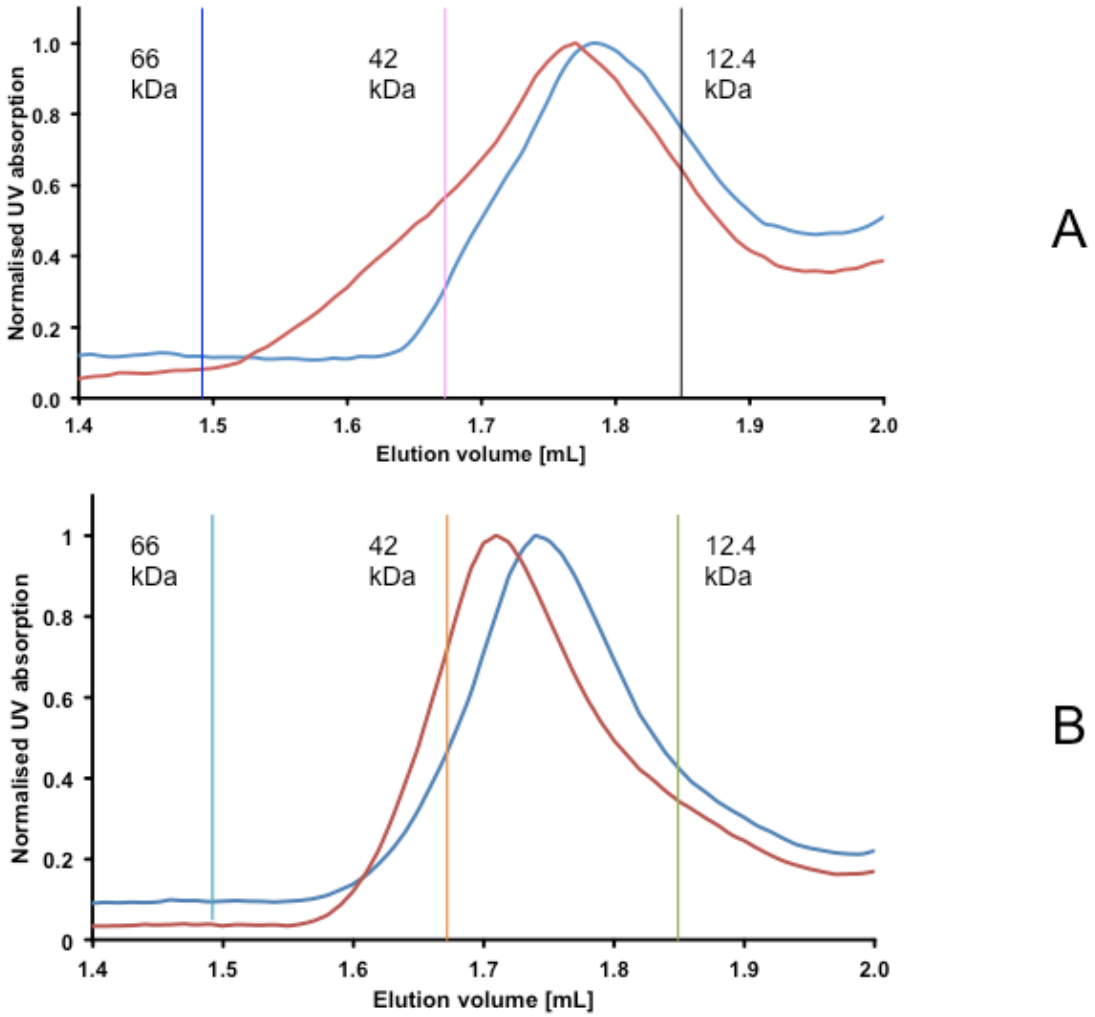

Figure 27: Analytical SEC of HlyB NBD wild type and H662A mutant from yeast. The experiments were performed in a buffer containing 50 mM malonate, 100 mM sodium acetate, 5% glycerol and pH 5.8. ATP was present in the solution at a concentration of 1 mM (red line) or not present (blue line). Vertical straight lines denote the elution peak maxima of proteins, used for the calibration of the column. **A:** Mobility of 50 µM HlyB NBD WT (28 kDa), separation via Superdex 200 PC 3.2/30 (*6*). **B:** Elution profile of 50 µM HlyB NBD H662A (28 kDa), separation via Superdex 200 PC 3.2/30.

HlyB NBD from yeast (28 kDa) showed a shift of the peak maximum upon ATP addition (Figure 27 A). The observed shift was rather small, however, the nucleotide addition clearly induced a widening of the peak toward higher

molecular weight, which was confirmed via SDS-PAGE (*6*). The elution profile supported the notion for a dimer formation and for a rapid monomer-dimer equilibrium after nucleotide addition in SEC experiments (*5*). HlyB NBD from *E. coli* showed a similar peak shift under the same experimental conditions (*5*), however the shift was more distinct compared to the yeast protein.

For a more comprehensive characterization of the nucleotide induced dimerization of HlyB NBD from yeast, the mutant HlyB NBD H662A was purified and analyzed. It has been already demonstrated that the homologously expressed H662A mutant is ATPase inactive but it shows a stable dimer in the presence of ATP in SEC experiments (*5*). The H662A mutant, heterologously expressed in *S. cerevisiae*, was examined as the wild type protein above (Figure 27 B). In this case, the addition of 1 mM ATP resulted in a distinct shift of the peak maximum towards a higher molecular weight. This protein mobility indicated the formation of a NBD dimer and it was highly similar to the elution profile of the H662A mutant from *E. coli* (*5*). This high degree of similarity between the SEC properties of the yeast and the bacterial protein indicated that the ATP induced dimerization of HlyB NBD H662A from *S. cerevisiae* does not differ significantly from the NBD mutant from *E. coli*. HlyB NBD H662A from yeast showed slightly different mobility compared to the wild type protein, however the difference was marginal. Furthermore, such difference between the mutant and the wild type protein was also observed for the *E. coli* HlyB NBD (*5*). The reason for this could be minor differences in the hydrodynamic radii between both proteins.

All these results revealed that the purification of HlyB NBD after heterologous expression in *S. cerevisiae* was possible. The biochemical analysis showed minimal differences between the properties of the yeast protein and the *E. coli* protein. This demonstrated that the yeast protein could be applied for the analysis of the intrinsic properties of HlyB NBD. For this purpouse, it was planned to incorporate the photo-caged compound DMNB-L-Ser at specific positions in the polypeptide chain of HlyB NBD.

Before the incorporation of DMNB-L-Ser at a particular position in the polypeptide chain of HlyB NBD, the impact of the according amino acid on the HlyB NBD function was investigated. For that purpose the according amino

acid was mutated to alanine or tyrosine. The resulting mutants were purified and biochemically characterized.

4.4.2 Properties of the S504 mutants of the HlyB NBD from *S. cerevisiae*

Serine 504 is located in the Walker A loop of HlyB NBD and it is not conserved among ABC transporters (*3*). The HlyB NBD structure in Figure 28 and the scheme in Figure 23 B reveal that serine 504 plays an important role in the coordination of ATP. It interacts through its side chain via a single hydrogen bond (2.7 Å) with the γ-phosphate of the nucleotide, which is crucial for the formation of the ATP-bound dimer (*12*). This indicates that a removal of its hydroxyl group could impact ATP hydrolysis.

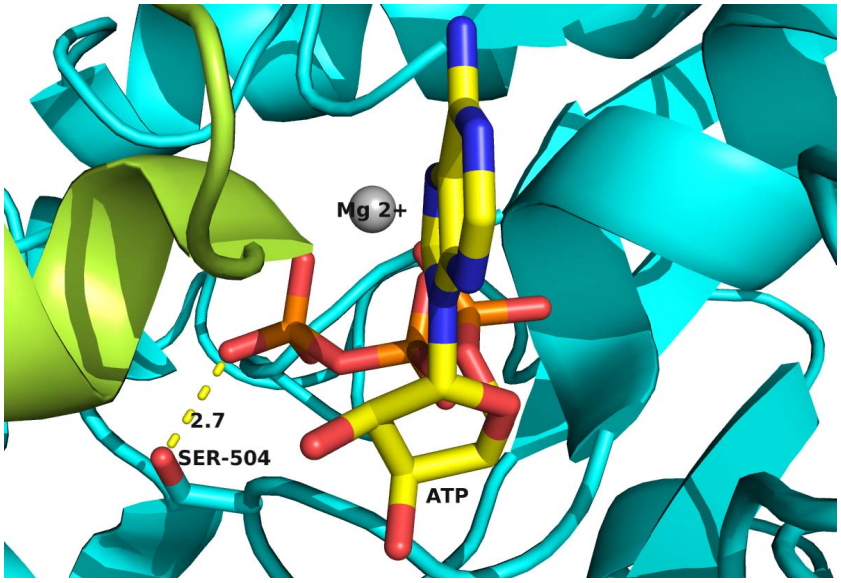

Figure 28: Role of serine 504 in the ATP binding pocket of HlyB NBD. The Walker A motif of the cis-monomer is shown in cyan, the C-loop of the trans-monomer is shown in green. The atoms of the adenine and ribose moiety are shown in the following colors: carbon in yellow; nitrogen in dark blue, oxygen in red. The phosphorus atoms of ATP are colored in orange. The nucleotide and the side chain of S504 are displayed in stick representation. The hydrogen bond (distance cutoff 3.5 Å) between S504 and the γ-phosphate of ATP is shown as dashed line in yellow, the interaction distance (in Å) is revealed next to it. This figure was created from the structure of HlyB NBD H662A, PDB-code 1XEF (*2*).

In fact, it already has been shown that this serine is essential for ATPase activity, however the mutation of S504A did not result in a severe negative influence on the nucleotide binding (*8*). Such an intact nucleotide binding suggested that the S504A mutant retains its ability to dimerize upon addition of ATP. Therefore, serine 504 was selected for DMNB-L-Ser mutagenesis.

The incorporation of the unnatural amino acid at this position would probably inactivate the protein. Before the incorporation Ser504 was replaced with alanine. The resulting S504A mutant was heterologously expressed in *S. cerevisiae*, purified and biochemically analyzed. The aim was to investigate whether the heterologous expression alters the properties of the S504A mutant.

4.4.2.1 Purification of HlyB NBD S504A

Figure 29 shows the results of the HlyB NBD S504A purification. The SDS gel revealed high protein purity after SEC. The mutant protein has the same size as the NBD (positive control) from *E. coli*. The elution profile of SEC displayed one major protein peak containing HlyB NBD S504A with maximum at an elution volume of 11.8 mL. The wild type HlyB NBD from *S. cerevisiae* showed an elution peak maxiumum at a volume of 10.5 mL. This observation indicated that the mutation S504A altered the hydrodynamic radius of HlyB NBD. The protein yield after purification amounted to 0.5 mg/L DO-URA medium. For this mutant no fermentation was performed, because the yield of the protein after the cultivation in shaking flasks and purification was suffucient for its characterization.

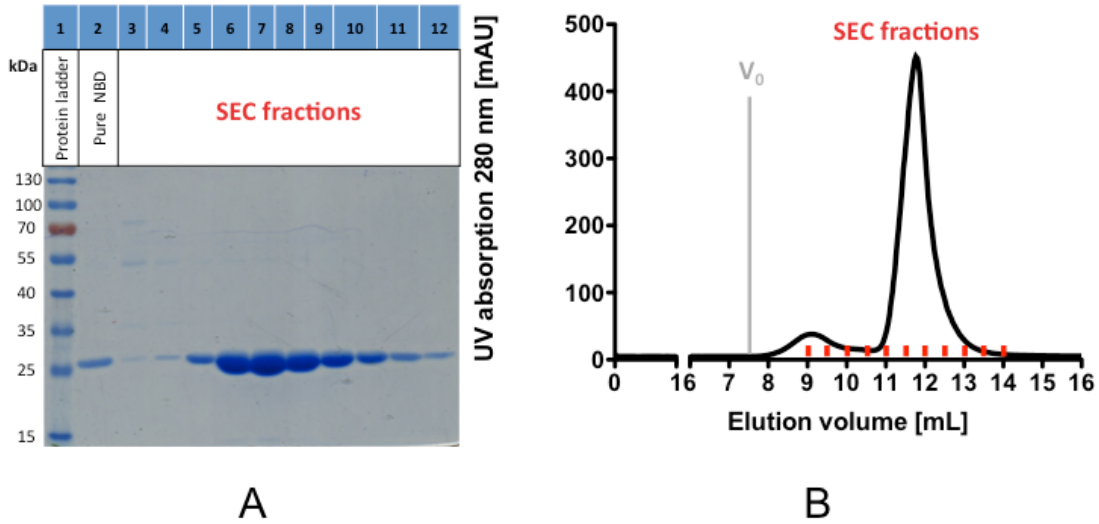

Figure 29: SEC of HlyB NBD S504A from yeast. A: SDS-PAGE analysis of fractions of SEC. The tanalyzed fractions correspond to the major protein peak shown in B. Pure HlyB NBD from *E. coli* was applied as positive control. **B:** Chromatogram of SEC using Superdex75 10/300 (GE Healthcare). The major peak contained pure HlyB NBD S504A. V_0 denotes the void volume of the column. The protein detection was performed via UV absorption at 280 nm.

4.4.2.2 Characterization of the purified HlyB NBD S504A

The mutant protein was examined for its ATPase activity, nucleotide binding and ATP induced dimerization. The ATPase activity assay was performed as a function of time in a buffer containing 100 mM HEPES, 20 % glycerol, 2 mM ATP, 10 mM $MgCl_2$ and pH 7.0. The concentration of the protein was 1.1 mM. The reaction temperature was 22 °C. HlyB S504A did not show any ATPase activity (Figure 30). This was expected because HlyB NBD S504A from *E. coli* showed no activity (*8*). Even after 60 minutes of incubation this mutant protein was not able to hydrolyze considerable amounts of ATP. Having the same concentration of 1.1 µM, the amount of free phosphate at this time-point, produced by HlyB NBD S504A, was only 6% of the amount, produced by the wild type enzyme. This result showed clearly that Ser504 plays an essential role in ATP hydrolysis despite the fact that it is not conserved.

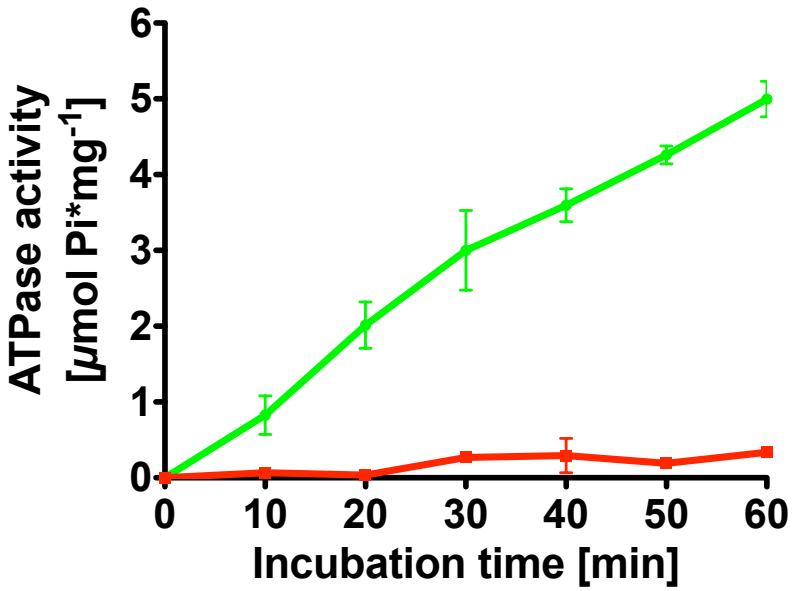

Figure 30: ATPase activity of HlyB NBD and S504A mutant as a function of time at an ATP concentration of 2 mM. The protein concentration was 1.1 µM at 22 °C in buffer containing 100 mM HEPES, 20 % glycerol, 10 mM $MgCl_2$ and pH of 7.0. The ATPase activity of 1.1 µM HlyB NBD S504A (red line) was compared to the activity of 1.1 µM wild type protein (green line).

In the next step the effect of this mutation on the nucleotide binding was examined. The ability of HlyB NBD S504A to bind ATP was analyzed with TNP-ATP as described for the wild type protein (the correction factors Q_1 and Q_2 are shown in the appendix). The curve, resulting from the nucleotide titration is shown in Figure 31. The calculated binding constant of HlyB NBD

S504A (2.4 ± 0.5 µM) was similar to the binding constant of the same mutant from *E. coli* (*8*) as summarized in Table 14.

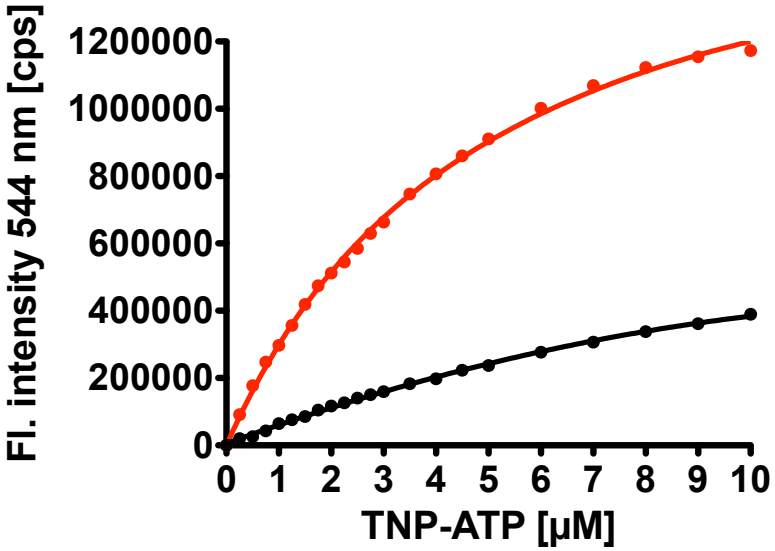

Figure 31: Binding of TNP-ATP to HlyB NBD S504A from yeast. The fluorescence signal, resulting from the TNP-ATP titration to HlyB NBD S504A, is displayed as a red line. The protein concentration was 4 µM. The data of the TNP-ATP titration to the solution with only buffer are shown in black. The fluorescence signal of TNP-ATP at 544 nm was recorded, calculated and fitted as described (*8*), see also "Material and Methods", chapter 3.2.2.7. Cps: counts per second.

Table 14: TNP ATP affinity of HlyB NBD and of the S504A mutant. The measurements were performed as described in "Materials and Methods". The protein concentration during the measurements was held constant 4 µM at 20 °C. The experiments were conducted in the absence of Mg^{2+}.

HlyB NBD	***K_D [µM]***	
	S. cerevisiae	*E. coli* (*8*)
Wild type	0.6 ± 0.2	0.8 ± 0.1
S504A	2.4 ± 0.5	2.1 ± 0.6

Furthermore, the K_D value of the S504A mutant of *S. cerevisiae* was higher than the K_D of the wild type HlyB NBD, expressed in the same organism. This indicated that the mutated amino acid influenced nucleotide binding, however, probably not significantly.

After exploring the nucleotide binding properties, analytical SEC was applied to monitor wether the HlyB NBD S504A mutant forms a dimer in solution in the presence of ATP. These experiments were conducted as already described (*5*). The SEC-buffer contained 50 mM malonate, 100 mM sodium acetate, 5 % glycerol and pH of 5.8. The oligomeric state of HlyB NBD S504A was analyzed with a chromatography column Superdex 75 PC 3.2/30. The

obtained result is displayed in Figure 32. The addition of ATP led to a very small peak shift toward higher molecular weight. The S504A mutant did not show a shift of the peak maximum as observed for HlyB NBD H662A. Therefore, it was concluded that the addition of ATP did not lead to the formation of a stable dimer of HlyB NBD S504A.

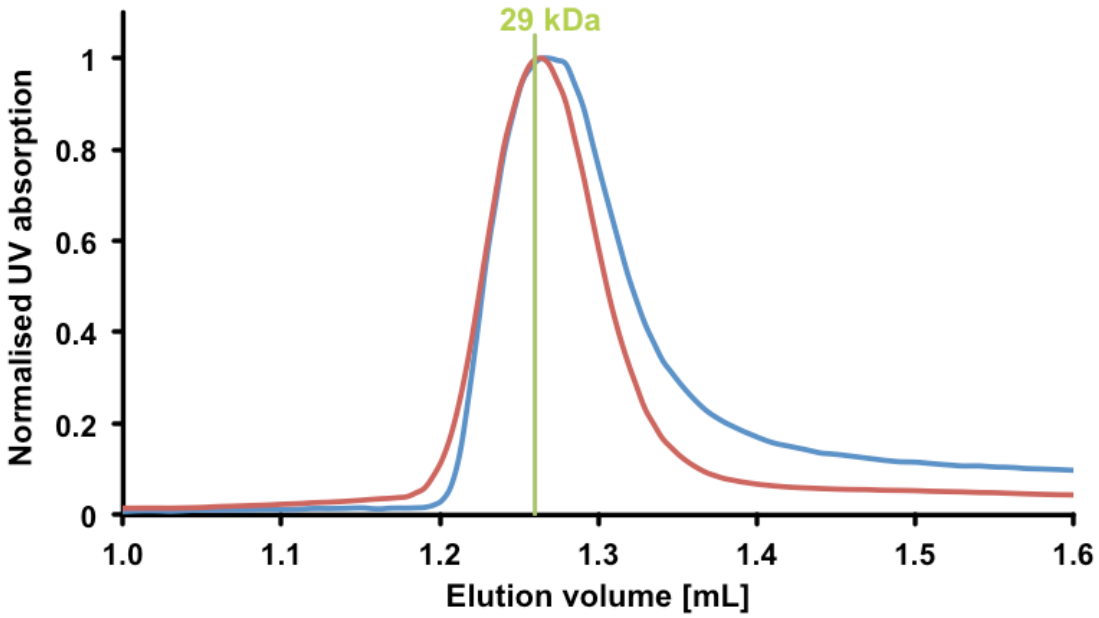

Figure 32: Analytical SEC of the HlyB NBD S504A mutant from yeast in 50 mM malonate, 100 mM sodium acetate, 5% glycerol and pH 5.8. ATP was not present in the solution (blue line) or added to a final concentration of 1 mM (red line). The green line indicates the elution maximum of the marker protein carbonic anhydrase (29 kDa). The analytical SEC was performed via Superdex 75 PC 3.2/30. The UV absorption at 295 nm was used for protein detection. For a better overview, the absorption values were normalised.

In summary (see Table 15), the mutation S504A resulted in an ATPase inactive protein. HlyB NBD S504A retained nucleotide binding, however, the formation of a dimer after ATP addition could not be shown.

Table 15: Comparison of the properties of HlyB NBD wild type (WT) with the mutant S504A.

	HlyB NBD	
Properties	S504A	WT
ATPase activity	-	+
TNP-ATP binding	+	+
Dimer formation	-	+

4.4.2.3 Purification of HlyB NBD S504DMNB-L-Ser from S. cerevisiae

Figure 33 shows the result of the HlyB NBD S504DMNB-L-Ser purification. Two peaks were observed after SEC was performed (Figure 33 B). The analysis of the SEC fractions via SDS-PAGE and Western blot (Figure 33 A) revealed that the minor peak (lanes 8-13) contained the DMNB-L-Ser-labeled HlyB NBD. This conclusion was supported by the observation that the addition of DMNB-L-Ser did result in the expression of full length HlyB NBD, which was shown in “Expression Studies” (Figure 18). The major peak contained aggregates of the NBD and protein impurities, as shown in Figure 33 A, lanes 4-7. The yield of the NBD S504DMNB-L-Ser was 0.06 mg / L YPD medium after fermentation and purification. This yield was lower compared to the yield of the wild type protein (3 mg/L) obtained by the application of the same protocol. This implied that the incorporation of the unnatural amino acid induced a decline of the yield by a factor of 50. The expression of this mutant in shaking flasks resulted in much lower yield and the purification did not deliver pure protein.

The chromatogram of SEC (Figure 33 B) displayed a different elution profile of the DMNB-L-Ser-mutant compared to the NBD S504A (Figure 29 B). The DMNB-L-Ser labeled NBD showed a peak maximum at 10.1 mL, the S504A mutant at 11.8 mL. The only obvious difference between both proteins was the side chains of the amino acid at position 504. Probably the incorporation of the unnatural amino acid results in a different hydrodynamic radius of HlyB NBD S504DMNB-L-Ser, which defines the running behavior during SEC.

4.4.2.4 Photolysis of isolated DMNB-L-Ser

The photolysis of the isolated DMNB-L-Ser in solution has been analyzed before the exploration of the properties of the DMNB-L-Ser labeled HlyB NBD. 110 µM DMNB-L-Ser was analyzed in two solvents: PBS and an acetonitrile/water mixture (2/1). The photolysis in PBS buffer was performed as a positive control because the decaging in this buffer was already

described (*102*). The less polar acetonitrile/water mixture (2/1) was chosen to simulate possible conditions within the HlyB NBD binding pocket. The photolysis was performed as described in “Materials and Methods”. The intensity of the laser was 0.095 J/s. The amount of DMNB-L-Ser was monitored via HPLC. UV-detection of DMNB-L-Ser was performed at 355 nm. The peak integrals were used to calculate the relative amount of the unnatural amino acid. The peak integral of the non-irradiated DMNB-L-Ser was set as 100 %. The results are shown in Figure 34.

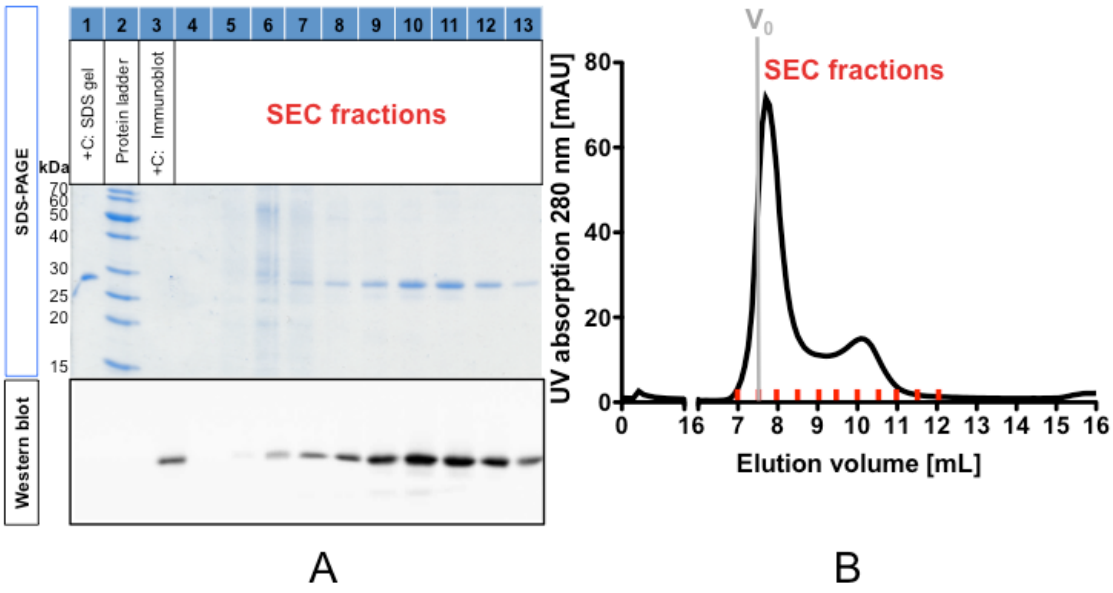

Figure 33: SEC of HlyB NBD S504DMNB-L-Ser and its analysis via SDS-PAGE. A: Analysis of the purity of HlyB NBD S504DMNB-L-Ser after SEC. The middle part shows SDS PAGE analysis of the SEC fractions. The lower part shows Western blot analysis of the same SEC fractions. The fractions containing the NBD mutant fit to the minor peak area in B. Detection with HlyB NBD antibody. +C: positive control (purified HlyB NBD from *E. coli*). **B:** Chromatogram of the SEC of HlyB NBD S504DMNB-L-Ser using Superdex75 10/300. The minor peak contains the labeled HlyB NBD. V_0 denotes the void volume of the column. The proteins were detected via UV absorption at 280 nm.

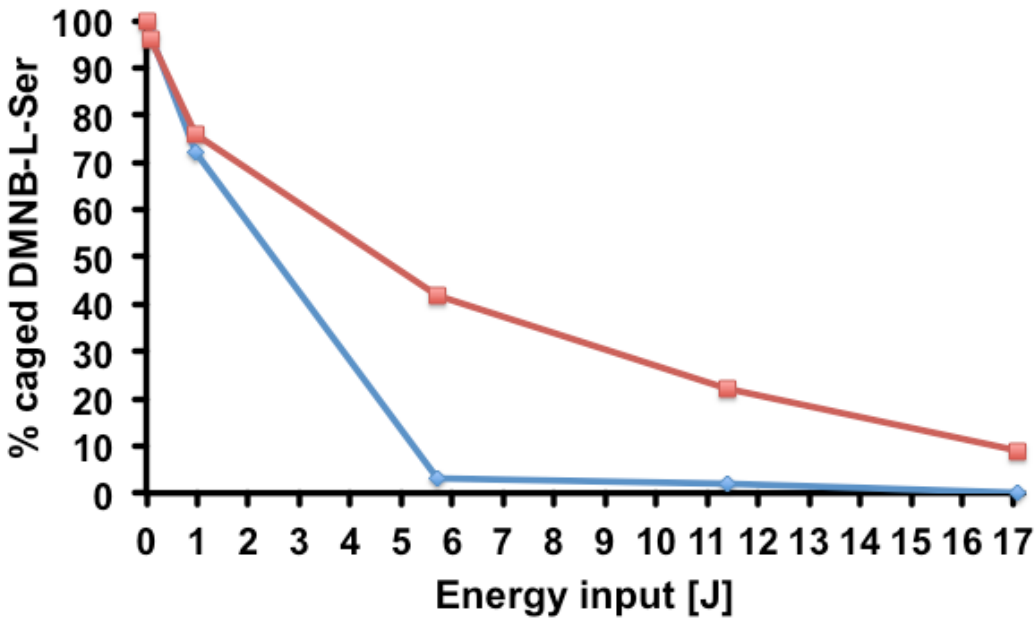

Figure 34: Photolysis of 110 µM DMNB-L-Ser in solution. The experiment was performed at 22 °C in PBS buffer (red line) or in acetonitrile/water mixture (2/1, blue line). The intensity of the laser was 0.095 J/s. The irradiation of the samples was performed for 0 s (0 J), 1 s (0.095 J), 10 s (0.95 J), 60 s (5.75 J), 120 s (11.4 J) and 180 s (17.1 J). The amount of DMNB-L-Ser was monitored via UV-detection (wavelength 355 nm) with HPLC. For the HPLC analysis a RP-18 Merck-column (125x4 mm) with silica based 5 µm particles (10 nm pore size) was applied (product code: LiCrospher 100 RP-18, 5 µm, LiChroCart 125-4). The non-irradiated samples were set as 100 %. The elution of the samples (110 µM, 100 µL injection) was performed via a linear methanol-gradient, which is described in “Matherials and methods”.

The results revealed that the decaging of DMNB-L-Ser is possible in PBS buffer (Figure 34, red line) as well as in the less polar acetonitrile/water mixture (Figure 34, blue line). In both cases the increase of the energy input led to a decrease of the amount of the caged compound. Interestingly, the efficiency of the photolysis differed in both solvents. 5.7 J (60 s) irradiation in acetonitrile/water mixture led to a complete decaging (97 %) of the unnatural amino acid. The same energy input in PBS buffer resulted in a photolysis of 58 % of DMNB-L-Ser. Even the input of 17.1 J (180 s) did not lead to a complete decaging in PBS. This suggested that in a more polar environment the decaging of this unnatural amino acid was less efficient. This indicated that the photolysis of DMNB-L-Ser might be more efficient when the amino acid is located in the binding pocket of the protein and less efficient when DMNB-L-Ser is incorporated at positions in the NBD, which are rather exposed to the polar solvent.

4.4.2.5 Characterization of the purified HlyB NBD S504DMNB-L-Ser

After the incorporation of the unnatural amino acid, the HlyB NBD S504DMNB-L-Ser was explored for its ability to hydrolyze ATP after irradiation with light. The aim was to examine wether the light irradiation led to decaging and reactivation of the DMNB-L-Ser-labeled HlyB NBD. This experiment was performed in two separate steps. In the first step the labeled protein was irradiated with laser light of a wavelength of 355 nm. In the second step the irradiated protein was analyzed for its ability to hydrolyze ATP.

The exposure of HlyB NBD S504DMNB-L-Ser to laser light was performed in accordance with the photolysis tests of the isolated DMNB-L-Ser (Figure 34). The only difference was that during irradiation the protein was in a buffer containing 100 mM CAPS, 20 % glycerol, 10 mM DTT and pH 10.4 because of its high stability in this buffer. The duration of the irradiation was 60 s, the light intensity was 0.34 J/s. As a control experiment, wild type HlyB NBD was also exposed to laser light.

The ATPase activity of the irradiated protein was monitored as a function of time at a constant temperature (22 °C), constant protein concentration and constant ATP concentration of 2 mM (see “Materials and Methods”, chapter 3.2.2.6). HlyB NBD S504DMNB-L-Ser has been diluted in the ATPase buffer shortly before the start of the ATPase assay. The assay was performed in a buffer containing 100 mM HEPES, 20 % glycerol at pH of 7.0.

Figure 35 shows the results of the ATPase assay after light irradiation of HlyB NBD S504DMNB-L-Ser. Its concentration was 2.4 µM. This concentration was higher than the concentration of wild type protein (1.1 µM), used routinely in ATPase assays. The reason was the assumption that the light irradiation would not lead to a full recovery of the ATPase activity compared to the wild type protein (*101*). The higher protein concentration should result in an ATPase signal, which is high enough for detection due to a reasonable signal-to-noise ratio. The wild type protein was also subjected to a laser light irradiation with an energy input of 270 J. The irradiated protein mutant did not show ATPase activity after the energy input (Figure 35 A, blue line). The ATPase activity of the wild type protein (Figure 35 A, black line) was not influenced by the light irradiation. This indicated that the light irradiation was

not the reason for the unsuccessful reactivation of the S504DMNB-L-Ser mutant. Nevertheless the experiment did not reveal wether the unsuccessful reactivation was a result of a failed decaging, an irreversible protein inactivation because of the modification within the essential Walker A motif or due to toxic byproducts generated during the decaging (*73, 138, 139*).
These results proved that the purification of HlyB NBD S504DMNB-L-Ser from *S. cerevisiae* was possible. The incorporation of DMNB-L-Ser at position 504 inactivated the protein as expected (*8*). However, it was not possible to restore the protein activity after irradiation with light.

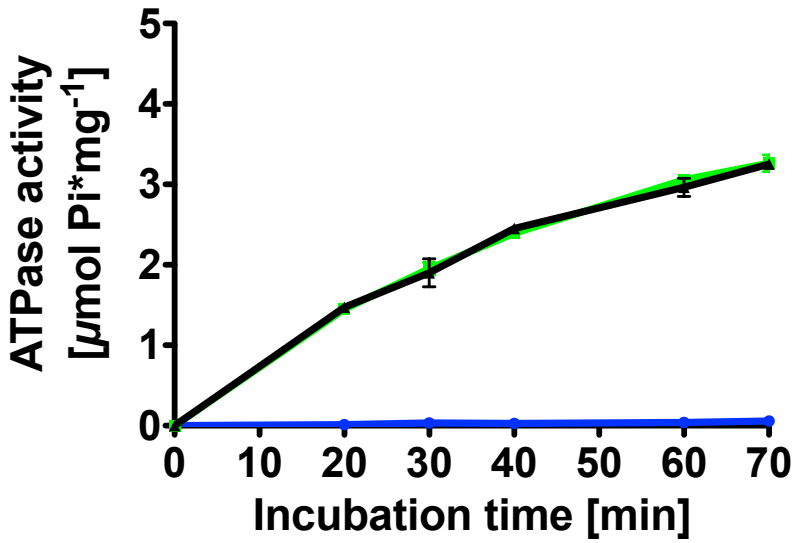

Figure 35: ATPase activity of 2.4 µM HlyB NBD S504DMNB-L-Ser (blue line) as a function of time after 1 min (20.4 J) laser irradiation. The light illumination was performed in a buffer containing 100 mM CAPS, 20 % glycerol, 10 mM DTT, pH 10.4 at room temperature. The ATPase assay was conducted in a buffer containing 100 mM HEPES, 20 % glycerol, 2 mM ATP and pH 7.0 at 22 °C. For comparison, the ATPase activity of the wild type protein is shown: black line – wild type NBD before illumination, green line – wild type protein after exposure to laser light (20 min, 270 J).

4.4.3 Properties of the S607 mutant of the HlyB NBD

Serine 607 resides in the signature motif of HlyB NBD. It is highly conserved and plays an important role in the formation of the composite dimer (*2*). The interaction scheme in Figure 23 B and the binding pocket of HlyB NBD in Figure 36 show how serine 607 is involved in the nucleotide binding. The side chain coordinates the γ-phosphate of ATP via its hydroxyl group by two hydrogen bonds. In the HlyB NBD composite dimer structure (*2*) these represent the majority of the interactions with the γ-phosphate coming from

the C-loop. Therefore, this serine should be essential for the ATPase activity by stabilizing the dimer after ATP binding. The mutation of this residue against cysteine, for example, resulted in an abolished ATPase hydrolysis of OpuAA (*140*). Furthermore, it has been shown experimentally that the mutation of this residue in HlyB (S607A) (*141*) and in HisP (S155F) (*142*) leads to an abolishment of the ATPase activity without disruption of the nucleotide binding. In the DNA repair protein Rad50 (class 2 ABC ATPase) the exchange of the C-loop serine against arginine resulted in a protein unable to form a dimer (*143*). These results made serine 607 a candidate for an exchange against DMNB-L-Ser. This mutant should be able to bind ATP, but not to hydrolyze it. Based on the structural analysis (Figure 36) and data from Rad50 and OpuAA, HlyB NBD S607DMNB-L-Ser might not be able to form a dimer after nucleotide binding. Therefore, this mutant could enable the trapping of HlyB NBD as an ATP bound monomer in its ATP hydrolysis cycle.

4.4.3.1 Purification of the HlyB NBD S607A from E. coli

Protein production and purification of HlyB NBD S607A from *E. coli* cells was performed as described (*115*). The results of a typical purification are displayed in Figure 37. The chromatogram displayed a single symmetrical peak of HlyB NBD S607A. This indicated a homogeneous protein preparation. The SDS-PAGE analysis (Figure 37 A) of the SEC fractions (Figure 37 B) revealed that the protein preparation was pure apart from minor impurities in one of the fractions (Figure 37 A, lane 4). This fraction was not used in the functional characterization of this protein.

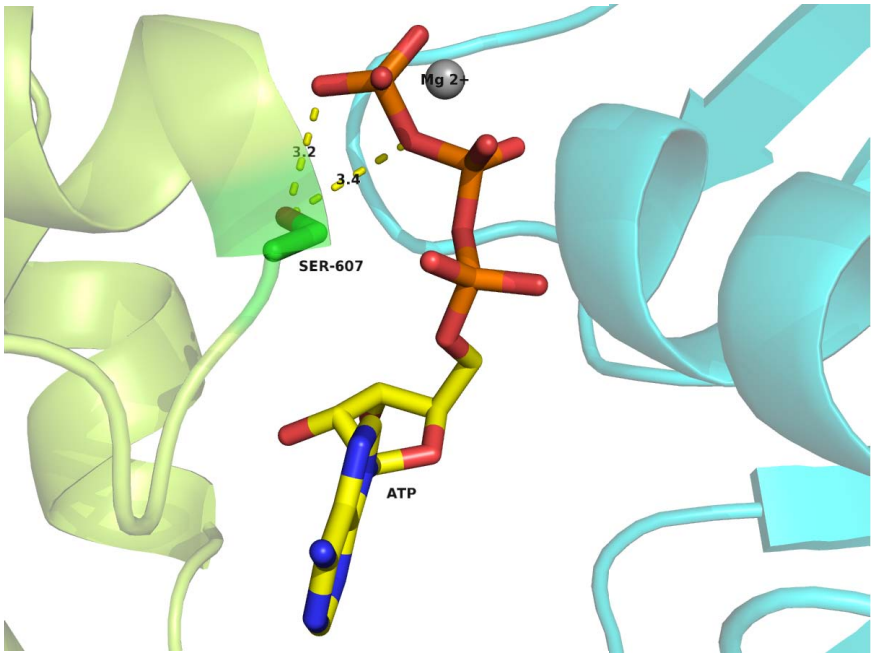

Figure 36: Influence of serine 607 on the ATP binding within the HlyB NBD composite dimer. One NBD monomer is colored in green, the other one is colored in cyan. S607 and ATP are shown in stick representation. Magnesium is displayed as a grey sphere. The oxygen atoms are colored in red, the nitrogen atoms in dark blue. The carbon atoms of S607 are colored in green, the carbon atoms of ATP are colored in yellow. The phosphorus atoms of ATP are colored in orange. Yellow dashed lines represent hydrogen bonds between the side chain of S607 and ATP (distance cutoff of 3.5 Å). The numbers next to the dashed lines reveal the length of the interaction distances in Å. The picture was modified after the crystal structure of HlyB NBD H662A (*2*), PDB code 1XEF.

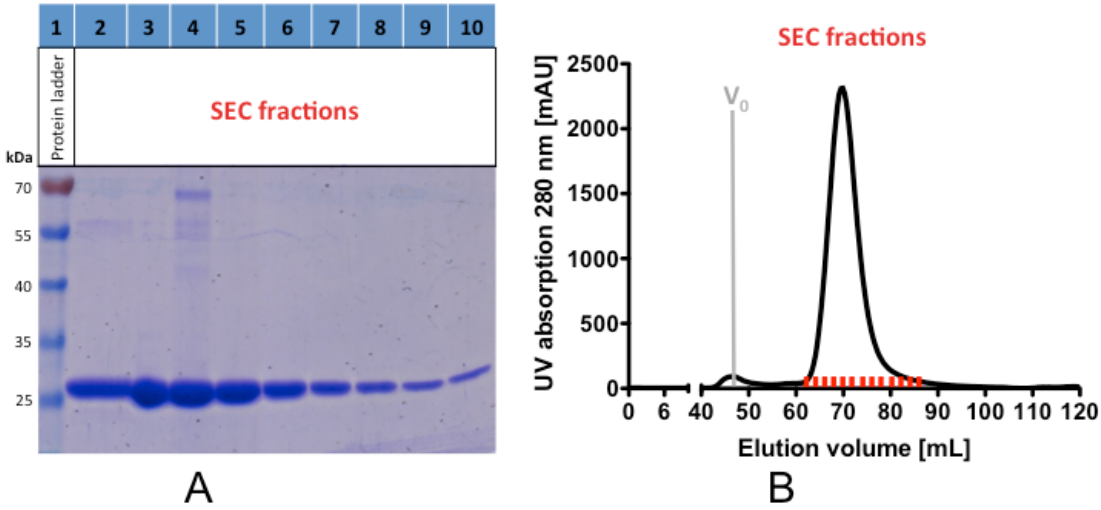

Figure 37: SEC of HlyB NBD S607A from *E. coli* cells. A: SDS-PAGE analysis of the peak fractions of SEC (B). On the left gel side the protein ladder is shown. **B:** Chromatogram of SEC of HlyB NBD S607A. The protein of interest eluted in a single symmetrical peak with a maximum at 70 mL elution volume. V_0 denotes the void volume of the column. The protein detection was performed via UV absorption at 280 nm. A Superdex 75 16/60 prep grade column (GE Healthcare) was used

4.4.3.2 Characterization of the purified HlyB NBD S607A from E. coli

The ability of HlyB NBD S607A to hydrolyze ATP was analyzed as a function of time as described in “Materials and Methods”, chapter 3.2.2.6. Compared to the wild type protein, the activity of the mutant was extremely low. This result demonstrated that the mutation S607A led to an inactivation of the protein. This experiment revealed that the hydroxyl group of the side chain of serine 607 is essential for the function of the isolated HlyB NBD (Figure 38).

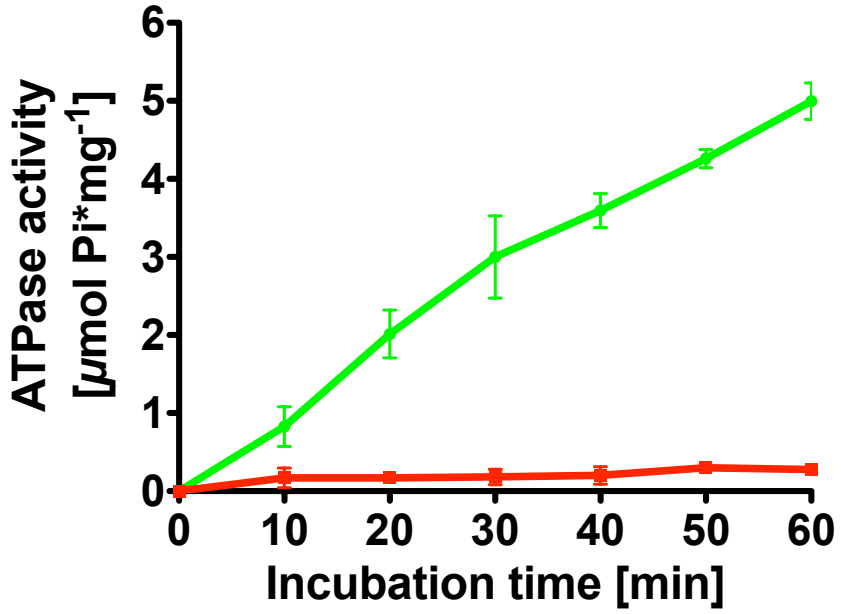

Figure 38: ATPase activity of HlyB NBD S607A from *E.coli* (in red) as a function of time. The experiment was performed at 22 °C in a buffer containing 100 mM HEPES, pH 7.0, 20 % glycerol, 2 mM ATP and 10 mM $MgCl_2$. The ATPase activity of HlyB NBD S607A is shown in red. Its concentration was 3.6 µM. As a green line the ATPase activity of wild type HlyB NBD from *S. cerevisiae* is presented.

Subsequently, analytical SEC was performed to investigate the oligomerization behavior of HlyB NBD S607A when ATP is present in the solution. Compared to the nucleotide-free solution (Figure 39, blue line), the ATP addition did not induce a shift in the protein elution profile towards lower elution volume (Figure 39, red line), which would indicate a dimerization. This result suggested that HlyB NBD S607A was not able to form a stable dimer in a solution upon nucleotide addition.

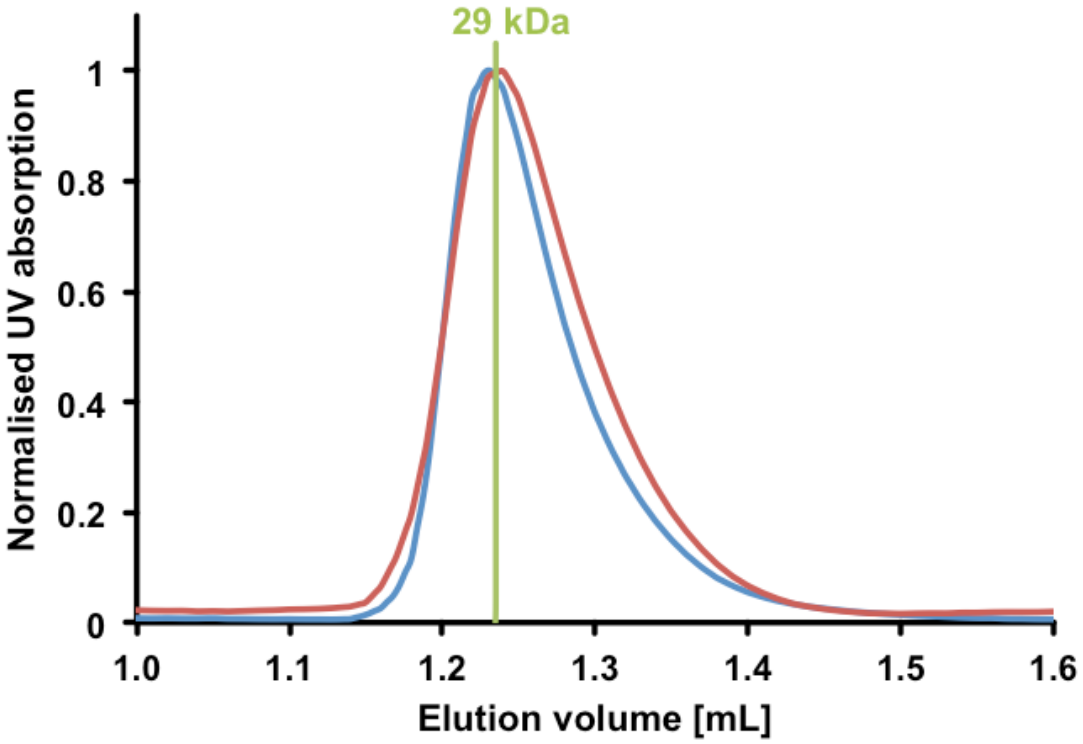

Figure 39: Analytical SEC of HlyB NBD S607A from *E. coli*. The enzyme concentration amounted to 50 µM. The SEC was performed at 4 °C in a buffer containing 50 mM malonate, 100 mM sodium acetate, pH 5.8. ATP was not present in the solution (blue curve) or added to a final concentration of 1 mM (red curve). The green line indicates the elution maximum of the marker protein carboanhydrase (29 kDa). A Superdex75 3.2/30 column (GE Healthcare) was used. The UV absorption at 295 nm was used for protein detection. For better overview the absorption values were normalized.

The experimental results discussed above did not answer the question wether the S607A mutation had an impact on the nucleotide binding. A TNP-ATP binding experiment was performed to examine the binding properties of the NBD S607A mutant (the calculated correction factors Q_1 and Q_2 are shown in the appendix). The result is summarized in Figure 40. The nucleotide titration indicated a binding of TNP-ATP to HlyB NBD S607A (Figure 40, displayed in red). A value of 1.3 ± 0.2 µM was calculated for the dissociation constant of the protein. This K_D was slightly higher than the K_D of the wild type protein from *E. coli* (0.8 µM (*8*)). This indicated that the S607A mutation did not influence the nucleotide binding significantly.

These results indicated that the mutation S607A blocks the ability of HlyB NBD to hydrolyse ATP without abrogation of the nucleotide binding. A dimer formation after the ATP addition was not detected. This suggested that this mutation could be used for trapping of the protein at the stage of an ATP-bound monomer within the ATP hydrolysis cycle.

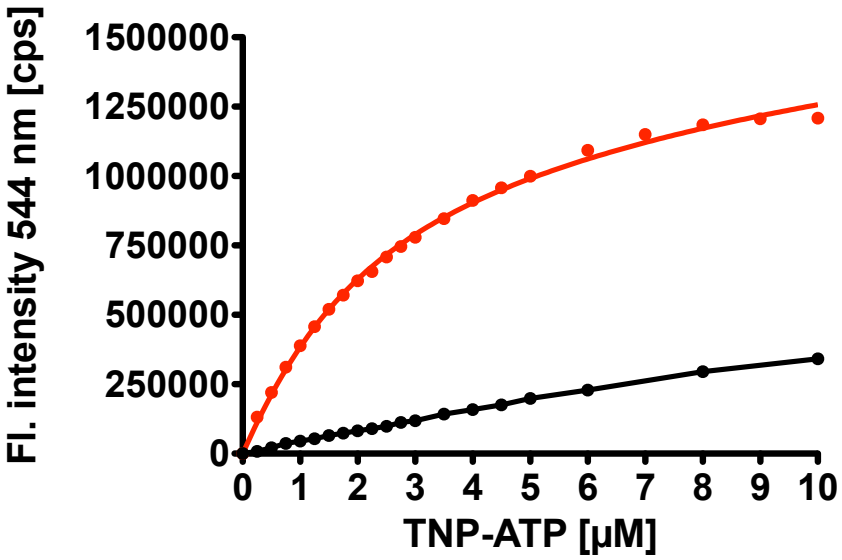

Figure 40: Nucleotide binding study of HlyB NBD S607A from *E. coli*. The concentration of the protein was 4 µM. The experiment was performed at 20 °C in a buffer containing 100 mM HEPES, 20 % glycerol, pH 7.0. The fitted fluorescence signal of TNP-ATP at 544 nm emission is shown as a red curve. The data of the TNP-ATP titration to the solution with only buffer are shown in black. Data was calculated and fitted as described (*8*), see also chapter 3.2.2.7. CPS: counts per second.

4.4.3.3 Purification of the HlyB NBD S607A from S. cerevisiae

The mutant HlyB NBD S607A was expressed and purified as described in "Materials and Methods". The results are presented in Figure 41. The SDS-PAGE analysis of the IMAC (Figure 41 A) revealed that none of the analyzed fractions contained pure HlyB NBD S607A. The comparison of the content of these fractions with the positive control (pure HlyB NBD, Figure 41 A, lane 4) demonstrated that only the fractions, which eluted with 100 mM imidazole, clearly contained protein with the size of HlyB NBD. However, these fractions contained a lot of impurities. This showed that the yield of HlyB NBD S607A after heterologous expression in yeast and purification by IMAC was extremely low.

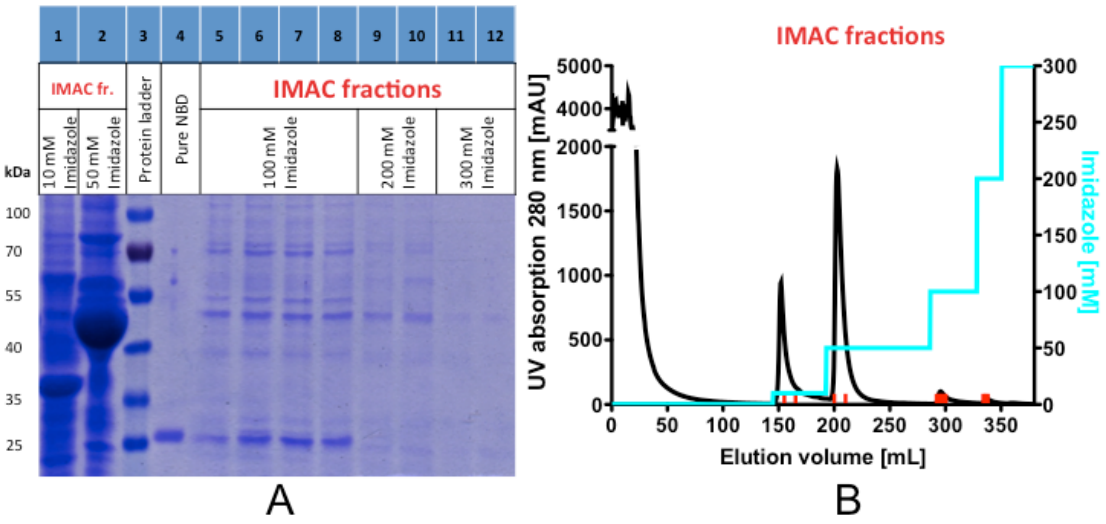

Figure 41: Purification of HlyB NBD S607A from *S. cerevisiae*. A: SDS-PAGE analysis of the major peak fractions of IMAC (B). On the left gel side is the protein ladder. Pure HlyB NBD was used as positive control. **B:** Chromatogram of the IMAC of HlyB NBD S607A. The protein was eluted with imidazole via step gradient, which resulted in different protein peaks. The imidazole concentrations are colored in cyan blue and are plotted on the right y-axis. The protein detection was performed via UV absorption at 280 nm. This UV signal is plotted on the left y-axis. A HiTrap Zn^{2+}/IDA Chelating column (GE) was used. The collected and analyzed fractions of the different protein peaks are colored in red.

When the mutant HlyB NBD S607A was expressed in *E. coli*, the isolation of highly pure protein was possible and the yields were sufficient for its biochemical characterization. However, when the same mutant was expressed in *S. cerevisiae* the protein yield was low, which was unexpected. It was not clear how the S607A mutation influenced protein expression. Furthermore, the similarity between alanine and DMNB-L-Ser was too low. On the other side DMNB-L-Ser was only obtainable on custom synthesis order and its quantity was not unlimited. Therefore, tyrosine, which is more similar to DMNB-L-Ser, was applied in the next experiments to examine whether a certain amino acid of HlyB NBD is suitable for an exchange with DMNB-L-Ser.

4.4.4 Properties of the HlyB NBD S506Y mutant

The non conserved serine 506 is located in the Walker A motif. From the structure of the dimeric HlyB NBD (Figure 42) and from the scheme in Figure 23 B the influence of this amino acid within the protein binding pocket can be estimated. Both, the nitrogen of the S506-main chain and the oxygen from the side chain interact with the β-phosphate of ATP via a hydrogen bond (Figure

42). Furthermore, the nitrogen of the S506-main chain interacts with the α-phosphate of ATP via a van der Waals interaction.

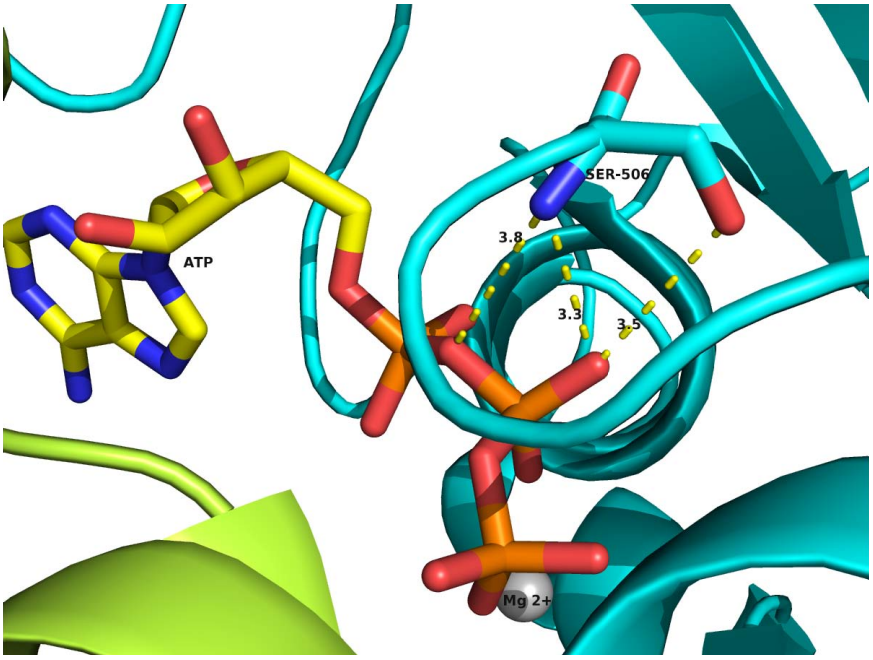

Figure 42: Influence of S506 on ATP binding in the HlyB NBD dimer. The protein monomers are displayed as a cartoon, one monomer is colored in green, the other one in cyan. The magnesium ion is presented as a grey sphere. Serine 506 and the ATP molecule are shown in stick representation. The oxygen atoms are colored in red, the nitrogen atoms in dark blue. The carbon atoms of the S506-cide chain are colored in cyan blue, the carbon atoms of ATP are colored in yellow. The phosphorus atoms of ATP are colored in orange. The dashed lines represent hydrogen bonds (distance cutoff 3.5 Å) and van der Waals interactions (distance cutoff 4.0 Å) between S506 and ATP. This figure is adapted from the X-Ray structure of HlyB NBD H662A (*2*), PDB code 1XEF.

This structural analysis suggested that a replacement of the hydroxyl group of the side chain at position 506 by a mutation of the serine would impact the coordination of ATP by HlyB NBD. As a consequence, this could inhibit the capability of HlyB NBD to hydrolyze ATP. This analysis implied that the incorporation of DMNB-L-Ser at position 506 would influence the ability of HlyB NBD to coordinate ATP and hydrolyze it due to the different chemical properties of the hydroxyl group and the DMNB moiety. Furthermore, the side chain of DMNB-L-Ser differs from the side chain of natural serine in its steric properties. The incorporation of a much bulkier side chain like DMNB could have a massive impact on the protein conformation within the binding pocket.

4.4.4.1 Purification of the HlyB-NBD S506Y from E. coli

Figure **43** summarizes the results of the HlyB NBD S506Y purification (*144*). For SEC of this NBD mutant (Figure **43** B) a Superdex 75 16/60 prep grade (GE) was employed. This is the reason for the different elution profile of HlyB NBD S506Y compared to the wild type protein and the other mutants. SEC (Figure **43** B) resulted in two well separate peaks. According to the data file of the chromatoghraphy column the first peak (elution maximum at 42 mL) contained aggregates (*145*). Furthermore, the peak with an elution maximum at 63 mL corresponded to a molecular weight of approx. 30 kDa. The analysis via SDS-PAGE (Figure **43** A) strongly supported the notion that this peak contained HlyB NBD S506Y. This experiment also showed that the eluted protein was highly pure. The obtained protein yield of 1 mg protein/L cells was 10 % of the wild type protein (10 mg / L cells (*115*)). However this amount was sufficient for the functional studies. The HlyB NBD S506Y protein was concentrated up to 11.6 mg/mL and stored at 4°C for further experiments.

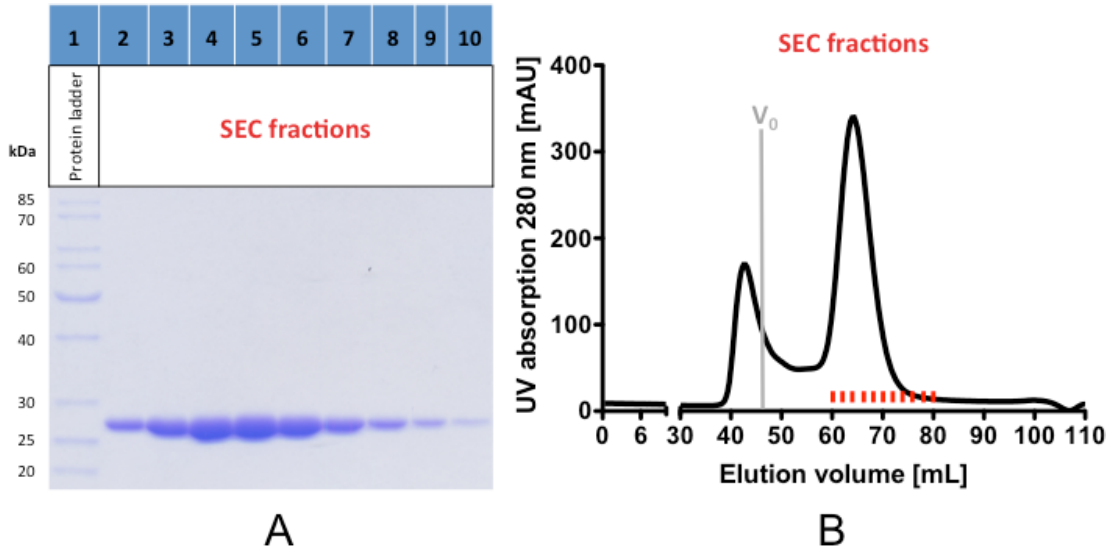

Figure 43**: SEC of HlyB NBD S506Y from *E. coli.* A:** SDS-PAGE analysis of the protein fractions of SEC (B). These fractions originated from the peak in B with maximum at 63 mL elution volume. **B:** SEC of HlyB NBD S506Y. The major peak with elution maximum at 63 mL contained HlyB NBD S506Y. The minor peak with elution maximum at 42 mL contained aggregates. V_0 denotes the void volume of the column. The protein was detected via UV absorption at 280 nm.

4.4.4.2 Characterization of the purified HlyB NBD S506Y

The ability of the HlyB NBD S506Y mutant from *E. coli* to hydrolyze ATP was analyzed (*144*). The result of a typical ATPase measurement is shown in Figure 44. Over time no significant increase of the free phosphate in the ATPase sample of the S506Y mutant could be detected. This result showed that serine 506 is essential for the ability of HlyB NBD to hydrolyze ATP.

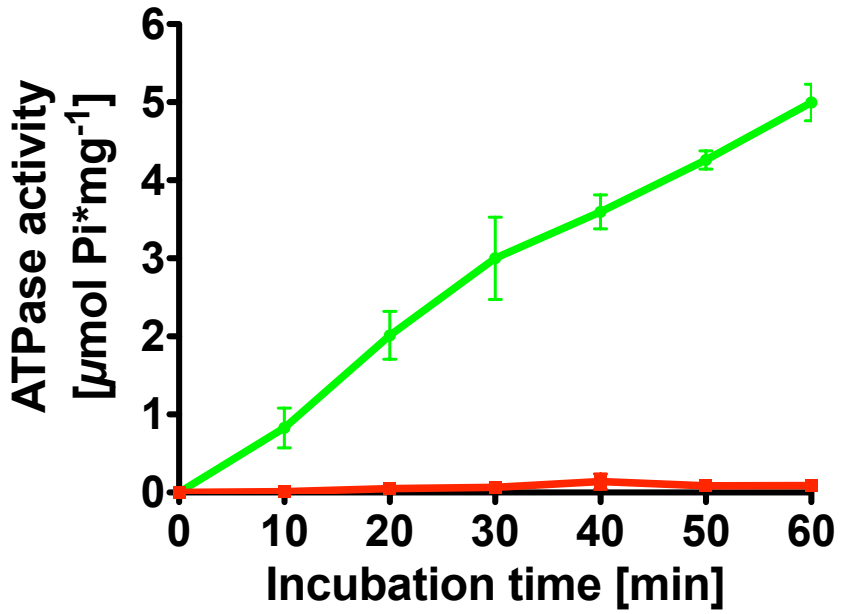

Figure 44: ATPase activity of HlyB NBD S506Y from *E. coli*. The activity was tested as a function of time at 22 °C in a buffer containing 100 mM HEPES, pH 7.0, 20 % glycerol, 2 mM ATP and 10 mM $MgCl_2$. The concentration of HlyB NBD S506Y amounted to 3.6 µM. Its ATPase activity is displayed as a red line. For comparison the ability of wild type HlyB NBD to hydrolyze ATP is shown as green line. The concentration of the wild type protein was 1.1 µM.

The next question was how exactly does this mutation inhibit the nucleotide hydrolysis – does it influence ATP binding and / or protein dimerization? To investigate the nucleotide binding, the ability of HlyB NBD S506Y to bind TNP-ATP was explored as described (*8*). The calculated correction factors Q_1 and Q_2 are shown in the appendix. From the TNP-ATP titration to the mutant protein, a binding constant of 0.2 ± 0.08 µM was calculated. This value was lower than the K_D of the wild type enzyme from *E. coli* (0.8 ± 0.1 µM, (*8*)). This result indicated that the mutation S506Y increased the affinity of HlyB NBD towards the nucleotide, which was surprising. The structural analysis (Figure 42) did not provide any evidence of the contribution of Y506 to the increased affinity.

The ability of HlyB NBD S506Y to form a functional dimer after nucleotide binding was analyzed too. For this purpose analytical SEC was applied. The experimental procedures were performed as described (*5*). A typical result from such an experiment is shown in Figure 45.

If a dimer formation upon nucleotide addition occurs, the S506Y mutant should show a peak shift towards higher molecular weight when 1 mM ATP is present in the solution. However, the analytical SEC did not show such a shift in the elution profile of HlyB NBD S506Y after addition of ATP (Figure 45, red curve). This implied that this protein mutant bound the nucleotide, however the ATP binding did not result in dimerization. These results indicated that an incorporation of DMNB-L-Ser at position 506 in the polypeptide chain of HlyB NBD might enable the trapping of HlyB NBD as a nucleotide bound monomer within the ATP hydrolysis cycle.

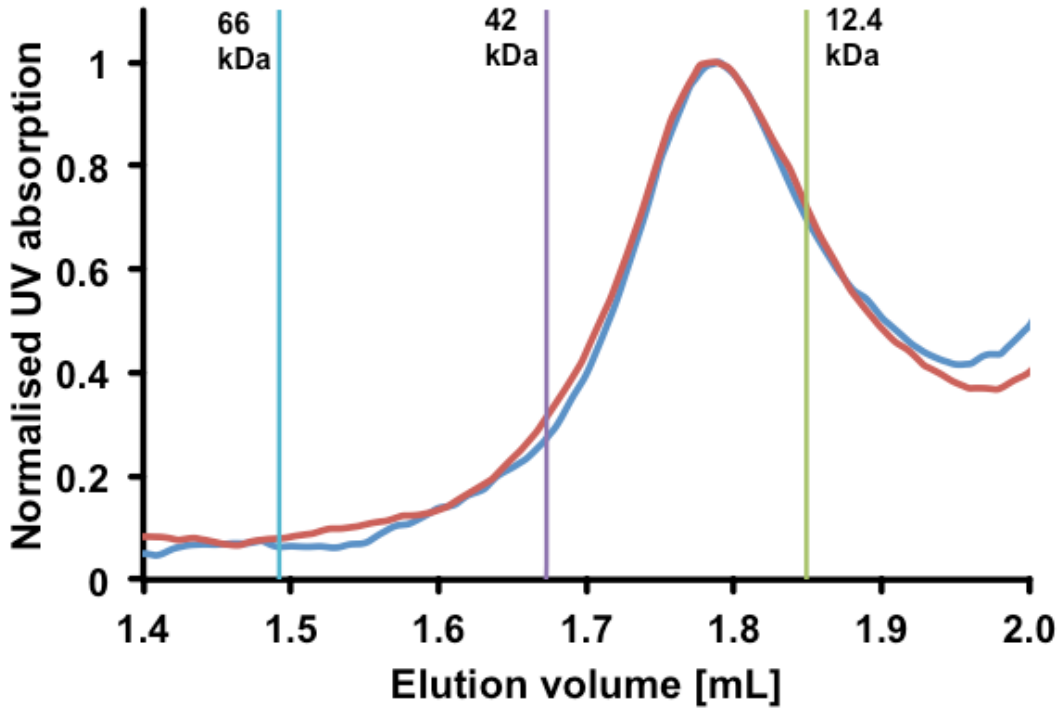

Figure 45: Analytical SEC of HlyB NBD S506Y from *E. coli*. The buffer of this experiment contained 50 mM malonate, 100 mM sodium acetate, 5 % glycerol and pH 5.8. ATP was not present in the solution (blue line) or added to a final concentration of 1 mM. The protein concentration was 68 µM. SEC was performed at 4 °C with a column Superdex 200 PC 3.2/30. UV absorption at 295 nm was used for protein detection. For better overview the absorption values were normalized. As vertical lines the elution maxima of calibration proteins, colored differently, are displayed.

4.4.4.3 Properties of the HlyB NBD S506DMNB-L-Ser from S. cerevisiae

It was not possible to characterize HlyB NBD S506DMNB-L-Ser from yeast because the heterologous expression of this protein in *S. cerevisae* was not successful, as described in “Expression studies of HlyB NBD in yeast”, Figure 21.

4.4.5 Properties of the HlyB NBD S509Y

Serine 509, which resides in the Walker A motif, is highly conserved among ABC transporters and is involved in nucleotide coordination. The schematic overview in Figure 23 B and the structure of the nucleotide bound dimer of HlyB NBD in Figure 46 show how serine 509 is involved in the coordination of ATP.

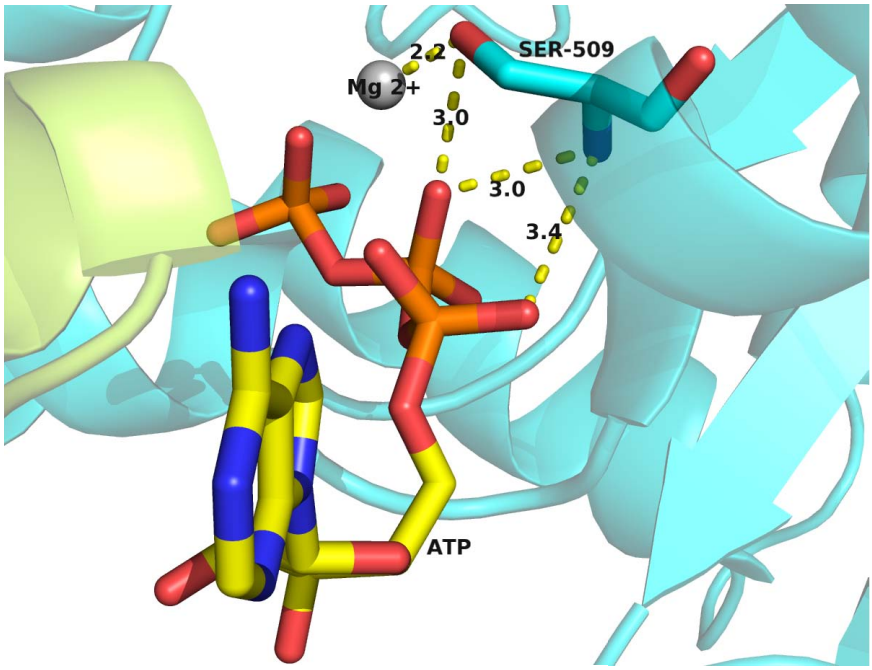

Figure 46: Role of serine 509 within the binding pocket of dimeric HlyB NBD with bound Mg^{2+} and ATP. One monomer is colored in cyan, the other one in green. The atoms of the adenine and the ribose moiety are shown in the following colors: carbon in yellow, nitrogen in dark blue, oxygen in red. The phosphorus atoms of ATP are colored in orange. The nucleotide and the side chain of S509 are displayed in stick representation. The hydrogen bonds (distance cutoff 3.5 Å) between S509 and ATP/Mg^{2+} are shown as dashed lines in yellow, the interaction distances (in Å) are revealed next to them. This figure was modified after the X-ray structure of HlyB NBD H662A (*2*), PDB code 1XEF.

The side chain of this amino acid interacts via hydrogen bonds with the β-phosphate of ATP and with the magnesium ion, while the nitrogen of the main chain coordinates the α- and β-phosphate of the nucleotide via hydrogen

bonds. This implies that S509 plays an important role in ATP binding and highlights the reason for its high conservation among ABC transporters. Non-conservative mutation of this serine to asparagine in HisP resulted in protein inactivation however this HisP mutant retained the ability to bind ATP (*142*). The mutation of the homolog serine in ABCB1 to alanine abolished the ability of the protein to hydrolyze ATP, but the exchange to threonine did not (*146*). However, the nucleotide binding was not impaired. These data, together with the structural analysis, led to the conclusion that the hydroxyl group of the conserved serine in the Walker A motif is essential for the protein activity but not for the ATP binding. Therefore, Ser509 from HlyB NBD was estimated as suitable for an exchange against DMNB-L-Ser. The protein construct still should be able to bind ATP, however it should not be able to hydrolyze it. Before the incorporation of the unnatural amino acid, S509 was mutated to tyrosine, which mimics sterically DMNB-L-Ser and the resulting mutant was characterized (*147*).

4.4.5.1 Purification of the HlyB NBD S509Y

The purification of HlyB NBD S509Y was performed as described (*147*). The result of a purification of this mutant is shown in Figure 47. The chromatogram of SEC displayed a single elution peak with an elution maximum at 18 mL (Figure 47 B). The SDS-PAGE analysis of that peak (Figure 47 A) demonstrated the presence of two additional minor protein bands next to the NBD band (28 kDa) in the elution peak. The positive control on the SDS-gel (Figure 47 A, lane 2) contained a band at the same height (56 kDa) as one of the additional bands in the fractions of the elution peak. This band corresponded to a disulfide dimer of HlyB NBD (*115*). This observation led to the conclusion that this band in the elution fractions of the S509Y mutant represented most probably the dimeric form of the protein. The other additional band (34 kDa) represented a contamination, however compared to the amount of HlyB NBD S509Y its amount was extremely low.

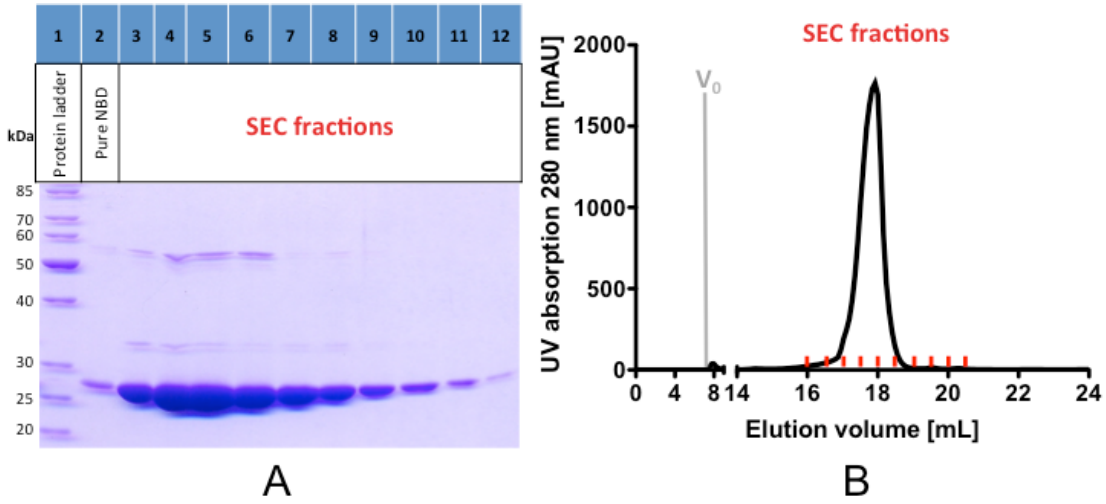

Figure 47: Purification of HlyB NBD S509Y from *E. coli*. A: SDS-PAGE analysis of the elution peak from SEC. The gel lanes contain the SEC fractions, which corresponded to the peak in B with an elution maximum at 18 mL. The major band at the height of 28 kDa was HlyB NBD S509Y, the band at 56 kDa represented probably the dimeric form of the same protein. There was a contaminating protein band at a height of approx. 34 kDa. Pure HlyB NBD was used as positive control. **B:** SEC of HlyB NBD S509Y. The mutant protein eluted as a single peak with maximum at 18 mL elution volume. Superdex 200 10/300 (GE) was used for SEC. V_0 denotes the void volume of the column. The protein detection was performed via UV absorption at 280 nm.

4.4.5.2 Characterization of the purified HlyB NBD S509Y

The ability of HlyB NBD S509Y to hydrolyze ATP was explored as a function of the time at a constant nucleotide concentration (2 mM), constant protein concentration (180 µM) and variable incubation time. As shown in Figure 48, no increase of the amount of free inorganic phosphate could be observed. It was concluded from this result that the mutation S509Y blocked the ability of HlyB NBD to hydrolyze ATP.

The inactivation of the protein by the S509Y mutation raised the question, which step of the nucleotide hydrolysis cycle was inhibited by this mutation. To investigate one of the steps, nucleotide binding, a TNP-ATP binding experiment was performed in the same way as for the mutants described above. In the appendix the correction factors Q_1 and Q_2 are summarized. The analysis implied specific binding of TNP-ATP to HlyB NBD S509Y with a K_D of 1.4 ± 0.5 µM. This value is similar to the K_D value of the wild type protein from *E. coli* (0.8 µM, (*8*)). This revealed that the mutation of the highly conserved serine 509 did not have a substantial impact on nucleotide binding.

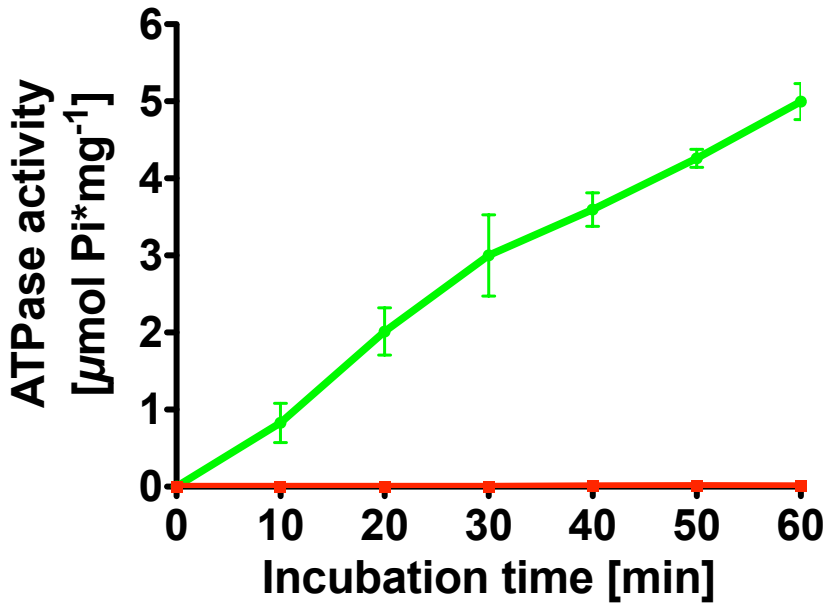

Figure 48: ATPase activity of HlyB NBD S509Y from *E. coli* as a function of time (red line). The experiment was performed at a temperature of 22 °C. The ATPase buffer contained 100 mM HEPES, pH 7.0, 20 % glycerol, 2 mM ATP and 10 mM $MgCl_2$. The concentration of the protein amounted to 180 µM. As a positive control the ATPase activity of wild type HlyB NBD is shown (green line). The concentration of the wild type protein was 1.1 µM

To investigate whether the mutation S509Y has an influence on the ATP induced dimerization of HlyB NBD, analytical SEC in the presence and absence of the nucleotide was applied. The result is shown in Figure 49. In both cases (no ATP or 1 mM ATP) the protein displayed basically the same elution profile. The addition of the nucleotide did not result in a shift of the peak maximum towards lower elution volume. The formation of a second peak was also not observed. This implied that the addition of ATP to the S509Y mutant did not lead to the formation of a HlyB NBD dimer.

All these data revealed that S509 is essential for the ATPase activity of HlyB NBD. The replacement of this amino acid with the bulky tyrosine resulted in an inactive protein. This mutant protein showed nucleotide binding, however, a nucleotide induced dimerization was not detected. These results suggested that position 509 is suitable for the incorporation of DMNB-L-Ser because the mutation of S509 inactivated the protein but did not abolish the nucleotide binding.

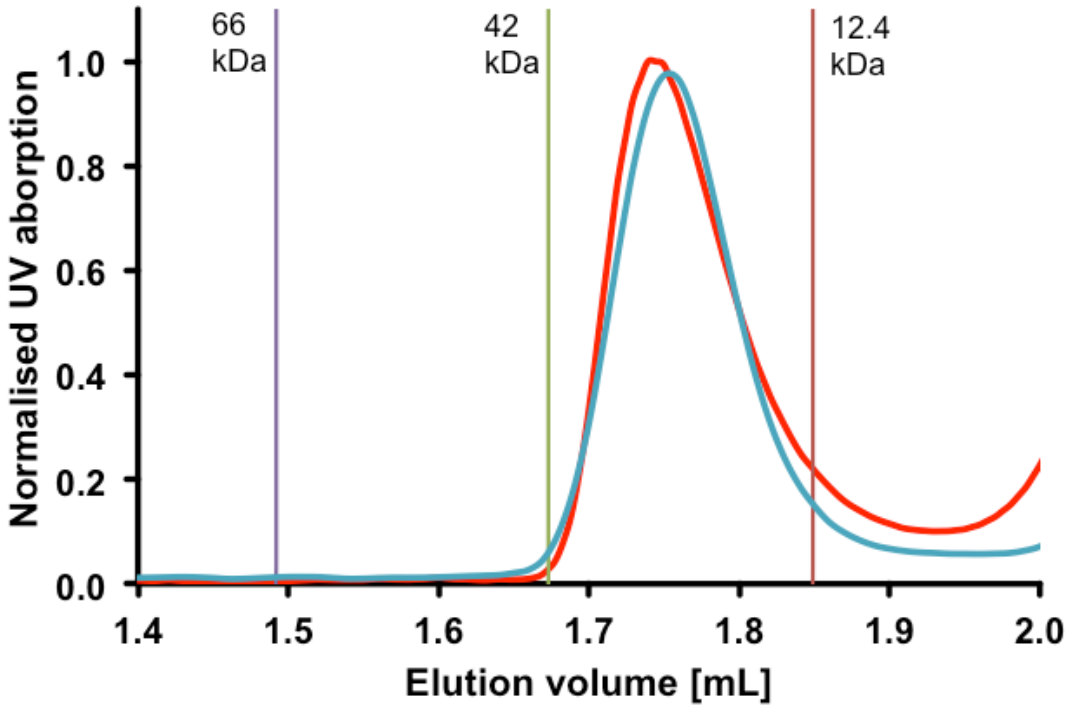

Figure 49: Analytical SEC of HlyB NBD S509Y from *E. coli*. The experiments were performed in a buffer containing 50 mM malonate, 100 mM sodium acetate, pH 5.8. The protein concentration was 50 µM. ATP was added to a final concentration of 1 mM (blue line) or absent from the solution (red line). The protein detection was performed via UV absorption at 295 nm. For better overview, the absorption values were normalized. As vertical lines the elution maxima of calibration proteins, colored differently, are displayed.

4.4.6 Properties of the HlyB NBD T510Y mutant

Threonine 510 is located in the Walker A motif and is conserved among ABC transporters (*19*). The interactions of threonine 510 within the ATP bound dimer of HlyB NBD are shown in Figure 23 B and Figure 50 A. The nitrogen atom from the main chain coordinates the α-phosphate of ATP via a hydrogen bond. The oxygen atom of the side chain interacts via hydrogen bonds with the phosphate moiety and beyond this with tyrosine 477 (Figure 50), which coorinates the adenine ring and is critical for binding of ATP (*148*). In this way the interaction T510–Y477 connects the adenine binding region with the Waker A motif (*2*). This structural analysis suggested that threonine 510 plays an important role for the ability of HlyB NBD to hydrolyze ATP. The mutation of this amino acid to alanine in HisP resulted in a protein, incapable of ATP hydrolysis, however nucleotide binding was not abolished (*142*).

This led to the conclusion that the incorporation of DMNB-L-Ser at position 510 in HlyB NBD might inactivate the protein without disruption of its capability to bind ATP. Thus, the incorporation of DMNB-L-Ser should enable the trapping HlyB NBD in its ATP hydrolysis cycle. The decaging of DMNB-L-Ser should result in a NBD T510S mutant, however this is a conservative exchange. Furthermore, a serine at position 510 should be able to establish the same interactions via the side chain hydroxyl group as threonine (Figure 50). The methyl group of the side chain of Thr510 establishes two van der Waals contacts with the hydroxyl group of the side chain of Tyr477 and with the oxygen of its own main chain. The absence of these interactions in the T510S mutant should not influence negatively the protein conformation because the side chain hydroxyl group of Ser510 would coordinate Tyr477 and the main chain oxygen of Ser510 would be coordinated by interactions with other amino acids (not shown). Therefore, mutation T510S should not abolish the nucleotide binding and the ATPase activity of HlyB NBD.

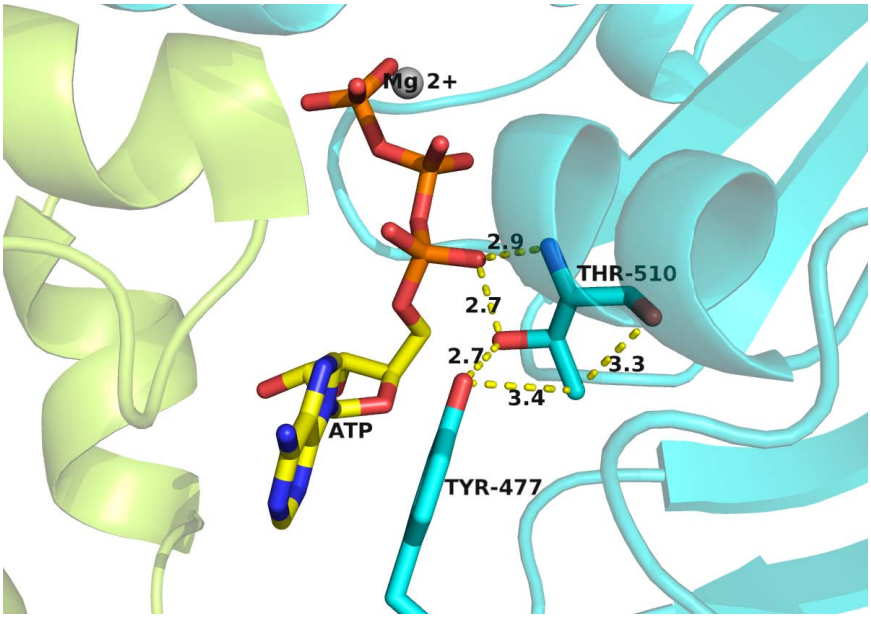

Figure 50: Role of threonine 510 within the HlyB NBD composite dimer. One NBD monomer is colored in green, the other one is colored in cyan. T510, Y510, Y477 and ATP are shown in stick representation. The magnesium ion is displayed as a grey sphere. The oxygen atoms are colored in red, the nitrogen atoms in dark blue. The carbon atoms of Y477 and T510 are colored in cyan. The carbon atoms of ATP are colored in yellow. The phosphorus atoms of ATP are colored in orange. Yellow dashed lines represent hydrogen bonds (distance cutoff 3.5 Å). The numbers next to the dashed lines reveal the length of the interactions distance (in Å). This picture was generated via Pymol from the crystal structure of HlyB NBD H662A (*2*), PDB code 1XEF.

To estimate the impact of the Thr510 mutation on the HlyB NBD properties Thr510 was mutated to tyrosine, which is sterically similar to DMNB-L-Ser and biochemically characterized (*144*).

4.4.6.1 Purification of the HlyB NBD T510Y

HlyB NBD T510Y was purified from *E. coli* as described (*115*). The analysis of the protein purity was performed via SDS-PAGE, which is shown in Figure 51 A. The major band in the lanes containing SEC fractions represented monomeric HlyB NBD T510Y (28 kDa). The band at the height below the 60 kDa marker band (Figure 51 A, lanes 7-11) represented most probably the disulfide dimer (56 kDa) of the NBD (*115*). There was also a faint band at 34 kDa visible, which represented a contaminating protein. However, the amount of this contamination was by far lower than the amount of HlyB NBD T510Y. The chromatogram (Figure 51 B) showed that the protein eluted as single symmetric peak, which indicated a highly homogeneous protein after purification. The yield of pure HlyB NBD T510Y was 8 mg / L expression medium, which was 80 % of the typical yield of the wild type protein (*115*).

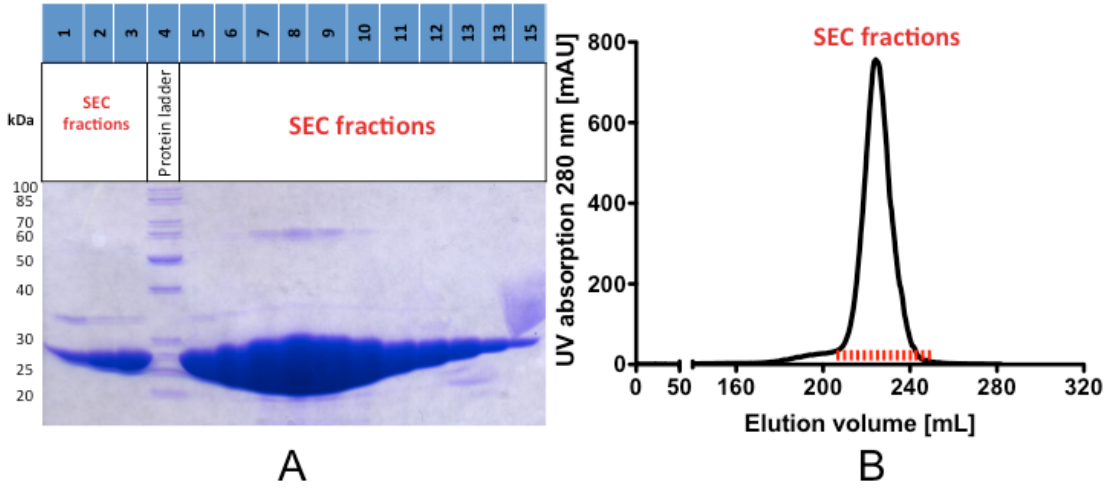

Figure 51: SEC of HlyB NBD T510Y from *E. coli*. A: SDS-PAGE analysis of the fractions from SEC (B). The major band at a height of 28 kDa represents the monomeric protein of interest; the minor band at 56 kDa is most probably the dimer of HlyB NBD T510Y. The faint band at the height of approx. 34 kDa represents a protein contamination. **B:** SEC chromatogram of HlyB NBD T510Y. The major peak with an elution maximum at ca. 220 mL elution volume contains HlyB NBD T510Y, which was analyzed via SDS-PAGE. The red bars show the fractions, which were collected during SEC. This purification step was performed with a Superdex 200 26/60 column (GE Healthcare). The protein detection was done via UV absorption at 280 nm.

4.4.6.2 Characterization of the purified HlyB NBD T510Y

HlyB NBD T510Y was analyzed for its ability to hydrolyze ATP as a function of time (*144*). The result is shown in Figure 52. As revealed, the T510Y mutation did not abolish completely the ability of HlyB NBD to hydrolyze ATP. However, the mutant protein displayed lower level of ATPase activity compared to the wild type NBD. This showed that threonine 510 plays an important but not essential role for nucleotide hydrolysis. This result was surprising, because due to the high conservation of T510, a complete inactivation of the enzym was expected. Thiat result turned this amino acid to an unsuitable candidate for an exchange against DMNB-L-Ser. Due to the sterical similarity between DMNB-L-Ser and tyrosine it is highly probable that the incorporation of DMNB-L-Ser at position 510 would also not inactivate HlyB NBD. This would not allow the isolatation of intermediate states of the ATP hydrolysis cycle of HlyB NBD.

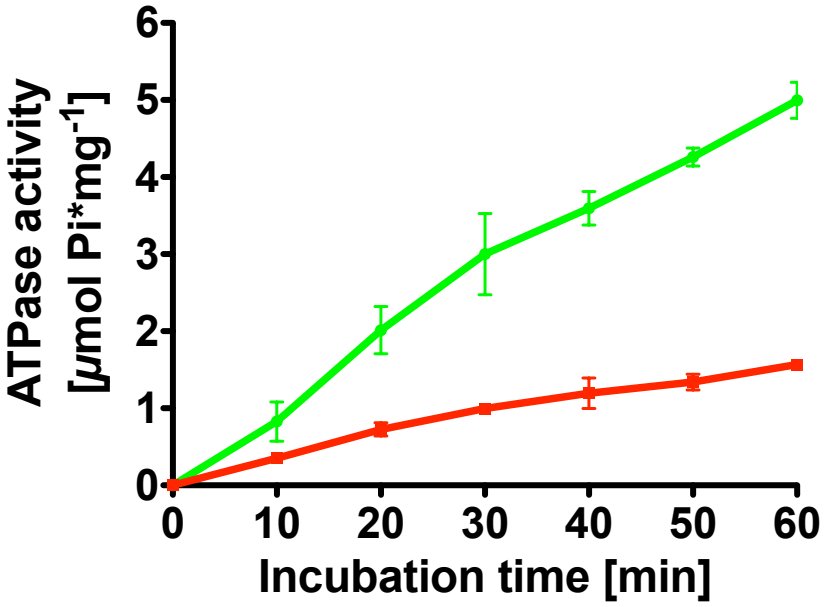

Figure 52: ATPase activity of HlyB NBD T510Y from *E. coli* as a function of time. The ATPase activity of the mutant protein is shown as a red line. The concentration of NBD T510Y was 3.6 µM. The ATPase activity of wild type HlyB NBD (positive control) is shown as a green line. Its concentration was 1.1 µM. The experiment was performed at 22 °C in a buffer containing 100 mM HEPES, pH 7.0, 20 % glycerol, 10 mM $MgCl_2$ and 2 mM ATP.

4.4.7 Properties of the S634 mutants of HlyB NBD from *S. cerevisiae*

Serine 634 resides in the D-loop (*35*). Residues from the D-loop together with residues from Walker B (Walker B/D-loop region, 629-635) and helix 6 (residues 644-645 and 647-648) act as effective hinges during the ATP hydrolysis cycle of HlyB NBD in the transition from the ATP/Mg^{2+}-bound to nucleotide-free state of the protein (*1*). In this way, S634 is involved in the conformational transitions of HlyB NBD during ATP hydrolysis. Furthermore, S634 is important for NBD-NBD communication (*1*). This amino acid is not highly conserved among ABC transporters, however it is represented in the D-loop consensus sequence (SALD) of many ABC transporters (*35*). Its role within the ATP/Mg^{2+} bound dimer of HlyB NBD is shown in Figure 53.

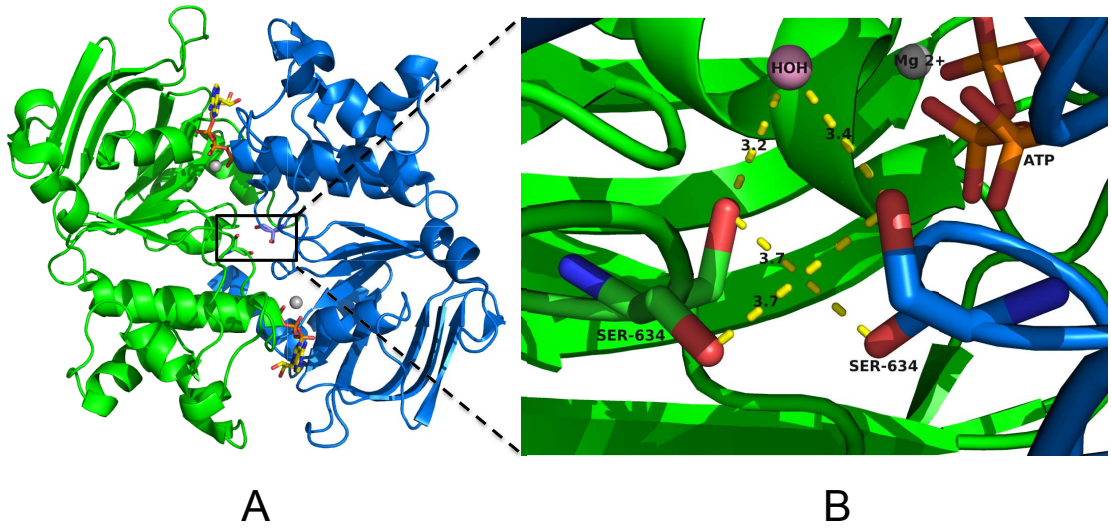

Figure 53: Role of serine 634 within the composite dimer of HlyB NBD. A: Overview of the ATP/Mg^{2+} bound dimer of HlyB NBD H662A (*2*), PDB code 1XEF. The monomers are shown in a cartoon representation in green and dark blue. Serine 634 and ATP are shown in stick representation. The carbon atoms of the nucleotide are colored yellow; the carbon atoms of the protein are in the same color as the according monomer. The black box shows the position of S634. **B:** Zoom in of the interactions between the serines 634 of both monomers. The monomers are presented in different colors; the serines 634 are shown in stick representation. A water molecule is shown as a pink sphere. A magnesium ion is shown as a grey sphere. The hydrogen bonds (distance cutoff 3.5 Å) and the van der Waals interactions (distance cutoff 4.0 A) are shown as dashed yellow lines. The distance lengths (in Å) are shown next to the yellow lines.

S634 is located at the interface of the monomers and participates in symmetrical inter-monomer interactions (*1*). Serine 634 from the *cis*-monomer

interacts with the serine 634 from the *trans*-monomer such that the oxygen atom of the *cis*-side chain interacts with the oxygen atom of the *trans*-main chain and vice versa. It was shown experimentally that mutation S634Y in *E. coli* results in a protein, which is capable of nucleotide binding but unable to hydrolyze ATP (*147*). Because tyrosine is sterically similar to DMNB-L-Ser, these results made S634 a suitable candidate for DMNB-L-Ser mutagenesis. Based on the experimental data (*147*), the mutation of this serine to DMNB-L-Ser would inactivate HlyB NBD without inhibition of nucleotide binding. Based on the structure (Figure 53 B) the reason for this might be the impaired NBD-NBD contact because of the bulky amino acids at the interface of the monomers.

4.4.7.1 Purification of the HlyB NBD S634Y

HlyB NBD S634Y was expressed both in *E. coli* (*147*) and *S. cerevisae*. Subsequently, the protein was purified and characterized. Due to the fact that the properties of the proteins from both expression hosts were very similar, only the properties of the yeast NBD S634Y are described here. The results of the HlyB NBD S634Y purification are presented in Figure 54. SDS PAGE analysis (Figure 54 A) of the protein fractions from SEC (Figure 54 B) revealed that some of the fractions (lanes 5-9) contained highly pure HlyB NBD S634Y. These fractions represented the major peak of the chromatogram of SEC. The NBD S634Y mutant eluted as a symmetrical peak with maximum at a volume of 10.8 mL, which corresponded to the elution maximum of wild type HlyB NBD from yeast (Figure 24). Expression of this mutant protein was performed in shaking flasks, which usually yielded 0.2 mg pure HlyB NBD S634Y per liter selective DO-URA medium after purification.

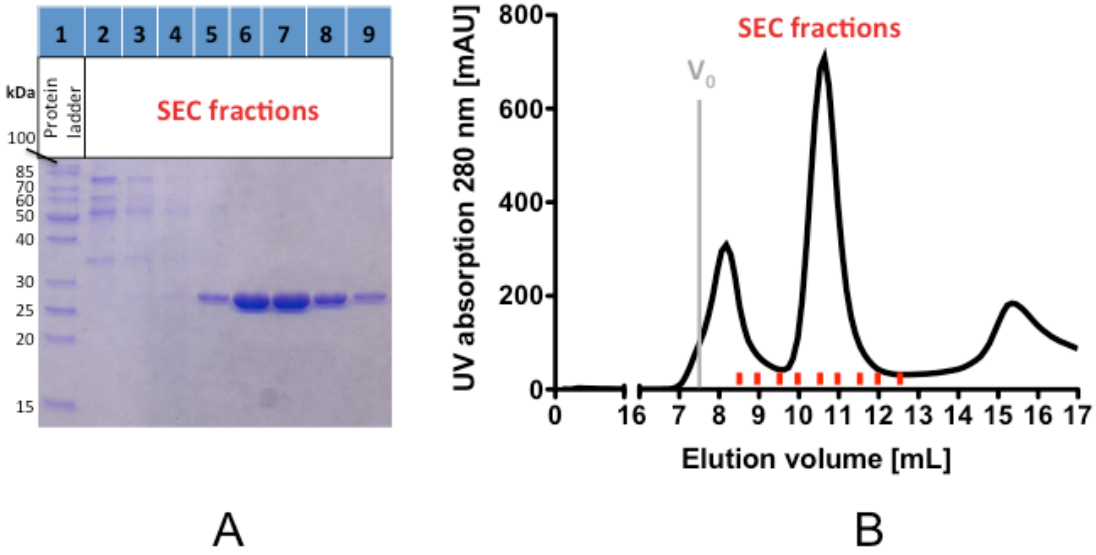

Figure 54: SEC of HlyB NBD S634Y from yeast. A: SDS PAGE of the fractions from SEC (B) of HlyB NBD S634Y from yeast. On the left side of the gel are the sizes of the proteins from the protein ladder (lane 1). The fractions containing pure HlyB NBD S634Y (28 kDa in lanes 5 – 9) represent the major protein peak of SEC. **B:** Chromatogram of SEC of HlyB NBD S634Y from yeast. A Superdex 75 10/300 (GE) column was used. V_0 denotes the void volume of the column. For better overview, the elution profile between 1 and 6 mL volume is not presented. The analyzed fractions are color-coded in red. The detection of the proteins was performed via UV absorption at 280 nm.

4.4.7.2 Characterization of the purified HlyB NBD S634Y

HlyB NBD S634Y from yeast was investigated for its ability to hydrolyze ATP as function of time (Figure 55). The experiment was performed in a buffer containing 100 mM HEPES, pH 7.0, 20 % glycerol, 1.1 µM protein and 2 mM ATP. The reaction temperature was 22 °C. The result demonstrated that serine 634 was essential for the ATPase activity of HlyB NBD. Compared to the wild type protein, no significant amounts of free inorganic phosphate could be detected in the reaction solution. The maximal amount of free inorganic phosphate, produced by this mutant (Figure 55, 50 min), was less than 4% of the phosphate level resulting from the ATP hydrolysis by the wild type HlyB NBD under the same conditions.

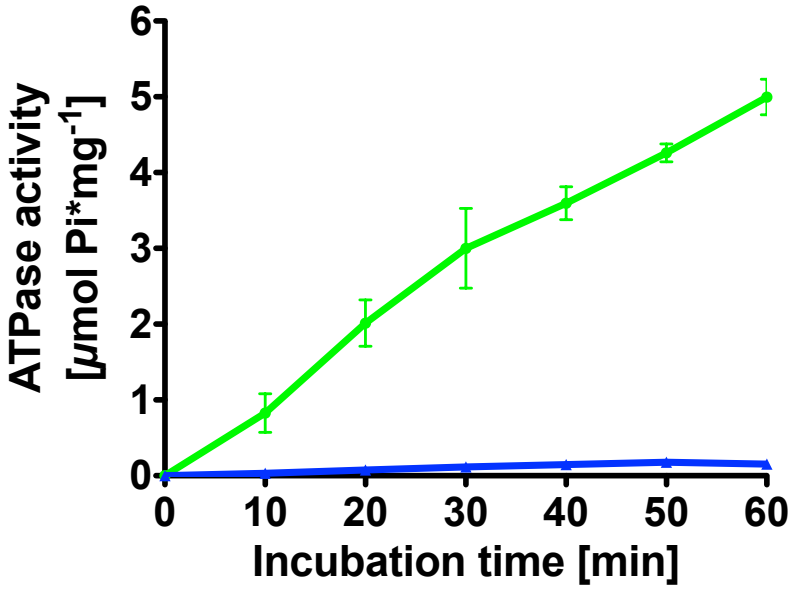

Figure 55: ATPase activity of the HlyB NBD S634Y mutant from yeast as a function of time. The protein concentration was 1.1 µM at 22 °C in a buffer containing 100 mM HEPES, 20 % glycerol, 10 mM $MgCl_2$, pH 7.0 and 2 mM ATP. The ATPase activity of HlyB NBD S634Y is shown as a blue line. As a positive control the ATPase activity of wild type HlyB NBD (1.1 µM, green line) under the same conditions is presented.

In the next step, the influence of the S634Y mutation on ATP binding was investigated (Figure 56). For this purpose, the nucleotide TNP-ATP was titrated to HlyB NBD S634Y as described (*8*). The experiments were conducted at 20 °C in a buffer containing 100 mM HEPES, 20 % glycerol, pH 7.0. The volume of the sample was 1.2 mL. The protein concentration was 4 µM. The increase of the TNP-ATP concentration resulted in a saturation of HlyB NBD S634Y with TNP-ATP, as could be judged from the curve in Figure 56. This implied that the nucleotide analog bound into the binding pocket of the mutant protein. A binding constant of 0.24 ± 0.05 µM was calculated for HlyB NBD S634Y (the calculated correction factors Q_1 and Q_2 are in the appendix). This value was lower than the K_D value of the wild type protein from *S. cerevisiae* (0.6 ± 0.2 µM). This suggested that the mutation S634Y altered the affinity of HlyB NBD towards TNP-ATP. However, this effect should be verified via other methods, e.g. surface plasmon resonance. The structural analysis of HlyB NBD (Figure 53) did not reveal how Tyr634 does influence nucleotide binding.

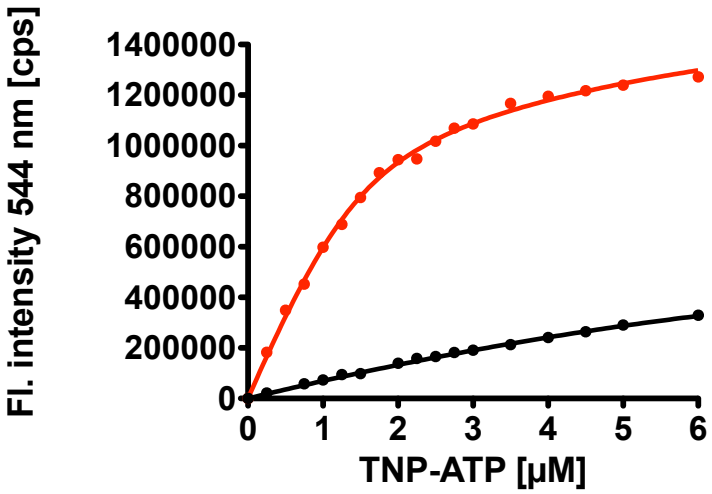

Figure 56: Titration of TNP-ATP to HlyB NBD S634Y from *S. cerevisiae*. The concentration of the protein was 4 µM. The experiment was performed at 20 °C in a buffer containing 100 mM HEPES, 20 % glycerol, pH 7.0. The fluorescence signal of TNP-ATP during the titration to the protein containing solution (shown in red) was recorded at 544 nm emission. The data of the TNP-ATP titration to the solution with only buffer are shown in black. The data were calculated and fitted as described (*8*), see also chapter 3.2.2.7. Cps: counts per second.

After nucleotide binding, the ability of HlyB NBD S634Y to dimerize after ATP addition was investigated. Analytical SEC was applied to monitor whether the protein was able to form a dimer in solution. These experiments were conducted as described (*5*). The reaction buffer (pH 5.8) contained 50 mM malonate, 100 mM sodium acetate, 5 % glycerol. A Superose 12 PC 3.2 / 30 SEC column (GE) was used. Typical results of these experiments are displayed in Figure 57. The addition of ATP led to an insignificant shift of the monomeric peak of the S634Y mutant toward a higher molecular mass. This shift was not comparable with the shift of the peak maximum of HlyB NBD H662A (Figure 27). These SEC results indicated that HlyB NBD S634Y was not able to form a dimer after ATP addition.

Taken together, these results implied that position 634 of the NBD was suitable for the incorporation of DMNB-L-Ser. The exchange of S634 against tyrosine, which is sterically similar to DMNB-L-Ser, resulted in an inactive HlyB NBD. The results suggested that the S634Y mutant retained the ability for nucleotide binding but not the ability for dimer formation after the addition of ATP.

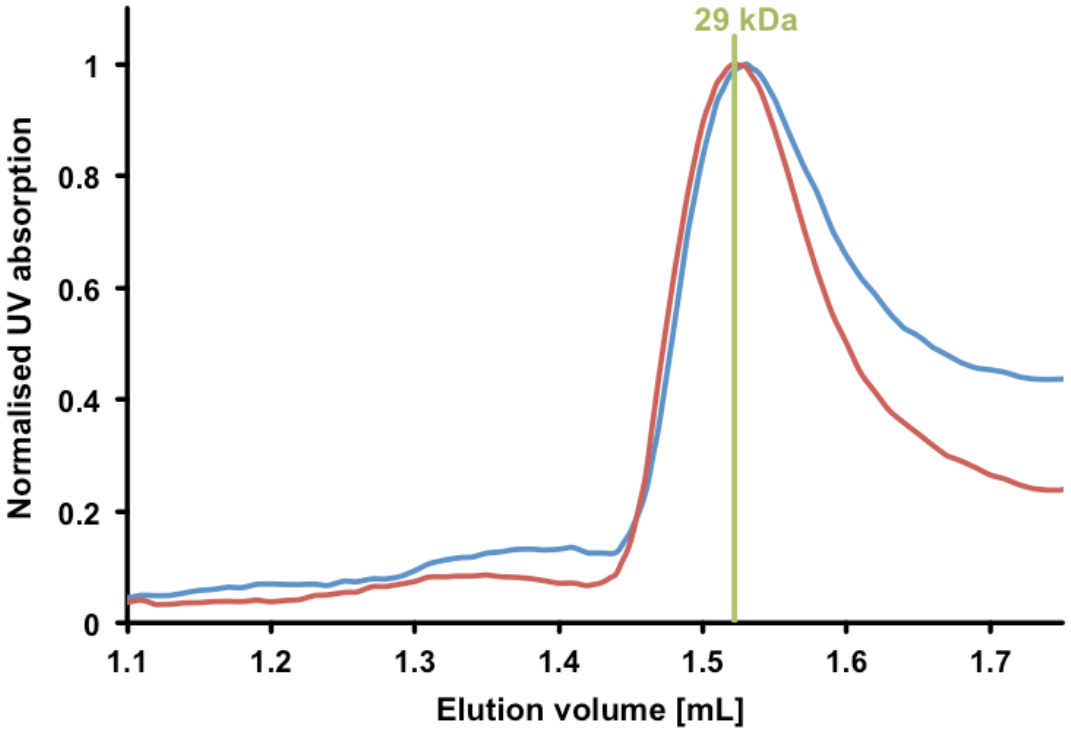

Figure 57: Analytical SEC of HlyB NBD S634Y from yeast in 50 mM malonate, 100 mM sodium acetate, 5% glycerol and pH 5.8. ATP was not present in the solution (blue line) or added to a final concentration of 1 mM (red line). The green line displays the elution maximum of the marker protein carbonic anhydrase (29 kDa). The separation was performed via Superose 12 PC 3.2/30 chromatography column (GE). UV absorption at 295 nm was used for the protein detection. For better overview the absorption values were normalized.

4.4.7.3 Purification of the HlyB NBD S634DMNB-L-Ser

In Figure 58 the results from the purification of HlyB NBD S634DMNB-L-Ser are displayed. It was pure as judged from the SDS gel. Next to the monomeric protein (28 kDa) also dimeric NBD S634DMNB-L-Ser (56 kDa) was detected. The protein band at 56 kDa was also detected via Western blot with the anti-HlyB-NBD antibody (Figure 58 A). This led to the conclusion that the 56 kDa band corresponds to the dimeric protein. Most probably this dimer resulted from the formation of intermolecular disulfide bonds through the single cysteine (C652). This conclusion was based on previous experiments, where such a dimer formation was observed for homologously expressed HlyB NBD (*115*). In the present work the HlyB NBD S634DMNB-L-Ser S-S dimer was detected by SDS-PAGE despite the boiling of the samples and the addition of DTT to the SDS sample buffer. SEC of HlyB NBD S634DMNB-L-Ser resulted in three peaks (Figure 58 B). The major peak contained labeled NBD. Its elution maximum was at 11.9 mL elution volume, which differed from the SEC

elution profile of the wild type protein (Figure 24 B) and from the profile of the S634Y mutant (Figure 54 B, both at 10.8 mL). The incorporation of DMNB-L-Ser might probably influence the protein conformation and subsequently the hydrodynamic radius of the protein, which resulted in the observed SEC elution behavior. This indicated that despite their sterical similarity L-Tyr and DMNB-L-Ser had different impact on the NBD conformation. The yield of HlyB NBD S634DMNB-L-Ser after fermentation, IMAC and SEC amounted to 0.25 mg/L YPD medium.

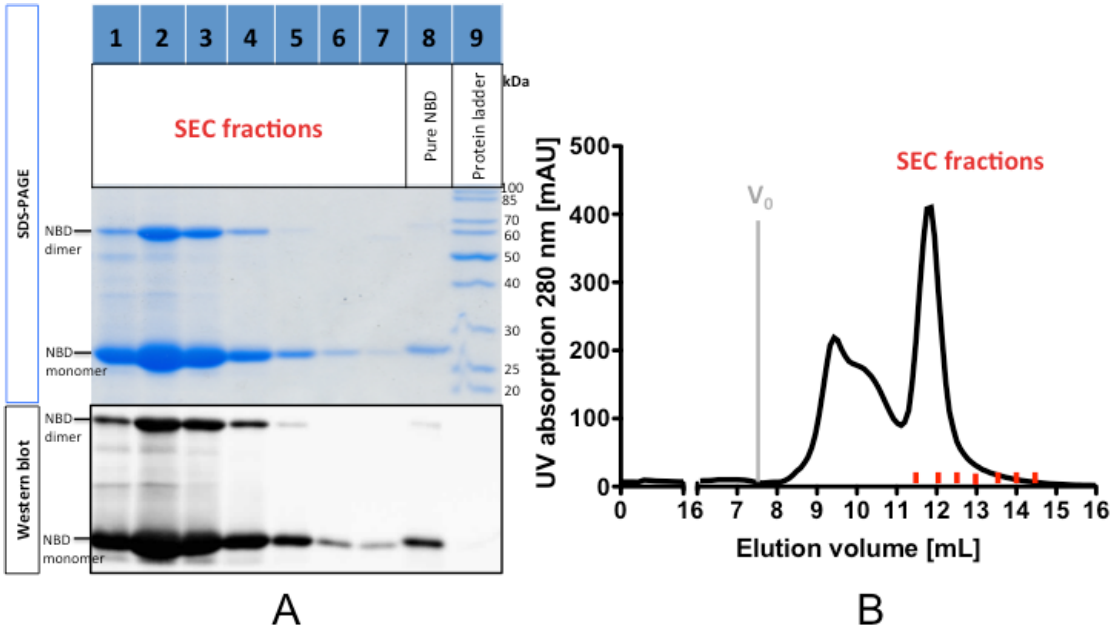

Figure 58: SEC of HlyB NBD S634DMNB-L-Ser from *S. cerevisiae*. A: Protein analysis via SDS-PAGE (middle part) and western blot (lower part, detection with anti-HlyB NBD antibody). In both parts the monomeric and dimeric NBD are marked. Pure HlyB NBD was used as a positive control. **B:** Chromatogram of SEC of HlyB NBD S634DMNB-L-Ser. A Superdex 75 10/300 chromatography column was used. V_0 denotes the void volume of the column. The major peak with elution maximum at 11.9 mL contained the protein of interest. The analyzed fractions are color-coded in red. The protein detection was performed via UV absorption at 280 nm.

4.4.7.4 Properties of the purified HlyB NBD S634DMNB-L-Ser

4.4.7.4.1 Mass spectrometry of HlyB NBD S634DMNB-L-Ser

To demonstrate the incorporation of DMNB-L-Ser into HlyB NBD and the removal of the DMNB photolabile group after irradiation with light, mass spectrometry (ESI-TOF) was applied. The ionization method was electrospray ionization (ESI) and the detection method was double-quadrupole time of flight (QQTOF). HlyB NBD (wild type or S634DMNB-L-Ser mutants) was in a

buffer, containing 100 mM CAPS, pH 10.4 and 20 % glycerol, and was immobilized on a C_{18}-matrix (ZipTipC_{18}) at room temperature. For an optimal detection in ESI-TOF the protein was eluted with a solution containing 60 % methanol and 5 % formic acid. Wild type HlyB NBD from *E. coli* (88 µg), *S. cerevisiae* (44 µg), HlyB NBD S634DMNB-L-Ser (40 µg) and decaged HlyB NBD S634DMNB-L-Ser (40 µg) were analyzed. The energy input for the decaging of the labeled NBD was 277 J. This dose was more then 10 times higher than the dose, which was applied for photolysis of the S504DMNB-L-Ser mutant. With the increased energy input the photolysis of the majority of the fraction of the caged protein was purposed. In this way the fraction of the decaged protein would probably prevail over the fraction of the caged protein after light irradiation. This would result in a reasonable intensity of the obtained ATPase signal after photolysis, contrary to an insufficient energy input with predominance of the caged protein fraction.

The different 6xHis-tagged protein constructs showed the following masses: 27857 Da for HlyB NBD from *E. coli*, 27854 Da for HlyB NBD from yeast, 28052 Da for HlyB NBD S634DMNB-L-Ser and 27859 Da for the decaged HlyB NBD S634DMNB-L-Ser, which are shown in Figure 60 - Figure 63.

The expected average mass of the wild type protein with a 6xHis-tag amounted to 27842 Da (calculated via ProtParam-tool at www.expasy.org). This mass deviated from the observed masses for the wild type HlyB NBD from *E. coli* (27857 Da, Figure 60) and *S. cereviae* (27854 Da, Figure 61).

The bacterial NBD provided very high signal intensities and a reliable signal to noise ratio, as shown in the charge series spectrum in Figure 59. The deconvolution of these TOF-data series led to mass signals with very low deviation among each other. The averaging of these mass signals resulted in a protein mass, which was higher than the expected mass by 15 Da. The reason for that deviation was most probably a single cysteine or methionine oxidation, resulting in a mass difference of +16 Da, combined with the inherent inaccuracy of ±1 Da of this method.

For the yeast wild type protein (Figure 61) an average mass of 27854 Da was observed, which was higher than the expected mass by 12 Da and lower than the observed mass of the *E. coli* NBD by 3 Da. Most probably the higher observed mass compared to the expected mass was a result of cysteine or

methionine oxidation (difference of +16 Da) in combination with the inherent inaccuracy (±1 Da) of that method, which was discussed above. The residual difference of 3 Da resulted most probably from the lower concentration of yeast NBD. This led to lower signal intensities and lower signal to noise ratio of these charge series data (Figure 71, appendix) compared to the NBD from *E. coli*. The deconvolution of these data and the subsequent averaging of the obtained masses resulted in the mass deviation of 3 Da.

The expected average mass of HlyB NBD S634DMNB-L-Ser with a N-terminal 6xHis-tag is 28037 Da. A molecular weight of 28052 Da was observed, as shown in Figure 62. The difference of 15 Da between the expected and the observed mass of the labeled protein corresponded with the difference between the expected and the observed molecular weight of wild type HlyB NBD from *E. coli* (see above). This indicated that the higher observed mass of HlyB NBD S634DMNB-L-Ser could be ascribed to a cysteine or methionine oxidation and the inaccuracy of this method, discussed above in the case of the wild type protein. This result demonstrated that HlyB NBD was successfully labeled with the unnatural amino acid.

The irradiation with light of HlyB NBD S634DMNB-L-Ser should convert the unnatural amino acid to L-serine. In that way after photolysis the decaged protein corresponds to the wild type NBD (expected mass 27842 Da). To avoid misinterpretation the photolysed NBD was called here decaged HlyB NBD S634DMNB-L-Ser. The detected mass (27859 Da) of the decaged protein (Figure 63) was higher than the expected mass by 17 Da. The wild type NBD (from *E. coli* and *S. cerevisiae*) as well as the caged NBD showed also higher masses than expected, which was probably caused by cysteine or methionine oxidation. Therefore, the higher mass, observed for the decaged HlyB NBD S634DMNB-L-Ser, was probably also a consequence of a methionine oxidation. As discussed above, for this experimental setup this results in a mass difference of +15 Da. The reason for the residual difference of +2 Da might be the low signal to noise ratio of this sample, which resulted in low signal intensities in the charge series spectrum (Figure 73, appendix). The deconvolution of the data from this spectrum resulted in masses, which slightly deviated from each other. Their averaging led to the additional difference of +2 Da.

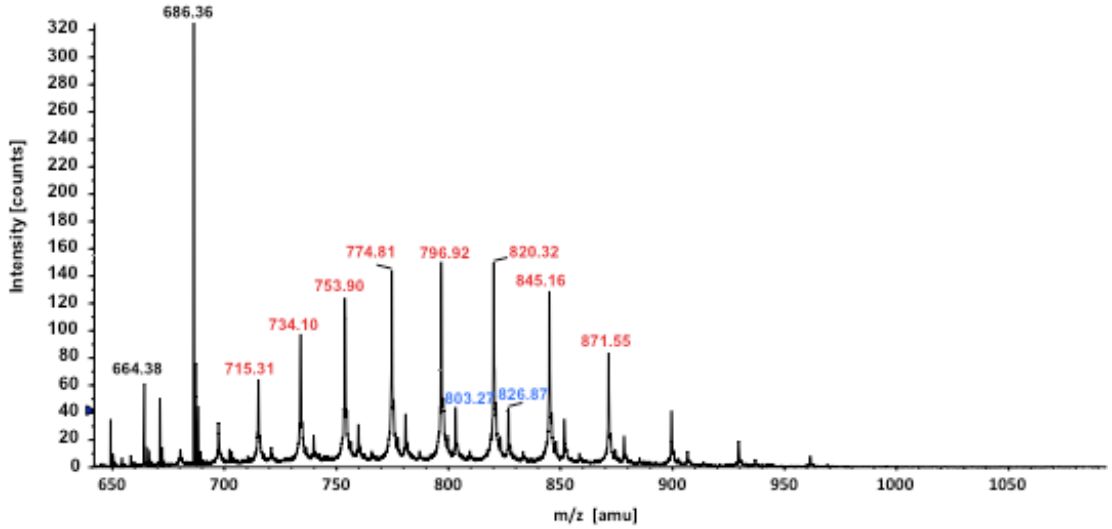

Figure 59: Charge series spectrum of HlyB NBD from *E. coli* after ESI-QQTOF. From this spectrum the masses in **Figure 60** were calculated by deconvolution. On the x-axis the mass / charge ratio (m / z) of the obtained ions is plotted. On the y-axis the signal intensity is plotted. From the peaks with the red signals the mass of HlyB NBD (27857 Da) was calculated. From the smaller peaks with the blue colored signals the mass of the second peak (28079 Da) in **Figure 60** was calculated. It corresponded to HlyB NBD from *E. coli* with one attached molecule CAPS (221 Da). The peak showing a mass of 664 Da corresponded to 3 molecules CAPS. The peak showing a mass of 686 Da corresponded to 3 molecules CAPS plus one sodium ion (23 Da).

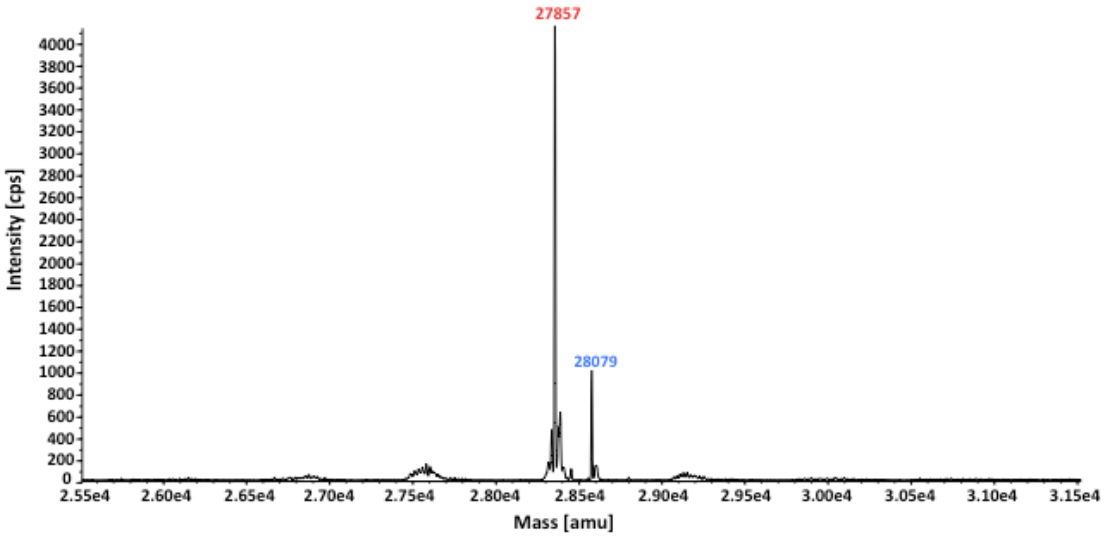

Figure 60: ESI-QQTOF MS spectrum of purified HlyB NBD from *E. coli* containing 6xHis-tag. Shown is an ESI-TOF derived, deconvoluted MS spectrum of the protein in 60 % methanol and 5 % formic acid. The obtained mass for HlyB NBD is shown in red. The expected average mass was 27842 Da, the observed average mass was 27857 Da, caused probably by an oxidized cysteine or methionine. The obtained mass for HlyB NBD with one attached CAPS molecule (28079 Da) is shown in blue. Amu – atom mass units, cps – counts per spectra.

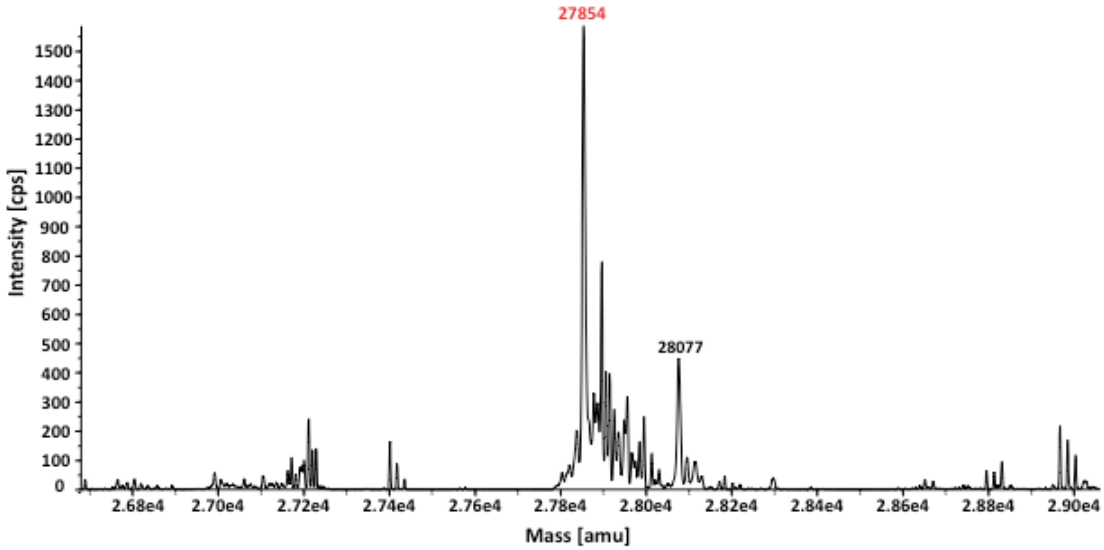

Figure 61: ESI-QQTOF MS spectrum of purified HlyB NBD from *S. cerevisiae* containing 6xHis-tag. Shown is an ESI-TOF derived, deconvoluted MS spectrum of the protein in 60 % methanol and 5 % formic acid. The obtained mass for HlyB NBD is shown in red. The expected average mass was 27842 Da, the observed average mass was 27854 Da. The average mass of 28077 Da corresponded to the protein with one attached molecule CAPS. Amu – atom mass units, cps – counts per spectra.

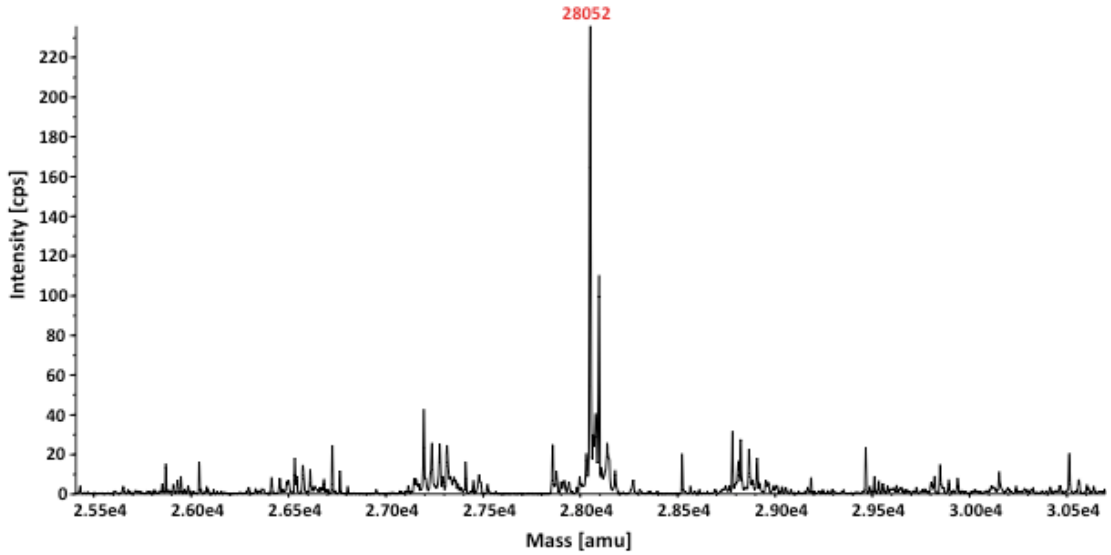

Figure 62: ESI-QQTOF MS spectrum of purified HlyB NBD S634DMNB-L-Ser from *S. cerevisiae* containing 6xHis-tag. Shown is an ESI-TOF derived, deconvoluted MS spectrum of the protein in 60 % methanol and 5 % formic acid. The obtained mass for the caged HlyB NBD S634DMNB-L-Ser is shown in red. The expected average mass was 28037 Da, the observed average mass was 28052 Da, caused probably by a cysteine or methionine oxidation. Amu – atom mass units, cps – counts per spectra.

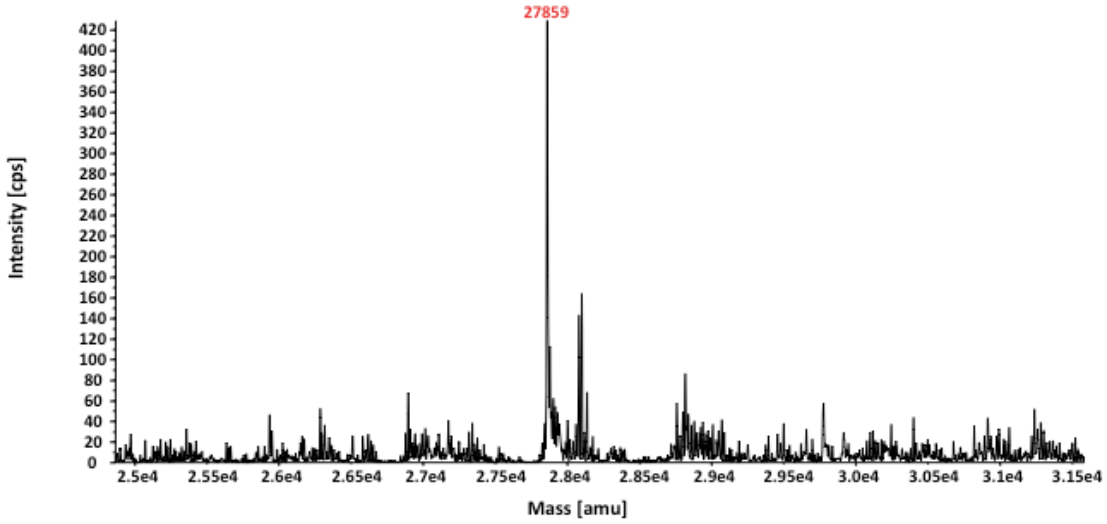

Figure 63. ESI-QQTOF MS spectrum of purified decaged HlyB NBD S634DMNB-L-Ser from *S. cerevisiae* containing 6xHis-tag. Shown is an ESI-TOF derived, deconvoluted MS spectrum of the protein in 60 % methanol and 5 % formic acid. The obtained mass for the decaged HlyB NBD S634DMNB-L-Ser is shown in red. The expected average mass was 27842 Da, the observed average mass was 27859 Da, caused probably by oxidized cysteine or methionine. Amu – atom mass units, cps – counts per spectra.

Taken together, the mass spectrometry data clearly showed that the purified HlyB NBD S634DMNB-L-Ser had a higher molecular weight than the wild type protein. The mass difference corresponded within experimental error to the mass of the DMNB photolabile protecting group. Furthermore, the Western blot data from the expression studies (Figure 20 A) provided a strong argument for the notion that DMNB-L-Ser was incorporated into the polypeptide chain of HlyB NBD. These data led to the conclusion that after the incorporation, HlyB NBD contained DMNB-L-Ser. The analysis of the DMNB-L-Ser-labeled protein after light irradiation showed a decrease of the protein mass, which corresponded to the mass of the DMNB moiety within the experimental error. This result strongly indicated a successful photolysis of the unnatural amino acid after the irradiation with light.

4.4.7.4.2 ATPase activity of HlyB NBD S634DMNB-L-Ser

HlyB NBD S634DMNB-L-Ser was analyzed for its ability to hydrolyze ATP. The ATPase activity was monitored as a function of time at constant temperature (22 °C). The protein concentration was adjusted to 3 µM. This concentration was higher than the concentration of the wild type protein (1.1 µM). With the higher concentration of the mutant protein, a high signal to

noise ratio of the ATPase assay was expected. The concentration of ATP (2 mM) was constant. The assay was performed in buffer containing 100 mM HEPES, 20 % glycerol at pH of 7.0. HlyB NBD S634DMNB-L-Ser was analyzed for hydrolytic activity before and after irradiation with laser light. The aim was to compare whether the caging at position 634 inactivates the protein and whether light irradiation reactivates it. The irradiation with laser light (wavelength 355 nm) was performed for 20 min with an intensity of 225 mJ/s resulting in a total energy amount of 270 J. Compared to the irradiation of HlyB NBD S504DMNB-L-Ser (20.4 J for 1 min) this was more than 10 times longer and more intensive. It was shown via mass spectroscopy that the prolonged irradiation resulted in the decaging of HlyB NBD S634DMNB-L-Ser (see chapter 4.4.7.4.1). The protein exposure to laser was performed in a buffer containing 100 mM CAPS, 20 % glycerol, pH 10.4, 10 mM DTT. The results of the ATPase measurements are shown in Figure 64.

The activity regain of HlyB NBD S634DMNB-L-Ser was successful. Before irradiation the caged protein showed no significant ATPase activity (Figure 64, red line). The protein exposure to laser light resulted in the recovery of its ATPase activity (Figure 64, blue line), which amounted to 0.15 µmol/mg (30 min), 0.21 µmol/mg (40 min), 0.29 µmol/mg (60 min) and 0.31 µmol/min (70 min). The regained activity reached 70 % of the activity of the non-irradiated wild type protein (Figure 64, black line) after 70 min of incubation. DTT seemed to influence the reactivation because in previous experiments with the same mutant no protein activity could be regained without this reagent (data not shown). To assure that light exposure did not reduce protein activity, wild type NBD was irradiated under the same conditions like the S634DMNB-L-Ser mutant. No reduction of the protein activity was observed (Figure 64, green line). This showed that DMNB-L-Ser-labeling at position S634 led to an inactivation of HlyB NBD. This inactivation was reversible and activity could be regained by irradiation with light at a wavelength of 355 nm. This provided the proof of princple that the DMNB photolabile protecting group could be cleaved off. Furthermore, the caging at this position and the UV irradiation did not damage the protein irreversibly.

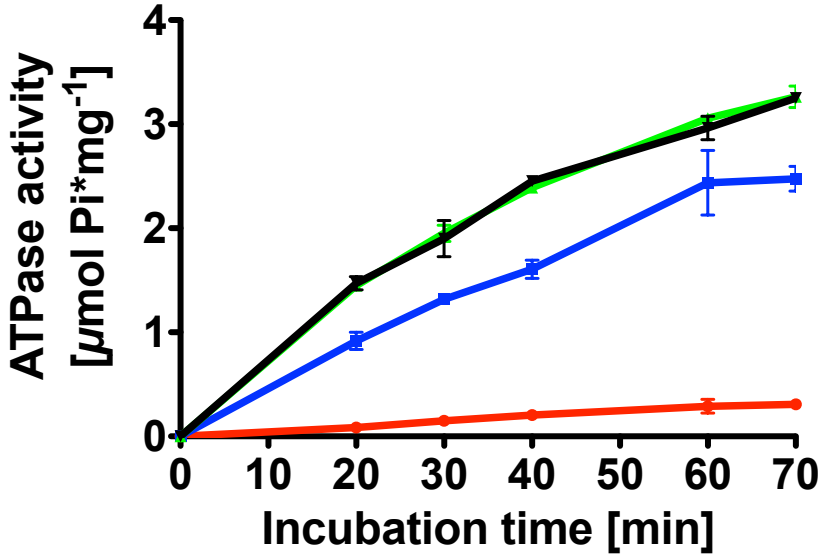

Figure 64: ATPase activity of 3 µM HlyB NBD S634DMNB-L-Ser as a function of time before and after exposure to laser light. The light illumination was performed in SEC buffer containing 100 mM CAPS, 20 % glycerol, 10 mM DTT, pH 10.4 at room temperature. The ATPase assay was conducted in a buffer containing 100 mM HEPES, 20 % glycerol and pH 7.0 at 22 °C. Red line shows HlyB NBD S634DMNB-L-Ser before illumination, the blue line shows the protein after irradiation (22 min, 277 J). The diagram reveals also the ATPase activity of the wild type protein (for comparison): black line – NBD before illumination, green line – wild type protein after the exposure to laser light (22 min, 277 J).

Without doubt, light irradiation of HlyB NBD S634DMNB-L-Ser resulted in reactivation of the protein. However, the energy input (and the duration of the irradiation) in this case was much higher compared to the energy input, which was required for the decaging of isolated DMNB-L-Ser. Such intensive light irradiation could influence the protein properties. Therefore, the ATPase activity of HlyB NBD S634DMNB-L-Ser was investigated as a function of the duration of the irradiation. The aim of this experiment was to monitor the progress of the photolysis and its impact on the ATPase activity. The buffer conditions were the same as described above. 3 µM HlyB NBD S634DMNB-L-Ser and 2 mM ATP (final concentrations) were added to the reaction mixture. The intensity of the laser irradiation amounted to 12.6 J/min. The duration of irradiation was 1 min (12.6 J), 7 min (88.2 J), 15 min (189 J) and 22 min (277.2 J). The result is shown in Figure 65.

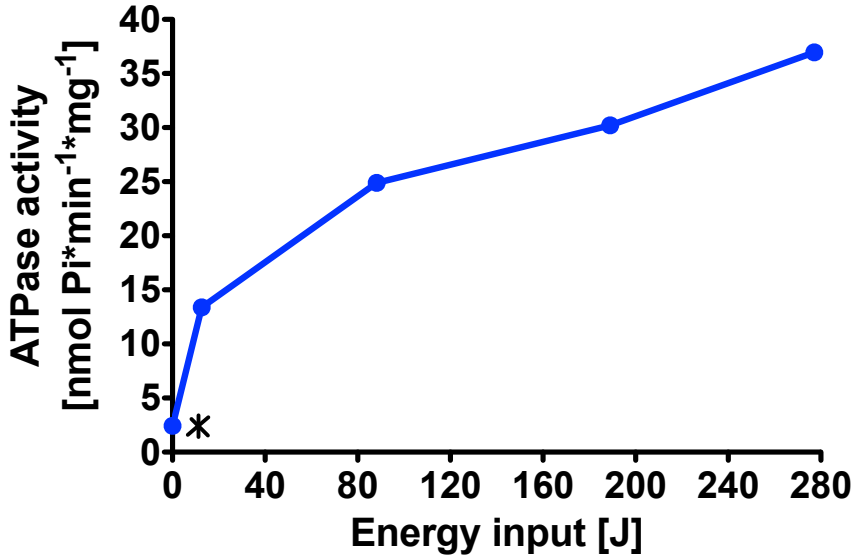

Figure 65: Dependence of the ATPase activity of the recovered NBD S634DMNB-L-Ser on the laser irradiation duration. The experiment was performed at 22 °C in a buffer containing 100 mM HEPES, 20 % glycerol, 10 mM $MgCl_2$ and pH 7.0. The protein concentration was 3 µM, the ATP concentration was 2 mM. The intensity of the laser irradiation was 12.6 J/min, the irradiation duration amounted to 1, 7, 15 and 22 min. The duration of the ATPase assay was 60 min. The dtata point at 0 J is marked with an asterisk. Due to the background activity of HlyB NBD S634DMNB-L-Ser (**Figure 64**, red line) the activity value at 0 J was higher than 0 nmol $Pi*min^{-1}*mg^{-1}$.

The results clearly demonstrated that the variation of the energy input influenced decisively the hydrolytic activity of the DMNB-L-Ser-labeled HlyB NBD after photolysis. The higher the energy input, the higher the ATPase activity. The irradiation with laser light in the UV range could lead to a photo-oxidation of the side chains of Cys, Met, Trp, Tyr, Phe or His (*149*). Such amino acid modification could result, for example, in enzyme inactivation (*150*), protein unfolding (*151, 152*), protein fragmentation or in an alteration of the properties of the protein (*149*). Furthermore, the higher energy input required irradiation duration of up to 22 min, which would make the performance of time resolved measurements impossible. Therefore, a lower energy input of 12.6 J (1 min irradiation) was chosen for decaging of HlyB NBD S634DMNB-L-Ser for further enzymatic assays. However, this would lead to lower signal to noise ratio of the ATPase assays compared to the decaging with higher amount of energy (Figure 65) and to lower specific ATPase activity.

The reactivation success of the S634DMNB-L-Ser raised the question wether the properties of the reactivated HlyB NBD differed from the properties of the wild type protein. To examine this, the ability of the reactivated protein to

hydrolyze ATP was investigated as a function of the ATP concentration, which varied between 0.1 and 3 mM. This assay was performed as described above (chapter 4.4.1.2), however, with some differences. The protein concentration was 3 µM. The incubation time of the samples was 70 min. The aim was to obtain a reliable signal to noise ratio. HlyB NBD S634DMNB-L-Ser was exposed to laser light for 1 min (12.6 J) in order to establish photolysis conditions, which might enable future time resolved measurements. The ATPase activity (Figure 66) was the result of three independent experiments.
These results demonstrated a non-linear dependency of the ATPase activity of the photolysed HlyB NBD S634DMNB-L-Ser on the substrate concentration. Data were fitted with the Hill equation, which resulted in a sigmoidal curve shape as described for the wild type protein from yeast. The calculation of the Hill coefficient resulted in a value of 1.51 ± 0.24. The V_{max} value was 8.2 ± 0.8 nmol*min^{-1}*mg^{-1}, the value for $K_{0.5}$ was 1.01 ± 0.25 mM ATP. The reaction rate was 0.28 ± 0.08 min^{-1}. These kinetic parameters are summarized in Table 16 and were compared to wild type NBD from *S. cerevisiae* and from *E. coli* (see below).
Clearly, the decaged HlyB NBD S634DMNB-L-Ser showed more differences than similarities to the wild type protein after the comparison of the properties (Table 16). The Hill coefficient of the reactivated enzyme (1.51) was similar to this of the wild type protein from yeast (1.87) and to this of the *E. coli* NBD (1.31), however there was certainly a difference between the Hill coefficients of both, wild type NBD from *E. coli* and from *S. cerevisiae*. Together with the sigmoidal curve shape these results indicated that ATP hydrolysis occurs in a cooperative fashion. V_{max} and k_{cat} of the reactivated protein were clearly below the according values of the wild type enzymes. The decline of these properties was not surprising because of the short duration of the laser decaging (1 min, Figure 65). This irradiation behavior had as a consequence a lower energy input and the photolysis of only a fraction of the caged protein. Therefore, only a small fraction of the total amount of the HlyB NBD molecules was able to hydrolyze ATP, which resulted in the low V_{max} value. The $K_{0.5}$ value of the recovered protein differed by a factor of 3-4 from the values of wild type NBD (1.01 vs. 0.24 and 0.36). This demonstrated that the affinity of the decaged protein towards ATP was altered. These data also

revealed that photolysis did not yield a protein with properties of the wild type NBD, which in theory should be the case.

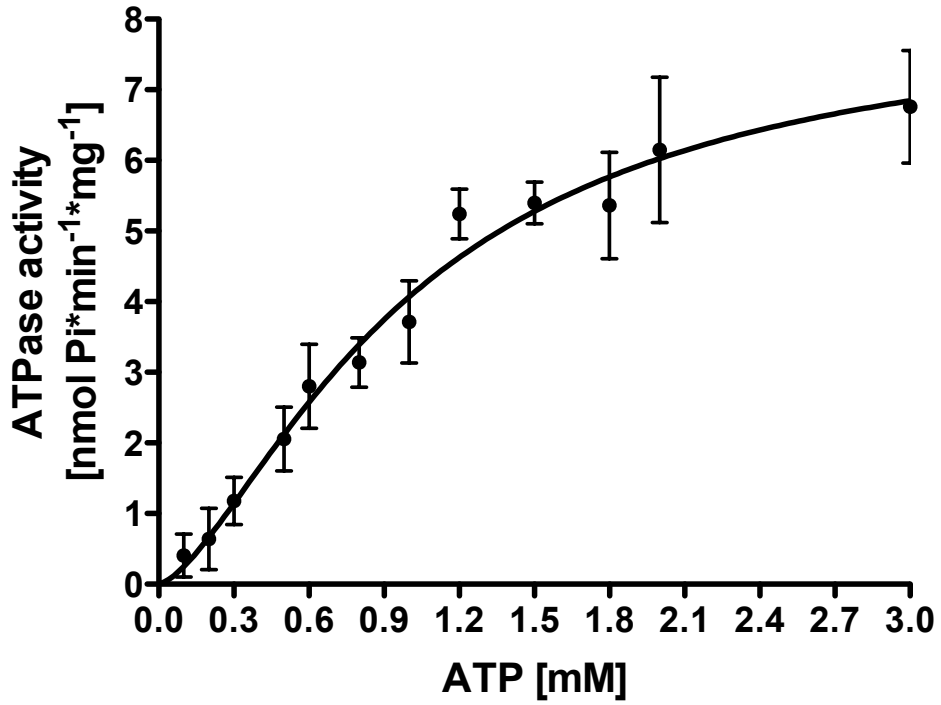

Figure 66: ATPase activity of HlyB NBD S634DMNB-L-Ser after light irradiation as a function of the ATP concentration. The protein was irradiated for 1 min with a laser light of a wavelength 355 nm. The intensity of the irradiation was 12.6 J/min. The enzymatic activity was measured at 22 °C in a buffer containing 100 mM HEPES, 20% glycerol, 10 mM $MgCl_2$ and pH 7.0. The protein concentration was 3 µM. The ATP concentration was between 0.1 and 3 mM. Data were fitted according to the Hill equation. The data points are average of three independent experiments. The error bars show standard deviation. The ATPase activity is lower compared to wild type enzyme because of not fully photo-deprotection due to the short duration of light irradiation, which resulted in lower energy input.

Table 16: Catalytic properties of the decaged (reactivated) HlyB NBD S634DMNB-Ser after light irradiation compared to the wild type protein from *S. cerevisiae* and *E. coli*.

HlyB NBD	V_{max} $[nmol*min^{-1}*mg^{-1}]$	k_{cat} $[min^{-1}]$	$K_{0,5}$ [mM]	*h*
S634-decaged *S. cerevisiae*	8.2 ± 0.8	0.28 ± 0.08	1.01 ± 0.25	1.51 ± 0.2
S. cerevisiae WT	149 ± 7	4.1 ± 0.2	0.24 ± 0.07	1.87 ± 0.24
E. coli WT	202 ± 16	5.6 ± 0.7	0.36 ± 0.05	1.31 ± 0.13

.

5 Discussion

Transport of molecules across biological membranes is essential for every cell. Different protein families are involved in this task (*11*). Proteins from the family of the ABC transporters translocate a wide range of transport substrates (allocrites) (*13*). The NBDs energize the transport process across the membrane by binding and hydrolysing ATP. These domains share a high degree of conservation, in contrast to the TMDs (*12*). In recent years, based on structural and biochemical data, tremendous progress in the mechanistic understanding of ABC transporters was achieved (*25*). These data led to the postulation of two different general models for the allocrite transport, the "Alternating Access Switch Model" and the "Alternating Catalytic Site Model" (*63*). Generally, these models differ in the dimerization behaviour of the NBDs during a "steady state" ATP hydrolysis when the allocrite is transported (*62*). In the "Alternating Access Switch Model" the NBDs form a symmetric closed dimer upon nucleotide binding (*65*). ATP hydrolysis leads to the dissociation of the NBD dimer. In contrast to this, the "Alternating Catalytic Site Model" postulates that the NBDs remain in contact during the transport process (*58*). Dimer opening/nucleotide exchange and ATP hydrolysis occur in an alternating fashion. This means that at any given time point only one nucleotide binding site of the dimer is occupied with ATP whereas the other is not. ATP hydrolysis in the nucleotide-occupied NBD results in a dimer opening at this particular site and in an ATP binding and dimer closure at the opposite NBD.

Isolated NBDs have been successfully used as model systems to investigate the mechanism of ATP hydrolysis mechanism of ABC transporters (*26, 38, 56*). The NBD of the ABC transporter HlyB is one of the best characterized model systems (*5*). Based on structural and biochemical data a catalytic cycle of HlyB NBD was proposed (*1*). It postulates dimerization of the NBDs after nucleotide binding, sequential hydrolysis of ATP, which is followed by sequential release of inorganic phosphate and dimer dissociation (*1*).

The main aim of this work was the further elucidation of the mechanism of hydrolysis of ATP of ABC ATPases. HlyB NBD was applied as a model system. The unnatural, photo-caged amino acid DMNB-L-Ser was applied in order to trap reactivatable intermediates from the catalytic cycle of the NBD. The analyzis of these intermediates could reveal further information about the mechanism of ATP hydrolysis. Prior to achieving this aim, several objectives had to be attained. First, the expression of HlyB NBD in *S. cerevisiae* had to be established. This was dictated by the fact that the fidelity of the DMNB-L-Ser incorporation was optimized for this host organism. Second, the heterologously expressed HlyB NBD had to be purified, characterized and its properties had to be compared to these of the NBD from *E. coli*. Third, NBD mutants, which would enable the trapping of the NBD at defined stages of its catalytic cycle, had to be identified, purified and characterized. Fourth, DMNB-L-Ser had to be incorporated in HlyB NBD at positions, which are essential for the ATPase activity of the protein. These positions were defined in the previuos step. The incorporation occurred via the “Amber stop codon” strategy *in vivo* in *S. cerevisiae* (*102*). For this purpose an orthogonal aaRS/tRNA pair was applied (*153*). This pair from *E. coli* has been generated for the application in *S. cerevisiae* after repetitive rounds of directed evolution with the aim to recognize only DMNB-L-Ser and to mediate its incorporation into the polypeptide chain by suppressing the “Amber” stop codon (TAG) (*102*). Fifth, the DMNB-L-Ser-labeled HlyB NBD had to be characterized. Sixth, the photo-caged HlyB NBD had to be photolysed and the properties of the decaged protein had to be analyzed. Finaly, the catalytic cycle of the ATP hydrolysis of HlyB NBD had to be investigated. Information about the coordinated ATP hydrolysis process should be extracted from the trapped (photo-caged) intermediates and their reactivation (photo-deprotection). This information might gain greater insight into the ATP hydrolysis mechanism of HlyB NBD and could contribute to the further understanding of the principles how ABC ATPases hydrolyse ATP.

5.1 Heterologous expression of the HlyB NBD in *S. cerevisiae* and its characterization

In the first place, the heterologous expression of HlyB NBD in *S. cerevisiae* was established. For this purpose, the expression of the NBD gene from plasmids with different promoters was performed on an analytical scale. The analysis (Figure 13) led to two conclusions: the heterologous expression of HlyB NBD in *S. cerevisiae* is possible and the highest protein level was obtained after the NBD expression from the plasmid with the strong constitutive active promoter GPD. This promoter was derived from the gene encoding the glyceraldehde-3-phosphate dehydrogenase. With regard to the establishment of the heterologous expression of HlyB NBD this result was reasonable. The expression system with the strong constitutive active promoter enabled simple handling of the yeast cells during their cultivation, which was also important for the establishment of the HlyB NBD expression on a preparative scale.

After the successful expression in *S. cerevisiae*, wild type HlyB NBD was purified and characterized. The purification resulted in a homogeneous protein. Its properties were compared with the properties of the homologously expressed HlyB NBD. The binding affinity of HlyB NBD from yeast towards TNP-ATP showed a value of 0.6±0.2 µM, which is within experimental error identical to the value of 0.8 µM of the bacterial protein (*8*). The data from the ATPase activity tests of the heterologously expressed protein could be fitted with the Hill equation (Figure 25 and Table 13). The properties of the yeast enzyme (V_{max} of 149±7 nmol*min^{-1}*mg^{-1} and $K_{0.5}$ of 0.24±0.07 mM) were similar to the properties of the *E. coli* enzyme (V_{max} of 202±16 nmol*min^{-1}*mg^{-1} and $K_{0.5}$ of 0.36±0.05 mM). The Hill coefficient of the yeast HlyB NBD (1.87±0.24) indicated that this protein like the *E. coli* NBD hydrolyzes ATP in a cooperative fashion. However the comparison with the Hill coefficient of the *E. coli* protein (1.31±0.13) showed a difference between the values of the coefficients. This difference between the Hill coefficients was surprising and it could not be explained untill now.

The analysis of the ATP-induced dimerization of HlyB NBD from *S. cerevisiae* via analytical SEC indicated the formation of a dimer in solution (Figure 27),

as already observed for the *E. coli* HlyB NBD (*5*). However, the observed elution shift of the yeast NBD was clearly less distinct compared to shift of the *E. coli* NBD. This observation was surprising. Considering that both proteins showed ATPase activity and similar biochemical properties, and in accordance with the current opinion that the NBD dimerizes during a steady state ATPase (*1*), it is to conclude that the NBD from *S. cerevisiae* should show the same oligomerization behavior like the *E. coli* NBD. The difference, observed via analytical SEC, suggested that the alteration of the hydrodynamic radius of the yeast NBD as a consequence of the ATP-binding differed from this alteration of the *E. coli* NBD. However, this assumption means both proteins differ in their folding, which would result in significant diference between their biochemical properties. Since these properties were similar, this led to the conclusion that analytical SEC was probably not well suited for the investigation of the oligomerization behavior in this case. As an alternative method fluorescence anisotropy could be applied for the determination of the oligomeric state of the protein in solution (*154, 155*). For this purpose, the intrinsic Trp-fluorescence of HlyB NBD could be monitored. HlyB NBD contains a unique tryptophane (W540). After ATP addition the fluorescence anisotropy would reveal the oligomeric state of the protein.

Taken together, the characterization of the yeast NBD showed that its biochemical properties were similar to the properties of the *E. coli* NBD. These results provided the basis for the incorporation of DMNB-L-Ser into HlyB NBD in the host *S. cerevisiae* and for the subsequent investigation of the properties of the photo-caged protein.

5.2 Incorporation of DMNB-L-Ser into the HlyB NBD via the "Amber" stop codon strategy

In this work the unnatural amino acid DMNB-L-Ser was incorporated into HlyB NBD from *E. coli*. The incorporation was performed *in vivo* during expression in *S. cerevisiae*.

HlyB NBD was successfully labeled with DMNB-L-Ser at two positions, S504 (Walker A) and S634 (D-loop). In both cases the purification of the labeled HlyB NBD resulted in sufficient quantities of pure protein. The analysis of the

expression of HlyB NBD S504DMNB-L-Ser in the absence of DMNB-L-Ser showed the presence of HlyB NBD (Figure 18 B). This observation implied that the fidelity of the DMNB-L-Ser incorporation might be lower than 100 % and suggested the tolerance of the aaRS/tRNA-pair towards another amino acids. In fact it was already shown that the fidelity of the DMNB-L-Ser incorporation in the human superoxide dismutase did not reach 100 % and resulted in the incorporation of other amino acids (*102*). The incorporation of "other" amino acids is based on the tolerance of aaRSs (natural or engineered) towards sterically similar amino acids (*156, 157*). This could lead to the synthesys of protein fractions, which contain not only proteins labeled with the desired amino acid and could eventually negatively influence the protein characterization. However, in the case of the labeling of HlyB NBD at position 504 the amount of the "wrong" labeled protein was extremely low (Figure 18 B). Furthermore, the incorporation of a natural amino acid instead of DMNB-caged serine was not observed for HlyB NBD S634DMNB-L-Ser (Figure 20 A). Therefore, it was concluded that the "wrong" labeling did not impact the experimental results significantly.

Surprisingly, the labeling with DMNB-L-Ser at position S506 was not successful. No HlyB NBD was detected in the lysates of the yeast cells. This suggested that the incorporation of DMNB-L-Ser at this position led to a misfolding, which resulted in the degradation of the protein.

The heterologous expression resulted in a yield, which in both cases (HlyB NBD S504DMNB-L-Ser and S634DMNB-L-Ser) was sufficient for biochemical studies. However, the comparison between the purified mutants S504DMNB-L-Ser (0.06 mg/L medium) and S634DMNB-L-Ser (0.25 mg/L medium) revealed that the labeling at these positions resulted in different protein amounts. This result suggested that the expression yield is dependent on the position of the unnatural amino acid.

Taken together, the labeling via the "Amber" stop codon strategy enabled the site specific incorporation of DMNB-L-Ser with high fidelity at single sites.

5.3 Photolysis of DMNB-L-Ser within HlyB NBD or as an isolated compound, comparison with other photo-caged proteins and with photo-caged compounds

The reactivation of a protein, caged with DMNB-L-Ser, is directly depending on the decaging of the DMNB group of the unnatural amino acid. In this work the photolysis of the photo-caged HlyB NBD was performed *in vitro*. For this reason the decaging of isolated DMNB-L-Ser was first investigated in different solvents (Figure 34). Cleavage of the DMNB photolabile protecting group after light irradiation in PBS buffer and in the hydrophobic acetonitrile/water mixture showed different results. In the polar PBS solution nearly 3 times more energy (17 J) input was required for the decaging of 110 µM DMNB-L-Ser compared to the hydrophobic acetonitrile/water mixture (6 J). This indicated that a hydrophobic environment, such as a protein binding pocket, would facilitate cleavage of the photolabile protecting group upon irradiation with light. These results were compared with the decaging behavior of DMNB-L-Ser within HlyB NBD at position 634 (HlyB NBD S634DMNB-L-Ser), as shown in Figure 64. The comparison revealed that for 3 µM labeled protein (33 times lower concentrated than the isolated compound) much more energy (280 J) was required for the decaging of the majority of the incorporated DMNB-L-Ser. Accordingly, the protein sample was irradiated much longer (22 min) compared to the free DMNB-L-Ser in acetonitrile/water (1 min, Figure 34). This was a problem in terms of future kinetic measurements because of the long duration of the irradiation. These results implied also that the protein environment had a huge impact on the photolysis of the incorporated DMNB-L-Ser. It is difficult to determine how exactly the HlyB NBD environment exerted influence on the properties of DMNB-L-Ser. Furthermore, at this point it was not clear whether the observed alteration of the DMNB-L-Ser photolysis is caused by the HlyB NBD environment or in general by any protein environment. To address this question, the impact of the environment of other proteins on the DMNB-properties and on the properties of similar photolabile protecting groups were compared.

The DMNB-caging group was incorporated via direct conjugation to cysteine in the heavy chain of meromyosin (*158*) and in the bacterial *SssI* DNA

methyltransferase (*159*), which in both cases resulted in an inactivation of the proteins.

In the case of the bacterial *SssI* DNA methyltransferase, the caged enzyme (0.5 µM) was irradiated with UV light from a 100 W mercury arc lamp by using a 320-400 nm band pass filter. An irradiation of 0.5 min (approx. 11 J energy input) led to an aprox. 50 % restoration and an irradiation of 5 min (approx. 111 J energy input) led to an approx. 60 % restoration of the enzymatic activity (*159*). Despite their highly sensitive detection method (^{3}[H]-radioactivity, femtomolar range) (*160*) and the high energy input the authors did not try the reactivation of the caged *SssI* with lower energy input.

Heavy meromyosin is the subdomain of the actin-based motor protein myosin (*161*). This protein is able to bind and hydrolyze ATP and subsequently to generate the force for actin movement (*162*). The photolysis of DMNB-caged heavy meromyosin (18.6 µM) was performed by irradiation with a 100 W mercury arc lamp with 340-400 nm light. The photolysis was monitored by absorption spectrometry, which revealed that the photo-deprotection was dependent on the irradiation dosis. 30 sec irradiation (approx. 9 J) resulted in detectable photolysis, 4 min irradiation (approx. 70 J) led to the removal of the majority of the DMNB protecting group and 30 min irradiation (approx. 525 J) to a complete photo-deprotection (*158*). Nevertheless, photolysis of the DMNB-caged heavy meromyosin was also observed after irradiation, which lasted for less than a second. In this experiment DMNB-caged hevy meromyosin (nanomolar concentration) was immobilized on a cover slip, then actin filaments labeled with the fluorescence marker tetramethylrhodamine phalloidin were bound to the heavy meromyosin and then ATP was added. The ability of heavy meromyosin to hydrolyze ATP and to generate force for the movement of actin was restored after a 500 ms light flash (approx. 16 mJ). The photo-deprotection of the caged protein was monitored indirectly via the movement of the actin filaments on a time scale of seconds, which was detected with fluorescence imaging microscopy (*158*). With this experimental setup it is difficult to estimate the fraction of the photo-deprotected heavy meromyosin molecules. It is enough to photolyse small number of molecules in close proximity to observe an actin movement. The authors did not investigate the ratio of the photolysed to the non-photolysed molecules,

nevertheless with this highly sensitive detection methods they were able to observe a biological response.

DMNB-L-Ser was incorporated via the “Amber stop codon” strategy in the transcription factor Pho4 (*102*). The objective of this study was to analyze the influence of the phosphorylation of different serine residues on the properties of this protein (*102*). The phosphorylation of certain serines leads to an export of Pho4 out of the cell nucleus (*102*). Several of these serines were replaced with DMNB-L-Ser, which prevented their phosphorylation and also the transport of Pho4 out of the nucleus to the cytoplasm. To observe nuclear export in real time, Pho4 was fused to GFP. Decaging and regaining of protein transport was demonstrated *in vivo* by confocal laser scanning microscopy. Photolysis was performed via an exposure of the cells to a laser light (405 nm wavelength) with approx. 410 nJ energy input and 1 msec irraditation duration per nucleus. This allowed kinetic measurements on the time scale of seconds to minutes (*102*). The authors showed the photolysis of DMNB-L-Ser indirectly by monitoring the decrease in the GFP-fluorescence within the nuclei over time. This experimental setup offered a highly sensitive detection, which could detect minor fluorescence differences even after minimal photolysis rate. The authors did not analyze the ratio between photolysed and non-photolysed DMNB-L-Ser.

Furthermore, the influence of the protein microenvironment on the photolysis properties of a caged compound was examined by analyzing the photolysis of proteins, which were labeled with *ortho*-nitrobenzyl-group (*o*-NB-group). This compound is similar to the DMNB- photolabile protecting group (Figure 67).

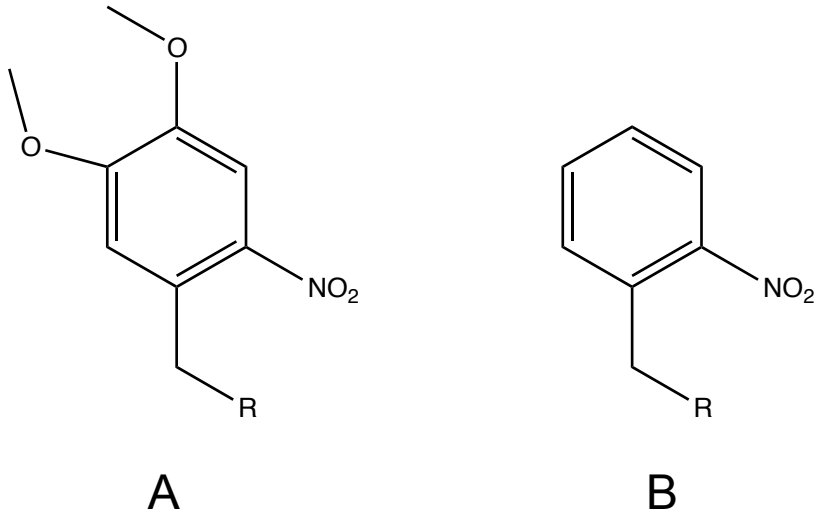

Figure 67: Comparison of the DMNB- (A) and the *o*-NB-photolabile caging group (B).

The restriction endonuclease *PvuII* was caged with the *o*-NB-group via conjugation to the cysteine thiol group (*101*). The authors aimed to investigate residues of the enzyme, which are essential for its activity. The incorporation of the caging compound enabled the reversible inhibition of the protein activity. For the photolysis of 1 µM *PvuII* (He Cd laser, 40 mW) with UV light (325 nm), 10 s irradiation (400 mJ) was sufficient to detect approx. 5 % activity. 50 % activity restoration was obtained after 1 min irradiation (2.4 J) and 80 % after 20 min irradiation (48 J). In this way the authors assessed indirectly the approximate level of photolysis of the *o*-NB-group.

In another example, β-Galactosidase from *E. coli* was caged with the *o*-NB-group by incorporating it via the "Amber" stop codon strategy (*163*). This resulted in an inhibition of the protein activity, which was monitored by absorption spectroscopy. After 5 min of UV irradiation (365 nm, approx. 33 J energy input) the enzyme (10 µM) showed detectable activity and 30 min irradiation (approx. 198 J energy input) resulted in an activity, which amounted to 54 % of the wild type enzyme activity (*163*).

In a further example*, o*-NB-tyrosine and *o*-NB-cysteine were incorporated into the M2 transmembrane segment of the γ-subunit of the muscle nicotinic ACh receptor, which was expressed in *Xenopus* oocytes (*90*). The aim was to inactivate the protein and to analyze channel kinetics after reactivation with light via the two-electrode voltage clamp method. By the application of 3 s

flashes (in the range 300-350 nm, approx. 2 J energy input) the photolytic efficiency of *o*-NB-Tyr was approx. 88 % and the photolytic efficiency of *o*-NB-Cys was approx. 36 %. Furthermore, the channel response was analyzed via photolysis by series of 1 ms flashes with UV light (350-400 nm, energy input not shown). The authors were able to investigate the channel kinetics on a time scale of seconds (*90*).

With the examples mentioned above the photolysis of the isolated DMNB-L-Ser was compared with the photolysis of the protein-incorporated DMNB- and the incorporated *o*-NB-photolabile protecting group. In order to gain a comprehensive view whether and how the protein environment influences the photolysis of an *o*-NB-caged compound, the properties of *o*-NB-caged compounds are presented below.

Different *o*-NB-caged compounds, e.g. caged nucleotides and their analogs, caged Ca^{2+}, caged protons and caged fluorophors have been developed and successfully applied (*138, 164*). For the sake of simplicity only the properties of the widely used *o*-NB derivative NPE-ATP (ATP, P^3-(1-(2-Nitrophenyl)Ethyl) ester, Figure 68) are discussed.

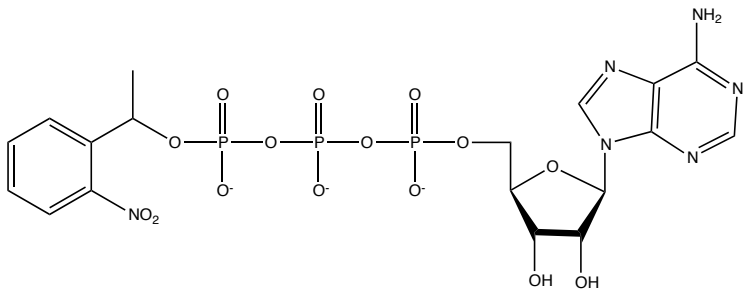

Figure 68: NPE-ATP (ATP, P^3-(1-(2-Nitrophenyl)Ethyl) ester).

NPE-caged ATP was often applied for time-resolved studies of ATP-dependent model systems. The reaction mechanism of the catalytic fragment CopB-B of the heavy metal-translocating P-type ATPase CopB from *S. solfataricus* was studied with caged NPE-ATP (*165*). In this case the pulse flash photolysis (8.1 J energy input, 120 ms duration) with UV light (308 nm) led to the photodeprotection of 90 % ATP from the caged ATP (15.3 mM),

which resulted in an ATPase activity of the protein (*165*). Furthermore, NPE-ATP was applied for time-resolved investigations of the efficiency of contraction in rabbit skeletal muscles by determining the release rate of inorganic phosphate (*166*). Single laser pulse (50-100 mJ energy input, 30 ns duration) with UV light (347 nm) led to the photolytic release of 1.5 mM ATP from 5 mM caged ATP. The following hydrolysis of the photodeprotected nucleotide by myosin, which led to a muscle contraction, was observed on the time scale of milliseconds to seconds (*166*). Similar results with NPE-ATP were obtained when the dissociation kinetics of actomyosin were analyzed (*167*). Laser flash photolysis (25 mJ energy input, 30 ns pulse duration) with UV light (347 nm) resulted in the generation of 0.5 mM ATP from 2.5 mM caged ATP. This caused the actomyosin dissociation, which was detected in the time range of milliseconds (*167*).

The comparison between the caged proteins and the caged compounds revealed a significant difference between their photolysis properties. The photodeprotection of the caged proteins (0.5-20 µM) required energy input in the range of tens or hundreds of joules for the photolysis of a significant amount of the photolabile groups. In contrast to this, the photolysis of the caged compounds (0.11-15.3 mM) from the presented examples required energy inputs in the range of millijoules to a few joules. The comparison indicated that the photodeprotection of caged compounds of higher concentration (compared to the discussed caged proteins) requires lower energy input. This analysis also suggested that not only the HlyB NBD environment but also the protein environment in general impacts the photolysis properties of NB-caged compounds in a way that the required energy input for the photodeprotection increases. The difference between protein-incorporated caged groups and caged compounds is the size of the molecule, which they are covalently bound to. Probably the covalent conjugation of the caged compound to a protein caused the observed effect.

The reasons for the observed effect could be twofold. First, (surrounding) side chains of Cys, Met, Trp, Tyr, Phe or His absorb UV radiation, which probably leads to their photooxidation (*149*), whithout impact on the photophysical and photochemical properties of the caging group. The second reason could be the alteration of the photophysical and photochemical properties of the

incorporated caging compound by the microenvironment of the protein such that e.g. the absorbed light does not result only in photolysis, but in a non-radiative relaxation from the excited state. Both effects lead to a dissipation of the irradiated energy to processes other than photolysis. This provides an explanation, why compared to “caged” compounds the protein-integrated caging groups need more energy for the photolysis and for the triggering of the biological responce. Indeed it is difficult to determine whether one of these effects or the combination of both led to the observed impact on the properties of the incorporated nitrobenzyl photolabile protecting group. It was observed nevertheless that a low energy input (11.5 mJ) was enough for the complete photolysis of the caged NPE-ATP (0.22 mM), which was coordinated (but not covalently conjugated) in the binding pocket of kinesin prior to photolysis (*168*). In this case protein residues, which could be photo-oxidized (*149*), also surrounded the caged ATP. However, this did not result in an energy input for photodeprotection in the range of tens or hundreds of joules. This supported the conclusion that the protein environment and the covalent conjugation impact the photophysical properties of the *o*-NB- and of the DMNB-photolabile protecting group.

Given the observation that the protein environment substantially influences the photolysis properties of the *o*-NB- and the DMNB-caging group the question arose whether these protein-incorporated groups are in general suitable for kinetic studies of the function of proteins and especially of HlyB NBD. The comparison between the labeled HlyB NBD and the discussed labeled proteins led to the conclusion that the detection setup is crucial for the time scale of the measured biological response. The fluorescence microscopy (caged/decaged Pho4 (*102*) and heavy meromyosin (*158*)) and the current measurements via the voltage clamp method (nicotinic ACh receptor (*90*)) provide high sensitivity. Therefore, low amounts of a decaged sample (e.g. a single channel or a single cell) are required for a detection of a signal (*169*). Accordingly, flash photolysis of a duration below a second led to a detectable biological response. In contrast, the detection of ATPase activity of the decaged HlyB NBD via absorption spectroscopy requires higher protein amounts (micromolar concentration), as shown in Figure 64 and (*5*). The photolysis of this higher protein amount for the established assay required the

use of a cuvette (10 mm length) and a higher energy input, compared the examples discussed above. The photon flux through such cuvettes is rather modest (*170*). Therefore, a modified experimental setup, e.g. the use of thiner cuvette might result in a decrease of the energy input, which is required for the complete photolysis of the NBD-incorporated DMNB. Alternatively, the application of another photo-caging group might be considered (*138*). Furthermore, a more sensitive detection setup might enable the detection of minimal amounts of the photodeprotected protein and real time kinetic measurements. For example, a glucose oxidase coupled ATPase assay (*171*), performed on a surface with an immobilized glucose oxidase, could be applied for this purpose. The reaction product hydrogen peroxide might be employed for the generation of fluorescent dichlorofluorescein from leucodiacetyldichlorofluorescein and the resulting fluorescence could be monitored by fluorescence microscopy (*172*). Fluorescence could be also applied as a read out for ATP hydrolysis via a coumarin-labeled phosphate binding protein, which binds inorganic phosphate resulting in an enhancement of its fluorescence (*166, 173*). In addition, fluorescence anisotropy might be utilized for a kinetic study of the oligomerization of HlyB NBD after ATP binding. As a fluorophor the unique tryptophane of the DMNB-labeled HlyB NBD (W540) could be exploited. This approach would enable the monitoring of the ATP-induced NBD oligomerization after photolysis.

Furthermore, the photolysis properties of caged ATP raised the question whether a strategy with a caged compound could be used alternatively for the caging of HlyB NBD with the aim of investigating its catalytic cycle. An advantage of this method is the possibility of time-resolved measurements due to the short irradiation, required for photolysis. Furthermore, there would be no need for heterologous expression. This would enable the application of the homologously expressed HlyB NBD to study questions, which are related to the nucleotide binding site like ATP-induced dimerization. However, a disadvantage of caged ATP is that the photolabile protecting group might impact the affinity of the protein towards the caged nucleotide. The coordination of the caged nucleotide by the protein might be influenced. In some cases binding is impaired (*174*), but in other cases not (*165*). In case of binding it might be possible to crystallize a dimer of HlyB NBD with bound

caged ATP and to investigate nucleotide hydrolysis within the cristall. The approach with photocaged ligands was already successfully applied to study the enzyme isocitrate dehydrogenase within an anzyme-substrate complex (*105*). On the other hand, the strategy of incorporating a caging group provides the opportunity to label HlyB NBD also outside of the nucleotide binding site. This enables much more detailed investigation of the influence of different subdomains on the enzymatic properties (e.g. allosteric regulation). Therefore, caged compounds could be used alternatively to caged proteins, however the latter strategy enables higher flexibility in terms of position labeling, which makes it probably more suitable for the investigation of the complex cycle of HlyB NBD.

5.4 Properties of the DMNB-L-Ser labeled HlyB NBD after light irradiation

In this work HlyB NBD was successfully labeled with DMNB-L-Ser at two positions of its polypeptide chain – Ser504 in the Walker A and Ser634 in the D-loop. This resulted in an abolishment of the ability of the protein to hydrolyze ATP. Illumination with light allowed the recovery of the activity only for the HlyB NBD S634DMNB-L-Ser mutant. This implied that both mutants behave differently in terms of photolysis of the incorporated unnatural amino acid and of the subsequent reactivation.

Serine 504 coordinates via its side chain through a hydrogen bond the γ-phosphate of ATP within the ATP/Mg^{2+}-bound dimer of HlyB NBD (Figure 28 and (*2*)). Its mutation to alanine in *E. coli* (*8*) and in *S. cerevisiae* (this work) abolished ATPase activity of the protein, however it did not influence significantly nucleotide binding. The S504DMNB-L-Ser mutant was also not able to hydrolyze ATP, however light irradiation did not lead to a recovery of protein activity (Figure 35).

One explanation for this observation could be the failed (or impaired) photolysis of this caged mutant. As discussed above (chapter 5.3), the complex protein environment impacts the photo-cleavage of the caging group in a way that it leads to an increase of the energy required for photolysis. Unfortunately the protein yield of HlyB NBD S504DMNB-L-Ser was insufficient

to validate these hypotheses. Another reason for the failed reactivation of HlyB NBD S504DMNB-L-Ser could be the impact of the unnatural amino acid on the protein conformation. The bulky aromatic DMNB-residue within the ATP binding pocket of HlyB NBD instead of the polar hydroxyl group of serine might cause conformational changes in the Walker A motif. SEC showed that the S504DMNB-L-Ser (Figure 33 B) mutant eluted at lower elution volume compared to the S504A mutant (Figure 29 B). This indicated that the incorporation of the unnatural amino acid impacts the hydrodynamic radius of this mutant and also its conformation. Maybe the incorporation of the unnatural amino acid interferes with the folding of HlyB NBD and makes the protein more prone to aggregation, which causes the failure of protein reactivation after light irradiation. Further analysis via other methods, e.g. dynamic light scattering (*175*), fluorescence anisotropy (*176*), and fluorescence correlation spectroscopy (*177*), might shed light on this hypothesis.

The light irradiation of HlyB NBD S634DMNB-L-Ser resulted in a recovery of the ATPase activity of the protein (Figure 64). Together with mass spectrometry data (Figure 62 and Figure 63) these results demonstrated the success of the DMNB-L-Ser photolysis and of the conversion of the protein to its active form. These observations revealed also that the chosen system for caging and photolysis of HlyB NBD does function. Contrary to the S504DMNB-L-Ser mutant, the reactivation of the 634 mutant was possible. The difference between both mutants was the labeling position, which suggested that the activity regain might depend on the location of the caging compound. Serine 634 resides outside of the ATP binding pocket and is not involved in nucleotide binding, but in intermonomeric communication within the ATP bound dimer of HlyB NBD (*178*). Probably due to the distance of DMNB-L-Ser634 from other residues, essential for ATPase activity, the resulting highly reactive *o*-nitrosobenzaldehyde compound (*73, 139, 164*) did not have the possibility to react with such residues and thereby irreversibly eliminated the protein function after photolysis. After reactivation the decaged HlyB NBD showed catalytic properties (especially $K_{0.5}$), which were different to wild type HlyB NBD (Table 16). Untill now there is no obvious explanation for this effect. Maybe a crystal structure of the decaged HlyB NBD could give

an inside into the conformation of the protein and might explain the altered catalytic properties. However, for this purpose the yield of HlyB NBD S634DMNB-L-Ser after expression and purification should be increased.

Alteration of the protein properties was observed after photolysis of other caged proteins too. In heavy meromyosin the velocity of the actin movements after photolysis was lower compared to the movements, induced from unmodified heavy meromyosin (*158*). Decaging of the restriction endonucleases *PvuII* and *MunI* did also not lead to full recovery of their activities (*101*). These results are similar to the activity restoration of DMNB-labeled HlyB NBD (Figure 64). This difference between the properties of wild type and photodeprotected proteins suggested that photo-caging and photolysis alters in general the protein properties.

All these data demonstrated that the incorporation of a caging unnatural amino acid into HlyB NBD via the “Amber” stop codon strategy was possible. The ATPase activity regain of the mutant HlyB NBD S634DMNB-L-Ser after photolysis revealed that the protein function could be controlled via an external switch. Therefore, the model system HlyB NBD in a combination with a caged unnatural amino acid could be used in the future to answer open questions about the mode of action of ABC transporters. However, possible alterations of the protein properties as a result of photolysis should be taken into account.

5.5 The ATP hydrolysis cycle of the HlyB NBD

Within the nucleotide bound dimer the D-loops are located on the contacting surface between both monomers, which was structurally shown in HlyB NBD (*2*), in other isolated NBDs (*38, 179*) or in a complete ABC transporter (*49*). Structural analysis of the D-loop interactions in HlyB NBD suggested that together with residues from the Walker B motif and helix 6 this loop acts as a hinge during ATP-ADP transitions and it is involved in inter-monomer communication by sensing the functional state of the opposite ATP binding site (*1*). Serine 634 from the D-loop interacts with the same amino acid from the opposite monomer, as shown in Figure 53. Its replacement against tyrosine or DMNB-L-Ser revealed, that the side chain hydroxyl group of this

amino acid is essential for the ability of HlyB NBD to hydrolyze ATP (Figure 55 and Figure 64). Interestingly, mutation of the amino acid at the same position in MJ0796 (G174) against tryptophan did not abolish the ATPase activity and ATP induced dimerization (*180*). However, contrary to S634 from HlyB NBD, the D-loop glycine from MJ0796 does not participate in inter-monomer contacts, which might be the reason for its successful exchange without abolishment of the enzymatic activity. Activity regaining after photolysis of DMNB-L-Ser at position 634 revealed that the inactivation of HlyB NBD is reversible. This implied that the D-loop region is dynamic and features certain flexibility, which probably allows its reversible manipulation with a bulky residue. Due to the fact that S634 from the D-loop is not involved in ATP binding, this amino acid is probably essential for ATPase activity after nucleotide binding. Maybe the incorporation of a bulky residue at this position influences the D-loop conformation and prevents protein dimerization after ATP binding, which is supported by analytical SEC (Figure 57). As a consequence, the communication (and the allosteric coupling) between the NBDs is maybe disrupted. Interestingly, the dynamic role of the D-loop in the allosteric communication between NBDs during ATP hydrolysis was predicted (*181*).

5.6 Outlook

Understanding the ATP hydrolysis cycle of ABC transporters during transport is still a challenge. The isolation of further intermediates would probably be further envisaged with the aim to obtain a more complete picture of this cycle. Isolated NBDs are excellent model systems to achieve this aim. Photo-caging of HlyB NBD provides a great opportunity to isolate different intermediates, which can be reactivated and analysed. Optimization of the ATPase assay and the detection setup should enable real time kinetic measurements of the nucleotide hydrolysis after photolysis of the caged HlyB NBD. Furthermore, the HlyB NBD S634DMNB-L-Ser mutant, which might represent an ATP bound monomer after ATP binding, should enable the real time observation of the NBD-oligomerization during steady state nucleotide hydrolysis. This could be achieved for example by monitoring the fluorescence of the unique Trp540 and by analyzing the fluorescent anisotropy after laser flash photolysis. Beyond this, one could further screen for mutants, which can be trapped as an ATP bound dimer via a photo-caging compound. Crystallization of such a mutant with bound nucleotide might allow time resolved monitoring of ATP hydrolysis after photolysis within the crystal. In this manner new insights into the exact mode of action of the nucleotide binding domain of HlyB could be gained, which could be related to the other ABC transporters.

6 References

1. Zaitseva, J., Oswald, C., Jumpertz, T., Jenewein, S., Wiedenmann, A., Holland, I. B., and Schmitt, L. (2006) A structural analysis of asymmetry required for catalytic activity of an ABC-ATPase domain dimer, *The EMBO Journal 25*, 3432-3443.
2. Zaitseva, J., Jenewein, S., Jumpertz, T., Holland, I. B., and Schmitt, L. (2005) H662 is the linchpin of ATP hydrolysis in the nucleotide-binding domain of the ABC transporter HlyB, *The EMBO Journal 24*, 1901-1910.
3. Schmitt, L., Benabdelhak, H., Blight, M. A., Holland, I. B., and Stubbs, M. T. (2003) Crystal structure of the nucleotide-binding domain of the ABC-transporter haemolysin B: identification of a variable region within ABC helical domains, *Journal of molecular biology 330*, 333-342.
4. Hvorup, R. N., Goetz, B. A., Niederer, M., Hollenstein, K., Perozo, E., and Locher, K. P. (2007) Asymmetry in the structure of the ABC transporter-binding protein complex BtuCD-BtuF, *Science 317*, 1387-1390.
5. Zaitseva, J., Jenewein, S., Wiedenmann, A., Benabdelhak, H., Holland, I. B., and Schmitt, L. (2005) Functional characterization and ATP-induced dimerization of the isolated ABC-domain of the haemolysin B transporter, *Biochemistry 44*, 9680-9690.
6. Reich, A. (2012) Optimization of the expression of the NBD of the ABC transporter HlyB, In *Institute of biochemistry*, Heinrich Heine University, Duesseldorf.
7. Adams, S. R., Kao, J. P. Y., and Tsien, R. Y. (1989) Biologically useful chelators that take up Ca2+ upon illumination, *J Am Chem Soc 111*, 7957-7968.
8. Oswald, C., Jenewein, S., Smits, S. H., Holland, I. B., and Schmitt, L. (2008) Water-mediated protein-fluorophore interactions modulate the affinity of an ABC-ATPase/TNP-ADP complex, *Journal of Structural Biology 162*, 85-93.
9. Dawson, R. J., and Locher, K. P. (2006) Structure of a bacterial multidrug ABC transporter, *Nature 443*, 180-185.
10. Young, T. S., and Schultz, P. G. (2010) Beyond the canonical 20 amino acids: expanding the genetic lexicon, *The Journal of biological chemistry 285*, 11039-11044.
11. Saier, M. H., Jr. (2000) A functional-phylogenetic classification system for transmembrane solute transporters, *Microbiology and molecular biology reviews 64*, 354-411.
12. Davidson, A. L., Dassa, E., Orelle, C., and Chen, J. (2008) Structure, function, and evolution of bacterial ATP-binding cassette systems, *Microbiology and Molecular Biology Reviews 72*, 317-364, table of contents.
13. Holland, I. B., and Blight, M. A. (1999) ABC-ATPases, adaptable energy generators fuelling transmembrane movement of a variety of

molecules in organisms from bacteria to humans, *Journal of molecular biology 293*, 381-399.
14. Schmitt, L., and Tampe, R. (2002) Structure and mechanism of ABC transporters, *Current opinion in structural biology 12*, 754-760.
15. I.B. Holland; K. Kuchler, C. F. H., S.P.C. Cole. (2003) ABC Proteins: From Bacteria to Man, *Academic Press, London, United Kingdom*.
16. Holland, I. B., Kuchler, K., Higgins, C. F., and Cole, S. P. C. (2003) ABC Proteins: From Bacteria to Man, *Academic Press, London, United Kingdom*.
17. Dassa, E., and Bouige, P. (2001) The ABC of ABCS: a phylogenetic and functional classification of ABC systems in living organisms, *Research in Microbiology 152*, 211-229.
18. Jones, P. M., O'Mara, M. L., and George, A. M. (2009) ABC transporters: a riddle wrapped in a mystery inside an enigma, *Trends in biochemical sciences 34*, 520-531.
19. Zolnerciks, J. K., Andress, E. J., Nicolaou, M., and Linton, K. J. (2011) Structure of ABC transporters, *Essays Biochem 50*, 43-61.
20. Higgins, C. F. (2007) Multiple molecular mechanisms for multidrug resistance transporters, *Nature 446*, 749-757.
21. Linton, K. J., and Higgins, C. F. (1998) The Escherichia coli ATP-binding cassette (ABC) proteins, *Mol Microbiol 28*, 5-13.
22. Boursiac, Y., Leran, S., Corratge-Faillie, C., Gojon, A., Krouk, G., and Lacombe, B. (2013) ABA transport and transporters, *Trends Plant Sci 18*, 325-333.
23. Lee, M., Choi, Y., Burla, B., Kim, Y. Y., Jeon, B., Maeshima, M., Yoo, J. Y., Martinoia, E., and Lee, Y. (2008) The ABC transporter AtABCB14 is a malate importer and modulates stomatal response to CO2, *Nature cell biology 10*, 1217-1223.
24. Terasaka, K., Blakeslee, J. J., Titapiwatanakun, B., Peer, W. A., Bandyopadhyay, A., Makam, S. N., Lee, O. R., Richards, E. L., Murphy, A. S., Sato, F., and Yazaki, K. (2005) PGP4, an ATP binding cassette P-glycoprotein, catalyzes auxin transport in Arabidopsis thaliana roots, *Plant Cell 17*, 2922-2939.
25. Holland, I. B. (2011) ABC transporters, mechanisms and biology: an overview, *Essays Biochem 50*, 1-17.
26. Chen, J., Lu, G., Lin, J., Davidson, A. L., and Quiocho, F. A. (2003) A tweezers-like motion of the ATP-binding cassette dimer in an ABC transport cycle, *Molecular Cell 12*, 651-661.
27. Kuhnau, S., Reyes, M., Sievertsen, A., Shuman, H. A., and Boos, W. (1991) The activities of the Escherichia coli MalK protein in maltose transport, regulation, and inducer exclusion can be separated by mutations, *Journal of bacteriology 173*, 2180-2186.
28. Dean, D. A., Reizer, J., Nikaido, H., and Saier, M. H., Jr. (1990) Regulation of the maltose transport system of Escherichia coli by the glucose-specific enzyme III of the phosphoenolpyruvate-sugar phosphotransferase system. Characterization of inducer exclusion-resistant mutants and reconstitution of inducer exclusion in proteoliposomes, *The Journal of biological chemistry 265*, 21005-21010.

29. Nelson, S. O., and Postma, P. W. (1984) Interactions in vivo between IIIGlc of the phosphoenolpyruvate:sugar phosphotransferase system and the glycerol and maltose uptake systems of Salmonella typhimurium, *European journal of biochemistry / FEBS Journal 139*, 29-34.
30. Stein, A., Seifert, M., Volkmer-Engert, R., Siepelmeyer, J., Jahreis, K., and Schneider, E. (2002) Functional characterization of the maltose ATP-binding-cassette transporter of Salmonella typhimurium by means of monoclonal antibodies directed against the MalK subunit, *European journal of biochemistry / FEBS Journal 269*, 4074-4085.
31. Oldham, M. L., Khare, D., Quiocho, F. A., Davidson, A. L., and Chen, J. (2007) Crystal structure of a catalytic intermediate of the maltose transporter, *Nature 450*, 515-521.
32. Locher, K. P., Lee, A. T., and Rees, D. C. (2002) The E. coli BtuCD structure: a framework for ABC transporter architecture and mechanism, *Science 296*, 1091-1098.
33. Schneider, E., and Hunke, S. (1998) ATP-binding-cassette (ABC) transport systems: functional and structural aspects of the ATP-hydrolyzing subunits/domains, *FEMS Microbiology Reviews 22*, 1-20.
34. Ye, J., Osborne, A. R., Groll, M., and Rapoport, T. A. (2004) RecA-like motor ATPases--lessons from structures, *Biochim Biophys Acta 1659*, 1-18.
35. Hanekop, N., Zaitseva, J., Jenewein, S., Holland, I. B., and Schmitt, L. (2006) Molecular insights into the mechanism of ATP-hydrolysis by the NBD of the ABC-transporter HlyB, *FEBS letters 580*, 1036-1041.
36. Jones, P. M., and George, A. M. (1999) Subunit interactions in ABC transporters: towards a functional architecture, *FEMS Microbiology Letters 179*, 187-202.
37. Oswald, C., Holland, I. B., and Schmitt, L. (2006) The motor domains of ABC-transporters. What can structures tell us?, *Naunyn Schmiedebergs Arch Pharmacol 372*, 385-399.
38. Smith, P. C., Karpowich, N., Millen, L., Moody, J. E., Rosen, J., Thomas, P. J., and Hunt, J. F. (2002) ATP binding to the motor domain from an ABC transporter drives formation of a nucleotide sandwich dimer, *Molecular Cell 10*, 139-149.
39. Davidson, A. L., and Chen, J. (2004) ATP-binding cassette transporters in bacteria, *Annu Rev Biochem 73*, 241-268.
40. Dawson, R. J., Hollenstein, K., and Locher, K. P. (2007) Uptake or extrusion: crystal structures of full ABC transporters suggest a common mechanism, *Molecular microbiology 65*, 250-257.
41. Chen, H. L., Gabrilovich, D., Tampe, R., Girgis, K. R., Nadaf, S., and Carbone, D. P. (1996) A functionally defective allele of TAP1 results in loss of MHC class I antigen presentation in a human lung cancer, *Nat Genet 13*, 210-213.
42. Saveanu, L., Daniel, S., and van Endert, P. M. (2001) Distinct functions of the ATP binding cassettes of transporters associated with antigen processing: a mutational analysis of Walker A and B sequences, *The Journal of biological chemistry 276*, 22107-22113.
43. Mourez, M., Hofnung, M., and Dassa, E. (1997) Subunit interactions in ABC transporters: a conserved sequence in hydrophobic membrane

proteins of periplasmic permeases defines an important site of interaction with the ATPase subunits, *The EMBO journal 16*, 3066-3077.
44. Tsui, L. C. (1992) The spectrum of cystic fibrosis mutations, *Trends in Genetics 8*, 392-398.
45. Locher, K. P. (2009) Review. Structure and mechanism of ATP-binding cassette transporters, *Philos Trans R Soc Lond B Biol Sci 364*, 239-245.
46. Oldham, M. L., Davidson, A. L., and Chen, J. (2008) Structural insights into ABC transporter mechanism, *Current opinion in structural biology 18*, 726-733.
47. Hunke, S., Mourez, M., Jehanno, M., Dassa, E., and Schneider, E. (2000) ATP modulates subunit-subunit interactions in an ATP-binding cassette transporter (MalFGK2) determined by site-directed chemical cross-linking, *The Journal of biological chemistry 275*, 15526-15534.
48. Hollenstein, K., Frei, D. C., and Locher, K. P. (2007) Structure of an ABC transporter in complex with its binding protein, *Nature 446*, 213-216.
49. Oldham, M. L., and Chen, J. (2011) Snapshots of the maltose transporter during ATP hydrolysis, *Proceedings of the National Academy of Sciences of the United States of America 108*, 15152-15156.
50. Pinkett, H. W., Lee, A. T., Lum, P., Locher, K. P., and Rees, D. C. (2007) An inward-facing conformation of a putative metal-chelate-type ABC transporter, *Science 315*, 373-377.
51. Ward, A., Reyes, C. L., Yu, J., Roth, C. B., and Chang, G. (2007) Flexibility in the ABC transporter MsbA: Alternating access with a twist, *Proceedings of the National Academy of Sciences of the United States of America 104*, 19005-19010.
52. Kimura, Y., Kioka, N., Kato, H., Matsuo, M., and Ueda, K. (2007) Modulation of drug-stimulated ATPase activity of human MDR1/P-glycoprotein by cholesterol, *Biochem J 401*, 597-605.
53. Davidson, A. L., Shuman, H. A., and Nikaido, H. (1992) Mechanism of maltose transport in Escherichia coli: transmembrane signaling by periplasmic binding proteins, *Proceedings of the National Academy of Sciences of the United States of America 89*, 2360-2364.
54. Petronilli, V., and Ames, G. F. (1991) Binding protein-independent histidine permease mutants. Uncoupling of ATP hydrolysis from transmembrane signaling, *The Journal of biological chemistry 266*, 16293-16296.
55. Ernst, R., Kueppers, P., Stindt, J., Kuchler, K., and Schmitt, L. (2010) Multidrug efflux pumps: substrate selection in ATP-binding cassette multidrug efflux pumps--first come, first served?, *European journal of biochemistry / FEBS Journal 277*, 540-549.
56. Janas, E., Hofacker, M., Chen, M., Gompf, S., van der Does, C., and Tampe, R. (2003) The ATP hydrolysis cycle of the nucleotide-binding domain of the mitochondrial ATP-binding cassette transporter Mdl1p, *The Journal of biological chemistry 278*, 26862-26869.
57. Jardetzky, O. (1966) Simple allosteric model for membrane pumps, *Nature 211*, 969-970.

58. Senior, A. E., al-Shawi, M. K., and Urbatsch, I. L. (1995) The catalytic cycle of P-glycoprotein, *FEBS letters 377*, 285-289.
59. Jones, P. M., and George, A. M. (2007) Nucleotide-dependent allostery within the ABC transporter ATP-binding cassette: a computational study of the MJ0796 dimer, *The Journal of biological chemistry 282*, 22793-22803.
60. Lee, J. Y., Urbatsch, I. L., Senior, A. E., and Wilkens, S. (2008) Nucleotide-induced structural changes in P-glycoprotein observed by electron microscopy, *The Journal of biological chemistry 283*, 5769-5779.
61. Oloo, E. O., and Tieleman, D. P. (2004) Conformational transitions induced by the binding of MgATP to the vitamin B12 ATP-binding cassette (ABC) transporter BtuCD, *The Journal of biological chemistry 279*, 45013-45019.
62. Jones, P. M., and George, A. M. (2013) Mechanism of the ABC transporter ATPase domains: catalytic models and the biochemical and biophysical record, *Crit Rev Biochem Mol Biol 48*, 39-50.
63. Al-Shawi, M. K. (2011) Catalytic and transport cycles of ABC exporters, *Essays Biochem 50*, 63-83.
64. Linton, K. J., and Higgins, C. F. (2007) Structure and function of ABC transporters: the ATP switch provides flexible control, *Pflugers Arch 453*, 555-567.
65. Higgins, C. F., and Linton, K. J. (2004) The ATP switch model for ABC transporters, *Nature Structural & Molecular Biology 11*, 918-926.
66. Urbatsch, I. L., Sankaran, B., Weber, J., and Senior, A. E. (1995) P-glycoprotein is stably inhibited by vanadate-induced trapping of nucleotide at a single catalytic site, *The Journal of biological chemistry 270*, 19383-19390.
67. Sauna, Z. E., Kim, I. W., Nandigama, K., Kopp, S., Chiba, P., and Ambudkar, S. V. (2007) Catalytic cycle of ATP hydrolysis by P-glycoprotein: evidence for formation of the E.S reaction intermediate with ATP-gamma-S, a nonhydrolyzable analogue of ATP, *Biochemistry 46*, 13787-13799.
68. Siarheyeva, A., Liu, R., and Sharom, F. J. (2010) Characterization of an asymmetric occluded state of P-glycoprotein with two bound nucleotides: implications for catalysis, *The Journal of biological chemistry 285*, 7575-7586.
69. Korkhov, V. M., Mireku, S. A., and Locher, K. P. (2012) Structure of AMP-PNP-bound vitamin B12 transporter BtuCD-F, *Nature 490*, 367-372.
70. Eckford, P. D., and Sharom, F. J. (2009) ABC efflux pump-based resistance to chemotherapy drugs, *Chem Rev 109*, 2989-3011.
71. Samanta, S., Ayvaz, T., Reyes, M., Shuman, H. A., Chen, J., and Davidson, A. L. (2003) Disulfide cross-linking reveals a site of stable interaction between C-terminal regulatory domains of the two MalK subunits in the maltose transport complex, *The Journal of biological chemistry 278*, 35265-35271.
72. Engels, J., and Schlaeger, E. J. (1977) Synthesis, structure, and reactivity of adenosine cyclic 3',5'-phosphate benzyl triesters, *J Med Chem 20*, 907-911.

73. Kaplan, J. H., Forbush, B., 3rd, and Hoffman, J. F. (1978) Rapid photolytic release of adenosine 5'-triphosphate from a protected analogue: utilization by the Na:K pump of human red blood cell ghosts, *Biochemistry 17*, 1929-1935.
74. Yu, H., Li, J., Wu, D., Qiu, Z., and Zhang, Y. (2010) Chemistry and biological applications of photo-labile organic molecules, *Chem Soc Rev 39*, 464-473.
75. Barsotti, R. J., and Ferenczi, M. A. (1988) Kinetics of ATP hydrolysis and tension production in skinned cardiac muscle of the guinea pig, *The Journal of biological chemistry 263*, 16750-16756.
76. Goldman, Y. E., Hibberd, M. G., McCray, J. A., and Trentham, D. R. (1982) Relaxation of muscle fibres by photolysis of caged ATP, *Nature 300*, 701-705.
77. Hibberd, M. G., Dantzig, J. A., Trentham, D. R., and Goldman, Y. E. (1985) Phosphate release and force generation in skeletal muscle fibers, *Science 228*, 1317-1319.
78. Kaplan, J. H. (1982) Sodium pump-mediated ATP:ADP exchange. The sided effects of sodium and potassium ions, *The Journal of general physiology 80*, 915-937.
79. Morad, M., Goldman, Y. E., and Trentham, D. R. (1983) Rapid photochemical inactivation of Ca2+-antagonists shows that Ca2+ entry directly activates contraction in frog heart, *Nature 304*, 635-638.
80. Nerbonne, J. M., Richard, S., Nargeot, J., and Lester, H. A. (1984) New photoactivatable cyclic nucleotides produce intracellular jumps in cyclic AMP and cyclic GMP concentrations, *Nature 310*, 74-76.
81. Karpen, J. W., Zimmerman, A. L., Stryer, L., and Baylor, D. A. (1988) Gating kinetics of the cyclic-GMP-activated channel of retinal rods: flash photolysis and voltage-jump studies, *Proceedings of the National Academy of Sciences of the United States of America 85*, 1287-1291.
82. Lester, H. A., and Nerbonne, J. M. (1982) Physiological and pharmacological manipulations with light flashes, *Annu Rev Biophys Bioeng 11*, 151-175.
83. Khan, S., Meister, M., and Berg, H. C. (1985) Constraints on flagellar rotation, *Journal of molecular biology 184*, 645-656.
84. Shimada, K., and Berg, H. C. (1987) Response of the flagellar rotary motor to abrupt changes in extracellular pH, *Journal of molecular biology 193*, 585-589.
85. Albers, R. W., Koval, G. J., and Siegel. (1968) Studies on the interaction of ouabain and other cardio-active steroids with sodium-potassium-activated adenosine triphosphatase, *Molecular pharmacology 4*, 324-336.
86. Geissler, D., Kresse, W., Wiesner, B., Bendig, J., Kettenmann, H., and Hagen, V. (2003) DMACM-caged adenosine nucleotides: ultrafast phototriggers for ATP, ADP, and AMP activated by long-wavelength irradiation, *Chembiochem 4*, 162-170.
87. Furuta, T., Wang, S. S., Dantzker, J. L., Dore, T. M., Bybee, W. J., Callaway, E. M., Denk, W., and Tsien, R. Y. (1999) Brominated 7-hydroxycoumarin-4-ylmethyls: photolabile protecting groups with biologically useful cross-sections for two photon photolysis,

Proceedings of the National Academy of Sciences of the United States of America 96, 1193-1200.

88. Gurney, A. M., Tsien, R. Y., and Lester, H. A. (1987) Activation of a potassium current by rapid photochemically generated step increases of intracellular calcium in rat sympathetic neurons, *Proceedings of the National Academy of Sciences of the United States of America 84*, 3496-3500.
89. Fedoryak, O. D., Sul, J. Y., Haydon, P. G., and Ellis-Davies, G. C. (2005) Synthesis of a caged glutamate for efficient one- and two-photon photorelease on living cells, *Chem Commun (Camb)*, 3664-3666.
90. Philipson, K. D., Gallivan, J. P., Brandt, G. S., Dougherty, D. A., and Lester, H. A. (2001) Incorporation of caged cysteine and caged tyrosine into a transmembrane segment of the nicotinic ACh receptor, *Am J Physiol Cell Physiol 281*, C195-206.
91. Zor, T., Bar-Yaacov, M., Elgavish, S., Shaanan, B., and Selinger, Z. (1997) Rescue of a mutant G-protein by substrate-assisted catalysis, *European journal of biochemistry / FEBS Journal 249*, 330-336.
92. de Graaf, A. J., Kooijman, M., Hennink, W. E., and Mastrobattista, E. (2009) Nonnatural amino acids for site-specific protein conjugation, *Bioconjug Chem 20*, 1281-1295.
93. Wang, L., Xie, J., and Schultz, P. G. (2006) Expanding the genetic code, *Annu Rev Biophys Biomol Struct 35*, 225-249.
94. Hendrickson, T. L., de Crecy-Lagard, V., and Schimmel, P. (2004) Incorporation of nonnatural amino acids into proteins, *Annu Rev Biochem 73*, 147-176.
95. Benzer, S., and Champe, S. P. (1962) A change from nonsense to sense in the genetic code, *Proceedings of the National Academy of Sciences of the United States of America 48*, 1114-1121.
96. Garen, A., and Siddiqi, O. (1962) Suppression of mutations in the alkaline phosphatase structural cistron of E. coli, *Proceedings of the National Academy of Sciences of the United States of America 48*, 1121-1127.
97. Xie, J., and Schultz, P. G. (2005) Adding amino acids to the genetic repertoire, *Curr Opin Chem Biol 9*, 548-554.
98. Wang, L., Brock, A., Herberich, B., and Schultz, P. G. (2001) Expanding the genetic code of Escherichia coli, *Science 292*, 498-500.
99. Wang, L., and Schultz, P. G. (2001) A general approach for the generation of orthogonal tRNAs, *Chem Biol 8*, 883-890.
100. Wang, L., and Schultz, P. G. (2004) Expanding the genetic code, *Angew Chem Int Ed Engl 44*, 34-66.
101. Silanskas, A., Foss, M., Wende, W., Urbanke, C., Lagunavicius, A., Pingoud, A., and Siksnys, V. (2011) Photocaged variants of the MunI and PvuII restriction enzymes, *Biochemistry 50*, 2800-2807.
102. Lemke, E. A., Summerer, D., Geierstanger, B. H., Brittain, S. M., and Schultz, P. G. (2007) Control of protein phosphorylation with a genetically encoded photocaged amino acid, *Nature Chemical Biology 3*, 769-772.
103. Blight, M. A., Menichi, B., and Holland, I. B. (1995) Evidence for post-transcriptional regulation of the synthesis of the Escherichia coli HlyB

haemolysin translocator and production of polyclonal anti-HlyB antibody, *Molecular & general genetics : MGG 247*, 73-85.
104. Dyballa, N., and Metzger, S. (2009) Fast and sensitive colloidal coomassie G-250 staining for proteins in polyacrylamide gels, *J Vis Exp*.
105. Stoddard, B. L., Cohen, B. E., Brubaker, M., Mesecar, A. D., and Koshland, D. E., Jr. (1998) Millisecond Laue structures of an enzyme-product complex using photocaged substrate analogs, *Nat Struct Biol 5*, 891-897.
106. Hanahan, D. (1983) Studies on transformation of Escherichia coli with plasmids, *Journal of molecular biology 166*, 557-580.
107. Ito, H., Fukuda, Y., Murata, K., and Kimura, A. (1983) Transformation of intact yeast cells treated with alkali cations, *Journal of bacteriology 153*, 163-168.
108. Kawai, S., Hashimoto, W., and Murata, K. (2010) Transformation of Saccharomyces cerevisiae and other fungi: methods and possible underlying mechanism, *Bioeng Bugs 1*, 395-403.
109. Vogelstein, B., and Gillespie, D. (1979) Preparative and analytical purification of DNA from agarose, *Proceedings of the National Academy of Sciences of the United States of America 76*, 615-619.
110. Birnboim, H. C., and Doly, J. (1979) A rapid alkaline extraction procedure for screening recombinant plasmid DNA, *Nucleic acids research 7*, 1513-1523.
111. Madigan, M. T., and Martinko, J. M. (2006) *Brock Biology Of Microorganisms*, 11 ed., Pearson Education, Inc.
112. Hardjito, L., Greenfield, P. F., and Lee, P. L. (1993) Recombinant protein production via fed-batch culture of the yeast Saccharomyces cerevisiae, *Enzyme Microb Technol 15*, 120-126.
113. Franken, K. L., Hiemstra, H. S., van Meijgaarden, K. E., Subronto, Y., den Hartigh, J., Ottenhoff, T. H., and Drijfhout, J. W. (2000) Purification of his-tagged proteins by immobilized chelate affinity chromatography: the benefits from the use of organic solvent, *Protein Expr Purif 18*, 95-99.
114. Stellwagen, E. (1990) Gel filtration, *Methods in enzymology 182*, 317-328.
115. Zaitseva, J., Holland, I. B., and Schmitt, L. (2004) The role of CAPS buffer in expanding the crystallization space of the nucleotide-binding domain of the ABC transporter haemolysin B from Escherichia coli, *Acta Crystallogr D Biol Crystallogr 60*, 1076-1084.
116. Gill, S. C., and von Hippel, P. H. (1989) Calculation of protein extinction coefficients from amino acid sequence data, *Anal Biochem 182*, 319-326.
117. Bradford, M. M. (1976) A rapid and sensitive method for the quantitation of microgram quantities of protein utilizing the principle of protein-dye binding, *Anal Biochem 72*, 248-254.
118. Laemmli, U. K. (1970) Cleavage of structural proteins during the assembly of the head of bacteriophage T4, *Nature 227*, 680-685.
119. Baykov, A. A., Evtushenko, O. A., and Avaeva, S. M. (1988) A malachite green procedure for orthophosphate determination and its

use in alkaline phosphatase-based enzyme immunoassay, *Anal Biochem 171*, 266-270.
120. Segel, I. H. (1993) *Enzyme kinetics*, Wiley-Interscience.
121. Bagshaw, C. (2001) ATP analogues at a glance, *J Cell Sci 114*, 459-460.
122. Yount, R. G. (1975) ATP analogs, *Adv Enzymol Relat Areas Mol Biol 43*, 1-56.
123. Faller, L. D. (1989) Competitive binding of ATP and the fluorescent substrate analogue 2',3'-O-(2,4,6-trinitrophenylcyclohexadienylidine) adenosine 5'-triphosphate to the gastric H+,K+-ATPase: evidence for two classes of nucleotide sites, *Biochemistry 28*, 6771-6778.
124. Chait, B. T., and Kent, S. B. (1992) Weighing naked proteins: practical, high-accuracy mass measurement of peptides and proteins, *Science 257*, 1885-1894.
125. Cech, N. B., and Enke, C. G. (2001) Practical implications of some recent studies in electrospray ionization fundamentals, *Mass Spectrom Rev 20*, 362-387.
126. Liu, J., Ro, K. W., Busman, M., and Knapp, D. R. (2004) Electrospray ionization with a pointed carbon fiber emitter, *Anal Chem 76*, 3599-3606.
127. Bonvin, G., Schappler, J., and Rudaz, S. (2012) Capillary electrophoresis-electrospray ionization-mass spectrometry interfaces: fundamental concepts and technical developments, *J Chromatogr A 1267*, 17-31.
128. Mendez, M. A., Prudent, M., Su, B., and Girault, H. H. (2008) Peptide-phospholipid complex formation at liquid-liquid interfaces, *Anal Chem 80*, 9499-9507.
129. Mumberg, D., Muller, R., and Funk, M. (1994) Regulatable promoters of Saccharomyces cerevisiae: comparison of transcriptional activity and their use for heterologous expression, *Nucleic Acids Res 22*, 5767-5768.
130. Mumberg, D., Muller, R., and Funk, M. (1995) Yeast vectors for the controlled expression of heterologous proteins in different genetic backgrounds, *Gene 156*, 119-122.
131. Funk, M., Niedenthal, R., Mumberg, D., Brinkmann, K., Ronicke, V., and Henkel, T. (2002) Vector systems for heterologous expression of proteins in Saccharomyces cerevisiae, *Methods in enzymology 350*, 248-257.
132. Kirov, M. S. (2008) Die Verwendung einer nicht-natürlichen Aminosäure zum Studium von ABC Transportern, Heinrich Heine University, Duesseldorf.
133. Figler, R. A., Omote, H., Nakamoto, R. K., and Al-Shawi, M. K. (2000) Use of chemical chaperones in the yeast Saccharomyces cerevisiae to enhance heterologous membrane protein expression: high-yield expression and purification of human P-glycoprotein, *Arch Biochem Biophys 376*, 34-46.
134. Benabdelhak, H., Schmitt, L., Horn, C., Jumel, K., Blight, M. A., and Holland, I. B. (2005) Positive co-operative activity and dimerization of the isolated ABC ATPase domain of HlyB from Escherichia coli, *Biochem J 386*, 489-495.

135. Koronakis, V., Hughes, C., and Koronakis, E. (1993) ATPase activity and ATP/ADP-induced conformational change in the soluble domain of the bacterial protein translocator HlyB, *Molecular microbiology 8*, 1163-1175.
136. Patkar, A., and Seo, J. H. (1992) Fermentation kinetics of recombinant yeast in batch and fed-batch cultures, *Biotechnol Bioeng 40*, 103-109.
137. Horn, C., Bremer, E., and Schmitt, L. (2003) Nucleotide dependent monomer/dimer equilibrium of OpuAA, the nucleotide-binding protein of the osmotically regulated ABC transporter OpuA from Bacillus subtilis, *Journal of molecular biology 334*, 403-419.
138. Pelliccioli, A. P., and Wirz, J. (2002) Photoremovable protecting groups: reaction mechanisms and applications, *Photochem Photobiol Sci 1*, 441-458.
139. Walker, J. W., Reid, G. P., McCray, J. A., and Trentham, D. R. (1988) Photolabile 1-(2-nitrophenyl)ethyl phosphate esters of adenine nucleotide analogues. Synthesis and mechanism of photolysis., *J Am Chem Soc 110*, 7170-7177.
140. Horn, C., Jenewein, S., Tschapek, B., Bouschen, W., Metzger, S., Bremer, E., and Schmitt, L. (2008) Monitoring conformational changes during the catalytic cycle of OpuAA, the ATPase subunit of the ABC transporter OpuA from Bacillus subtilis, *Biochem J 412*, 233-244.
141. Koronakis, E., Hughes, C., Milisav, I., and Koronakis, V. (1995) Protein exporter function and in vitro ATPase activity are correlated in ABC-domain mutants of HlyB, *Mol Microbiol 16*, 87-96.
142. Shyamala, V., Baichwal, V., Beall, E., and Ames, G. F. (1991) Structure-function analysis of the histidine permease and comparison with cystic fibrosis mutations, *The Journal of biological chemistry 266*, 18714-18719.
143. Hopfner, K. P., Karcher, A., Shin, D. S., Craig, L., Arthur, L. M., Carney, J. P., and Tainer, J. A. (2000) Structural biology of Rad50 ATPase: ATP-driven conformational control in DNA double-strand break repair and the ABC-ATPase superfamily, *Cell 101*, 789-800.
144. Bruderer, F. (2012) Influence of point mutations on the nucleotide binding domain of the ABC transporter HlyB, In *Institute of Biochemistry; Membrane Transport Group*, Heinrich Heine University, Düsseldorf.
145. GE, Healthcare, and Sciences, L. (2011) Data file 18-1100-52 AE / HiLoad Superdex 30 prep grade, HiLoad Superdex 75 prep grade, HiLoad Superdex 200 prep grade.
146. Urbatsch, I. L., Gimi, K., Wilke-Mounts, S., and Senior, A. E. (2000) Conserved walker A Ser residues in the catalytic sites of P-glycoprotein are critical for catalysis and involved primarily at the transition state step, *The Journal of biological chemistry 275*, 25031-25038.
147. Touloumtzidis, M. (2010) Struktur-Funktionsanalyse der Nukleotid-bindenden Domäne des ABC-Transporters HlyB, In *Institute of biochemistry*, Heinrich Heine University, Duesseldorf.
148. Kim, I. W., Peng, X. H., Sauna, Z. E., FitzGerald, P. C., Xia, D., Muller, M., Nandigama, K., and Ambudkar, S. V. (2006) The conserved tyrosine residues 401 and 1044 in ATP sites of human P-glycoprotein are critical for ATP binding and hydrolysis: evidence for a conserved

subdomain, the A-loop in the ATP-binding cassette, *Biochemistry 45*, 7605-7616.
149. Pattison, D. I., Rahmanto, A. S., and Davies, M. J. (2012) Photo-oxidation of proteins, *Photochem Photobiol Sci 11*, 38-53.
150. Davies, M. J. (2003) Singlet oxygen-mediated damage to proteins and its consequences, *Biochem Biophys Res Commun 305*, 761-770.
151. Dalsgaard, T. K., Otzen, D., Nielsen, J. H., and Larsen, L. B. (2007) Changes in structures of milk proteins upon photo-oxidation, *J Agric Food Chem 55*, 10968-10976.
152. Silva, E., De Landea, C., Edwards, A. M., and Lissi, E. (2000) Lysozyme photo-oxidation by singlet oxygen: properties of the partially inactivated enzyme, *J Photochem Photobiol B 55*, 196-200.
153. Liu, C. C., and Schultz, P. G. (2010) Adding new chemistries to the genetic code, *Annu Rev Biochem 79*, 413-444.
154. Ross, J. A., Chen, Y., Muller, J., Barylko, B., Wang, L., Banks, H. B., Albanesi, J. P., and Jameson, D. M. (2011) Dimeric endophilin A2 stimulates assembly and GTPase activity of dynamin 2, *Biophys J 100*, 729-737.
155. Yu, P., and Pettigrew, D. W. (2003) Linkage between fructose 1,6-bisphosphate binding and the dimer-tetramer equilibrium of Escherichia coli glycerol kinase: critical behavior arising from change of ligand stoichiometry, *Biochemistry 42*, 4243-4252.
156. Hartman, M. C., Josephson, K., and Szostak, J. W. (2006) Enzymatic aminoacylation of tRNA with unnatural amino acids, *Proceedings of the National Academy of Sciences of the United States of America 103*, 4356-4361.
157. Mejlhede, N., Nielsen, P. E., and Ibba, M. (2001) Adding new meanings to the genetic code, *Nat Biotechnol 19*, 532-533.
158. Marriott, G., and Heidecker, M. (1996) Light-directed generation of the actin-activated ATPase activity of caged heavy meromyosin, *Biochemistry 35*, 3170-3174.
159. Rathert, P., Rasko, T., Roth, M., Slaska-Kiss, K., Pingoud, A., Kiss, A., and Jeltsch, A. (2007) Reversible inactivation of the CG specific SssI DNA (cytosine-C5)-methyltransferase with a photocleavable protecting group, *Chembiochem 8*, 202-207.
160. Roth, M., and Jeltsch, A. (2000) Biotin-avidin microplate assay for the quantitative analysis of enzymatic methylation of DNA by DNA methyltransferases, *Biol Chem 381*, 269-272.
161. Kneussel, M., and Wagner, W. (2013) Myosin motors at neuronal synapses: drivers of membrane transport and actin dynamics, *Nat Rev Neurosci 14*, 233-247.
162. Walcott, S., Fagnant, P. M., Trybus, K. M., and Warshaw, D. M. (2009) Smooth muscle heavy meromyosin phosphorylated on one of its two heads supports force and motion, *The Journal of biological chemistry 284*, 18244-18251.
163. Deiters, A., Groff, D., Ryu, Y., Xie, J., and Schultz, P. G. (2006) A genetically encoded photocaged tyrosine, *Angew Chem Int Ed Engl 45*, 2728-2731.

164. McCray, J. A., and Trentham, D. R. (1989) Properties and uses of photoreactive caged compounds, *Annu Rev Biophys Biophys Chem 18*, 239-270.
165. Vollmecke, C., Kotting, C., Gerwert, K., and Lubben, M. (2009) Spectroscopic investigation of the reaction mechanism of CopB-B, the catalytic fragment from an archaeal thermophilic ATP-driven heavy metal transporter, *European journal of biochemistry / FEBS Journal 276*, 6172-6186.
166. He, Z. H., Chillingworth, R. K., Brune, M., Corrie, J. E., Webb, M. R., and Ferenczi, M. A. (1999) The efficiency of contraction in rabbit skeletal muscle fibres, determined from the rate of release of inorganic phosphate, *J Physiol 517 (Pt 3)*, 839-854.
167. McCray, J. A., Herbette, L., Kihara, T., and Trentham, D. R. (1980) A new approach to time-resolved studies of ATP-requiring biological systems; laser flash photolysis of caged ATP, *Proceedings of the National Academy of Sciences of the United States of America 77*, 7237-7241.
168. Higuchi, H., Muto, E., Inoue, Y., and Yanagida, T. (1997) Kinetics of force generation by single kinesin molecules activated by laser photolysis of caged ATP, *Proceedings of the National Academy of Sciences of the United States of America 94*, 4395-4400.
169. Hesse, J., Wechselberger, C., Sonnleitner, M., Schindler, H., and Schutz, G. J. (2002) Single-molecule reader for proteomics and genomics, *J Chromatogr B Analyt Technol Biomed Life Sci 782*, 127-135.
170. Lee, H. M., Larson, D. R., and Lawrence, D. S. (2009) Illuminating the chemistry of life: design, synthesis, and applications of "caged" and related photoresponsive compounds, *ACS Chem Biol 4*, 409-427.
171. Avila, C., Kornilayev, B. A., and Blagg, B. S. (2006) Development and optimization of a useful assay for determining Hsp90's inherent ATPase activity, *Bioorg Med Chem 14*, 1134-1142.
172. Kelly, T. A., and Christian, G. D. (1982) Homogeneous enzymatic fluorescence immunoassay of serum IgG by continuous flow-injection analysis, *Talanta 29*, 1109-1112.
173. Vernon, G. G., Brune, M., Webb, M. R., and Woolley, D. M. (1999) Real-time visual detection of Pi released by flagellar dynein ATPase, *Pflugers Arch 437*, 771-775.
174. Moro, F., Fernandez-Saiz, V., and Muga, A. (2006) The allosteric transition in DnaK probed by infrared difference spectroscopy. Concerted ATP-induced rearrangement of the substrate binding domain, *Protein science : a publication of the Protein Society 15*, 223-233.
175. Jachimska, B., Wasilewska, M., and Adamczyk, Z. (2008) Characterization of globular protein solutions by dynamic light scattering, electrophoretic mobility, and viscosity measurements, *Langmuir 24*, 6866-6872.
176. Wang, X., Graveland-Bikker, J. F., de Kruif, C. G., and Robillard, G. T. (2004) Oligomerization of hydrophobin SC3 in solution: from soluble state to self-assembly, *Protein science : a publication of the Protein Society 13*, 810-821.

177. Pabbathi, A., Patra, S., and Samanta, A. (2013) Structural transformation of bovine serum albumin induced by dimethyl sulfoxide and probed by fluorescence correlation spectroscopy and additional methods, *Chemphyschem 14*, 2441-2449.
178. Zaitseva, J., Jenewein, S., Oswald, C., Jumpertz, T., Holland, I. B., and Schmitt, L. (2005) A molecular understanding of the catalytic cycle of the nucleotide-binding domain of the ABC transporter HlyB, *Biochem Soc Trans 33*, 990-995.
179. Procko, E., Ferrin-O'Connell, I., Ng, S. L., and Gaudet, R. (2006) Distinct structural and functional properties of the ATPase sites in an asymmetric ABC transporter, *Molecular Cell 24*, 51-62.
180. Zoghbi, M. E., Krishnan, S., and Altenberg, G. A. (2012) Dissociation of ATP-binding cassette nucleotide-binding domain dimers into monomers during the hydrolysis cycle, *The Journal of biological chemistry 287*, 14994-15000.
181. Jones, P. M., and George, A. M. (2012) Role of the D-loops in allosteric control of ATP hydrolysis in an ABC transporter, *J Phys Chem A 116*, 3004-3013.

7 Appendix

7.1 Plasmid maps

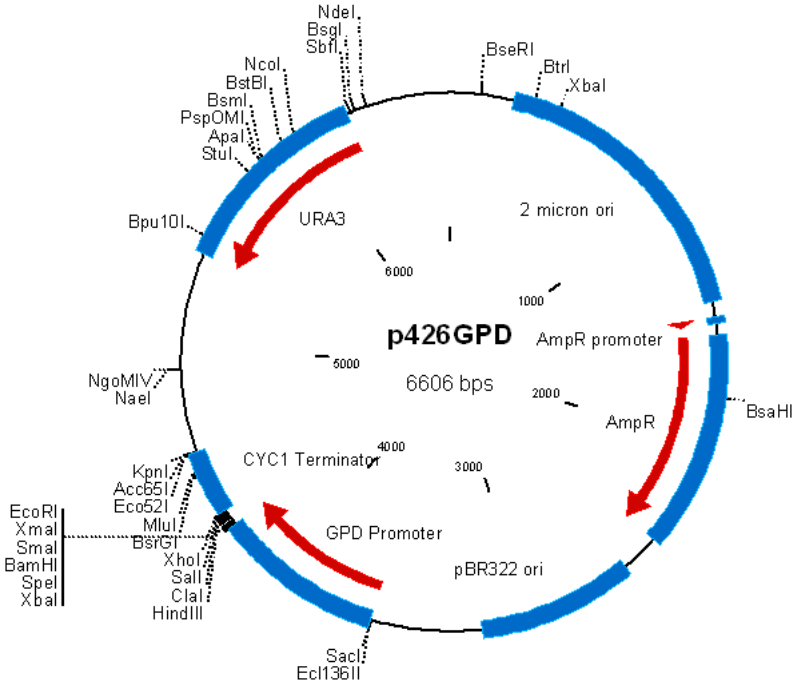

Figure 69: Map of the plasmid p426GPD.

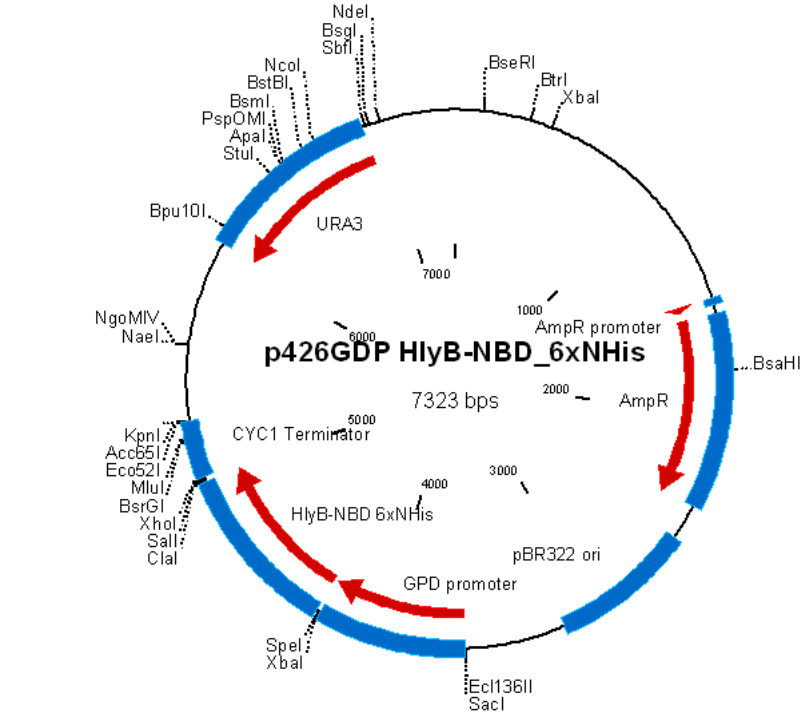

Figure 70: Map of the plasmid p426GPD_HlyB-NBD_6xNHis.

7.2 Charge series MS spectra

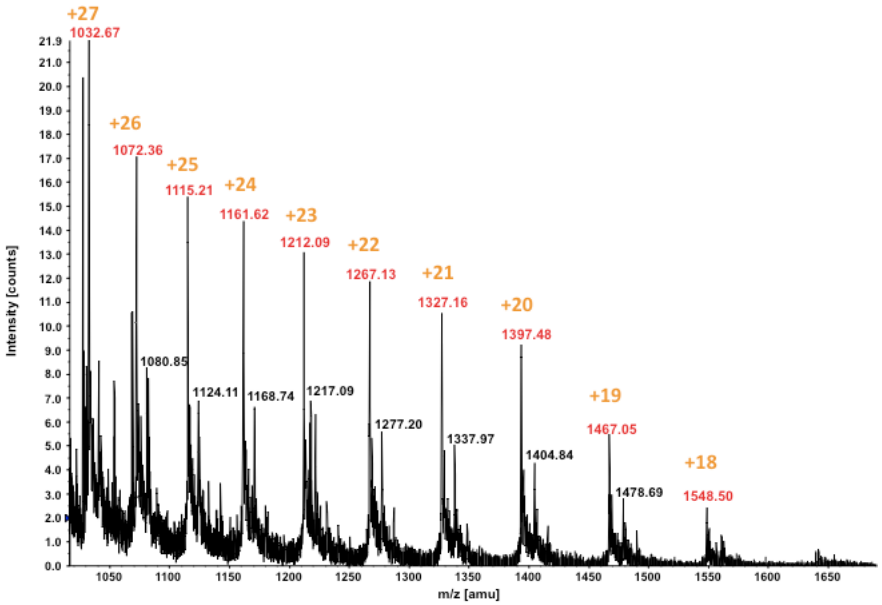

Figure 71: Charge series spectrum of purified HlyB NBD wild type from *S. cerevisiae* after ESI-QQTOF. On the x-axis the mass/charge ratio (m/z) of the obtained ions is represented. On the y-axis the signal intensity is represented. The mass/charge ratio of HlyB NBD is colored in red, the mass/charge ratio of the HlyB NBD with one attached molecule CAPS is shown in black. In orange the charges of the according protein peaks (below the charge) are shown. The mass of the protein from the according charge series is calculated by multiplication of the mass/charge ratio with the according charge. Subsequently, the charge value is subtracted. This calculation is performed for each peak from the according data series. Subsequently the obtained masses are averaged. This results in the mass of HlyB NBD and the mass of HlyB NBD with one attached molecule CAPS, which are shown in **Figure 61**.

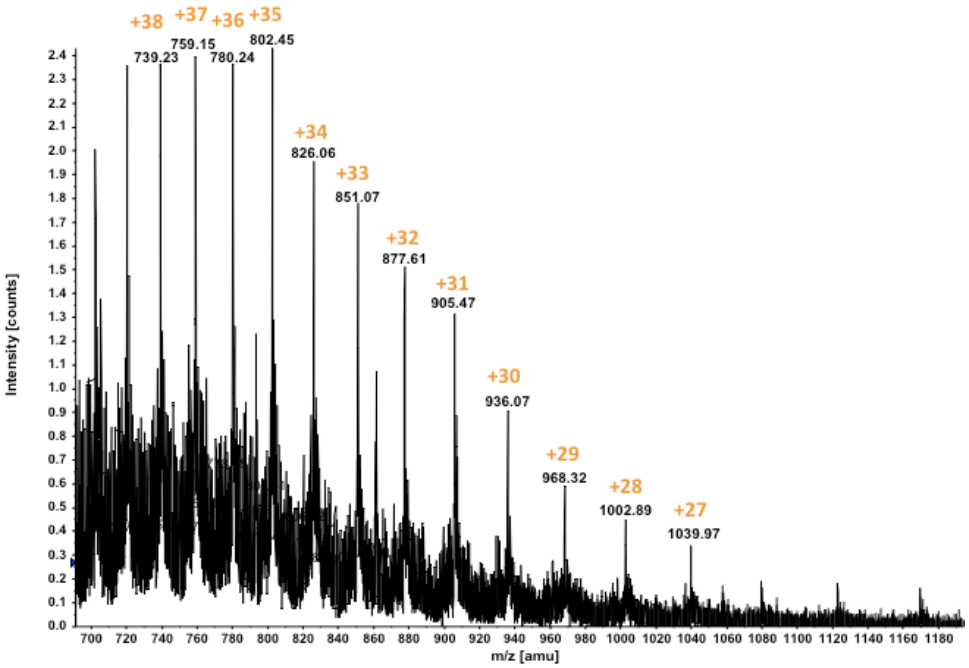

Figure 72: Charge series spectrum of purified caged HlyB NBD S634DMNB-L-Ser from *S. cerevisiae* after ESI-QQTOF. On the x-axis the mass/charge ratio (m/z) of the obtained ions is represented. On the y-axis the signal intensity is represented. The mass/charge ratio the protein is colored in black. In orange the charges of the according protein peaks are shown. The mass of the protein is calculated by multiplication of the mass/charge ratio with the according charge. Subsequently, the charge value is subtracted. This calculation is performed for each peak from the data series. Subsequently the obtained masses are averaged. This results in the mass of the caged HlyB NBD S634DMNB-L-Ser. The obtained mass is shown in **Figure 62**.

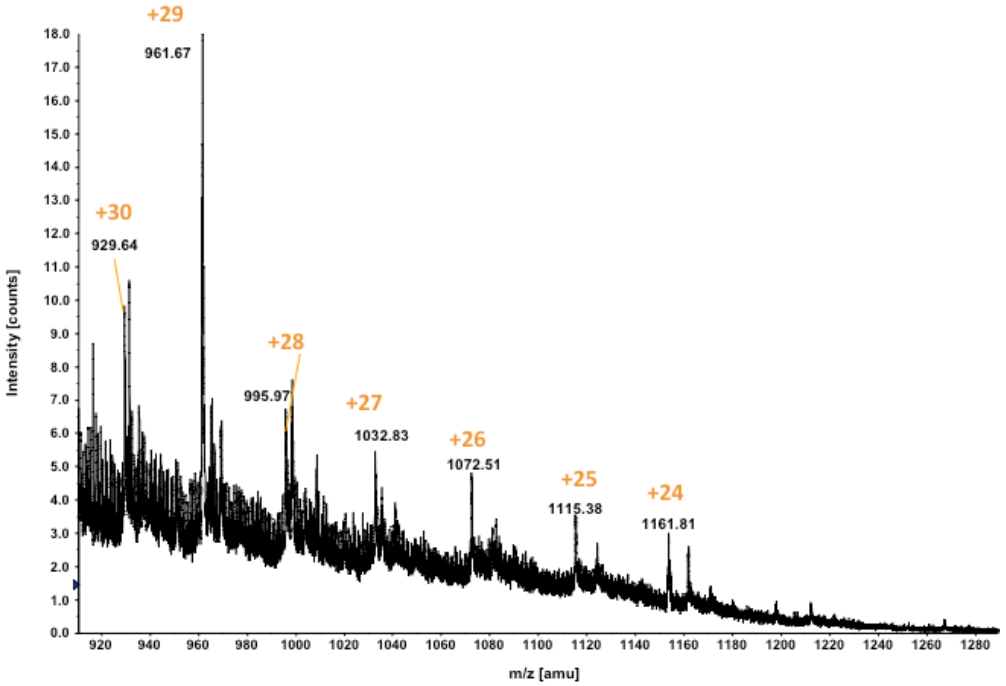

Figure 73: Charge series spectrum of purified decaged HlyB NBD S634DMNB-L-Ser from *S. cerevisiae* after ESI-QQTOF. On the x-axis the mass/charge ratio (m/z) of the obtained ions is represented. On the y-axis the signal intensity is represented. The mass/charge ratio the protein is colored in black. In orange the charges of the according protein peaks are shown. The mass of the protein is calculated by multiplication of the mass/charge ratio with the according charge. Subsequently, the charge value is subtracted. This calculation is performed for each peak from the data series. Subsequently the obtained masses are averaged. This results in the mass of the decaged HlyB NBD S634DMNB-L-Ser. The obtained mass is shown in **Figure 63**.

Table 17: Correction factors Q_1 and Q_2 for the inner filter effects for the titrations of different mutants of HlyB NBD with TNP-ATP.

HlyB NBD	Q_1 [a.u. μM^{-1}]	Q_2 [a.u. μM^{-2}]
Wild type (*S. cerevisiae*)	52337 ± 1941	-1275 ± 220
S504A (*S. cerevisiae*)	57006 ± 1141	-1914 ± 117
S506Y (*E. coli*)	77168 ± 6350	-847 ± 649
S509Y (*E. coli*)	38755 ± 1691	-536 ± 173
S607A (*E. coli*)	43511 ± 839	-902 ± 87
S634Y (*S. cerevisiae*)	72506 ± 1787	-3014 ± 200

7.3 Abbreviations

AARS	Amino acyl tRNA synthetase
ABC	ATP binding cassette
ADH	Alcohol dehydrogenase
ADP	Adenosine-5'-diphosphate
AP	Alkaline phosphatase
AP	Alkaline phosphatase
APS	Ammonium persulfate
ATP	Adenosine-5'-triphosphate
BSA	Bovine serum albumine
CAPS	Cyclohexylaminoethanesulfonic acid
CYC1	Cytochrome-C oxidase
DMNB-L-Ser	Dimethoxy nitrobenzyl-L-serine
DNA	Desoxyribonucleic acid
DO	Drop out
DTT	Dithiothreitol
EtOH	Ethanol
GAL	Galactose
GPD	Glyceraldehyde-3-phosphate dehydrogenase
HEPES	N-(2-hydroxyethyl)piperazine-N´-2-ethanesulfonic acid
HlyB NBD	Haemolysin B nucleotide binding domain
IDA	Iminodiacetic acid
IMAC	Immobilised metal ion affinity chromatography
MET	Methionine
NBD	Nucleotide binding domain
NEB	New England Biolabs
NPE-ATP	P^3-1(2-nitro)phenylethyladenosine 5´-triphosphate
o-NB	Ortho nitrobenzyl
OD	Optical density
PAGE	Polyacrylamide gel electrophoresis
PCR	Polymerase chain reaction
PVDF	Polyvinilidene difluoride
SDS	Sodium dodecylsulfate

TAP	Transporter associated with antigen processing
TEF	Translation elongation factor
TEMED	N, N, N', N'-Tetramethylethylendiamine
TNP-ATP	2'(or 3')-O-(2, 4, 6-trinitrophenyl)-adenosine-5'-monophosphate
TRP	Tryptophan
URA	Uracil
WT	Wild type

8 Danksagung

Vielen Dank an meinem Doktorvater Prof. Dr. Lutz Schmitt für die Möglichkeit, dass ich an diesem sehr interessanten Thema arbeiten konnte. Die Diskussionen mit ihm, seine Tipps sowie seine Kritik haben mich immer wieder motiviert. Nochmal vielen Dank für die Unterstützung Lutz!

Vielen Dank auch an Dr. Nils Hanekop für seine wertvollen Tipps und für die vielen Diskussionen, die mich immer inspiriert haben.

Ich möchte Dr. Sander Smits für seine stete Diskussionsbereitschaft und für die vielen Ideen danken.

Ein großer Dank geht an alle Kollegen um mich herum, die eine unglaublich gute Atmosphäre geschafft haben. Es hat mir unglaublich viel Spaß gemacht, täglich mit euch wissenschaftlich zu arbeiten und auch danach außerhalb des Labors Zeit zu verbringen. Die Zeit mit euch werde ich nie vergessen.

Großer Dank auch an Nadine Wolters, Paul Konieczny und Stefan Vossköter aus AG Prof. Dr. Rainer Weinkauf sowie an Dr. Renè Geißen aus AG Prof. Dr. Joachim Ernst für die Unterstützung bei den experimentellen Arbeiten an deren Instituten.

Vielen Dank an PD Dr. Klaus Schaper für die kritischen Diskussionen und für die Ratschläge.

Ein besonderer Dank geht an meine Freundin Doro und meiner Familie. Ich kann es kaum in Worten fassen, wie viel eure Unterstützung mir bedeutet. Ihr gebt mir immer wieder die Kraft für die Bewältigung jeder neuen Herausforderung.

Hiermit versichere ich, dass ich die vorliegende Dissertation eigenständig verfasst habe, und dass ich alle verwendeten Quellen und Hilfsmittel angegeben habe. Alles, was aus anderen Arbeiten in veränderter oder unveränderter Form übernommen wurde, wurde als solches kenntlich gemacht.

Miroslav Kirov
Düsseldorf, März 2014